The effects of patient specific alignment on the wear, kinematics and contact mechanics of total knee replacements using pre-clinical methods.

A combined computational and experimental approach

Bethany Lowe

Submitted in accordance with the requirements for the degree of Doctor of Philosophy

The University of Leeds
Institute of Medical and Biological Engineering, School of Mechanical Engineering

Under supervision of

Prof Louise M Jennings

Dr Abdellatif Abdelgaied

Dr David Wolfson

January 2023

The candidate confirms that the work submitted is his/her own and that appropriate credit has been given where reference has been made to the work of others.

This copy has been supplied on the understanding that it is copyright material and that no quotation from the thesis may be published without proper acknowledgement.

© 2023 The University of Leeds and Bethany Lowe

Acknowledgements

Firstly, I would like to thank my primary supervisor, Professor Louise Jennings for this opportunity and for her continuous guidance and expertise throughout my PhD project. Additional thanks to Dr Abdellatif Abdelgaied for his help with all things computational and for his patience. I would also like to thank my DePuy Synthes industry supervisor Dr Dave Wolfson for his expert knowledge and encouragement.

This PhD has been funded by an EPSRC industrial case studentship, kindly supported by DePuy Synthes including the provision of all samples used in this project and the equipment used during placement. It has been a pleasure to work with DePuy Synthes with special thanks to Mick Rock, Ioan Cracaoanu, Alice De Courcy-Grylls and Chase Maag.

During my PhD project I have worked within the Institute of Medical and Biological Engineering where I have had the constant support of many people including Dr Raelene Cowie, Phil Wood and Andrew Stockdale who I would like to thank for all their help with the simulators and fixtures.

Thanks to the brilliant PhD researchers of iMBE I have worked alongside over the years, especially Ahranee Canden and Elizabeth Young for keeping me laughing and healthy throughout Covid-19, and to my two housemates Genevieve Pounds and Sophie Hutchinson for their amazing friendship and kindness.

To the groups I've volunteered with at The Children's Society, Stand Together 4 Refugees (ST4R) and Team Gold. You all inspire me so much every day, thank you for always cheering me on.

I have been lucky to be surrounded by such a wonderful community of close friends and family, thank you for your unending support. A special thanks to the wonderful women who have always empowered me (Grandma, Mum, Auntie Mandy, Auntie Deborah and Auntie Nichola).

To 방탄소년단, *thanks for becoming my light*.

I would like to dedicate my thesis to my loving parents, Gail and Jeff Lowe for always believing in my dreams, thank you.

Abstract

Pre-clinical evaluation methods of total knee replacements have traditionally involved experimental simulations to determine the tribological performance of the bearing. However, as the popularity of patient specific surgical procedures increases, so does the demand on research to investigate the impact of these procedures on the longevity of implants. Adapting pre-clinical experimental simulator methodologies to investigate the large range of patient variables required to fully understand these impacts is both impractical and not economically viable. Therefore, it was proposed that recent developments in computational modelling may provide an opportunity to utilise finite element models as a fast and low-cost tool to aid in the pre-clinical assessment of patient specific variables. The aim of this study was to use a combined experimental and computational approach to develop a finite element model of a total knee replacement which could be used to investigate the effects of patient specific alignment variables on implant biomechanics and tribology.

The outputs investigated were kinematics, contact mechanics and wear during ISO 14243-1:2009 standard walking conditions. Agreement between the model predictions and experimental studies during neutral and 4° varus joint alignment developed trust in the capabilities of the model. This resulted in further adaptions of the model to investigate a wider range of joint alignment positions which showed that both sagittal and coronal planes of alignment impacted the walking kinematic outputs. Future work involving these studies has a wide scope which may include investigations with different total knee replacement systems, in a wider range of alignment combinations and under more clinically relevant input conditions.

In conclusion, a newly developed finite element model of an Attune AOX total knee replacement predicted kinematics, contact mechanics and wear values in good agreement with experimentally determined values under varying joint alignment conditions.

Table of Contents

Chapter 1 Introduction and Literature Review 1

1.1 Introduction 1

1.2 Anatomy and Physiology 2

1.2.1 Movement 3

1.2.2 Knee Kinetics and Kinematics 4

1.2.3 Knee Alignment 7

1.2.4 Osteoarthritis 9

1.3 Total Knee Replacements 10

1.3.1 Tribology 11

1.3.2 Polyethylene Implant Materials 12

1.3.3 UHMWPE and Cross Shear 13

1.3.4 Moderately Cross-linked UHMWPE 14

1.3.5 AOX Polyethylene 14

1.3.6 Total Knee Replacement Design 14

1.4 Primary Total Knee Replacement Surgical Procedure 16

1.4.1 Axes of Alignment, Joint Lines and Angles 17

1.4.2 Methods of Alignment 18

1.4.3 Mechanical Alignment 20

1.4.4 Patient Specific Alignment 22

1.5 Preclinical Wear Simulation 25

1.5.1 Total Knee Replacement Wear Under Standardised Conditions 25

1.5.2 Load Control Wear Simulation 26

1.5.3 Experimental Wear of UHMWPE Total Knee Replacements 30

1.6 Computational Simulation Methods Using Finite Element Analysis 32

1.6.1 Wear Laws 32

1.6.2 Computational Wear of Total Knee Replacements 34

1.7 Influence of Surgical Alignment on Wear 35

1.8 Aim and Objectives 37

1.8.1 Summary of Literature Review 37

1.8.2 Objectives 38

Chapter 2 Experimental Simulation Methods 40

2.1 Introduction 40

2.2 Materials 41

2.2.1 Study 1: Sigma XLK Components 41
2.2.2 Study 2: Attune AOX Components 41
2.3 Methods 44
2.3.1 Simulator Calibration 44
2.3.2 ISO 14243-1:2009 Force Control Inputs 44
2.3.3 Sample Setup Methods 47
2.3.4 Methods of Wear Determination 48
2.3.5 Kinematic Outputs 49
2.4 Study 1: Results 50
2.4.1 Sigma XLK Load Control Kinematics 50
2.4.2 Sigma XLK Wear Rates 52
2.5 Study 2: Results 53
2.5.1 Attune AOX Load Control Kinematics 53
2.5.2 Attune AOX Wear Rates 56
2.6 Discussion and Limitations 59
Chapter 3 Experimental Measurement of Total Knee Replacement Contact Mechanics 61
3.1 Introduction 61
3.2 Preliminary Study 1 – AMTI ViVo 62
3.2.1 Rationale 62
3.2.2 Materials 62
3.2.3 Methods 64
3.2.4 Results 70
3.2.5 Discussion 76
3.3 Preliminary Study 2 - Prosim Simulator Total Knee Replacement method development 77
3.3.1 Rationale 77
3.3.2 Materials 77
3.3.3 Methods 79
3.3.4 Results 80
3.3.5 Discussion 82
3.4 ProSim Attune Baseline Tekscan Study 83
3.4.1 Rationale 83
3.4.2 Methods 83
3.4.3 Results 85
3.4.4 Discussion 89

3.5 Measuring Contact Mechanics Using Pressure Sensors Discussion 89
Chapter 4 Finite Element Methods 92
4.1 Introduction 92
4.2 Development of Finite Element Simple Geometry Models 93
4.2.1 Introduction and Background 93
4.2.2 Cylinder on Plate model 93
4.2.3 Sphere on Plate model 99
4.2.4 Dynamic Models 103
4.2.5 Discussion 107
4.3 Development of a Displacement Control Attune Total Knee Replacement Model 107
4.3.1 Rationale 107
4.3.2 Finite Element Model Setup 107
4.3.3 Convergence Studies 109
4.4 Development of a Load Control Attune Total Knee Replacement Model 111
4.4.1 Rationale 111
4.4.2 Linear Spring Model 111
4.4.3 Non-linear Spring Model 114
4.4.4 Results 116
4.4.5 Discussion 117
4.5 Using the Attune Total Knee Replacement Model to Investigate Contact Mechanics 118
4.5.1 Rationale 118
4.5.2 Model Development Methods 118
4.5.3 Results 119
4.5.4 Discussion 122
4.6 Finite Element Model Discussion 123
Chapter 5 Patient Specific Alignment Experimental Simulation 126
5.1 Introduction 126
5.2 Patient Specific Alignment Background 127
5.2.1 Patient Specific Alignment Axes and Angles 127
5.2.2 Patient Specific Alignment Outcomes in Literature 130
5.2.3 PSA Surgical Guidelines 133
5.2.4 Conclusions 135
5.3 Development of Experimental Methods of Patient Specific Alignment... 136

5.3.1 Rationale 136
5.3.2 Simulator Capabilities 137
5.3.3 Designing Fixtures 139
5.4 Study 1 - 4° Varus Experimental Kinematics and Wear 141
5.4.1 Methods.....141
5.4.2 Results 143
5.4.3 Discussion 150
5.5 Study 2 - 4° Varus Experimental Contact Pressure 150
5.5.1 Methods.....150
5.5.2 Results 153
5.5.3 Discussion 156
5.6 Discussion.....156
Chapter 6 Computational Modelling of Patient Specific Alignment and Wear 158
6.1 Introduction 158
6.2 Developing 4 º Varus Alignment Finite Element Model 159
6.2.1 Rationale 159
6.2.2 4º Varus Model Setup Methods 159
6.2.3 Investigating Initial Contact 161
6.3 4º Varus Model Gait Cycle Simulation in Load Control 162
6.3.1 Methods of Simulation 162
6.3.2 Spring constraints study.....164
6.3.3 4º Varus Model Simulation Kinematics Results.....167
6.3.4 Discussion 170
6.4 4º varus Model Contact Mechanics Study 171
6.4.1 Rationale 171
6.4.2 Steps 171
6.4.3 Boundary Conditions 172
6.4.4 Model Outputs 172
6.4.5 4º Varus Model Contact Pressures 172
6.4.6 4º Varus Model Comparison to Experimental Contact Pressures 173
6.4.7 4º Varus Model Comparison to MA Contact Pressures 175
6.4.8 Discussion 176
6.5 The Effect of Coronal and Sagittal Alignment on Kinematics 176
6.5.1 Rationale 176

6.5.2 Alignment Input Parameters 177
6.5.3 Adapting Coronal and Sagittal Alignment Assembly 178
6.5.4 Level 1 Alignment Kinematic Results 179
6.5.5 Level 2 Alignment Kinematic Results 181
6.5.6 Discussion 186
6.6 The Effect of Coronal Alignment on Wear 186
6.6.1 Introduction 186
6.6.2 Background on Total Knee Replacement Wear Models 187
6.6.3 Inputs to Attune AOX Wear Model 188
6.6.4 MA and 4º Varus Alignment Computational Wear Predictions ... 188
6.6.5 Comparison of Computational and Experimental Wear Rates ... 189
6.6.6 Summary of Wear Model 190
6.7 Discussion 190
Chapter 7 Discussion and Limitations 194
7.1 Introduction 194
7.2 Experimental Simulation of Attune AOX Total Knee Replacements Under ISO 14243-1:2009 Load Control in Mechanical Alignment. 195
7.3 Experimental Investigation of Attune AOX Total Knee Replacement Contact Mechanics Using Pressure Sensors at a Range of Kinematic Positions and Loads 197
7.4 Developing an Attune AOX Finite Element Model to Predict Kinematics and Contact Mechanics Under ISO-14243-1:2009 Load Control Simulation Input Conditions 197
7.5 Creating Experimental Preclinical Methods of Simulating Patient Specific Alignment Joint Angles to Predict Kinematics, Contact Mechanics and Wear Rates. 198
7.6 Applying Alignment Simulation Parameters to an Attune AOX Finite Element Model to Predict Kinematics and Contact Mechanics 200
7.7 Using Computational Methods to Determine the Wear Rate of Attune AOX Simulated Under Mechanical Alignment and 4° Varus Alignment Conditions 201
7.8 Limitations 202
7.9 Future Work 204
7.10 Conclusion 207
Chapter 8 Bibliography 209
Appendix 220
Appendix A – Attune Baseline Component Details 220
Appendix B – Python script for extracting Abaqus data 221

List of Tables

Table 1-1: Abduction-adduction and Internal-external angles of a native tibiofemoral joint at different degrees of flexion (Roth et al., 2015) [9, 34] 7

Table 1-2: Definitions of surgical alignment procedures of total knee replacements in references to axes and angles of the lower limb [93]. 20

Table 1-3: ProSim 6-station electromechanical simulator capabilities 27

Table 2-1: Attune sample descriptions, part reference and images for the tibial insert, tibial tray and femoral component 42

Table 2-2: Sample pairings with corresponding wear station at each wear interval 42

Table 2-3: Sample cumulative volumetric wear at each measurement interval. 52

Table 2-4: Sample cumulative volumetric wear at each measurement interval. 57

Table 2-5: average volumetric wear rate of each wear station at 3 million cycles and 6-station average with 95% confidence interval. 57

Table 3-1: Mechanical Alignment Input Profiles 70

Table 3-2: Patient-specific Alignment Input Profiles 70

Table 3-3: Percentage difference between simulator applied load and Tekscan sensor measured load. Includes 101 (test 1, repeat 1), 102 (test 1, repeat 2) and 201 (test 2, repeat 1) 71

Table 3-4: Tekscan gait study input values at 10% intervals from 0%-100% for 4-degrees of freedom 84

Table 4-1: Extended cylinder Hertzian Predicted PMax values for a range of polyethylene material properties 97

Table 4-2: Hertzian predicted peak contact pressure values for a sphere loaded onto a plate with varying Young's Modulus and Poisson's ratio values 101

Table 4-3: Contour images of the tibial component contact area at 10% intervals of the gait cycle 120

Table 4-4: Average and peak contact pressure predictions of TKR baseline model 121

Table 5-1: Lower limb alignment axes and angles terminology [94, 160] 129

Table 5-2: Summary of reviewed literature on mechanical alignment versus patient specific alignment outcomes 130

Table 5-3: Post-operative joint alignment angles of the literature review of MA and PSA procedures 132

Table 5-4: Example of patient with out of "safe boundary" tibial coronal angle as per DePuy Synthes ATTUNE Knee System femur first PSA instrumented surgical technique..... 135

Table 5-5: 4° varus experimental wear simulation sample pairings with corresponding wear station at each wear interval 141

Table 5-6: Cumulative wear (mm^3) of each wear sample at wear intervals, with 3mc volumetric wear rate (mm^3/mc) for each sample..... 149

Table 5-7: 4° varus 10% gait interval tekscan input positions. 152

Table 6-1: Femoral and tibial component angle configurations in coronal and sagittal planes for first level of experiments 178

Table 6-2: Femoral and tibial component angle configurations in coronal and sagittal planes for second level of experiments 178

Table 6-3: Summary of maximum and minimum kinematic outputs for anterior-posterior displacement, internal-external rotation and abduction-adduction rotation for Level 2 alignment model simulations 185

Table 6-4: Computational predictions of contact stress, cross shear ratio and wear rate calculated in MATLAB using the computational wear framework developed by Abdelgaied et al., 2018 [119]..... 188

Table A-1: Attune Baseline Component Details 220

List of Figures

Figure 1-1: The anatomy of the knee [17] 3

Figure 1-2: The three joint coordinate axes and the three rotational motions of the knee as established by Grood, E. S., & Suntay, W. J. (1983) adapted from Noyes, F. R., & Grood, E. S. (1987) published by Noyes, F. R. (2009) [19-21] 4

Figure 1-3: Axes of rotation of the knee: (a) Flexion-extension about the frontal axis; (b) Internal-external rotation about the longitudinal axis; (c) Abduction-adduction rotation about sagittal axis by Marieswaran et al. (2018) [24] 5

Figure 1-4: X-ray contact maps comparing the medial and lateral compartment surface contact of the tibiofemoral joint (left knee) during increasing angles of flexion. The black dots are the centre of contact. By S Hamai et al, (2012)[29] 6

Figure 1-5: The axes and joint line of the knee in different positions a) neutral alignment b) valgus alignment c) varus alignment. By D.A. Dennis (2018) [35] 7

Figure 1-6: Knee adduction moment in healthy individuals calculated using different models by Meireles et al. (2017) [39] 8

Figure 1-7: DePuy Synthes ATTUNE Primary fixed bearing cruciate retaining knee implant [56] 11

Figure 1-8: Schematic showing the influence of chain sliding on the principal molecular orientation (PMO) of UHMWPE [70] 13

Figure 1-9: ATTUNE Knee System implants including posterior stabilised (back) posterior cruciate ligament retaining (front) [81] 15

Figure 1-10: Gradually reducing ATTUNE knee system femoral radius (Gradius) design highlighted in purple compared to a dual-radius design (PFC Sigma) in red and the Stryker Triathlon singe flexion radius design in green. [84] 16

Figure 1-11: Coronal view of the knee A) native knee B) with total knee replacement showing how the joint line orientation can be altered post-operatively in angle and in height from the epicondylar axis [87] 17

Figure 1-12: Defining angles between the axis of the lower limbs including 1. Lateral distal femoral angle (LDFA) 2. Medial proximal tibial angle (MPTA) 3. Mechanical hip-knee-ankle angle (mHKA) for a) mild constitutional varus knee b) degeneration of varus knee [89]. 18

Figure 1-13: A comparison of the various TKR alignment procedures with reference to the different leg axes and joint lines, release refers to release of soft tissues [92], annotations are added in black 19

Figure 1-14: Histogram of the distribution of hip-knee-ankle angles within a population of 250 asymptomatic volunteers, with an average of 1.3° varus [88] 23

Figure 1-15: The angles of the knee in the coronal plane include; the transfemoral axis (TFA) angle of the knee; the femoral angle (α) between the bottom of the femoral condyles and the anatomical axis of the femur; the tibial angle (β) between the base of the tibial tray and the anatomical axis of the tibia [108] 24

Figure 1-16: ProSim 6-station electromechanical total knee simulator by Simulation Solutions, Stockport, UK 27

Figure 1-17: ProSim electromechanical knee simulator component setup with directions of applied motions including Axial force, flexion-extension, anterior-posterior displacement and internal-external tibial rotation. 28

Figure 1-18: Gait profiles for standard walking under load control (ISO 14243-1:2009) including a) axial force, b) flexion-extension, c) anterior-posterior load, d) internal-external torque 29

Figure 1-19: ISO 14243-1:2009 cruciate retaining TKR spring stiffness profiles for a) anterior-posterior load and b) internal-external torque 30

Figure 1-20: The wear performance of Sigma XLK and Attune AOX TKR bearings over 5 million cycles. Presented by Dressler et al. at ORS 2012 [120]. 31

Figure 2-1: Attune femoral component centre of rotation 43

Figure 2-2 : Attune fixed bearing cruciate retaining Delrin fixtures 44

Figure 2-3: Gait profile inputs for standard walking under force control (ISO 14243-1:2009) a) axial force b) flexion angle c) anterior-posterior force d) tibial rotation torque [112] 46

Figure 2-4: ISO 14243-1:2009 cruciate retaining TKR spring stiffness profiles for AP load (left) and TR torque (right) 46

Figure 2-5: Contact prints of Attune AOX Baseline samples 48

Figure 2-6: Output Sigma XLK anterior-posterior kinematic positions 10 cycle average from the wear study and published data by Johnston et al. 2019 [129] 51

Figure 2-7: Output Sigma XLK tibial-rotation kinematic angles 100-cycle average from the wear study and published data by Johnston et al. 2019 51

Figure 2-8: Average volumetric wear rates with 95% confidence limits after 2MC Sigma XLK wear study compared to data published by Johnston et al., 2018 53

Figure 2-9: 100-cycle average anterior-posterior displacement for three wear intervals 0-1Mc, 1-2MC and 2-3MC. 54

Figure 2-10: 100-cycle average internal-external rotation angle for three wear intervals 0-1Mc, 1-2MC and 2-3MC. 54

Figure 2-11: Output baseline Attune AOX anterior-posterior displacement kinematic positions 100-cycle average 55

Figure 2-12: Output baseline Attune AOX internal-external rotation kinematic angles 100-cycle average 56

Figure 2-13: Output baseline Attune AOX abduction-adduction rotation angles 100-cycle average 56

Figure 2-14: 0-3 million cycles Attune AOX average cumulative volumetric wear with 95% confidence interval at each million-cycle wear interval. Includes a linear fit regression line. 57

Figure 2-15: Average Volumetric Wear Rate over 3 million cycles for each wear station. 58

Figure 2-16: Average 6-station volumetric wear rate with 95% confidence intervals displayed for 3 million cycles of wear of Attune AOX and 2 million cycles of wear of Sigma XLK 59

Figure 3-1: Tekscan 4000 Sensor 63

Figure 3-2: Tekscan Calibration Disks 63

Figure 3-3: Tekscan Calibration Equipment Setup 65

Figure 3-4: Tekscan 4000 calibration with default sensitivity (left) and Mid 2 sensitivity (right) settings. 65

Figure 3-5: TKR components setup on AMTI single station ViVo with Tekscan 4000 sensors, posterior view (left) and anterior view (right) 67

Figure 3-6: Kinematic profiles for mechanical alignment (MA) and anatomic alignment (AA) Tekscan study on AMTI VIVO as extracted from 6-DOF joint simulator model for cruciate retaining (CR) and posterior stabilised (PS) bearing designs. Including medial-lateral (ML) force, anterior-posterior (AP) force, Vertical force, flexion, varus-valgus (VV) torque and internal-external (IE) torque. (reproduced with permission from Maag et al., 2021 [130]) 68

Figure 3-7: VIVO output for flexion/extension angles and axial loads with the study input points located on the profile in a) MA b) PSA 69

Figure 3-8: VIVO output for medial/lateral and anterior/posterior displacement with the study input points located on the profile in a) MA b) PSA 69

Figure 3-9: VIVO output for adduction/abduction and internal/external angles with the study input points located on the profile in a) MA b) PSA 69

Figure 3-10: Contact pressure heat map scale 71

Figure 3-11: Test 2, repeat 2 contact pressure maps of MA and PSA over all 11 fixed points of the gait cycle. Greyed results represent no contact pressure on that sensor pad..... 73

Figure 3-12: Peak Contact Pressure (MPa) for MA Test 1 medial and lateral compartments. 74

Figure 3-13: Peak Contact Pressure (MPa) for MA Test 2 medial and lateral compartments. 74

Figure 3-14: Peak Contact Pressure (MPa) for PSA Test 1 medial and lateral compartments. 75

Figure 3-15: Peak Contact Pressure (MPa) for PSA Test 2 medial and lateral compartments. 76

Figure 3-16: Tekscan Prosim Calibration Setup 78

Figure 3-17: ProSim Total Knee Replacement Tekscan setup 79

Figure 3-18: Output contact pressure of applied load to TKR bearing with Vaseline applied after 6 measurements 81

Figure 3-19: Output contact pressure of applied load to TKR bearing with Vaseline applied after 12 measurements 81

Figure 3-20: Output contact pressures of applied load to TKR bearing with a reduced frequency of calibrations between measurements, including each ramp, 6 ,12 and 18 additional measurements. 82

Figure 3-21: Average Contact Pressure at an applied load with varying femoral flexion angles 85

Figure 3-22: Attune baseline Tekscan heat scale 86

Figure 3-23: Attune baseline contact pressure heat maps for one gait cycle at 10% intervals. 87

Figure 3-24: Average ±1 standard deviation contact pressure at 10% intervals of the gait cycle with input load of an ISO 14243-1:2009 standard walking gait cycle. 88

Figure 3-25: Average Contact Pressure (MPa) of medial and lateral compartments measure by the Tekscan sensor on ProSim simulator in Mechanical alignment 88

Figure 4-1: Cylinder on Plate model assembly 94

Figure 4-2: Abaqus Cylinder on Plate Model - Plate stress contours a) 63.5mm cylinder length b) 70+mm cylinder length 95

Figure 4-3: Cylinder mesh convergence study with the result for convergence circled in red. 95

Figure 4-4: Cylinder on Plate model predicted contact pressure for a range of material properties with differing values of Young's Modulus and Poisson's Ratio 98

Figure 4-5: Cylinder on Plate model predicted values for v=0.46 plotted with calculated values using Hertzian contact theory. Value highlighted red to show outside of 5% agreement 98

Figure 4-6: Sphere on plate mesh convergence study with maximum contact pressure values at a range of global element sizes with the result for convergence circled in red. 99

Figure 4-7: Hertzian Contact model of a sphere on plate (Cheneler et al., 2013) 100

Figure 4-8: Sphere on Plate model predicted contact pressure for a range of material properties with differing values of Young's Modulus and Poisson's Ratio 101

Figure 4-9: Sphere on Plate model predicted values for v=0.46 plotted with calculated values using Hertzian contact theory. 102

Figure 4-10: Peak contact pressure results at a range of coefficient of friction values.....102

Figure 4-11: Gait profiles for standard walking under displacement control adapted from (ISO 14243-3:2014) [114].....104

Figure 4-12: Sphere on plate output contact area and contact pressure for one gait cycle.....105

Figure 4-13: ISO 14243-1:2009 force control input profiles for AF, FE, AP and TR at a 1Hz frequency [112] 105

Figure 4-14: Sphere on plate load control model predicted output anterior-posterior displacement and calculated value for one gait cycle.....106

Figure 4-15: Sphere on plate load control model predicted output internal-external rotation and calculated value for one gait cycle.....106

Figure 4-16: Right: TKR Model setup with coordinate system of reference. +X is medial, Y+ is posterior and Z+ is superior. The directions of rotation are Mx+ is flexion, My+ is abduction and Mz+ is internal rotation. 108

Figure 4-17: Convergence study of the TKR contact pressure under a static load of 220N at a range of element sizes for finite element mesh created in HyperMesh versus ABAQUS software.....110

Figure 4-18: Mesh convergence study using ABAQUS mesh with a static load demand of 667N applied to a TKR finite element mesh with decreasing global element sizes (global element size of 1 highlighted red).....111

Figure 4-19: Wire elements applied to Attune finite element model to act as anterior-posterior spring and tibial rotation spring. 112

Figure 4-20: Linear spring model stiffness profiles for AP displacement (mm) and tibial rotation angle (°) 113

Figure 4-21: Linear spring model predicted kinematic values vs calculated values using Hooke's law -F=kx for AP displacement (left) and TR angle (right).....113

Figure 4-22: Linear spring model predicted kinematic values vs calculated values using Hooke's law -F=kx for AP displacement for spring lengths of 20mm, 30mm and to ground. 114

Figure 4-23: TKR model setup with the active kinetic and kinematic controls applied to each reference point constrained to the two components.....115

Figure 4-24: Model predicted AP displacement of the tibial component and experimental simulation measured 100 cycle average AP displacement with ±95% CI (represented with dashed lines) (r^2 = 0.766) 116

Figure 4-25: Model predicted TR angle of the tibial component and experimental simulation measured 100 cycle average TR angle with ±95% CI (represented with dashed lines) (r^2 = 0.828) 117

Figure 4-26: Contour scale for tibial contact images 120

Figure 4-27: Tibial insert model contact heat map medial and lateral condyles 120

Figure 4-28: Average contact pressure of baseline TKR model contact surface (black) medial compartment (orange) and lateral compartment (green). With axial force and flexion-extension graphs inputs of one gait cycle 121

Figure 4-29: Average contact pressure of baseline TKR model plotted with average baseline Tekscan study outputs with ±1 standard deviation. 122

Figure 5-1: The three axes that define tibiofemoral and patellofemoral kinematics including the longitudinal axis (yellow), transverse axis of tibial flexion (green) and transverse axis of patellar flexion (magenta) [155] 128

Figure 5-2: Frontal view leg axes in valgus and varus alignments, including the long bone axis, the femur mechanical axis and the tibia mechanical axis. 128

Figure 5-3: Frontal view lower leg alignment axes, angles and joint lines (JL) [94] 129

Figure 5-4: Total knee replacement patient specific alignment angles and axes for pre-operative cutting calculations [94] 134

Figure 5-5: Illustrated example of cutting angles to restore patients' post-operative alignment to within DePuy Synthes "safe boundaries" 135

Figure 5-6: Trial 1 - 4° tibial angle setup using abduction-adduction carriage a) CAD depiction of adaption to component alignment b) component alignment during simulator alignment trial 138

Figure 5-7: Trial 2 – Abduction-adduction rotation angle output kinematic profile with 4° adduction angle profile applied to simulator tibial carriage 139

Figure 5-8: 4° varus femoral Delrin fixture aligned with femoral fixture base to align screw holes for positioning in the joint simulator 140

Figure 5-9: 4° varus alignment femoral fixture drawing with adapted base, base plate screw holes and femoral peg centring holes 140

Figure 5-10: 4° varus experimental simulator setup with fixture adaptions. Axes of alignment labelled in accordance with DePuy alignment guidelines as femoral anatomical (red line) axis, femoral mechanical (purple dashed line) axis and tibial mechanical (red line) axis. F and T are the femoral joint line angle and tibial joint line angle respectively. 142

Figure 5-11: 4° varus alignment anterior-posterior displacement at each wear interval (100-cycle average of 6 stations) 144

Figure 5-12: 4° varus alignment internal-external rotation angle at each wear interval (100-cycle average of 6 stations) 144

Figure 5-13: 4° varus alignment abduction-adduction rotation angle at each wear interval (100-cycle 6 station average) 145

Figure 5-14: PSA 4deg anterior-posterior displacement 0-1MC 100-cycle average with 95% confidence intervals 146

Figure 5-15: PSA 4deg internal-external rotation angle 0-1MC 100-cycle average with 95% confidence intervals 146

Figure 5-16: PSA 4deg abduction-adduction rotation angle 0-1MC 100-cycle average with 95% confidence intervals 146

Figure 5-17: Baseline and 4º varus anterior-posterior displacement 100-cycle average with 95% confidence intervals 148

Figure 5-18: Baseline and 4º varus tibial rotation angle 100-cycle average with 95% confidence intervals 148

Figure 5-19: Baseline and 4º varus abduction-adduction rotation angle 100-cycle average with 95% confidence intervals 148

Figure 5-20: 4° varus and MA average cumulative wear with 95% confidence intervals at wear intervals over 3mc, and regression line with intercept at zero 150

Figure 5-21: 4° varus alignment experimental Tekscan setup in simulator ...152

Figure 5-22: PSA Tekscan average contact pressure and standard deviation (n=6) and input load and flexion of one gait cycle 153

Figure 5-23: Tekscan average contact pressures (n=6) for the total contact surface, the medial compartment, and the lateral compartment for each of the 10% gait cycle intervals 154

Figure 5-24: 4° varus and MA experimental total contact surface contact pressure average and standard deviation at 10% intervals of the gait cycle 155

Figure 5-25: 4° varus (triangles) and MA (diamonds) experimental contact pressure average at 10% intervals of the gait cycle for the medial compartment (orange) and lateral compartment (green) 155

Figure 6-1: 4° varus model alignment side and front views of setup of control nodes and coordinate system with control reference points of each component including the tibial insert (RP-1) and the femoral component (RP-2). 160

Figure 6-2: 4° varus alignment in finite element environment with axes and coordinate system 161

Figure 6-3: 4° varus alignment with small vertical displacement applied through femoral component, with initial contact pressure of 0.62MPa located at the bearing dwell point 162

Figure 6-4: Input profiles with "free-range" for a) anterior-posterior load and b) internal-external tibial torque 164

Figure 6-5: Input profiles with no "free-range" for a) anterior-posterior load and b) internal-external tibial torque 165

Figure 6-6: 4° varus alignment anterior-posterior displacement output with varying spring profile combinations (1), (2) and (3). 165

Figure 6-7: 4° varus alignment internal-external rotation angle output with varying spring profile combinations (1), (2) and (3). 166

Figure 6-8: Contact pressure map of tibial insert during 4° varus alignment gait cycle with both tibial rotation spring and anterior-posterior spring containing a "free range". 166

Figure 6-9: 4° varus finite element model output kinematics of one gait cycle for a) anterior-posterior displacement and b) internal-external rotation 168

Figure 6-10: Anterior-posterior displacement 4° varus output kinematics for experimental (±95%CI) and finite element model predicted outcome. 168

Figure 6-11: Internal-external rotation angle 4° varus output kinematics for experimental (±95%CI) and finite element model predicted outcome. 169

Figure 6-12: Anterior-posterior displacement kinematic output for MA and 4° varus finite element model outputs 170

Figure 6-13: Internal-external rotation angle kinematic output for MA and 4° varus finite element model outputs 170

Figure 6-14: Finite element model predicted medial and lateral compartment contact pressures at 10% gait intervals in 4° varus alignment 173

Figure 6-15: Finite element model PSA average contact pressure and experimental contact pressure with ±1 standard deviation at 10% intervals of the gait cycle 174

Figure 6-16: 4° varus experimental Tekscan contact pressure heat map at 30% configuration repeat-1 174

Figure 6-17: 4° varus 30% model contact pressure heat map 175

Figure 6-18: Finite element model predicted average contact pressure at eleven 10% intervals of the gait cycle for baseline mechanical alignment and 4° varus alignment. 175

Figure 6-19: Finite element model setup of coronal and sagittal planes of alignment 177

Figure 6-20: AP displacement kinematic outputs from the first level of interaction studies for a) coronal alignment and b) sagittal alignment and including baseline MA output kinematics 179

Figure 6-21: Internal-external angle kinematic outputs from the first level of interaction studies for a) coronal alignment and b) sagittal alignment and including baseline MA output kinematics 180

Figure 6-22: Abduction-adduction angle kinematic outputs from the first level of interaction studies for a) coronal alignment and b) sagittal alignment and including baseline MA output kinematics 181

Figure 6-23: Anterior-posterior displacement kinematic outputs from Level 2 model alignment study including a) coronal 3° sagittal 5°-7°, b) coronal 5° sagittal 5°-7°, c) coronal 7° sagittal 5°-7° 182

Figure 6-24: Internal-external rotation kinematic outputs from Level 2 model alignment study including a) coronal 3° sagittal 5°-7°, b) coronal 5° sagittal 5°-7°, c) coronal 7° sagittal 5°-7°.....183

Figure 6-25: Abduction-adduction rotation kinematic outputs from Level 2 model alignment study including a) coronal 3° sagittal 5°-7°, b) coronal 5° sagittal 5°-7°, c) coronal 7° sagittal 5°-7°.....184

Figure 6-26: Average 3 million cycle wear rates of baseline experimental study for each of the six wear stations, the experimental average wear rate with ±95% confidence interval, and the computational wear prediction in orange.....189

Figure 6-27: Average 3 million cycle wear rates of 4° varus experimental study for each of the five wear stations, the experimental average wear rate with ±95% confidence interval, and the computational wear prediction in orange.....190

List of Equations

Equation 1-1: Archard's Wear Law..... 11

Equation 1-2: Cross Shear calculation by Kang et al., 2008 [126] 33

Equation 1-3: Wear coefficient equation by Abdelgaied et al. (2018) 34

Equation 4-1: Young's Modulus – Poisson's Ratio relationship in Hertzian prediction 96

Equation 4-2: Semi-contact width (Cylinder on Plate) 96

Equation 4-3: Maximum Contact Pressure (Cylinder on Plate) 96

Equation 4-4: Radius of the contact circle 100

Equation 4-5: Maximum contact pressure for a sphere on plate 100

Equation 4-6: Hooke's Law where F is applied force, k is spring stiffness and x is the displacement. 112

Equation 6-1: Non-dimensional wear coefficient for UHMWPE as a function of cross shear and non-dimensional contact stress [119]..... 187

Nomenclature

ABBREVIATION	WORD
AA	Anatomic Alignment
ACL	Anterior Cruciate Ligament
AdAb	Adduction/Abduction
AF	Axial Force
aMA	Adjusted Mechanical Alignment
AP	Anterior/Posterior
BC	Boundary Condition
Co-Cr	Cobalt Chrome
CoR	Centre of Rotation
CPU	Central Processing Unit
CR	Cruciate Retaining
CS	Cross Shear
CSR	Cross-shear Ratio
DoF	Degrees of Freedom
EM	Electromechanical
FB	Fixed Bearing
FE	Finite Element
FFCS	Femoral Flexion Facets
G&S	Grood and Suntay
GPGPU	General-purpose Graphics Processing Unit
HKA	Hip-knee-ankle
IE	Internal/External
ISO	International Organization for Standardization
KA	Kinematic alignment
KAM	Knee Adduction Moment
KS8	Knee Simulator 8
KSS	Knee Society Score
LCL	Lateral Collateral Ligament
MA	Mechanical Alignment
MC	Million Cycles
MCL	Medial Collateral Ligament
ML	Medial/Lateral
OA	Osteoarthritis
PCA	Posterior Condylar Axis
PCL	Posterior Cruciate Ligament
PE	Polyethylene
PMO	Principal Molecular Orientation
PoP	Pin on Plate
PS	Posterior-stabilised
rKA	Restricted Kinematic Alignment
RP	Reference Point
SI	Superior/Inferior
TFA	Transfemoral Axis
TKR	Total Knee Replacement
TR	Tibial Rotation
UHMWPE	Ultra-High Molecular Weight Polyethylene
VV	Varus/Valgus

Chapter 1
Introduction and Literature Review

1.1 Introduction

From the first joint replacements developed nearly 100 years ago, to the work by John Charnley in the 1950's and 60's who successful developed a routine surgical procedure with low-friction arthroplasty design [1], the world of orthopaedic implants has advanced with research and technology into the modern day. In 2021, 68,974 primary total knee replacement surgeries were completed in the UK alone, an annual value which was decreased slightly from a figure of around 90,000 procedures annually in the five years before the COVID-19 pandemic [2]. The procedure is used to replace damaged surfaces of the knee, most commonly due to a joint degeneration disease known as osteoarthritis (OA) which accounts for 97% of knee replacement procedures in the UK [2]. Primary risk factors for developing OA include age, gender, obesity, joint injury, joint abnormalities and genetic factors [3]. OA is prevalent in around 80% of the population over 65 in well-developed countries and since the global population is living longer, the number of cases of OA globally is predicted to reach 130 million by 2050 [4, 5]

The success of a total knee replacement (TKR) implant is dependent on a range of variables including, but not limited to, surgical delivery, kinematics, patient population and biomaterial technology degradation [6]. The key factor in determining the longevity of joint replacements is biotribology, a multidisciplinary subject which applies the fundamentals of tribology to biological systems [7]. The pre-clinical determination and prediction of biotribology, specifically wear, is currently undertaken experimentally by joint simulators under a limited set of conditions, which do not take into account the wide variation of clinical conditions in the patient.

A new Stratified Approach For Enhanced Reliability (SAFER) has been developed which aims to understand what the outlier conditions are where there is an increased risk of early implant failure [6]. Malalignment of implants is among one of the top reasons for implant failure, therefore there has been an increased focus on how TKRs are aligned during surgery to help to reduce malalignment and improve the longevity of implants [2].

Traditional methods of implant alignment involve positioning the components with the hip-knee-ankle (HKA) axis, which joins the centre of each of the three joints to create

a neutral axis of alignment. However, the majority of patients have a natural varus or valgus angle to their joint line and therefore, creating a neutral joint line in TKR surgery effects the kinematics and loading of the joint post-surgery [8]. As a result, new surgical techniques have been developed which aim to restore the pre-arthritic, natural coronal angle of the joint line [9, 10].

Variations of this joint line restoration technique to create patient specific alignments have shown early indications of better clinical outcomes compared to mechanical alignment [11-13]. However, the effects of these procedures on the kinematics, contact mechanics and wear of total knee replacements is poorly understood. To determine potential failure mechanisms and the efficacy of the procedure, this research project will contextualise the impact of patient specific alignment of a total knee replacement on wear rates, kinematics and contact mechanics through the combined use of computational and experimental simulations.

1.2 Anatomy and Physiology

The knee is a major joint in the body located in the legs where the distal end of the thigh bone (femur) and proximal end of the shin bone (tibia) meet. The knee is composed of a combination of structures including bone, ligaments, muscles, tendons, cartilage, synovial fluid and blood vessels (Figure 1-1). The bones form the three compartments of the knee, the medial and lateral tibiofemoral joint and the patellofemoral joint. The three bones are:

- Tibial condyle (proximal end of the tibia or shin bone)
- Medial and lateral femoral condyles (distal end of the femur or thigh bone)
- Patella (knee-cap).

The articulation of the bones permits ambulation of the leg and a combination of soft tissues provides the main source of stability in the joint to restrict the movement of the joint to a permitted range of motion. Two fibrocartilage structures, the menisci, provide stability in the knee by increasing the surface contact area and distributing loads between the two compartments [14]. Articular cartilage is a smooth tissue covering the ends of the bones and has been shown to reduce friction providing a smooth and lubricated surface during articulation [15]. The whole joint is surrounded by synovial fluid which is contained in bursas, these are situated within the articular capsule and lubricate the joint to also reduce friction [16].

The capsule ligaments are; the posterior cruciate ligament and the anterior cruciate ligament, located in the intercondylar area, to prevent the excessive backward and forward rolling of the tibia respectively, There is also the medial collateral ligament and lateral collateral ligament, located exteriorly of the joint capsule, which prevent excessive medial and lateral translation [16].

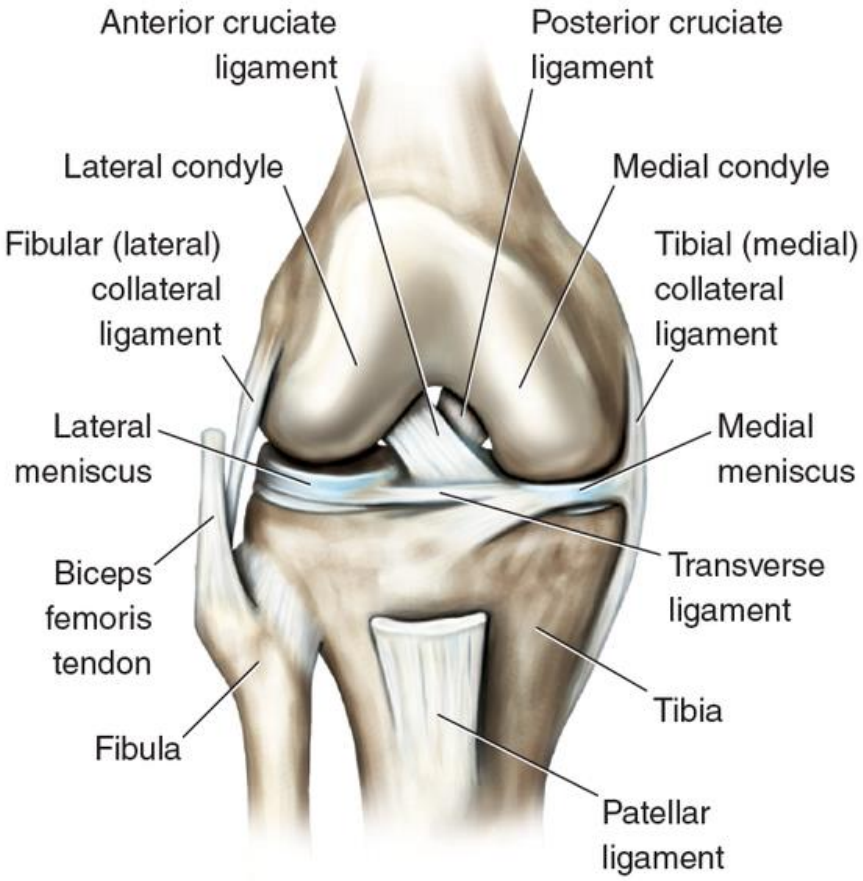

Figure 1-1: The anatomy of the knee [17]

1.2.1 Movement

The joint is responsible for the movement and positioning of the lower leg during locomotion tasks such as walking and running. The skeletal muscles of the knee control movement and provide strength to the knee by initiating a pulling action through muscle tensions to move the joint into the correct position. The muscles are supported by tendons which attach the muscles to the bones. The main muscles involved in the movement of the knee are the quadriceps muscle group, which are anterior to the femur and attached to the patellar by the quadriceps tendon and are

active in tibial extension, and the hamstring group posterior to the femur which control thigh extension and flexion [18].

1.2.2 Knee Kinetics and Kinematics

The study of biomechanics has enabled researchers to determine how the different joints of the body are loaded and how they articulate relative to each other and their surroundings during movement. Grood and Suntay (1983) determined that the knee has 6 degrees of freedom (DoF) (shown in Figure 1-2) which are [19]:

1) Translational (red arrows)
    - Anterior Posterior (AP)
    - Medial Lateral (ML)
    - Superior Inferior (SI)
2) Rotational (black arrows)
    - Flexion Extension
    - Abduction Adduction
    - Internal External

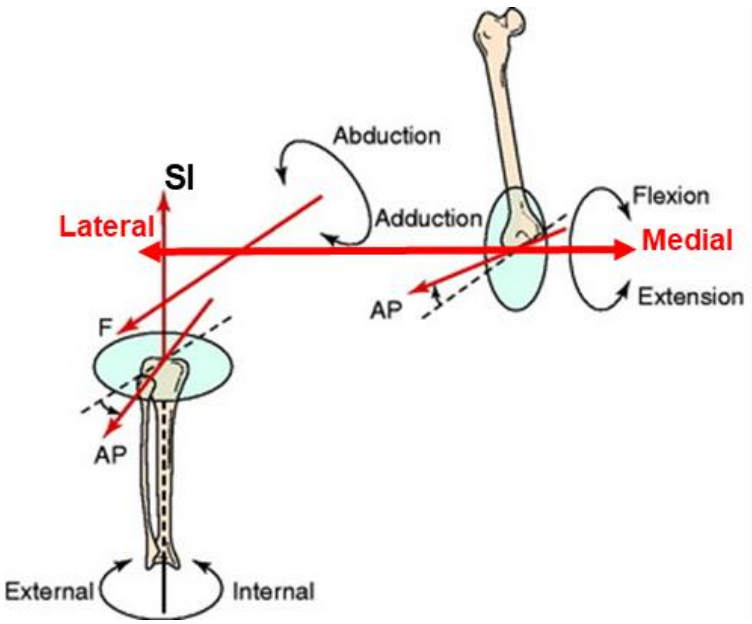

Figure 1-2: The three joint coordinate axes and the three rotational motions of the knee as established by Grood, E. S., & Suntay, W. J. (1983) adapted from Noyes, F. R., & Grood, E. S. (1987) published by Noyes, F. R. (2009) [19-21]

Flexion and extension of the knee, controlled by the hamstring muscles, is characterised by the rotation of the lower leg about the frontal axis (Figure 1-3). A study by Lafortune et al (1992) using inter-cortical traction pins to track the joint kinematics determined that the flexion range of motion (ROM) permitted in the knee during walking is typically -0.5° to +60° [22]. A study of the general population in the United States aged 25-74 (n=1683) recorded between 1971-1975 had an average maximum passive knee flexion angle of 132° which may be reached through activities such as squatting [23].

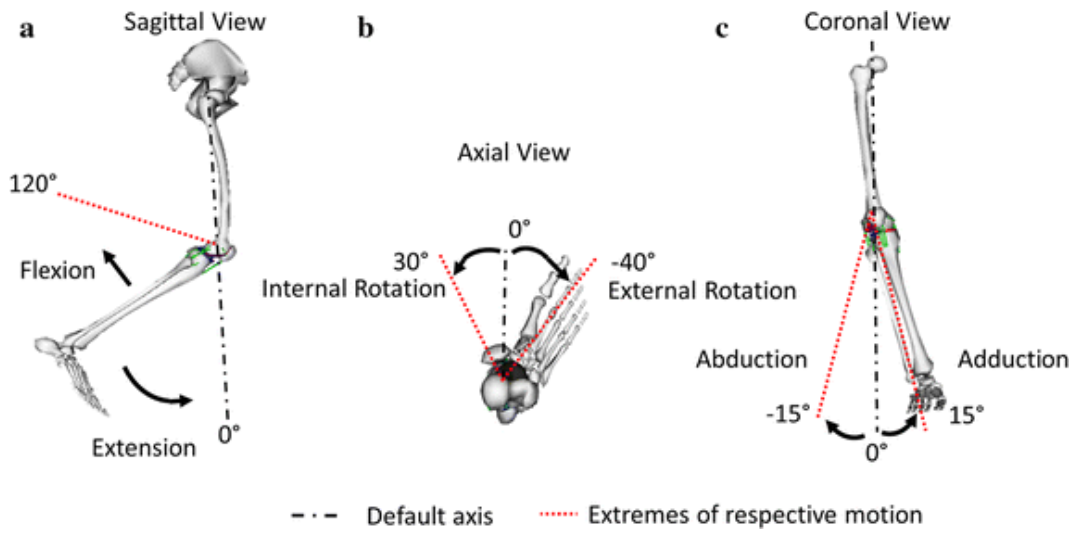

Figure 1-3: Axes of rotation of the knee: (a) Flexion-extension about the frontal axis; (b) Internal-external rotation about the longitudinal axis; (c) Abduction-adduction rotation about sagittal axis by Marieswaran et al. (2018) [24]

Unloaded cadaver knee and living knee studies by Iwaki et al. (2000) and Hill et al. (2000) using magnetic resonance imaging (MRI) determined that flexion of the knee involves a combined posterior translation and internal rotation of the femoral condyle, this is known as femoral rollback [25, 26]. Studies of living knees have tracked the medial and lateral femoral flexion facet centres which are the centre of the posterior circular surface of the femoral condyles, using MRI and found that the lateral condyle has a much larger posterior translation than the medial condyle, which causes an internal rotation of the joint with increased flexion (Figure 1-3b) [27, 28]. Hamai et al (2012) used X-rays of male participants' proximal tibial surface to track the movement of the centres of contact of the medial and lateral compartments during active flexion angles of 85° to 150°, these are illustrated in Figure 1-4 [29]. These images highlight the lateral posterior shift of the centre of contact (the black dots) with increasing angles of flexion.

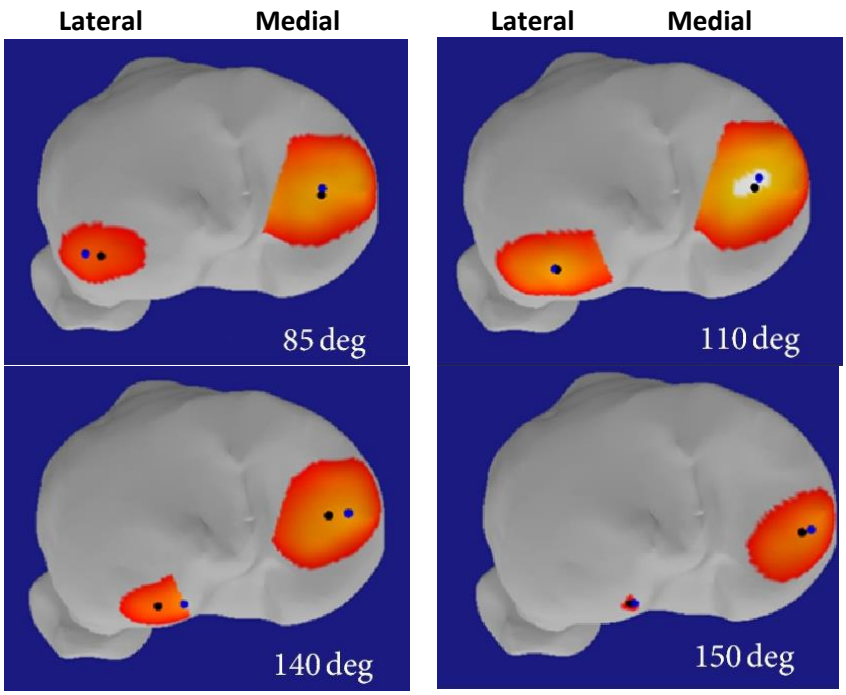

Figure 1-4: X-ray contact maps comparing the medial and lateral compartment surface contact of the tibiofemoral joint (left knee) during increasing angles of flexion. The black dots are the centre of contact. By S Hamai et al, (2012)[29]

The defined centre of rotation (CoR) of the transverse plane of the knee impacts the internal-external rotation because it determines the maximum degree about which the knee is able to rotate [30]. A medial offset of the CoR causes a large posterior translation of the lateral compartment during femoral rollback [31]. However, studies which have included ambulatory testing conditions have found the CoR was predominantly located on the lateral compartment of the knee during walking [32]. This suggests that active loading of the knee impacts the position of the CoR in the transverse plane.

Relatively small rotations of abduction and adduction are permitted about the sagittal axis (Figure 1-3c) of the knee. Abduction is the lateral rotation (valgus) of the knee opening the medial compartment, while adduction is the medial rotation (varus) opening the lateral compartment. This movement is allowed when the knee is flexed but limited during extension [9, 33, 34].

A study of ten cadaveric knees determined that at 0° flexion, abduction-adduction rotation in both directions is less than 1° but this value significantly increases when the knee is flexed to 45°-90° causing the varus angle to become 3.1°and valgus to become 1.4° (Table 1-1) [11, 34].

Table 1-1: Abduction-adduction and Internal-external angles of a native tibiofemoral joint at different degrees of flexion (Roth et al., 2015) [9, 34]

Flexion (°)	Adduction (°)	Abduction (°)	Internal (°)	External (°)
0	0.7	0.5	4.6	4.4
45-90	3.1	1.4	14.6	14.7

1.2.3 Knee Alignment

The natural alignment of the knee is determined by the vertical hip-knee-ankle axis (lines connecting the centre of each joint) and the transverse joint line, these are shown in Figure 1-5 [35].

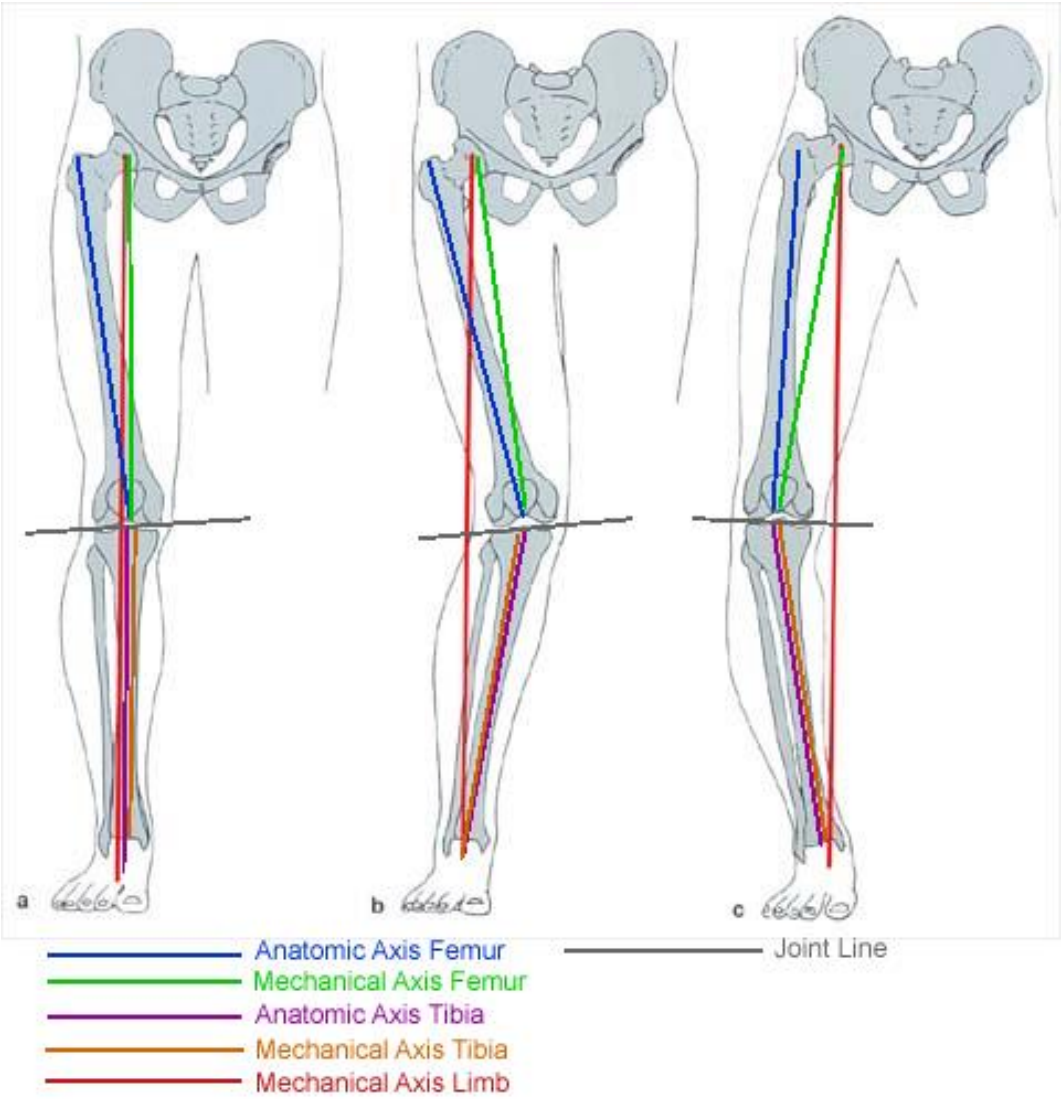

Figure 1-5: The axes and joint line of the knee in different positions a) neutral alignment b) valgus alignment c) varus alignment. By D.A. Dennis (2018) [35]

The joint line is a straight line representing the angle of the centre of the tibiofemoral joint and determines whether the knee is varus or valgus. Varus alignment is the internal rotation of the tibia in the coronal plane while valgus is the external rotation of the tibia in the coronal plane. Dossett et al. (2012) reported that only 2% of limbs have a neutral anatomical axis alignment, of the 98% without a neutral axis, 32% of men and 17% of women have a native anatomical axis of ≥3° varus rotation [8].

The stability of the knee joint is controlled by a combination of compressive loading forces from the muscles and loads transmitted through the soft tissue constraints. Tension in the ligaments varies depending on the position of the knee and is highest during extension and lowest during flexion. The amount of relaxation of the ligaments is referred to as the laxity. Collateral ligament laxity is a normal variable within the human knee and can be affected by variables such as sex, with women typically having more lax in their collateral ligaments [36]. A varus or valgus alignment of the knee may offset the loading of the knee. The dynamic distribution of load in the knee is determined biomechanically by calculating the external knee adduction moment in the frontal plane [37, 38]. Meireles et al. (2017) reported peak knee adduction moment in healthy individuals (using a weight-bearing functional axis of rotation model) to be 2.70 ± 1.17 at peak 1 and 1.59 ± 1.18 at peak 2 of the load plot, which is shown in Figure 1-6 [39].

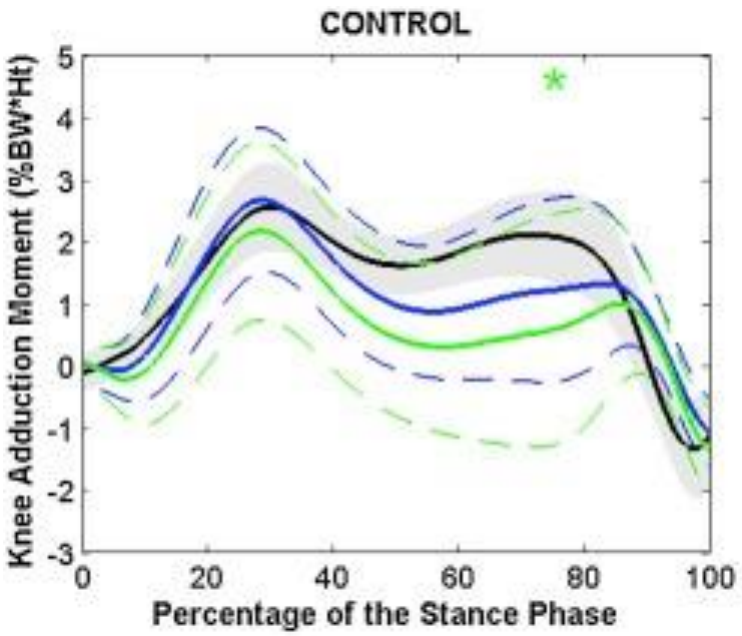

Figure 1-6: Knee adduction moment in healthy individuals calculated using different models by Meireles et al. (2017) [39]

The primary influence on transfemoral joints loads has been shown to be due to subject specific factors including the vertical hip load, femoral anterior-posterior force and tibial abduction-adduction torque [40]. These factors were closely correlated with the condylar contact area. Studies have also shown that an increase in knee adduction moment shifts the loading to the medial condyle; this increase in knee adduction moment is often seen in individuals with either a varus or valgus deformity and is commonly found in patients with OA [37, 41].

1.2.4 Osteoarthritis

OA is a chronic degenerative articular joint disease which is found to be associated with age, gender (in over 50-year olds), obesity, previous knee surgeries, and a history of sport-related joint injuries [42, 43]. OA is the most common form of arthritis and is prevalent in around 80% of the population over 65 in well-developed countries [5]. The global population is living longer and therefore there are more and more people world-wide suffering with OA, this number is predicted to reach 130 million by 2050 [4].

As OA progresses, the synovial fluid becomes gradually less effective at lubricating the joint and the worn cartilage becomes rougher. It is therefore often found that the coefficient of friction increases as OA progresses [44-46]. The matrix of the articular cartilage structure covering the ends of the bone becomes more permeable to water which reduces the modulus of elasticity [47]. This more rigid material cannot attenuate loading forces which does not protect the joint and can become extremely painful for the patient. An offset of loading in the knee to the medial compartment has been highlighted as a precursor for the development of OA [37, 39]. In a healthy knee, the usual offset is 60% to the medial side, but this is increased to 80-100% in those with OA [42]. Hall et al. (2017) found that there is a link between increased peak knee adduction moment (which reflects ML compartment joint loading distributions) and more severe OA symptoms, including pain levels measured by The Western Ontario and McMaster Universities Osteoarthritis Index (WOMAC) scores, developed at different levels of disease severity [37]. Additionally, Kumar et al. (2013) found an increased incidence of lateral compartment lift-off in patients with OA in addition to increased medial compartment loading caused by a greater knee adduction moment [48]. Therefore, knee adduction moment is often measured as a biomechanical marker for the progression of OA and the effectiveness of treatments, since reducing knee adduction moment reduces medial loading and slows the progressions of the disease [42, 49].

The initial stages of OA can be treated with Nonsteroidal anti-inflammatory drugs (NSAIDs) and other types of medication, however there is no cure and eventually the patient will require surgical interventions. Knee arthroplasties, which replace the diseased bone, were first developed in the 1970s and have since developed and improved into successful standardized treatment protocol for OA with good, long term clinical outcomes [50].

1.3 Total Knee Replacements

A TKR replaces an arthritic knee joint with an artificial substitute to restore structure and function of the joint. In 2021, 97% of primary TKRs (with or without cement) were completed due to joint degeneration caused by osteoarthritis with 68,974 primary procedures taking place in total [2]. This number has increased from just 46,557 primary TKR procedures in the UK in 2020, a marked decrease in procedures from previous years caused by the effect of procedure cancellations and delays due to Covid-19 [51].

Prior to Covid-19, the number of knee replacements was increasing yearly, largely accelerated by the increasing rate of obesity which is a major cause of knee joint degeneration [42]. In 2016 27.8% of TKR patients in the UK were obese (body mass index ≥ 35), this figure was just 18.6% in 2000 which highlights the rate of increase of this epidemic in the UK [52]. Additionally, younger patient demographics (under 60's) have been reported to have decreased satisfaction post-operatively [53, 54]. These younger and more active patient groups are more demanding on the function and durability of the joint replacement and have shown increased wear rates and increased rate of revision up to 35% in the under 50 age category [55]. Consequently, there is an increasing focus in orthopaedic research relating to the biomechanics and biotribology of implants, particularly those directly impacted by body mass index and activity levels. The after effects of Covid-19 on patient demographics are yet to be uncovered, however early reports from surgeons suggests an increase in complexity of the joint replacement cases they are seeing [2]. It is possible that the delays in treatment, caused by Covid-19, may have longer term impacts on TKR patient demographics.

A typical TKR is comprised of; a metal alloy (Cobalt-chrome) femoral component which replaces the femoral condyles of the native femur, a cobalt chrome tibial component which resurfaces the proximal end of the tibia, and an ultra-high-molecular-weight-polyethylene (UHMWPE) tibial insert on which the femoral component articulates (Figure 1-7).

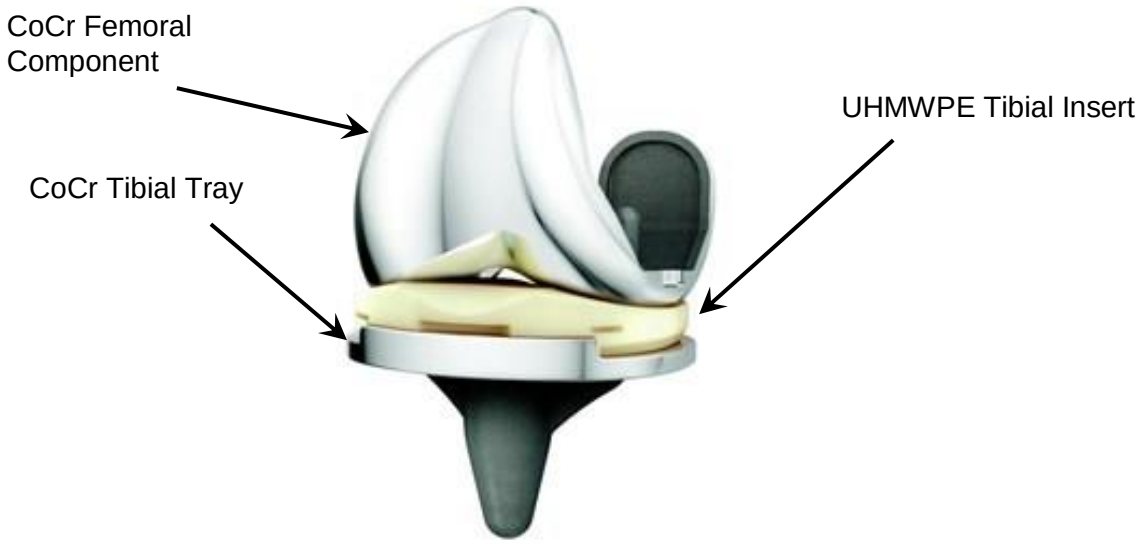

Figure 1-7: DePuy Synthes ATTUNE Primary fixed bearing cruciate retaining knee implant [56]

1.3.1 Tribology

Tribology is the study of the interaction of bearing surfaces which includes wear, friction and lubrication. Wear is the loss of material due to the interaction of motion at a surface which causes the release of particles. The biotribological performance of materials used in joint replacements is of particular interest since any wear particles produced by the interaction of the bearing surface is released into the surrounding tissues of the patient. Jin et al. (2006) highlighted 5 types of wear processes which occur within a joint replacement bearing including abrasive, adhesive, fatigue, erosive and corrosive [57]. The first three are caused by mechanical interactions within the bearing and can be minimised by developing the materials and design of the components.

Archard's wear law, based on sliding distance and load, was developed to calculate the surface wear of metallic materials. Overall, the theory states that wear rate is proportional to the applied load unless a change in the load causes the surface conditions to change. A coefficient of wear (K_1) was included in the wear formulation to account for changes in surface conditions effecting the wear rate. The wear law (Equation 1-1) formulated by Archard and Hirst (1956) is as follows, where W is the wear volume, P is the pressure, s is the sliding distance [58].

$$W = K_1 P s$$

Equation 1-1: Archard's Wear Law

Popular total knee replacements currently on the market have metallic cobalt chrome femoral and tibial tray components and have a polyethylene tibial insert component. The wear behaviour of a metal and polyethylene bearing requires further consideration for calculating volumetric surface wear. Visco-elastic polymers show wear rate dependent behaviour related to the contact area, cross-shear, surface roughness and cross-linking of the polyethylene component [59-62].

Friction is a force which opposes the direction of motion. When two surfaces articulate, friction is induced which can be reduced using appropriate lubrication, in the instance of joints this would be synovial fluid. The coefficient of friction (μ) is determined by dividing the friction by the normal force applied. The coefficient of friction of a natural human joint is around 0.01 [45, 63]. Coefficient of friction is material dependent and therefore cannot be presumed to be the same value for a total knee replacement bearing as for the natural knee structure. Literature has reported that a coefficient of friction of 0.04 is found for cobalt-chrome on polyethylene bearings [64].

1.3.2 Polyethylene Implant Materials

Wear debris released by polyethylene implant bearings into surrounding tissues can lead to osteolytic response of cells which is the loss of bone from resorption leading to aseptic loosening. Due to the severity of aseptic loosening, the current fourth leading cause for primary total knee replacement revisions, considerable research has been completed to reduce the volume of wear debris and the size of wear particles [2, 65]. Conventional polyethylene irradiated in gamma vacuum foil (GVF, DePuy Synthes, IN, USA) is a traditional material choice for total knee replacement bearing tibial insert material. Wear studies found that GUR 1020 material sterilised in GVF produced high proportions of wear particles, leading to the release of osteolytic cytokines, in comparison to moderately cross-linked GUR 1050 (5MRad) [65]. The material was also found to result in high wear rates when simulated under high kinematic profiles [62, 66].

Methods of sterilising the highly cross-linked polyethylene originally involved irradiation in air which was shown to result in delamination of the material due to the release of free radicals resulting in oxidative degeneration. Sterilisation methods in atmospheres without O_2 or new sterilisation methods were quickly adopted to remove this incidence of this fatigue wear mechanism [67].

As a result of the development of the material and sterilisation processes, polyethylene materials with increased cross-linking have become more popular

solutions for total knee replacement bearings. High levels of cross-linking of ultra-high molecular-weight polyethylene (UHMWPE) resins, including GUR1020 and GUR1050, have been shown to improve the wear resistance of the material in comparison to conventional polyethylene. However, high cross-linking has also been shown to decrease mechanical properties [60, 65].

1.3.3 UHMWPE and Cross Shear

UHMWPE is a polyethylene with very high molecular mass with high wear resistant properties. Its semi-crystalline structure allows it to have time-dependent responses to mechanical, chemical and thermal changes [68]. The amorphous part of the structure is anisotropic which means that under high tensile strains the polymer chains become oriented in the direction of stretching. This orientation of the polymer molecules changes the mechanical properties of the material making it more resistant to wear in the direction of alignment and less resistant in the perpendicular direction which is known as strain hardening [59, 69]. This process is detailed in Figure 1-8 where the polymer chains are initially randomly oriented but re-orient favourably in the principal molecular orientation direction resulting in strain hardening in that direction and strain softening in the perpendicular direction [70].

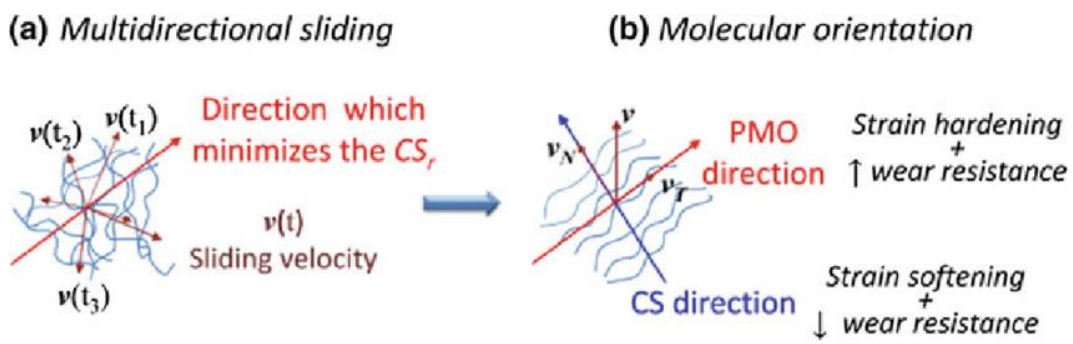

Figure 1-8: Schematic showing the influence of chain sliding on the principal molecular orientation (PMO) of UHMWPE [70]

Studies on the effect of cross shear in hip replacements on the surface wear have demonstrated that molecules of cross linked UHMWPE orient in the direction of sliding motion which results in increased resistance to wear due to strain hardening in this direction of molecular alignment [59]. Highly cross-linked polyethylene materials (10MRad) simulated on pin on plate studies have shown high resistance to wear [60]. However, there is typically a compromise of mechanical properties, such as fatigue strength, in highly cross-linked UHMWPE as a result of the additional heat

treatment process required to reduce the concentration of free radicals, hence there are concerns for using highly cross-linked UHMWPE for TKR inserts [62].

1.3.4 Moderately Cross-linked UHMWPE

Moderately cross-linked UHMWPE materials find a compromise between improving wear resistance through cross-linking without compromising the mechanical toughness of the material [60, 71]. XLK™ material (a 5MRad, moderately cross-linked UHMWPE material, DePuy Synthes, IN, USA) has shown high resistance to wear during simulations of walking [72, 73]. The lower cross shear experienced in the knee joint in comparison to the hip joint, have been studied on the XLK material and show that the high molecular weight resin GUR1020 with moderate cross-linking is subjected to enough cross shear for sufficient strain hardening in the principal molecular orientation to reduce wear rates [60].

1.3.5 AOX Polyethylene

In more recent years, the UHMWPE processing has been modified to reduce oxidative degeneration due to the release of free radicals, however most solutions have resulted in decreased mechanical properties as a consequence. One solution which has been shown to not hinder cross linking or reduce the mechanical properties of the material while being highly resistant to oxidative degradation is AOX™ Antioxidant-stabilized Polyethylene [74, 75], AOX is utilised in the ATTUNE™ Knee System tibial insert polyethylene material [56].

This AOX material is stabilised using the antioxidant COVERNOX™ (DePuy Synthes, IN, USA). COVERNOX is combined with a compression moulded, non-remelted polyethylene resin (GUR1020) which has optimised mechanical toughness and strength properties [76]. This combined material is irradiated to 8Mrads using gamma sterilization which initiates a free radical reaction where the free radicals in the resin bond with the antioxidant, stabilising the radicals and preventing oxidation. It also has increased fatigue crack propagation resistance compared to XLK material [77, 78]. The resultant material has optimised wear resistance characteristics, uncompromised mechanical properties and eliminates the need of an annealing process (which would compromise the mechanical properties) [79].

1.3.6 Total Knee Replacement Design

The design of TKRs can vary widely to suit factors such as disease progression, primary or revision surgery, the experience and preference of the operating surgeon, and whether the internal tissue structures of the knee are retained. It is important for

an implant to restore the kinematic movements and loading of the natural pre-arthritic joint.

The geometry of the implant components may be varied to control femoral rollback by the use of a post on the tibial insert and a cam on the femoral component wherein the post interacts (Figure 1-9), this is called a posterior-stabilised TKR. This posterior stabilised design alteration prevents the anterior translation of the femur with the tibia, restoring normal posterior translation (rollback motion) seen in the natural knee, in the absence of the posterior cruciate ligament to help improve the stability of the knee and restore natural kinematic movements [80].

Figure 1-9: ATTUNE Knee System implants including posterior stabilised (back) posterior cruciate ligament retaining (front) [81]

The conformity of the bearing is directly proportional to the contact area and therefore directly impacts the surface wear rates, reduced conformity gives reduced contact areas and reduced surface wear rates [82, 83]. Conformity is also inversely proportional to contact stress since reduced contact area increases contact stresses. However, there is a limit wherein the fatigue wear mechanisms will be activated if it is exceeded by too much reduction in conformity [82].

The Attune knee system includes a number of design optimisations. One of the key characteristics of the Attune femoral component design is the gradual change in sagittal curvature of the radius. This gradually reducing radius (Gradius™) facilitates the gradual attenuation of loads (Figure 1-10).

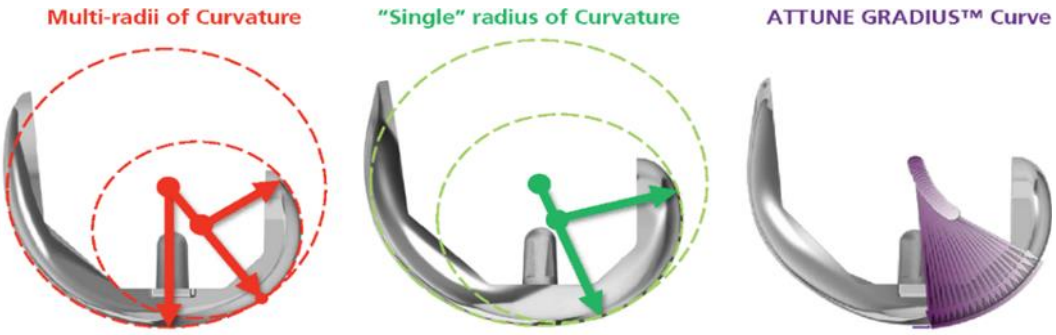

Figure 1-10: Gradually reducing ATTUNE knee system femoral radius (Gradius) design highlighted in purple compared to a dual-radius design (PFC Sigma) in red and the Stryker Triathlon singe flexion radius design in green. [84]

In-vivo fluoroscopic studies aimed at quantifying of the effect of these radius designs on the functional performance of the joint replacement have shown differences in the kinematic motions of cruciate retaining, fixed bearing designs during a range of flexion activities. The dual radius of the PFC Sigma® design is characterised by a sudden shift in anterior translation during mid-flexion (30°). This motion is not found in-vivo for the Attune Gradius design which instead showed femoral rollback of posterior translation of the lateral condyle [85]. This femoral rollback, found in healthy non-arthritic knees, highlights the optimised performance of the gradually reducing sagittal radius design of the Attune TKR bearing. Five-year in vivo outcomes comparing the clinical performance of thirty Attune and thirty PFC Sigma implants have shown no overall significant difference in patient satisfaction. However, patients implanted with the Attune bearing did show earlier recovery [86].

1.4 Primary Total Knee Replacement Surgical Procedure

Primary total knee replacement surgery is a common surgical procedure which accounts for 85% of all primary knee surgical procedures [2]. In an instrumented surgical procedure, bone cuts are measured and made using a combination of pre-operative planning from patient radiographs, and measurements made during the procedure with instrumentation usually provided by the manufacturer of the implant components. The resections of the femur and tibia set the alignment of the joint prosthesis joint line, hip-knee-ankle (HKA) axis and therefore the kinematic movements of the TKR.

1.4.1 Axes of Alignment, Joint Lines and Angles

Specific terminology is used in the surgical alignment procedure of a total knee replacement to identify angles and axes of the joint. These axes and angles define the alignment by orienting the joint in three planes: the coronal, sagittal and transverse planes. The coronal plane sets the varus or valgus angle, the sagittal plane sets the tibial slope and the transverse plane sets the rotational alignment of the femoral and tibial components.

When aligning total knee replacements in the patient, additional axes and angles must be taken into consideration. The joint line is determined using the frontal view of an extended knee by creating a tangent between the distal points of the medial and lateral compartments of the distal femoral condyle and proximal tibial surface (Figure 1-11).

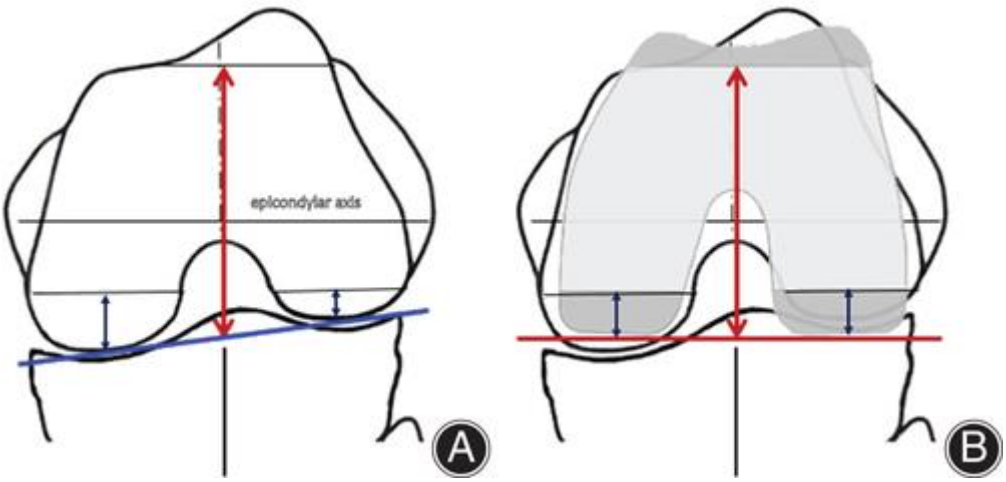

Figure 1-11: Coronal view of the knee A) native knee B) with total knee replacement showing how the joint line orientation can be altered post-operatively in angle and in height from the epicondylar axis [87]

Patients undergoing total knee replacement surgery due to arthritis usually have significant changes in their joint alignment in comparison to the pre-arthritic (constitutional) alignment of the joint [88]. The constitutional alignment of a patient, which is established once bones are fully formed after birth, can be established by measuring the angles between axes of the bone using a radiograph. The overall hip-knee-ankle angle may be established using the angles between the mechanical axes of the bone and the joint lines (Figure 1-12) using the following angles, [88]:

- LDFA - Lateral Distal Femoral Angle - lateral angle between femur mechanical axis and joint line of the distal femur.

- MPTA - Medial Proximal Tibia Angle - medial angle between tibial mechanical axis and joint line of the proximal tibia.
- mHKA – hip-knee-ankle angle defined as angle formed between mechanical axis of femur and tibia.

To restore the patients' pre-arthritic native anatomy in a patient specific alignment total knee replacement procedure, these joint angles and the overall hip-knee-ankle angle must be established.

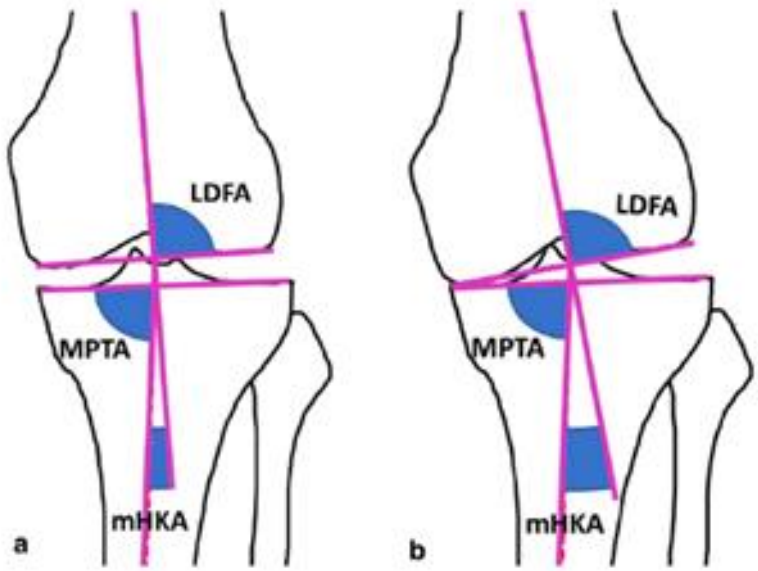

Figure 1-12: Defining angles between the axis of the lower limbs including 1. Lateral distal femoral angle (LDFA) 2. Medial proximal tibial angle (MPTA) 3. Mechanical hip-knee-ankle angle (mHKA) for a) mild constitutional varus knee b) degeneration of varus knee [89].

Studies have begun to develop an arithmetic hip-knee-ankle angle algorithm (aHKA) which is calculated by subtracting the LDFA from MPTA [89, 90]. However, due to the degeneration of the bone and surrounding structures during the progression of osteoarthritis, these measurements of the aHKA may not be possible in severe cases of osteoarthritis. When considering a patient specific alignment approach, it is important to restore the patients' native joint lines and therefore essential that the overall hip-knee-ankle angle is determined accurately.

1.4.2 Methods of Alignment

The definitions of the different alignment procedures can vary in literature, specifically when referencing whether the joint is completely resurfaced or whether there are limits applied to the surgical procedure cuts. Figure 1-13 depicts alignment

procedures commonly undertaken in primary total knee replacement surgeries, the alignments referenced are defined as follows [91]:

- Mechanical alignment – a systematic procedure creating a neutral joint line where the femoral component is set perpendicular to the femoral mechanical axis.
- Anatomic alignment (AA) – Creates a systematic oblique joint line of 2° to 3° varus to mechanical axis.
- Adjusted mechanical alignment (aMA) – typically applied in patients with large deformities with focus on balancing ligaments.
- Kinematic alignment (KA) – This may be a femur first or tibia first procedure. It aims to restore the native pre-arthritic joint line of the knee and balance the soft tissues. This is true resurfacing of the joint.
- Restricted kinematic alignment (rKA) – Applies a kinematic alignment procedure but within “safe boundaries” of 3° varus to 0° valgus.

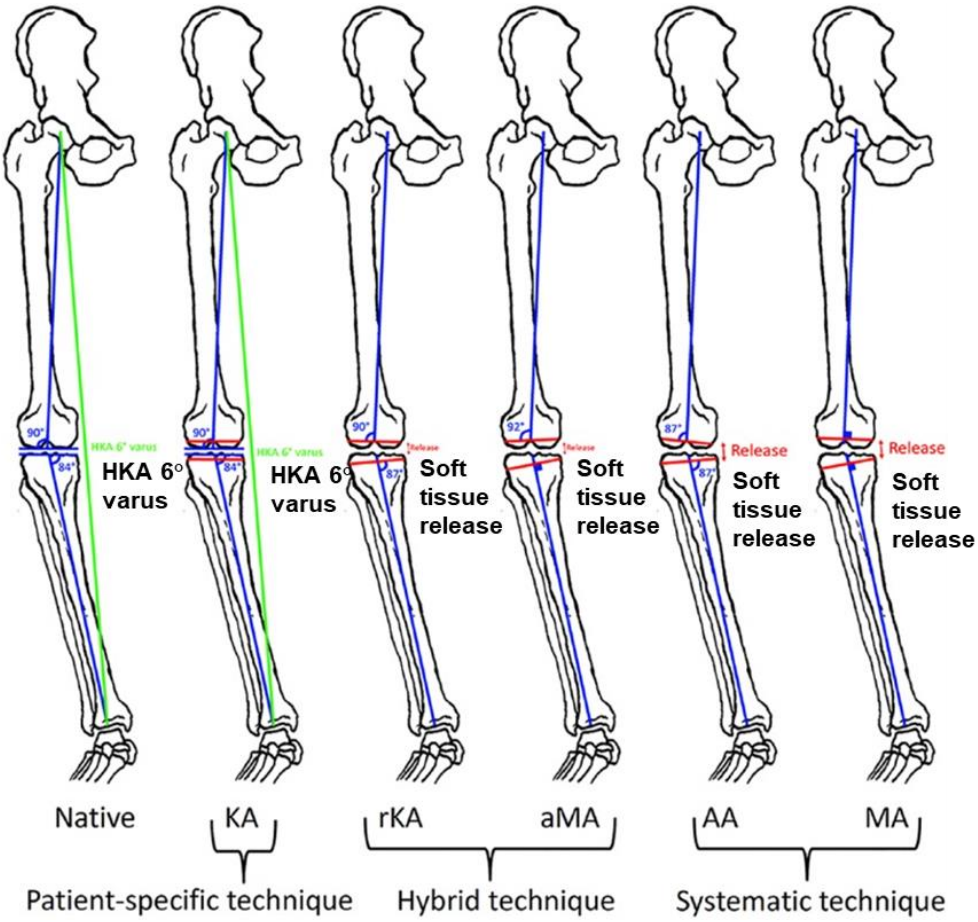

Figure 1-13: A comparison of the various TKR alignment procedures with reference to the different leg axes and joint lines, release refers to release of soft tissues [92], annotations are added in black.

A more in-depth look into the specific alignment values involved in these procedures is outlined in Table 1-2 which streamlines terminology and separates definitions of each surgical alignment procedure.

Table 1-2: Definitions of surgical alignment procedures of total knee replacements in references to axes and angles of the lower limb [93].

Alignment type	Mechanical	Anatomic	Patient specific alignment	
			Restricted Kinematic	Kinematic
Procedure	Neutral hip-knee-ankle alignment	Systematic 3° joint line	Restoring native alginment within boundaries. [94]	Native joint resurfacing [9]
Femoral Joint line	Perpendicular to femoral mechanical axis	Apply 3° valgus to angle between femoral joint line and femoral mechanical axis	Recreate a femoral joint line angle <99° to the femoral anatomic axis	Recreate femoral joint line angle
Tibial Joint line	Perpendicular to tibial axis	Apply 3° varus to tibia joint line angle	Recreate tibial joint line angle within 87°-90°	Restore tibial joint line angle
HKA axis	180°	Create a hip-knee-ankle angle of 177°	HKA = F + T – X Within limits 177°-180°	Restore hip-knee-ankle angle
Ligaments	Ligament release	Ligament release	May result in ligament release	No ligament release

1.4.3 Mechanical Alignment

Traditionally TKRs have been surgically positioned in mechanical alignment which created a neutral line of alignment with respect to the centres of the hip, knee and ankle, this was historically referred to as Maquet's line [95, 96]. The mechanical alignment surgical technique is able to balance the loading within the joint by reducing knee adduction moment by moving the loading to a central position [97, 98]. However, this technique takes no account of the natural position of the joint and, as highlighted previously, very few intact knees (2%) have a native neutral anatomical alignment [8].

1.4.3.1 Mechanical Alignment Resection Methods

There are two resection methods used by surgeons per their personal preference and evidence for the surgical outcome of each method. The first is a femur first approach which involves making femoral bone cuts first as follows [99]:

1. Cut the distal femur at 90° to the mechanical axis of the femur.
2. In flexion, make the anterior cut.
3. In flexion, make the posterior cut which can be determined from the transepicondylar axis (perpendicular to the anterior-posterior axis) or at around 3° of external rotation from the posterior condylar axis.
4. Resect the tibia to balance the joint in both extension and flexion.

The second method is a tibia first approach [99]:

1. Proximal cut of the tibia perpendicular to the tibial mechanical axis.
2. Distal cut of the femur perpendicular to the femur mechanical axis.
3. Knee moved into full extension to make extension cuts based on the bone anatomy.
4. Knee moved into flexion to make flexion cuts based on the soft tissue balance.

The second method allows independent cuts of anterior and posterior femur to balance the joint in both flexion and extension. Either flexion or extension balancing is usually compromised in the femur first approach since it is hard to account for both based on tibial cuts alone. Furthermore, mechanical alignment techniques using femur first frequently sacrifice the anterior cruciate ligaments which compromises the soft tissue balance of the knee. However, the method of femur first has more control over the alignment of the implant to the native anatomy. In mechanical alignment, the joint line orientation angle will have a valgus angle.

1.4.3.2 Mechanical Alignment Outcomes and Limitations

The mechanical alignment surgical technique often results in soft tissue release and is commonly associated with malalignment of the implant. A study of 18,065 knees, 405 of which underwent revision surgery, found that implant malalignment was the 6th most common TKA failure mechanism along with osteolysis/polyethylene wear, both resulting in 2.5% of the revision surgeries [100]. Implant malalignment may

include distal femoral malalignment, tibial malrotation and tibial malalignment (i.e. the offset from the mechanical axis). Andriacchi et al. (1986) showed that different alignment conditions of TKR components induces an offset of joint loading between the medial and lateral compartments of the knee. It was suggested that these variations in loading can cause issues leading to early failure of the implant [101].

Srivastava et al (2011) studied the effects of different degrees of tibial malpositioning on wear, component failure and ultimately TKR survival rates using retrieval implants. The study found that a varus tibial malalignment of above 3° resulted in double the wear rate due to shear forces at the tibiofemoral interface which altered the distribution of wear [102]. Andriacchi et al. (1993) demonstrated the influence of the joint line and varus and valgus alignment on the biomechanics of the knee post-operatively. This study found patellofemoral joint failures in implants where there had been changes in the joint line position, there was also femoral condylar lift off in implants where varus alignment was present [103].

Historically, mechanical alignment has been a favourable surgical procedure for creating a neutral mechanical axis and distributing the loading on the implant more evenly over the bearing surface to reduce wear rates and improve implant longevity. However, adjusting the patients' native alignment has resulted in poor functional outcomes and 15 year follow up outcomes show no improved implant survivorship in comparison to implants positioned in more anatomical alignments [104, 105]. These post-operative studies pose the question of whether adapting the patients' native anatomy to a corrected neutral alignment is more appropriate in comparison to creating joint alignments to restore native alignment.

1.4.4 Patient Specific Alignment

As technology has advanced and medical treatment aims towards providing patient specific solutions, new surgical techniques of alignment have been developed. Some alignment procedure methods are tailored towards the specific patients' anatomical axes. In the most basic terms, the knee joint can be split into 3 categories of alignment: neutral, varus and valgus. A study of 250 asymptomatic volunteers had a mean hip-knee-ankle angle value of 1.33° varus, with 32% of men and 17% of women having constitutional varus (above 3° varus) knee alignments (Figure 1-14) [88]. This study and other literature commonly agree that hip-knee-ankle angle of >183° is considered constitutional valgus while <177° is constitutional varus [88, 106, 107].

In patient specific alignment (PSA) procedures, the angles of the knee in the coronal plane are considered with respect to the anatomical axis of the femur and tibia. Figure

1-15 shows how the transfemoral axis angle, calculated as the angle between the femoral anatomical axis and tibial axis, is determined in addition to the femoral angle and tibial angle.

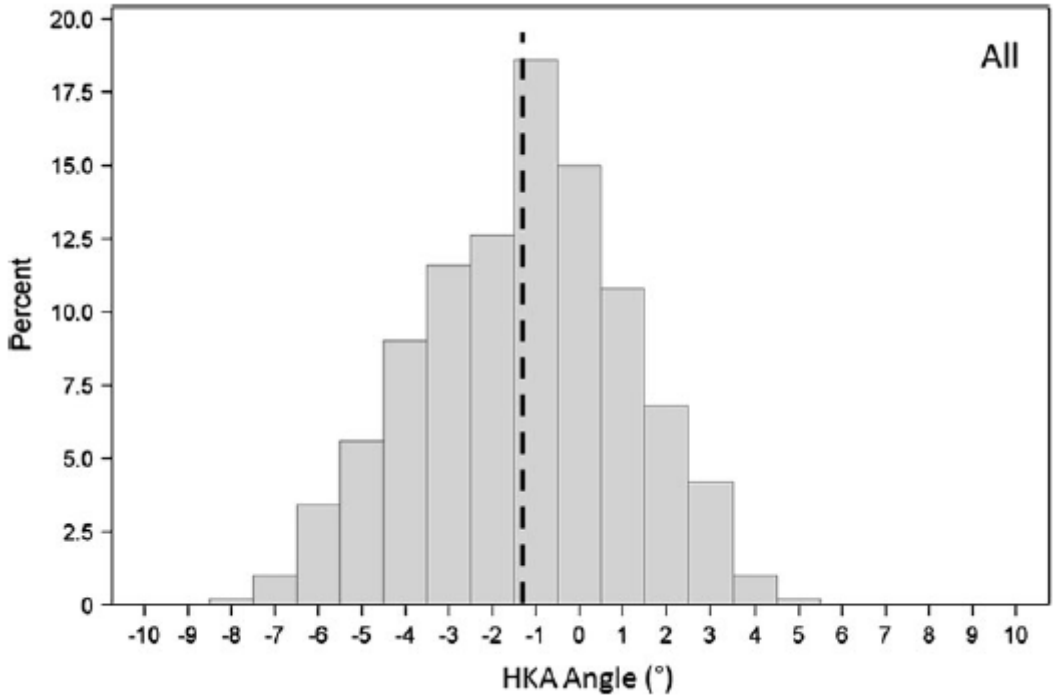

Figure 1-14: Histogram of the distribution of hip-knee-ankle angles within a population of 250 asymptomatic volunteers, with an average of 1.3° varus [88]

Figure 1-15: The angles of the knee in the coronal plane include; the transfemoral axis (TFA) angle of the knee; the femoral angle (α) between the bottom of the femoral condyles and the anatomical axis of the femur; the tibial angle (β) between the base of the tibial tray and the anatomical axis of the tibia [108]

1.4.4.1 True Kinematic Alignment

Early literature proposes that aligning the knee to match its pre-arthritic anatomical alignment position would be more appropriate than aligning the joint with the mechanical axis [8]. Broadly, this is referred to as kinematic alignment (KA) in literature although true kinematic alignment involves completely resurfacing the joint by replacing the exact amount of bone and cartilage removed [12].

One main advantage of true kinematic alignment techniques is that they do not require ligament release since the joint is balanced to the patients' native anatomy. In kinematic alignment the native anatomical axis is restored to the pre-arthritic joint alignment which does not adjust knee adduction moment, a possible precursor to OA [37]. The influence of not balancing knee adduction moment in kinematic alignment TKRs is still relatively unknown. However, Roth et al., (2018) showed that kinematic alignment restricts tibial forces between the lateral and medial compartments allowing a more even distribution of loading and a more natural posterior translation of tibial contact during passive flexion. This reportedly contributed to better restoration of the knee function compared to mechanical alignment outcomes [11]. Overall, studies comparing kinematic alignment and mechanical alignment clinical outcomes have found better restoration of function and kinematics and a reduction in pain in patients with kinematic alignment compared to mechanical alignment [10, 13, 109].

1.4.4.2 Restricted Kinematic Alignment (rKA)

Restricted kinematic alignment procedures have become increasingly popular over recent years to offer a hybrid between providing a patient specific solution while also being considerate of extreme anatomies. Studies have found that 3% of patients have an extreme varus or valgus anatomy (above 10°) [110] which therefore poses the question: is it safe to recreate these alignment angles with a TKR? Literature on these safe ranges is limited, especially with respect to the long-term effects. There is yet to be a conclusive agreement on what would be an acceptable value for restricted kinematic alignment, with some studies determining a HKA angle of 180°±3° to be the target [111]. This value would align with keeping reconstructed joint alignment within the values of what would be considered constitutional varus. However, using these safe ranges means that patients with extreme native alignments have their

post-operative HKA angle adjusted. Further studies will have to investigate whether current boundaries are appropriate for the longevity of the joint implants and how the boundaries affect the outlier patient populations.

One final consideration is whether current joint implant designs on the market are suitable for these patient specific alignment procedures. The majority of primary TKR's are developed to be placed in mechanical alignment. If the orthopaedic community wishes to continue to place components in patient specific alignments while minimising as far as possible any potential risk to the patient, there should be consideration into whether the current design of TKR's is appropriate.

1.5 Preclinical Wear Simulation

Pre-clinical simulation provides the means to investigate the function of a joint replacement under controlled experimental conditions. In-vitro and in-silico simulations can be developed to create environmental conditions and mechanical variables to replicate in-vivo conditions. The control of variables such as biomechanical inputs, lubrication conditions, component alignment and bearing material facilitates the investigation of the performance of a joint replacement in a standardised manner. The appropriate inputs to these simulations has been the topic of research throughout the years, with the aim being to ensure that joint replacements are as safe as possible for patients.

1.5.1 Total Knee Replacement Wear Under Standardised Conditions

International standards for the pre-clinical studies of total knee replacement are published to inform the inputs to these simulations. Currently, these standards provide inputs for an average patient of an average weight under normal walking gait. ISO 14243-1:2009 outlines the testing procedure for using an experimental simulator in force control, ISO 14243-2:2016 outlines the measurement methodology, and ISO 14243-3:2014 outlines the testing procedure for using an experimental simulator in displacement control [112-114]. The difference between the force control standard and displacement control standard is that the anterior-posterior and internal-external axes are controlled by forces and spring constraints in the former, and displacement motions in the latter. These standards were created to simulate the conditions of the average patient, of an average weight and under basic activity levels of walking gait cycles.

However, this is not representative of the vast variation seen in the patient population. Studies of the biomechanics of walking in younger, healthy subjects showed that in-

vivo kinematic levels are higher than these average kinematics [22, 66]. Pre-clinical wear studies using kinematic profiles more representative of more active patients reported evidence of abrasive wear on GVF polyethylene samples [115]. When the tibial rotation kinematic was completely removed from the wear simulation, which essentially removes multidirectional sliding, the wear rate decreased, which highlights the impact of cross-shear on wear rates of UHMWPE tibial inserts [116]. These studies show that the magnitude and direction of internal-external and anterior-posterior input affect the resultant wear mechanism and ultimately, the wear rate.

The femoral centre of rotation (CoR), the point about which all axes are centred and motions orientate about is specified in ISO 14243-1 as the average of the distal and posterior radii of the component. Brockett et al. (2016) demonstrated that the preclinical simulation of a PFC Sigma total knee replacement, using the distal radius as indicated on the device design, results in a significantly higher mean wear rate compared to the ISO defined CoR under high kinematic displacement control walking conditions [117]. The distal CoR position causes a posterior translation of the contact point during flexion which replicates femoral rollback as seen in vivo. A distal CoR results in a higher conformity of the bearing surface due to femoral rollback and therefore a greater cross shear ratio.

1.5.2 Load Control Wear Simulation

Experimental simulators can investigate pre-clinical wear and walking kinematics under a range of input conditions. ProSim electromechanical (EM) simulators (Figure 1-16) based in the iMBE laboratories at the University of Leeds are produced by Simulation Solutions, Stockport, UK. The simulators have six wear stations, each with five independently controlled axes of motion.

The capabilities of the simulator allow the tibial component to be controlled through input profiles according to ISO 14243-1:2009 force control kinematics and load profiles which apply motions to the femoral component and tibial component (Figure 1-17) [112]. The simulator is able to be run at a frequency of up to 2.0Hz and has the capability to simulate high kinematic input profiles up to 5kN load, anterior-posterior translation of ±25mm and internal-external rotation up to ±25° (Table 1-3).

Figure 1-16: ProSim 6-station electromechanical total knee simulator by Simulation Solutions, Stockport, UK

Table 1-3: ProSim 6-station electromechanical simulator capabilities

Parameter	Limit	Axis Control	Input profile
Axial force	5kN	Fully controlled	**Force**
Flexion-extension	±90°	Fully controlled	**Displacement**
Internal-external	±25°	Fully controlled	**Displacement and Force**
Abduction-adduction	±10°	Fully controlled or passive	**Displacement**
Anterior-posterior	±25mm	Fully controlled	**Displacement and Force**
Medial-lateral	±10mm	Pre-defined/fixed	**Not profile controlled**

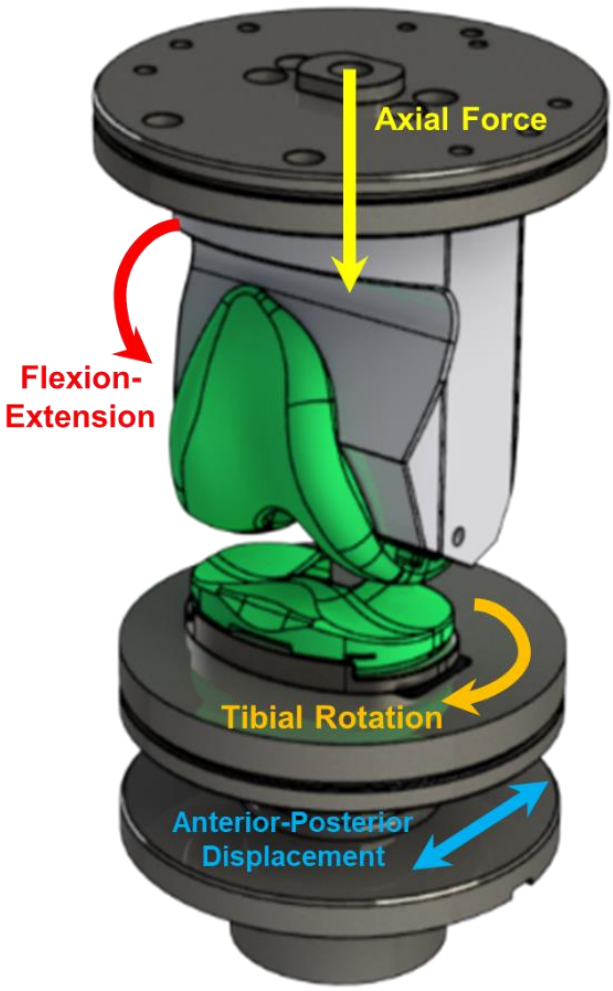

Figure 1-17: ProSim electromechanical knee simulator component setup with directions of applied motions including Axial force, flexion-extension, anterior-posterior displacement and internal-external tibial rotation.

Force control applies axial force (168-2600N), angular rotations including flexion (0°-58°), anterior-posterior force (-265-110N) and internal-external tibial rotation torque (-1-6Nm) profiles (Figure 1-18). In this method the simulator is able to control the movement of the joint using spring constraints to apply the restraining action of cruciate ligaments. Abduction-adduction is left as a passive motion to allow the tibial component to move freely, relative to the motion of the femoral component. The medial-lateral position of the tibial component is fixed at zero.

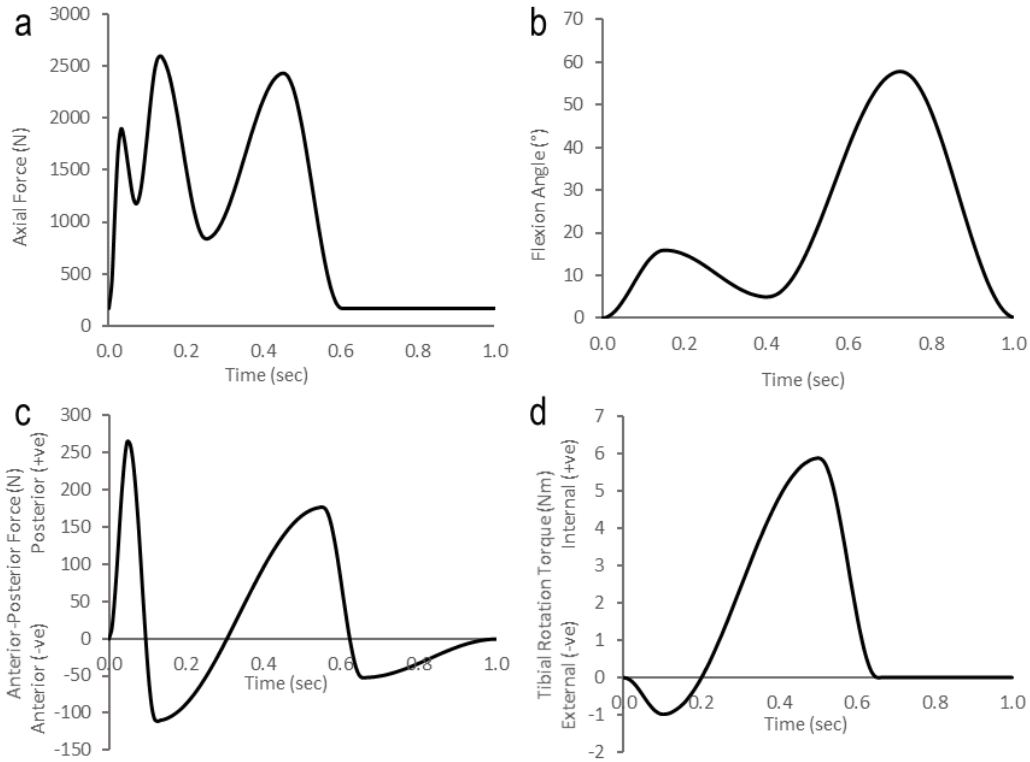

Figure 1-18: Gait profiles for standard walking under load control (ISO 14243-1:2009) including a) axial force, b) flexion-extension, c) anterior-posterior load, d) internal-external torque

Soft tissue tensions are crucial for the stability of the joint and are adjusted during surgery to balance the tensions in flexion and extension. Physical or virtual spring constraints are used to replicate the restraint mechanisms of soft tissue constraints in the natural knee [118]. For a cruciate retaining implant design, the force control standard ISO 14243-1:2009 specifies the spring stiffness values for constraint of anterior-posterior load and internal-external tibial torque [112]. The tibial spring stiffness is assigned a constant of proportionality of 0.36 ±0.02 Nm/°, and a “spring gap” of 0Nm/° between ±6°. The anterior-posterior spring stiffness is 44 ±2.2 N/mm in posterior motion, 9.3 N/mm in anterior motion and a spring gap of 0N/mm at ±2.5 mm (Figure 1-19).

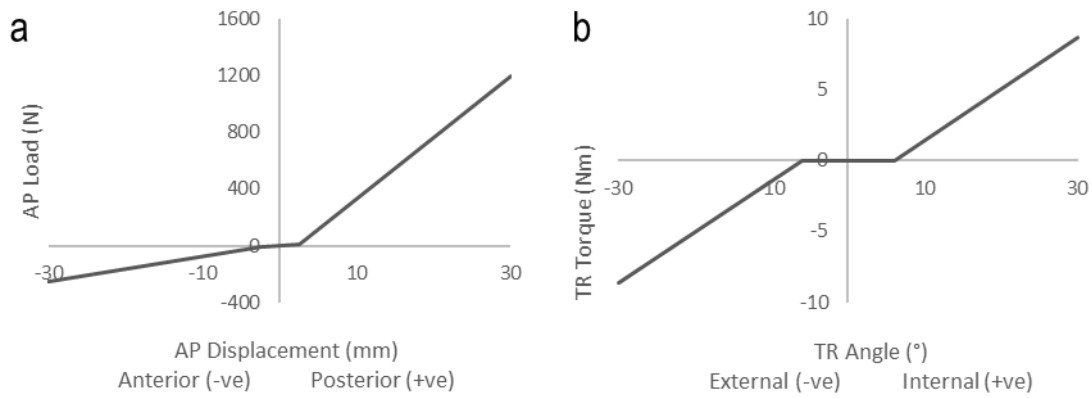

Figure 1-19: ISO 14243-1:2009 cruciate retaining TKR spring stiffness profiles for a) anterior-posterior load and b) internal-external torque

Overall, force control is sensitive to variables which directly affect the kinematics of the joint due to the motion of the tibial insert relative to the femoral component. Furthermore, the implant design should be considered when determining whether force control is the most appropriate control system for a pre-clinical simulation study. Highly conforming tibial inserts have been shown to restrict the full kinematic motions applied through load control simulations [73]. This study using a ProSim electromechanical knee simulator also demonstrated the effects of internal friction of the independently controlled simulator stations on the variability of kinematic outputs.

1.5.3 Experimental Wear of UHMWPE Total Knee Replacements

Over the last twenty years, wear simulations have evolved to more accurately simulate the conditions of in-vivo knee replacements in controlled laboratory environments. These studies have driven the developments in materials and design of total knee replacements, such as studies comparing the wear of GUR1020 GVF conventional polyethylene and moderately crosslinked XLK material on the dual-radius Sigma design. Displacement control simulations under high activity kinematics defined by [66], reported a significantly higher wear rate at 3 million cycles on GVF (9.2 ± 2.9 mm^3/Mc) in comparison to XLK (5.9 ± 2.1 mm^3/Mc) [71]. Subsequent studies on second generation electromechanical simulators under high kinematic displacement control conditions reported the wear rate of Sigma XLK at 3 million cycles as 5.8 ± 1.4 mm^3/Mc [119]. A 2 million cycle simulation study on the same second-generation wear simulator reported lower wear rates of 4.7 ± 1.3 mm^3/Mc for Sigma XLK under ISO 14243-1:2009 force control [73].

More recent wear simulation studies have reported 50% lower wear rates after 5 million cycles under displacement control kinematics in Attune AOX (3.6mg/Mc) in

comparison to Sigma XLK (7.2mg/Mc) [120]. This study, completed on an AMTI wear simulator (Watertown, MA), demonstrated how a combination of differences in tibial insert material and femoral component curvature geometries impact wear rates (Figure 1-20).

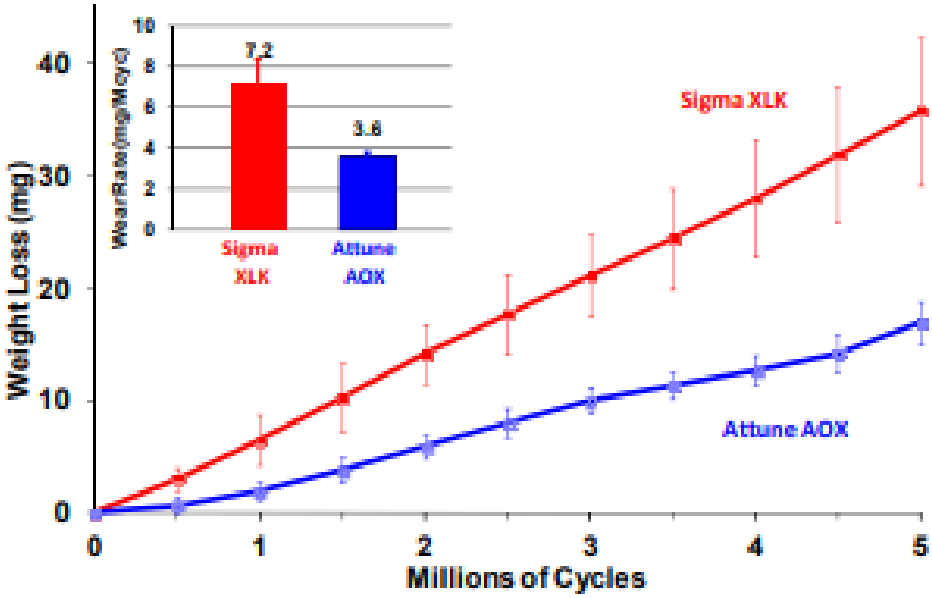

Figure 1. Wear for Sigma XLK and Attune AOX knee systems. Inset shows wear rate. Error bars represent ±1 standard deviation.

Figure 1-20: The wear performance of Sigma XLK and Attune AOX TKR bearings over 5 million cycles. Presented by Dressler et al. at ORS 2012 [120].

The lower wear rates of Attune AOX, also reported under force control conditions after 3 million cycles of wear on an AMTI wear simulator (Watertown, MA) of 3.5±0.5mg/Mc [121], indicates improved implant longevity in comparison to alternative moderately cross-linked material solutions.

However, the wear rate of Attune AOX total knee replacements on second-generation ProSim simulators is not yet established and therefore direct comparison of wear rates of this bearing design to 5MRad Sigma XLK on the same simulator, under the same wear conditions is unknown. The variability in wear rates shown between individual stations within a wear simulator [73], partly due to mechanical characteristics such as internal friction, demonstrates why comparison of wear rates under the same conditions on the same wear simulators is essential to draw a true comparison in the wear performance of different wear bearing designs.

1.6 Computational Simulation Methods Using Finite Element Analysis

Computational modelling environments offer methods of in-silico pre-clinical simulation of joint replacements using finite element (FE) analysis. This resource reduces both time and the cost in comparison to using experimental methods, however computational simulations must be validated with experimental data. One favourable type of computational modelling is finite element analysis which can be used to apply forces and displacements to a model and determine the corresponding stresses, strains and displacements to the specific input conditions. Finite element analysis involves the formulation and solving of partial differential equations of complex geometries by dividing the shape or “body” into finite elements and nodes and formulates a solution which is known as a mesh. The approximation can be made more accurate through decreasing the global element size, however this vastly increases the computation time [122]. FE models are more frequently being applied to investigate the interactions of surfaces with the body in the medical industry. This includes the interaction of implant bearing surfaces such as TKRs. These FE model outputs can then be used in computational wear predictions to determine other variables such as wear and friction. Although it is necessary to validate models of this kind, by comparing the results to experimental results, they can be used to study a range of different clinical conditions, component designs and material changes.

Studies of total knee replacement bearings using computational models to simulate joint kinematics found that changes in a coefficient of friction affected the anterior-posterior translations of TKRs when investigated using finite element analysis. Models were simulated using friction values of 0.01, 0.04 and 0.07 and output kinematics were compared with experimental kinematics to determine the correct coefficient of friction. A friction coefficient of 0.04 estimated anterior-posterior translation parameters in closest agreement with experimental data [64].

1.6.1 Wear Laws

Archard’s wear law established a computational method to calculate wear volume (W). This wear law, derived from studies on metallic materials, does not account for the elastic-plastic behaviour of polyethylene materials used in joint replacements. Determining the wear of polyethylene materials must account for the effect of cross shear on the wear rate formulation. In elastic-plastic materials such as UHMWPE, the molecules orient in the direction of sliding motion which results in increased resistance to wear due to strain hardening in this direction of molecular alignment.

The transverse direction is left weakened and susceptible to accelerated wear mechanisms resulting in increased wear particles. To produce computational models capable of accurately predicting the wear rate of joint replacement bearings, it is crucial that cross shear is accounted for. Adaptions to Archard's wear law have been developed and optimised to account for the effects of cross-shear and creep on wear rates of polyethylene materials [59, 123]. However, these models which calculate a wear factor are all contact pressure-dependent.

One series of studies incorporated sliding distance into the computational wear formulation, independent of pressure, using a pin on plate rig and total hip replacement wear simulators. The studies found that as surface area reduced or contact pressure increased, the cross-shear ratio reduced causing the surface wear of the material to reduce [83, 124, 125].

Further work by Kang et al., 2008 [126] investigated the cross shear of highly cross-linked UHMWPE (10MRad GUR1050) and non-cross-linked polyethylene under compressive loads on a pin on plate rig with ±55° rotation. The study defined principal molecular orientation as the average direction of the sliding direction on the plate. The direction perpendicular to the principal molecular orientation was determined as the direction of strain softening. Frictional work in the direction perpendicular to the principal molecular orientation ($W_{cross\text{-}shear}$) was divided by the total work (W_{total}) to calculate the cross shear (Equation 1-2) [126].

$$Cross - shear = \frac{W_{cross-shear}}{W_{total}}$$

Equation 1-2: Cross Shear calculation by Kang et al., 2008 [126]

Research has since aimed to evolve the computational wear models, to calculate a wear coefficient independent of pressure, optimised for total knee replacements. One study developed a total wear damage formulation (δ_{total}) as the sum of compressive creep (δ_{creep}) and linear wear depth (δ_{wear}). Linear wear depth was calculated from multiplying the wear coefficient, derived from pin on plate studies, by sliding distance [61]. To investigate the efficacy of this new wear law, a finite element model of a Sigma TKR design was simulated under standard walking conditions to predict sliding distance and contact pressure [61]. The new wear law predicted wear rates in agreement with experimental wear data demonstrating the efficacy of this new non-dimensional wear coefficient model for predicting wear of total knee replacements. The study also demonstrated how wear factors were dependent on applied contact

pressure making the predictions inaccurate as wear progresses and contact areas change on the worn bearing surface.

Finally, Abdelgaied et al. (2018) expanded on these findings to develop a fully independent computational framework for TKR pre-clinical wear validated by experimental methods simulated under standard walking conditions using displacement control inputs. An equation for the wear coefficient (C) was developed and is shown in Equation 1-3 where CS is cross-shear, P/E is a non-dimensional contact stress, W is the wear volume, A is the contact area and S is the sliding distance.

$$C\left(fun\left(CS,\frac{P}{E}\right)\right) = \frac{W}{AxS}$$

Equation 1-3: Wear coefficient equation by Abdelgaied et al. (2018)

The study aimed to measure more accurate, material specific mechanical properties, under compressive loading conditions and reported an elastic modulus of 553±51MPa and Poisson's ratio of 0.32±0.08 for XLK polyethylene.

1.6.2 Computational Wear of Total Knee Replacements

A number of studies have demonstrated how finite element models can be used for the pre-clinical simulation of total knee replacements to predict kinematics, contact mechanics and wear rates. Among these studies are simulations of different total knee replacement designs, materials and kinematic activity inputs. One study successfully developed a finite element model of a Sigma XLK (GUR 1020, 5MRad) replicating a ProSim joint simulator setup with independently experimentally determined material properties [119]. This study, which simulated displacement control standard walking conditions, calculated a wear rate of 4.5mm^3/Mc, comparable to the wear rate of an experimental simulation completed under the same input conditions of 5.8 mm^3/Mc.

Other wear simulation finite element models have been developed to replicate AMTI wear simulators, with all six degrees of freedom of the total knee replacement motion fully controlled through input gait cycles [127]. In this study, two total knee replacement designs were simulated (PFC Sigma and Attune), under load driven inputs derived from literature [128]. Both the femoral component and tibial insert were modelled as rigid body in this instance, not accounting for the elastic-plastic behaviour of the polyethylene insert but with increased computational efficiency. The

kinematic outputs of this model were validated against experimental values determined using an AMTI joint simulator.

Computational models of total knee replacements have successfully predicted wear rates of dual radii PFC Sigma design with XLK material properties and the kinematic outputs under load control walking simulation of the Gradius Attune design. However, further work is required to develop finite element models of the Gradius Attune design with AOX material properties to predict kinematics and contact mechanics to computationally predict wear rates.

1.7 Influence of Surgical Alignment on Wear

The surgical alignment method of total knee replacements is of high interest with a focus on how variations of patient specific alignment impact the function and longevity of the implant post-operatively. Patient specific alignment procedures result in a large range of total knee replacement setups with an increased complexity of variables dependent on the individual case [93]. There are still unknowns about the impact of patient specific alignment on the load distribution in the total knee replacement.

Adaptions of traditional mechanical alignment experimental simulations have been used to understand the impact of coronal alignments on kinematic motions and wear. An experimental study of Sigma XLK tibial and femoral components oriented to 4° varus alignment reported similar anterior-posterior translation, internal-external tibial rotation and abduction-adduction rotation kinematic outputs in comparison to mechanical alignment under the same load control kinematic input conditions [129]. This was also reported by a similar study which found no significant difference in output kinematics for Attune AOX between mechanical alignment, a 4° varus ‘malalignment’ without load axis adaptions, and a 4° patient specific alignment with adapted loading axes [121]. The study showed no significant difference between wear rates for mechanical alignment (3.8 ± 0.5 mg/Mc) and 4° patient specific alignment (4.1 ± 0.2 mg/Mc) under ISO 14243-1 load control input conditions. These two studies were completed on different joint simulators, ProSim electromechanical for the former and AMTI for the latter. A combined experimental and computational simulation study was also reported to have no significant difference in kinematics or wear rate between mechanical alignment and 5° varus patient specific alignment for Attune AOX when simulated on an AMTI joint simulator [130]. In this simulation, a lower limb model [131] was used to create more representative inputs of loads and kinematics during walking with a patient specific aligned total knee replacement.

Other pre-clinical simulation studies have begun to utilise the versatility and speed of computational models to investigate these patient specific alignment variables. Simulation models have been adapted from a previously validated mechanically aligned musculoskeletal model (KneeSIM, LifeModeler, San Clemente, California) [132], to simulate patient specific alignment conditions.

One study created two alignment models including 3° tibial varus with 3° femoral valgus and 5° tibial varus with 5° femoral valgus [133]. A high compressive load 4kN (5 times body weight) was applied to this model at a range of flexion angles between 0° and 120°. These patient specific alignment models produced higher patellofemoral and tibiofemoral contact stresses and resulted in greater femoral rollback and more external rotation, more closely aligned with normal knee kinematics than is seen in mechanically alignment. However, the study did not simulate other kinematics of knee motion during normal daily activities, such as anterior-posterior translations or internal-external tibial rotations.

Another study simulated ISO 14243-1 load control motions using the same validated KneeSIM musculoskeletal model, adapted into patient specific alignment with 3° tibial varus and 3° femoral valgus [134]. The study reported no significant difference in output kinematic motions and loads between this setup and mechanical alignment, concluding that the alignments were not functionally different. Furthermore, the study reported lateral compartment lift-off in the 3° alignment setup which has previously been reported of resulting in increased wear damage on the medial compartment [135]. Although the original musculoskeletal model was validated using clinical retrieval wear scars and wear simulator studies prior to being applied to this study, the results from these patient specific alignment models should be compared to clinical data or pre-clinical experimental data to validate the accuracy of the model in an alternate alignment.

Studies have shown that patient specific alignment setups within restricted kinematic alignment boundaries do not result in significantly different kinematic outcomes. However, they do indicate more pronounced loading offset, in comparison to mechanical alignment, and even lateral compartment lift off in some instances. Since an offset in compartment loading may affect the resulting contact mechanics of the bearing, it is important to research these variables using pre-clinical testing procedures to verify whether or not there is a significant impact on wear rates.

1.8 Aim and Objectives

1.8.1 Summary of Literature Review

Pre-clinical evaluation methods of total knee replacements have traditionally involved experimental simulation to determine the biomechanical and tribological performance of the bearing [6, 62]. Knee replacement design [84], materials [79] and surgical procedure [91] have developed over the years to meet the requirements of patients and to ensure that the implant lasts as long as possible before it requires a highly invasive surgical procedure, known as revision surgery, to replace it. However, these developments to improve implant longevity require studies, known as pre-clinical testing, to assure that the performance of the implant meets certain standards before they are approved to be used clinically. These pre-clinical studies investigate the tribology of the implants for example, which is the science of wear, friction and lubrication, over a long period of time. They have been predominantly experimental based using joint wear simulators which are able to replicate internal conditions of the knee during daily activities in a standardised and controlled environment [136].

Surgical alignment of total knee replacements is a known factor in the success of joint replacements. Surgical errors such as malalignment, where the knee replacement components are implanted at an incorrect angle, can lead to serious complications ending in implant failure which requires revision surgery. The most traditional method of knee replacement alignment is known as mechanical alignment where a 180° angle is created between the lines connecting the hip to the knee and the knee to the ankle (hip-knee-ankle angle). However, research has shown that roughly only 2% of the patient population have a 180° (straight leg) alignment [8]. In more recent years, procedures to recreate each individual patient's native hip-knee-ankle angle have become increasingly popular among surgeons in accordance with the increase in popularity of patient specific treatments. Patient specific alignment surgeries aim to recreate the patient's native pre-arthritic joint angles or adapt them as much as possible to within specific "safe boundaries" [111]. Early studies into the efficacy of these modified procedures on patient satisfaction and implant functionality are widely reported as improved [93]. Despite this, the long-term effects of these relatively new surgical procedure modifications on the longevity of the implants are mostly unknown.

Pre-clinical studies offer a method of evaluation of the effect of patient specific alignment on the tribology of total knee replacements over the implant lifespan. However, current methods of preclinical assessment are resource and time intensive.

Relatively recent developments in computational modelling provides an opportunity to utilise finite element models as a fast and low-cost tool to aid in pre-clinical assessment. Computational models of joint replacements offer a promising outlook in their contribution to research and development through being able to produce results quickly and also by their advantage of not being bound by the same physical restrictions of a joint simulator which are manufactured with control limits and safety precautions built into the software.

The drive of surgical procedures towards patient-specific treatment requires the use of these models to simulate more complex conditions, however, challenges still remain around the computational expense of building reliable and efficient models.

The aim of this research was to use a combined experimental and computational approach to investigate the influence of patient specific alignment under ISO 14243-1:2009 walking conditions on kinematics, contact mechanics and wear of a DePuy Synthes Attune AOX Total Knee Replacement.

1.8.2 Objectives

- Experimentally investigate kinematics and wear of Attune AOX total knee replacement bearings under ISO 14243-1:2009 standard walking gait load control conditions. This data will be used to validate computational simulation methods and establish wear in conventional mechanical alignment conditions.
- Develop repeatable experimental methodologies using pressure sensors to investigate the effect of load and kinematics on the contact mechanics of TKR bearings at intervals of a gait cycle.
- Develop a computational model of the Attune AOX TKR bearing and simulate one ISO 14243-1:2009 gait cycle to assess standard walking kinematics to predict kinematics and contact mechanics.
- Create a patient specific alignment package and necessary inputs to investigate the kinematics, contact mechanics and wear on an experimental simulator under ISO 14243-1:2009 conditions.
- Adapt mechanical alignment finite element setup to patient specific alignment to investigate the efficacy of the model to predict kinematics and contact mechanics outputs at an alternate alignment under ISO 14243-1:2009 conditions and compare to experimental results.

- Explore the potential of the finite element model to investigate various surgical alignment parameters an the individual and combined effect on kinematics.
- Computationally determine the wear under patient specific alignment setup of Attune AOX and compare with standard alignment conditions and experimental wear data.

Chapter 2
Experimental Simulation Methods

2.1 Introduction

Experimental simulation is a well-established method of investigating the wear of joint replacement bearings under standard input conditions. The inputs to these simulations have developed over time to account for changes in technology, research into standard walking gait and the development of prostheses and materials. There are currently three International Organization for Standardization (ISO) published standards for the wear of total knee replacements [112-114].

These standards help to inform the methods to complete wear simulations of total knee replacements, however the exact methodology is dependent on the design of the bearing and the scope of the study. For studies where the effect of input parameters on the output kinematics are of interest, force control is the most appropriate simulation control method to use. Since load control also uses spring constraints to constrain motions of the total knee replacement, replicating the action of soft tissue constraints, the output kinematics are susceptible to changes in the simulation setups and component design.

Previous studies, using load control simulation methods, have shown that spring constraint stiffness and spring gaps significantly affect output kinematics [73]. The methods developed in this study will be applied in future chapters to investigate the effect of total knee replacement alignment on kinematics and wear. Therefore, load control was chosen as the simulator control method for these studies.

This chapter outlines how methods were developed to implement ISO 14243-1:2009 load control [112], total knee replacement experimental wear simulation conditions on a DePuy Synthes Attune AOX bearing. The aim of the study was to determine the kinematic outputs and a baseline wear rate of the bearing design under ISO 14243-1:2009 standard walking gait. Two studies were completed in this Chapter which include:

Study 1 - A preliminary study using a Sigma XLK TKR bearing to determine output kinematics and measure wear rates. The objective of this study was to compare the results to published data completed under the same simulation methodology to establish the validity of the test methods.

Study 2 – An Attune AOX wear study where the objective was to adapt the preliminary study methods to be applicable to the alternate bearing and to determine output kinematics and measure wear rates.

2.2 Materials

The wear simulations were completed on University of Leeds 6-station electromechanical (EM) ProSim (Simulation Solutions, Manchester, UK) total joint simulators (Figure 1-12). The knee wear simulator had 6 independently controlled stations with up to five degrees of freedom on each station. The simulator was capable of running either displacement control or load control input requirements and recording kinematics outputs as displacements and loads for all required degrees of freedom. The wear bearings were lubricated with 25% (v/v) new-born calf serum/0.04% (w/v) sodium azide solution created in accordance with protocols and health and safety requirements. Each capsule contained 450ml of 25% bovine serum which was replaced with freshly made solution every 300,000 cycles.

2.2.1 Study 1: Sigma XLK Components

Sigma (DePuy Synthes, Leeds, UK) bearings were used as wear samples in Study 1. The UHMWPE tibial insert material was moderately crosslinked XLK (DePuy Synthes, Leeds, UK) 5MRad gamma irradiated, re-melted and compression moulded GUR1020. The study was completed using six stations for loaded wear (femoral component, tibial tray and tibial insert), and two tibial insert samples used as unloaded soak control samples. All samples were right knee, mid-size components and had already been used on previous wear studies. The design and size of each bearing component was as follows:

- 6 x Sigma CoCr femoral components (Size 3), cruciate retaining
- 8 x Sigma XLK tibial inserts (Size 3), cruciate retaining, fixed bearing, 10mm thickness
- 6 x Sigma CoCr tibial trays (Size 3), fixed bearing

2.2.2 Study 2: Attune AOX Components

The samples used for Study 2 were right knee Attune (DePuy Synthes, Leeds, UK) total knee replacement components. The UHMWPE tibial insert material was AOX (DePuy Synthes, Leeds, UK) 8MRad, with COVERNOX (DePuy Synthes, Leeds, UK)

antioxidant, compression moulded without re-melting, GUR1020. Six mid-size bearings were used as wear samples which included Attune femoral component, Attune tibial tray and Attune AOX tibial inserts (Table 2-1). Size 5 Attune components are equivalent in size to Sigma Size 3 components. Component identifiers were assigned to each component to allow tractability of the sample throughout this study and future studies. Further information on the components including the lot number and a summary of studies each sample was used on is displayed in Appendix A.

Table 2-1: Attune sample descriptions, part reference and images for the tibial insert, tibial tray and femoral component

Component description	8x Attune AOX tibial inserts (Size 5), cruciate retaining, fixed bearing 6mm thickness	6x Attune CoCr femoral components (Size 5) cruciate retaining	6x Attune CoCr tibial trays (Size 5), fixed bearing
Part Reference	1516-20-506	1504-00-205	1506-00-005
Component image			

Each component was assigned to a sample pairing for the total knee replacement bearing, and each sample pairing was assigned a fixture. The samples would remain with the assigned fixtures throughout the study. The sample pairings were moved onto a different wear station at each 1 million cycle (MC) wear interval to reduce any inter-station variability. The pairings of the samples and wear station at each test interval is shown in Table 2-2.

Table 2-2: Sample pairings with corresponding wear station at each wear interval

Sample Pairing	Tibial Insert	Tibial Tray	Femoral Component	Assigned station number at each wear interval		
				0-1MC	1-2MC	2-3MC
1	X1	T1	F1	4	6	5
2	X2	T2	F2	5	4	6
3	X3	T3	F3	6	5	4
4	X4	T4	F4	1	3	2
5	X5	T5	F5	2	1	3
6	X6	T5	F6	3	2	1

2.2.2.1 Attune Fixture Design

Fixtures were developed for the Attune cruciate retaining femoral components due to their unique geometry. They have a graduated radius (Gradius) meaning that locating the centre of rotation (CoR) is dependent on the rotation of the component. This method used in this study was determined by following the guidelines in ISO 1424-1:2009 which states that the CoR is found using an “imaginary plane perpendicular to the tibial axis” [112] at 30° and 60° of flexion. In the case of the Attune components, the first step was to identify the CoR of the dwell point at 0° of flexion which was completed using SolidWorks Premium 2018 x64 Edition (Dassault Systèmes SolidWorks Corp, US). The CoR found at the dwell point was identified as the “Distal CoR”. The component was then rotated 30° about the Distal CoR and by 60° about the CoR identified on the component drawing. A perpendicular line was drawn relative to the dwell point at each rotation (shown in Figure 2-1) and the intersection of these lines was determined to be the ISO CoR of the femoral component.

In addition, there was a medial-lateral offset of the CoR point of 0.07 times the width of the component. The femoral component centre of rotation was then used to determine the geometry of the femoral fixture. Six femoral fixtures were machined from delrin blocks for the Attune fixed bearing, cruciate retaining implants (Figure 2-2).

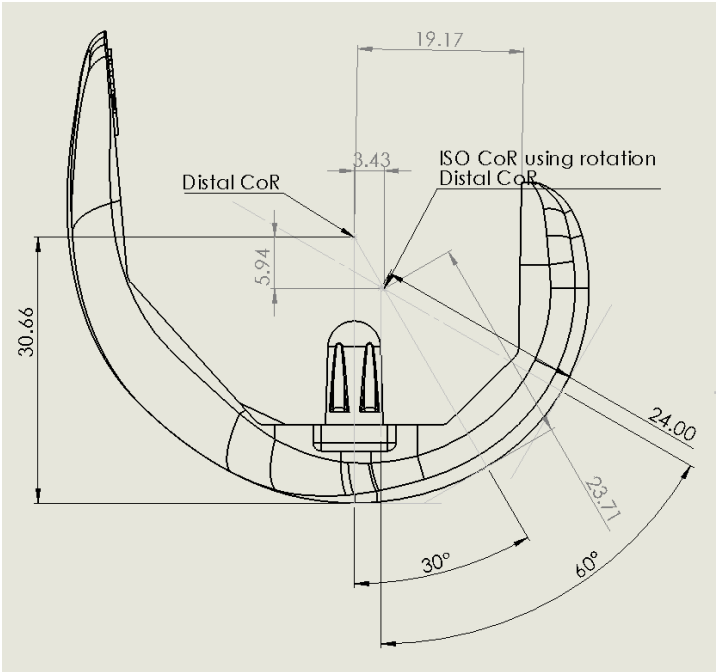

Figure 2-1: Attune femoral component centre of rotation

Figure 2-2 : Attune fixed bearing cruciate retaining Delrin fixtures

2.3 Methods

2.3.1 Simulator Calibration

A calibration procedure, provided by the manufacturer of the simulator and adapted into a standard operating procedure at the University of Leeds [137], was carried out between wear studies to verify the function of the simulator. All six axes of the simulator were calibrated during this procedure and the axes which would be used to control the components using forces were assigned additional measures of calibration to ensure that the demand forces resulted in a correct measurement of displacement, rotation or load, depending on the axis. All calibration constants were documented for future reference during each calibration procedure. These constants were compared to new constants in accordance with the calibration SOP, to ensure calibration values were acceptable, otherwise calibration was repeated.

2.3.2 ISO 14243-1:2009 Force Control Inputs

The input conditions were adapted from BS ISO 14243-1:2009 “Implants for surgery – Wear of total knee-joint prostheses, Part 1: Loading and displacement parameters for wear-testing machines with load control and corresponding environmental conditions for test” [112]. Axial force (Figure 2-3a), flexion extension rotation (Figure

2-3b), anterior-posterior force (Figure 2-3c) and tibial rotation torque (Figure 2-3d) profiles were applied. Abduction-adduction rotation of the tibial insert was left as a passive motion and medial-lateral translation was fixed. The flexion-extension profile was modified to move through a range of -30° to +30° to ensure that the motion was within the simulator axis rotation limits. These flexion-extension limits were accounted for in the design of the femoral component fixture which had a built in 30° angle. The simulator was run at a frequency of 1Hz.

The tibial insert component was constrained by spring constraints replicate soft tissue constraints for both the anterior-posterior motion and tibial rotation. According to the ISO 14243-1:2009 standard, the elastic spring element profiles are determined by a constant of proportionality, the magnitude of which is determined by the prosthesis design; cruciate retaining or cruciate sacrificing.

The cruciate retaining prosthesis design used in this study was assigned a constant of proportionality of 0.36 ±0.02 Nm/° to the tibial rotation control springs, where the tibial rotation angle value was outside of the range of ±6°. Within this ±6° range, the tibial rotation control spring was assigned a constant of 0Nm/°.

The anterior-posterior spring control system was also assigned a constant of proportionality for the tibial component translation value. The value for the AP spring for a cruciate retaining tibial insert design was dependent on whether the motion of the tibial component was posterior (44 ±2.2 N/mm) or anterior (9.3 N/mm), between ±2,5 mm the value was 0N/mm. These inputs result in a spring control profile with three phases, depending on the magnitude of motion (Figure 2-4).

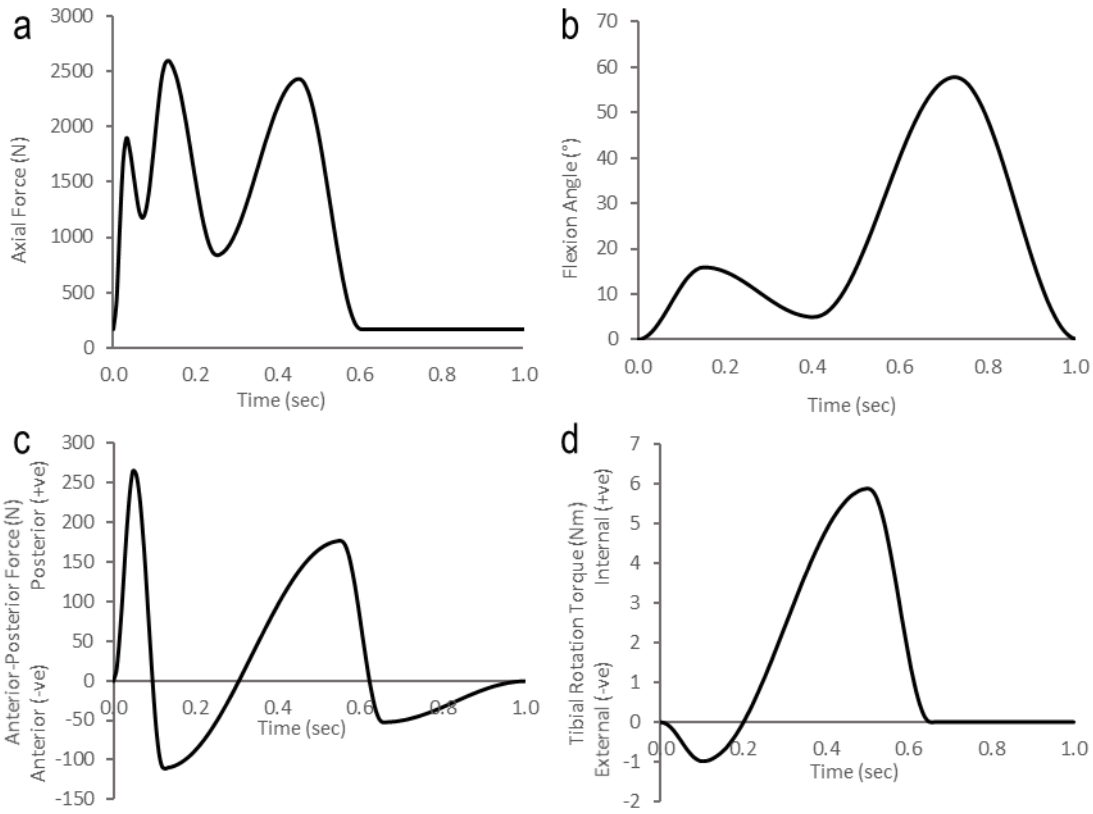

Figure 2-3: Gait profile inputs for standard walking under force control (ISO 14243-1:2009) a) axial force b) flexion angle c) anterior-posterior force d) tibial rotation torque [112]

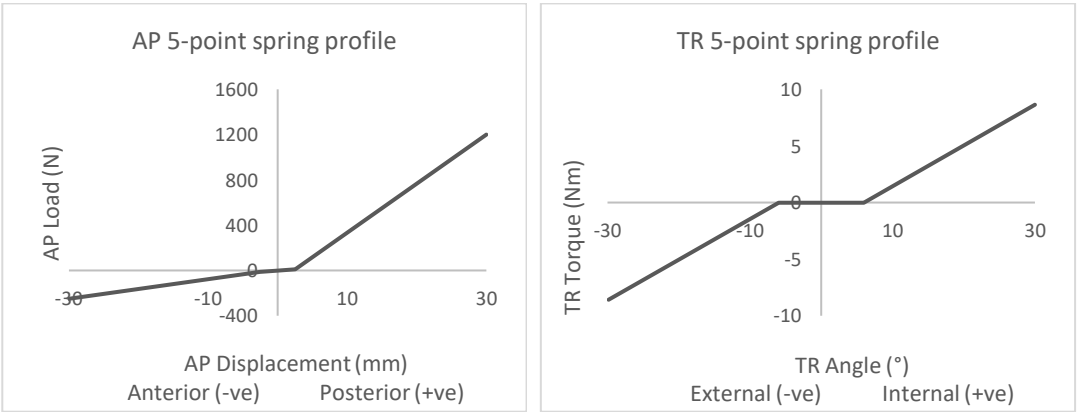

Figure 2-4: ISO 14243-1:2009 cruciate retaining TKR spring stiffness profiles for AP load (left) and TR torque (right)

Anterior-posterior load and internal-external tibial torque Potential, Integral and Differential (PID) Gain tuning was used to reduce the differences between input forces and applied forces to reduce station to station variation. These values were adjusted during setup of each wear interval. Occasionally the values were adjusted

during the wear interval to account for drift, this was usually during the first 24 hours after a serum change as the simulator axial force ramped up to the target load.

Each station was tuned individually using the potential gain value (P), profile scale and phase. Once the PID gains were optimised, the profile was normalised to average the value of the points around zero to prevent drift of values during simulation.

A measurement interval was performed at every 1MC. At each wear interval, the tibial inserts were cleaned and left in a controlled environment for 48 hours prior to weighing, this allowed the moisture of the components to stabilise and settle to the surrounding environment to improve measurement reliability. The simulator was also paused every 3-4 days (approximately 333,000 cycle intervals) for a change of serum due to serum degradation.

2.3.3 Sample Setup Methods

All inserts were soaked in deionised water for a minimum period of two weeks to allow an equilibrated fluid absorption level to reduce variability due to fluid weight gain. The centre of rotation position was identified in accordance with the ISO standard. The standard also specifies a 0.07 x width offset of the axial force axis towards the medial compartment from the neutral tibial component axis. This offset was built into the design of the femoral component fixture.

Components were cemented onto the fixtures in preparation for wear testing. Tibial trays were cemented into tibial fixtures and femoral components were cemented onto the femoral fixtures using laboratory procedures for cementing [138]. Acrylic bone cement (PMMA) was constructed from powder (cold cure) and monomer (rapid repair liquid) in a 2-to-1 weight ratio.

This procedure was carried out using appropriate health and safety considerations. After the cemented components were assembled into the simulator, a thin coating of Microset 101 fluid replicating compounds (Microset Product Ltd, Leicestershire, UK) was applied to the femoral components and loaded to 1kN. The prints of the contact were checked to ensure that all samples had contacts at the dwell point of the bearing and to ensure that they were located in the same place on all tibial insert components (as shown in Figure 2-5).

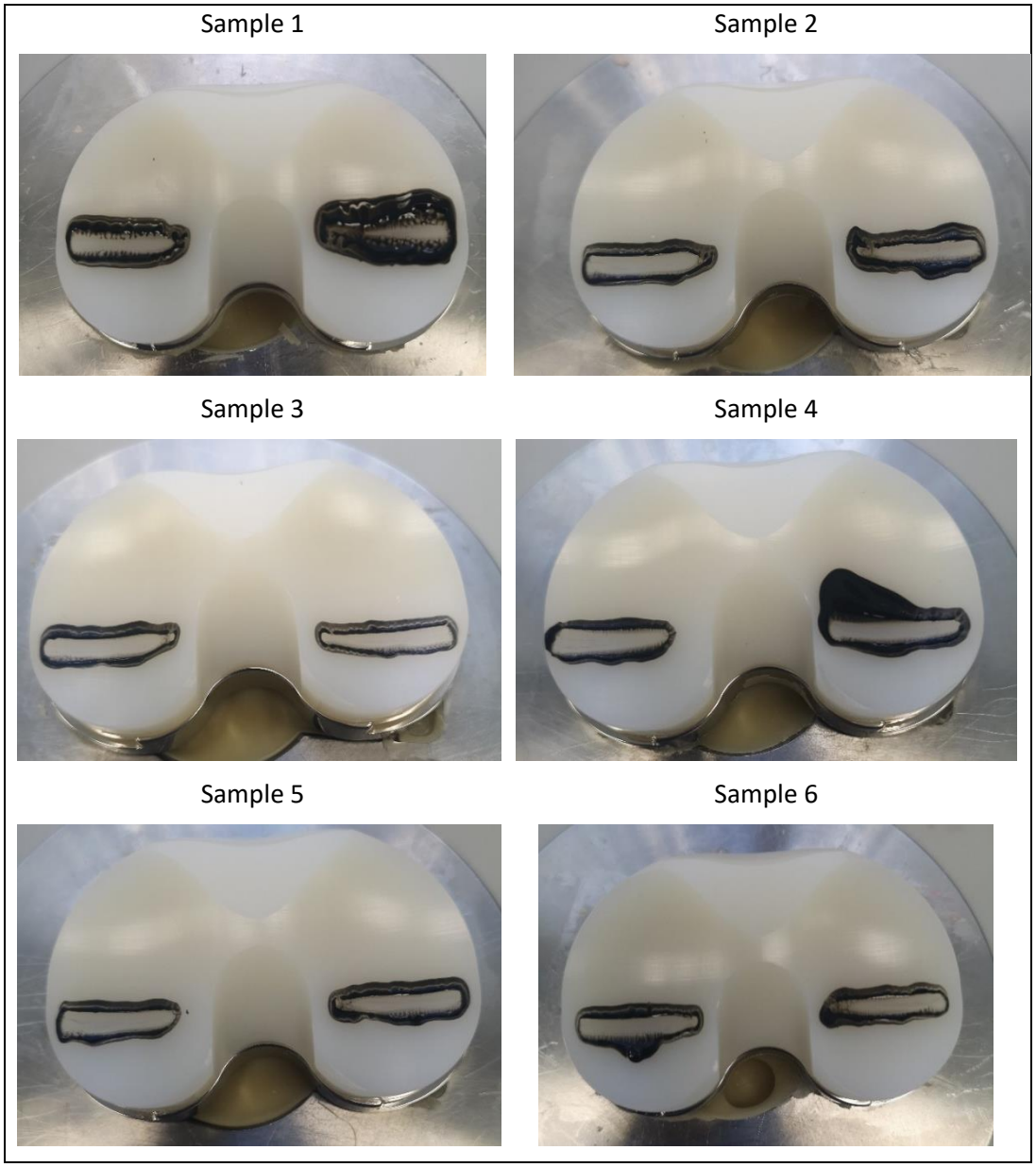

Figure 2-5: Contact prints of Attune AOX Baseline samples

2.3.4 Methods of Wear Determination

Gravimetric methods were used to measure the wear of the bearings on a Mettler XP205 balance (Mettler-Toledo Inc., OH, USA) with a 10µg resolution. Gravimetric measurements were taken at intervals of 1MC including a measurement at 0MC of wear simulation. The methods of determining the gravimetric wear of the implant

followed standard operating procedures at the University of Leeds which detailed methods adapted from ISO 14243-2:2016 [113, 139]. At each wear interval, the tibial inserts were removed from the simulator and cleaned with disinfectant (distel) followed by ultrasonic cleaning for 10 minutes in 70% iso-propanol/water solution. They were then left to dry in a temperature and humidity controlled (40-50% RH) room for 48 hours before weighing. Each tibial insert was weighed repeatedly until five consecutive measurements within 0.05mg were obtained. The gravimetric values were converted to volumetric values using the density of the polyethylene (934 kg/m^3) before a final average volumetric wear value was determined per each tibial insert [66]. A volumetric wear rate was then determined for each sample from the slope of the volumetric wear values at each wear interval. An average and 95% confidence interval was determined for the six samples. For Study 1 using Sigma XLK components, the study completed 2MC of wear. Study 2 Attune AOX components completed 3MC of wear.

To provide confidence in the validity of the methodology to determine kinematic displacement outputs and wear rates, the results from Study 1 on Sigma XLK were compared to data published by Johnston et al., 2018 [73]. The studies were comparable due to being completed on the same ProSim knee simulator (KS8), under the same wear conditions and with the same samples. The only difference between the two studies was that the samples used in the published study had undergone less wear cycles prior to testing. The kinematic outputs with 95% confidence intervals were compared quantitatively. A statistical analysis using a one-way ANOVA to compare the wear rate measured in this study to the historical data was performed, with significance taken at $p < 0.05$.

2.3.5 Kinematic Outputs

Output kinematic measurements from the simulator were recorded at regular time points during the wear study. The outputs required were determined by what would be used to determine the ability of the simulator to follow the input profiles and by which would be useful to determine the movement of the bearing in response to the input forces during the walking cycle. For the first point, output axial load, flexion-extension angle, anterior-posterior load and tibial rotation torque applied at the bearing were requested as outputs. The outputs requested to quantify the motions of the tibial insert as a result of the input forces, were anterior-posterior displacement and tibial rotation angle. Additional kinematic outputs for abduction-adduction rotation of the tibial insert were requested for the Attune AOX study. In future chapters, this

methodology will be used to investigate the impact of different TKR alignment on the kinematics. Understanding the medial-lateral load shift caused by these alignment parameters will be of value to understanding the impact on contact mechanics and wear. Therefore, abduction-adduction was selected as an additional kinematic output of interest.

A 100-cycle average was calculated using Excel 2016, for each of the kinematic outputs for each station. An average of the six stations was then calculated and the 127-point outputs for each cycle were presented as percentage values of a 100% gait cycle. 95% confidence intervals of the six stations output kinematic values were also calculated.

2.4 Study 1: Results

2.4.1 Sigma XLK Load Control Kinematics

A preliminary study was completed using Sigma XLK components in a load control wear study. The purpose was to determine whether the methodology is appropriate for investigating the variables required using the equipment available. The study was also used to highlight any limitations in the methodology. Tibial fixtures and femoral fixtures were used to mount the components in the simulator, aligned at the centre of rotation. The femoral fixtures had been designed previously for the specific design and centre of rotation of the Sigma design [117]. A sample size of 6 was included in this study. The output kinematic positions for anterior-posterior motion and internal-external rotation of the tibial insert component are displayed in Figure 2-6 and Figure 2-7 respectively.

The outputs were compared to outputs of a study completed with the same components on the same experimental equipment, published by Johnston et al. 2019. The outputs from both simulations are presented as a 100-cycle average of the six wear stations with ±95% confidence intervals.

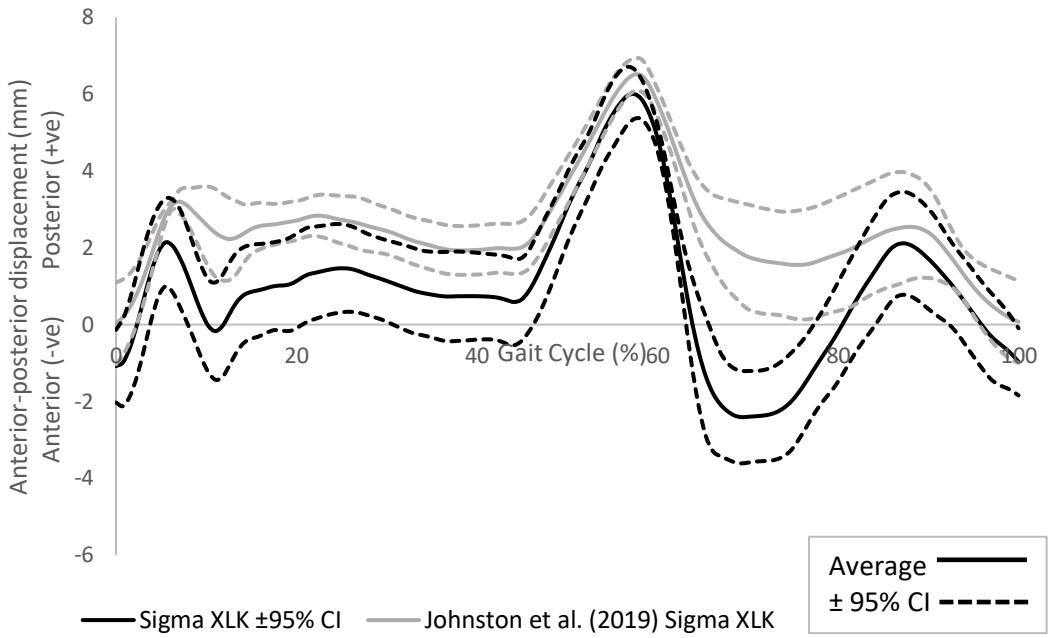

Figure 2-6: Output Sigma XLK anterior-posterior kinematic positions 10 cycle average from the wear study and published data by Johnston et al. 2019 [129]

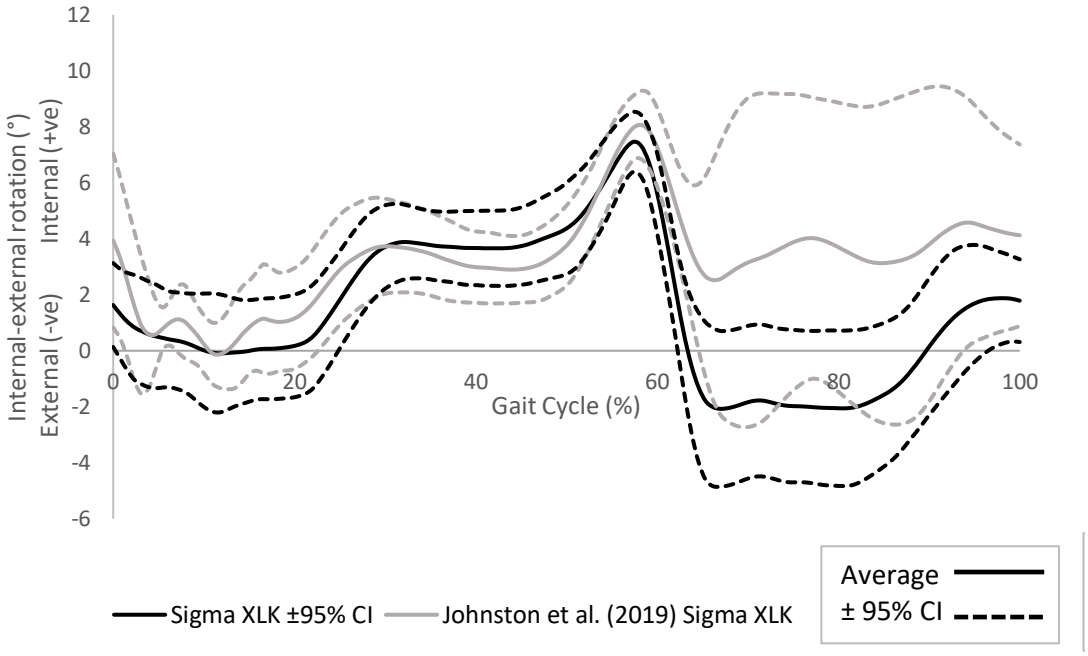

Figure 2-7: Output Sigma XLK tibial-rotation kinematic angles 100-cycle average from the wear study and published data by Johnston et al. 2019

The output anterior-posterior translation kinematics shows that the tibial insert moved posteriorly at the beginning of the gait cycle, with an average peak posterior position of 6mm at 58% of the gait cycle and an average peak anterior position of -2.4mm at 70% of the gait cycle. In comparison, the data published by Johnston et

al, 2019 did not show a negative displacement value over the whole gait cycle [73]. Both output datasets showed a similar 95% confidence interval range over the whole gait cycle.

The output internal-external rotation kinematics shows that the tibial insert had an average peak internal rotation of 7.5° at 57% of the gait cycle and an average peak external rotation of -2.1° at 67% of the gait cycle. The output rotation average value for the published data was positive over the whole gait cycle. Both outputs had a confidence interval range in the first 60% of the gait cycle of around 3-4°. However, this confidence interval range was increased to around 6° for this study and around 11° in the published study.

2.4.2 Sigma XLK Wear Rates

The cumulative volumetric wear for each sample at each measurement interval on Sigma XLK components using force control is displayed in Table 2-3. The average volumetric wear rate, calculated by linear regression fit, of the six samples after 2MC of wear was 5.6±2.1 mm^3/MC. This wear value was compared to data published by Johnston et al., 2018 [73] which was 4.7±1.3 mm^3/MC (Figure 2-8). There was no significant difference ($p = 0.36$) in the wear rates measured by the two studies using the same materials and methods of wear simulation.

Table 2-3: Sample cumulative volumetric wear at each measurement interval.

Measurement Interval (cycles)	**Volumetric Wear (mm^3)**					
	Sample 1	**Sample 2**	**Sample 3**	**Sample 4**	**Sample 5**	**Sample 6**
1,004,049	3.2	5.5	4.5	9.1	5.8	7.7
2,028,178	6.1	12.7	9.7	16.2	8.4	15.3

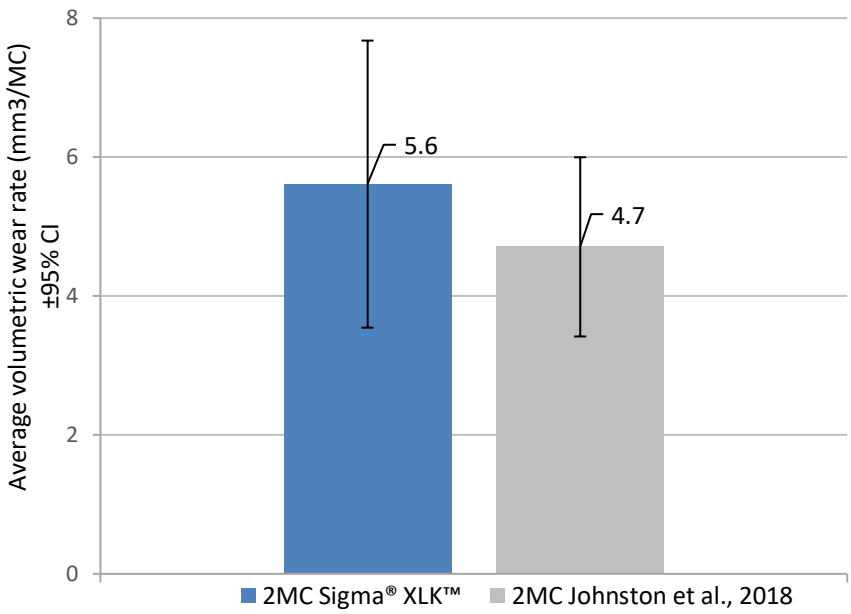

Figure 2-8: Average volumetric wear rates with 95% confidence limits after 2MC Sigma XLK wear study compared to data published by Johnston et al., 2018

2.5 Study 2: Results

2.5.1 Attune AOX Load Control Kinematics

The output kinematics for the entire 3MC wear study were recorded using the simulator software. For each wear interval, a 100-cycle average of the output was taken to check for any changes to the output kinematics incurred by removing samples and fixtures from the simulator. The comparison of the average for all three wear intervals for anterior-posterior displacement is shown in Figure 2-9 and for internal-exterior tibial rotation angle is shown in Figure 2-10. The results show that the output kinematics did not change greatly between wear intervals.

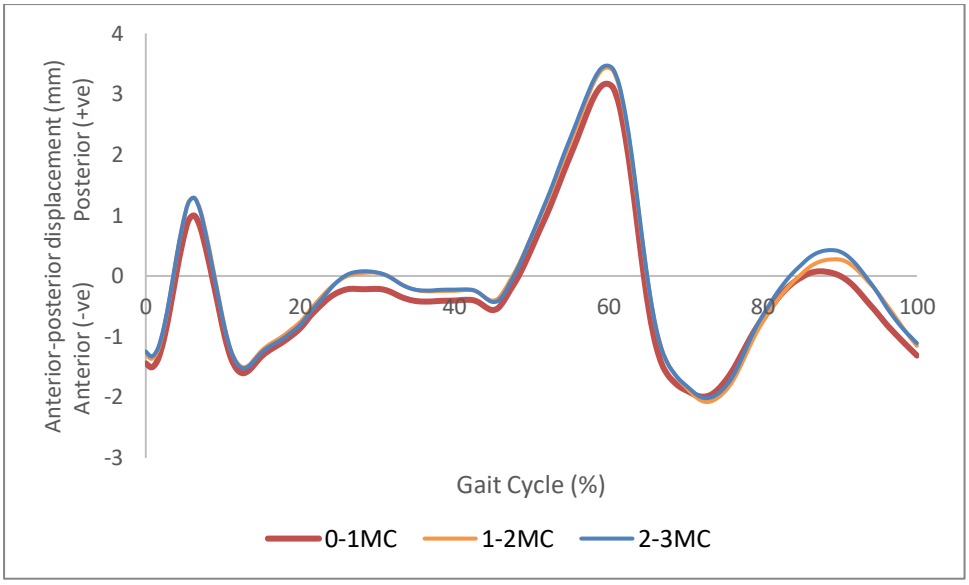

Figure 2-9: 100-cycle average anterior-posterior displacement for three wear intervals 0-1Mc, 1-2MC and 2-3MC.

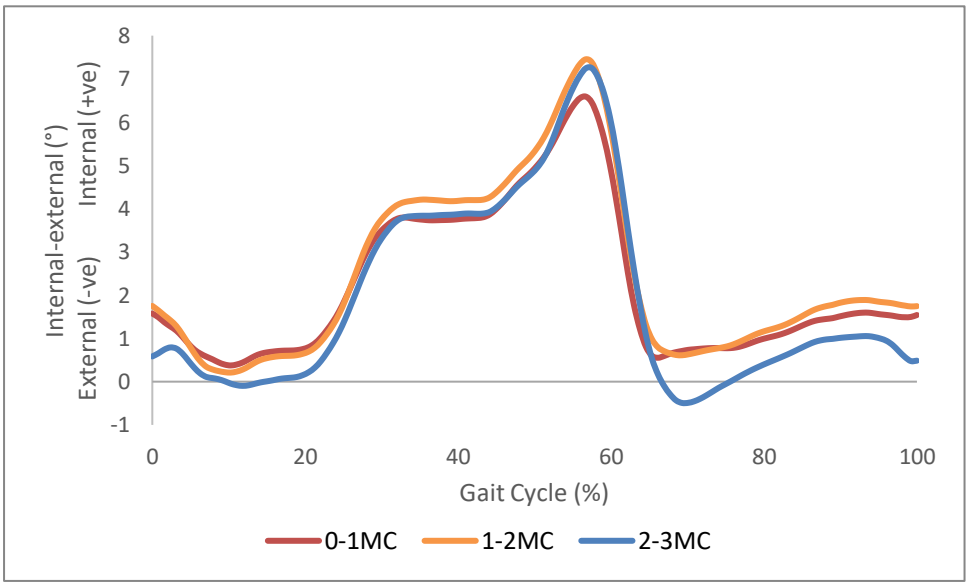

Figure 2-10: 100-cycle average internal-external rotation angle for three wear intervals 0-1Mc, 1-2MC and 2-3MC.

The 100-cycle average anterior-posterior displacement with ±95% confidence interval for the 0-1MC wear interval is shown in Figure 2-11. The tibial insert was initially in an anterior position at the start of the gait cycle and moved to a posterior position at 10% gait before moving back to an anterior position at 15%. The insert, on average, remained in an anterior position until 45% of gait. However, the 95% confidence interval shows that there were some samples which translated into a posterior position around 20% gait. The insert reached a peak posterior position

around 60% of the gait cycle and then moved to an anterior position as the gait cycle transitioned into swing phase (above 60%). The average position of the kinematic outputs of the tibial insert samples showed an anterior position for the final 40% of the gait cycle. However, the confidence intervals show that some samples translated to a posterior position during mid swing phase.

The 100-cycle average internal-external tibial rotation angle, with ±95% CI for the 0-1MC wear interval, is shown in Figure 2-12. The average tibial rotation position was internal during the whole gait cycle, reaching a peak of 6.5° around 60% of gait. On average, there was a plateau in the rotation angle during the swing phase of the gait cycle. However, the 95% confidence intervals show that the output tibial rotation of some samples had an external rotation during the swing phase and during the first 25% of the stance phase.

The average abduction-adduction rotation for the six stations was between zero and 0.2° adduction (Figure 2-13). There was a steep rotation to a peak adduction rotation of -0.5° around 60% of gait. The 95% confidence interval shows that there was increased variation between the station adduction rotation at this point and also at around 75% gait where peak abduction was reached. The peak average abduction value was 0.5° followed by continued rotation to smaller abduction values at 100% gait.

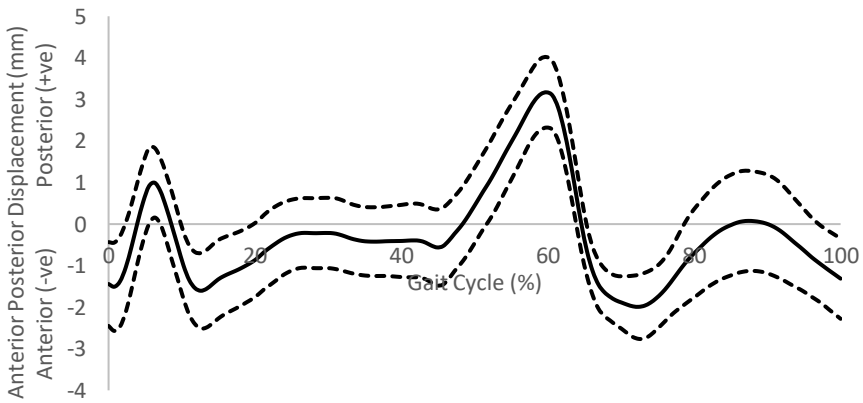

Figure 2-11: Output baseline Attune AOX anterior-posterior displacement kinematic positions 100-cycle average

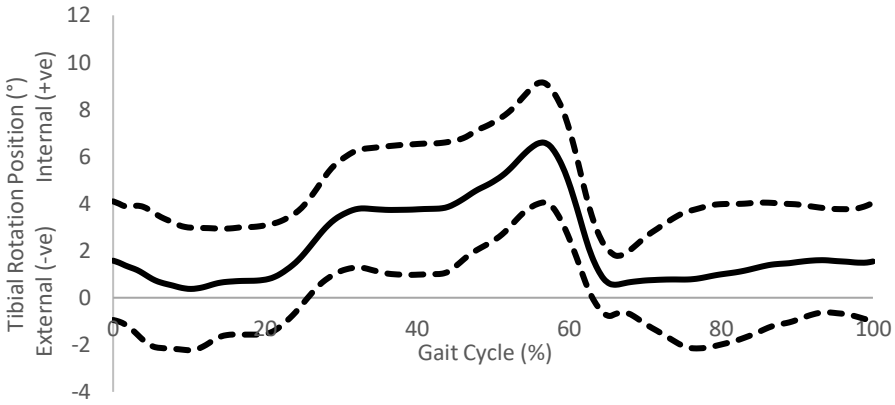

Figure 2-12: Output baseline Attune AOX internal-external rotation kinematic angles 100-cycle average

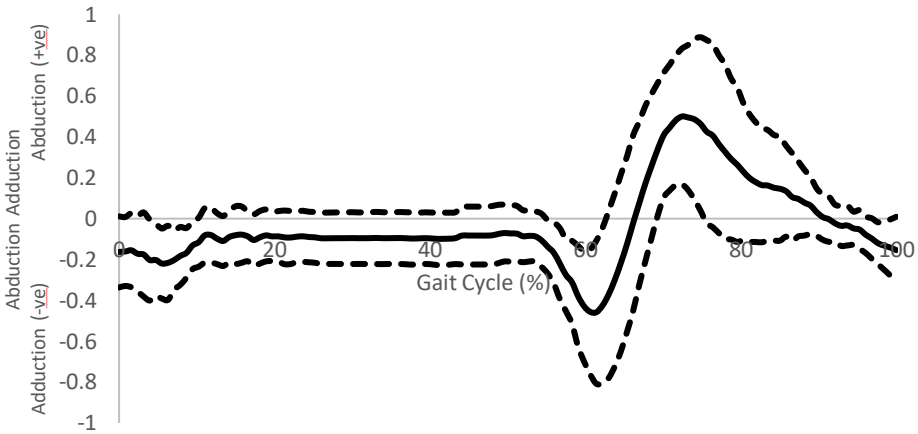

Figure 2-13: Output baseline Attune AOX abduction-adduction rotation angles 100-cycle average

2.5.2 Attune AOX Wear Rates

The volumetric wear for each sample at each measurement interval on Attune AOX fixed bearing, cruciate retaining components using force control is displayed in Table 2-4. The components were weighed at or around 1 million cycle intervals for efficiency of running the test continuously, 24 hours a day. The limitation to stopping the cycle at exact points of 1MC means that the components may be left loaded and in situ in the simulator until an operator was able to access the laboratory. The exact wear interval cycles were 0 cycles, 1,094,936 cycles, 2,089,830 cycles and 3,000,000 cycles. The largest cumulative volumetric wear value after 3MC was 13.85mm^3 for sample 3, the minimum was 4.25mm^3 for sample 6. The cumulative volumetric wear results are displayed with 95% confidence intervals at each wear interval of the wear

study (Figure 2-14). A linear regression line was fit to the average cumulative wear values at each wear interval.

The volumetric wear rate was calculated by linear regression of volumetric loss for each sample of the study (Table 2-5). The average was calculated as an average of the volumetric wear rate at each of the three wear intervals for each station. An overall average volumetric wear rate for the six wear samples was also calculated with a 95% confidence interval, displayed in Figure 2-15.

Table 2-4: Sample cumulative volumetric wear at each measurement interval.

	Volumetric Wear (mm^3)							
	Sample						**Average**	**95% CI**
Wear Cycles	**1**	**2**	**3**	**4**	**5**	**6**		
0-1MC	4.26	1.34	4.30	5.95	1.72	1.53	3.19	2.01
1-2MC	7.40	3.51	7.29	6.96	3.51	1.99	5.11	2.50
2-3MC	8.36	6.73	13.95	8.31	8.43	4.25	8.34	3.35

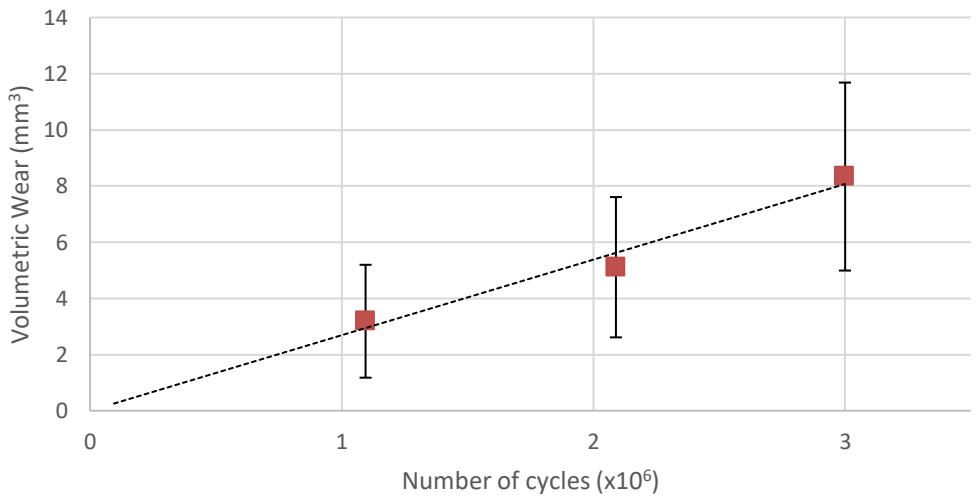

Figure 2-14: 0-3 million cycles Attune AOX average cumulative volumetric wear with 95% confidence interval at each million-cycle wear interval. Includes a linear fit regression line.

Table 2-5: average volumetric wear rate of each wear station at 3 million cycles and 6-station average with 95% confidence interval.

Volumetric wear rate (mm^3/MC)						**Average**	**95% CI**
Sample 1	**Sample 2**	**Sample 3**	**Sample 4**	**Sample 5**	**Sample 6**		
2.8	2.2	4.5	2.6	2.7	1.3	2.7	1.1

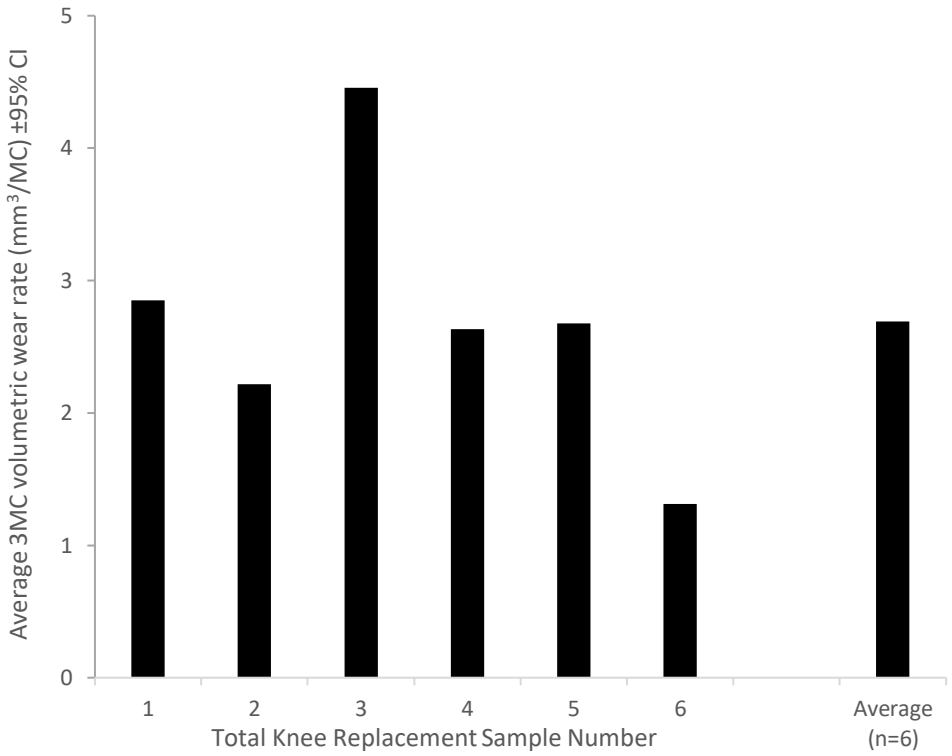

Figure 2-15: Average Volumetric Wear Rate over 3 million cycles for each wear station.

The overall average volumetric wear rate of the six wear samples after 3 million cycles of Attune AOX wear simulation was 2.7±1.1mm^3/MC (Figure 2-16). This is comparable to the average volumetric wear rate after 2MC on Sigma XLK bearing components, which was 5.6±2.1 95%.

The confidence intervals for the wear of Attune AOX samples had smaller confidence intervals than the Sigma XLK study. The variability in the wear rates of Study 2 may be a combination of the tuning of tibial rotation angle and the setup of the Attune components when cementing into fixtures. Although the dwell point was checked between samples and showed that all six samples were in a similar position, any slight changes in this could affect the output kinematics and therefore the wear.

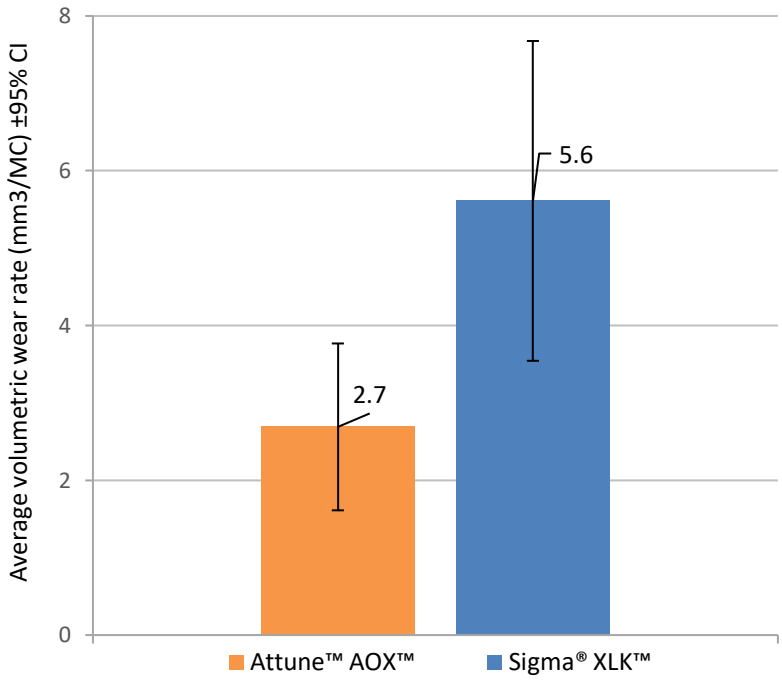

Figure 2-16: Average 6-station volumetric wear rate with 95% confidence intervals displayed for 3 million cycles of wear of Attune AOX and 2 million cycles of wear of Sigma XLK

2.6 Discussion and Limitations

The baseline wear simulation was a critical method development section of this project. The research objective was to experimentally investigate a baseline wear rate of Attune AOX total knee replacement bearings under ISO 14243-1:2009 standard walking gait load control conditions. To achieve this, studies were completed to determine appropriate methodologies for the setup of the TKR bearing on the wear simulator and established the capabilities of the wear simulator to apply load control inputs using spring constraints.

The wear rates found in Study 1 using Sigma XLK TKR components were not significantly different (($p = 0.36$) from published data under the same test conditions on the same implant [73]. The output kinematics of Study 1 showed good agreement during stance phase (0%-60% gait) in both anterior-posterior displacement and internal-external rotation. During swing phase (60%-100% gait), there was less agreement between the output kinematics of the two studies. While the published literature reported that the tibial insert remained in posterior translation and internal rotation throughout swing phase [129], this study found that there was a net anterior displacement between 65% and 80% gait and net external rotation between 65% and 90%. When comparing these results, it is important to consider the condition of the

tibial insert bearing prior to wear simulation. The same components were used in both studies which means that the tibial insert in the current study had already undergone multiple million cycles of wear simulation which would have impacted the surface condition of the tibial insert. Furthermore, differences in PID tuning may also have had an impact on these output profiles.

The wear results of Study 2 (2.7± 1.1mm^3/MC) were slightly lower than wear result reported in literature (3.8 mm^3/MC) for an Attune AOX bearing [130]. However, the wear rates for the published study were determined from a wear study simulated under load control, but using a different wear simulator (AMTI VIVO) and setup procedure. Output kinematics showed good repeatability between wear intervals. Anterior-posterior displacement outputs had a consistent confidence interval range throughout the whole gait cycle which showed good agreement between the outputs of all six stations of the simulator. The internal-external rotation angle outputs showed a slightly large confidence intervals of 5° to 6° throughout the gait cycle. However, they were not comparatively different to the kinematic output confidence intervals found in Study 1. Abduction-adduction rotation variability was consistent throughout the majority of the gait cycle with relatively larger confidence intervals in the high abduction range between 70%-90% of the gait cycle.

The variability of output kinematics between stations, for anterior-posterior displacement and internal-external rotation are affected by the PID tuning parameters developed at the beginning of the wear interval. Since tibial rotation was controlled through an input torque (Nm), tuning was more challenging than for an applied load, using PID control. As a result, the tibial rotation outputs showed more variability between stations than the anterior-posterior displacement outputs. The variability in the output kinematics between all six stations should be taken into account when assessing the other outputs of the study such as the impact this may have on the wear of the tibial inserts.

Overall, this chapter outlines the development and application of the methodology of completing a 3 million cycle wear study on Attune AOX total knee replacement components in load control. The results show that the methodology determine wear rates for the Attune bearing design and for the Sigma design. The methodology can be used and adapted to the needs of future studies.

Chapter 3
Experimental Measurement of Total Knee Replacement Contact Mechanics

3.1 Introduction

Understanding the contact mechanics between the two interacting surfaces of a total knee replacement bearing is a useful parameter in understanding the wear of a joint implant during daily activities [140]. Pressure sensor equipment can be used to measure a range of contact mechanics parameters including contact pressure and contact area. In this study the primary aim was to measure the contact pressure at various points of the gait cycle to understand how this varies as kinematics and loads change through an ISO 14243-1:2009 standard walking cycle. This experimental study, focussed on measuring the contact stresses of a total knee replacement, involved developing a method to investigate the contact mechanics of Attune fixed bearing cruciate retaining total knee replacement components using Tekscan equipment. Tekscan was chosen as the appropriate pressure sensitive film to use over Fuji Film as a result of reported literature of its effectiveness at measuring contact pressure, whereas Fuji Film has been reported to have improved accuracy in measuring contact area [141].

A combination of literature was used to develop the methods which include previous study reports from DePuy Synthes, the Tekscan I-Scan User Manual v7.6x and published works [142]. The preliminary procedures were adapted after experimental trials to suit the requirements of this study. The final methodology is outlined in this chapter where the following objectives are addressed:

1) Complete preliminary studies on AMTI and ProSim joint simulators to establish setup protocols of the TKR components in a range of fixed kinematic positions and loads.
2) Develop a repeatable method for calibrating the Tekscan equipment.
3) Create a protocol for measuring the contact pressure between the femoral component and tibial insert using both an AMTI and ProSim joint simulator
4) Determine the appropriate frequency for calibration of the Tekscan sensors between contact pressure measurements.
5) Complete a gait study to measure contact pressure under compressive load at fixed intervals of the gait cycle for mechanical alignment (MA).

3.2 Preliminary Study 1 – AMTI ViVo

3.2.1 Rationale

An initial understanding of the capabilities of the Tekscan sensors when used to measure contact mechanics of a TKR bearing design was required to determine whether the sensors were a viable option for use in this study. The aim of this study was to determine whether the Tekscan was capable of measuring contact pressures at various points of the gait cycle in different alignments and whether the setup was robust to take repeatable measurements. The AMTI VIVO simulator was selected as the ideal equipment for this preliminary investigation since previous studies on this simulator involved input kinematics for mechanical alignment and other variations of patient specific alignment. Therefore, the capabilities of the simulator to create this alignment had already been confirmed and was not a required element of this study.

3.2.2 Materials

This study was completed on a single station AMTI VIVO 6DoF joint simulator (AMTI, Watertown, MA) joint simulator at DePuy Synthes Leeds Tribology laboratory. The pressure sensitive films used in this study were Tekscan 4000 Sensors which was two independent pressure pads, made up of individual sensels, with a maximum pressure of approximately 62MPa (Figure 3-1). Each sensel of a Tekscan sensor is a variable resister and when a force is applied to the sensor the impedance of the sensels in the loaded area changes. This change in impedance is correlated to a digital value which determines the pressure or force applied to the sensor. The contact pressure values were recorded by the Tekscan I-Scan 6.03 software

A joint simulator was used to complete both the calibration procedure and the measurement of pressure between the bearings. In this preliminary study a DePuy Synthes 3-station AMTI VIVO Joint Simulator was used which controls all six degrees of freedom of the knee independently. The Attune cruciate retaining Size 5 CoCr femoral component was mounted on the simulator using an AMTI Femoral Shaft fixture while the Attune fixed bearing Size 5 CoCr tibial tray was cemented onto an AMTI tibial tray fixture [143]. An Attune AOX Size 5 tibial insert created the bearing surface with the femoral component. The sensors were connected to a laptop running I-Scan software using a Tekscan data handle.

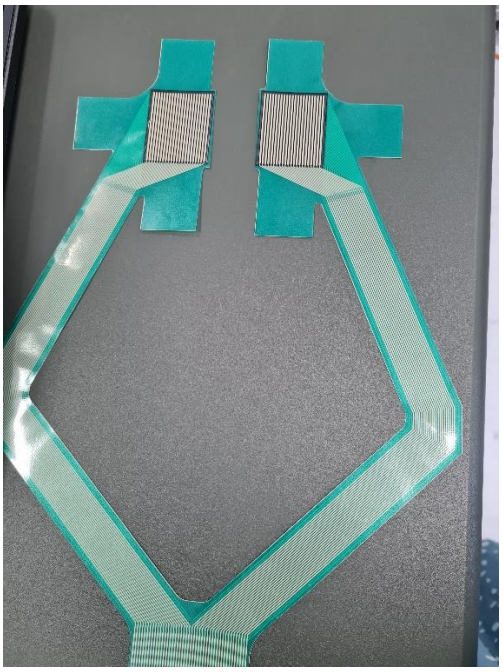

Figure 3-1: Tekscan 4000 Sensor

Two stainless-steel round disks were machined to a 25mm diameter be used to create the contact between the load and the pressure sensors during the calibration step (Figure 3-2). The diameter of the cylinders was determined to fit the disks within the area of each sensor pad, this prevented trapped air affecting the pressure measurements.

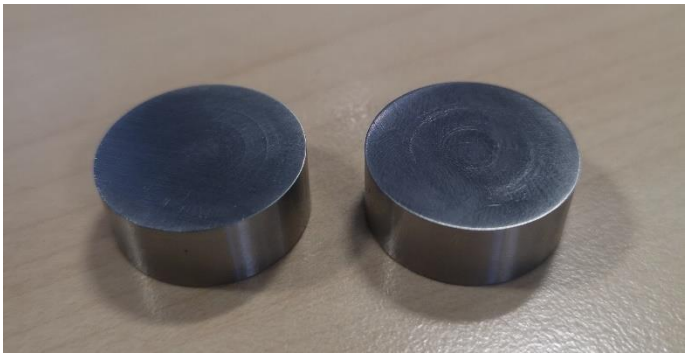

Figure 3-2: Tekscan Calibration Disks

3.2.3 Methods

3.2.3.1 Calibration Methods

Calibration of the Tekscan sensors is used to correlate the digital value (between 0 and 255) read by the sensors into an engineering value, such as pressure. To do this, a known load is applied to a known area on the sensor. If two loads are applied to the sensor, one at a ‘zero point’ and one at a ‘calibration point’ then a line can be used to connect the two measured points. The slope of the line can be deduced which equates to the calibration factor [144].

A methodology for the calibration procedure in the AMTI VIVO was developed and tested for repeatability. Firstly, a level calibration block was secured onto the flexion arm of the AMTI VIVO 3-station simulator and an AMTI signal controller was connected to a load cell to record the applied load to the sensors (Figure 3-3). Tekscan 4000 sensor pads secured onto a level metal block placed on top of the load cell and the machined metal disks were placed centrally on the sensor pad area. The Tekscan Data Handle was used to connect the sensors to the I-Scan software, ensuring that the sensors were inserted the correct way up. To create contact the AMTI software was used to apply a load to the level block which applied a load to the two metal disks in contact with the sensors. An initial low load of 50N was applied to check for an even load distribution and no trapped air using the software.

Once a steady load was obtained on the sensors, the sensitivity of the sensor was adjusted using the I-Scan software to increase the sensel load pickup and increase the colour contrast of pressure map (Figure 3-4).

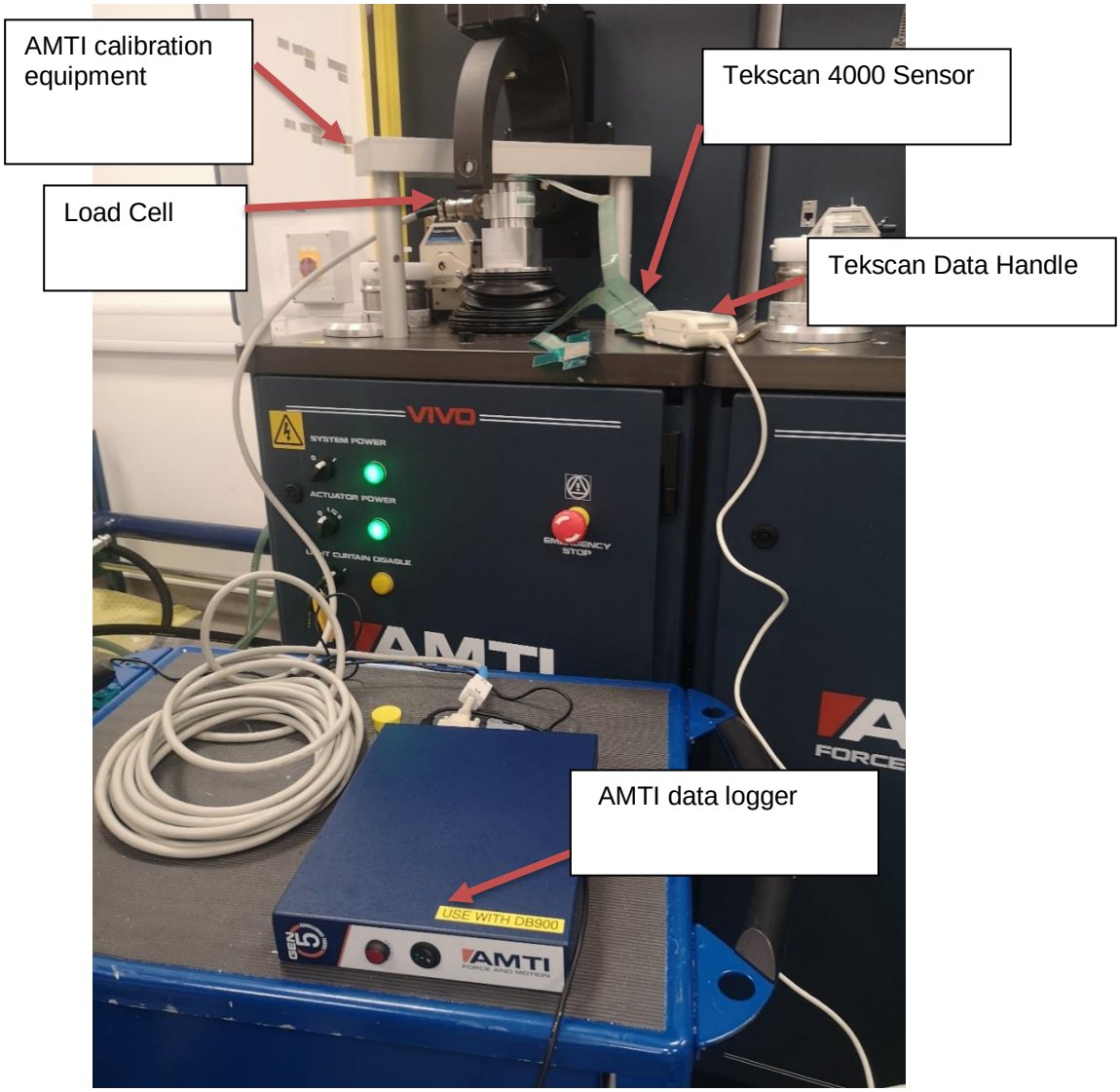

Figure 3-3: Tekscan Calibration Equipment Setup

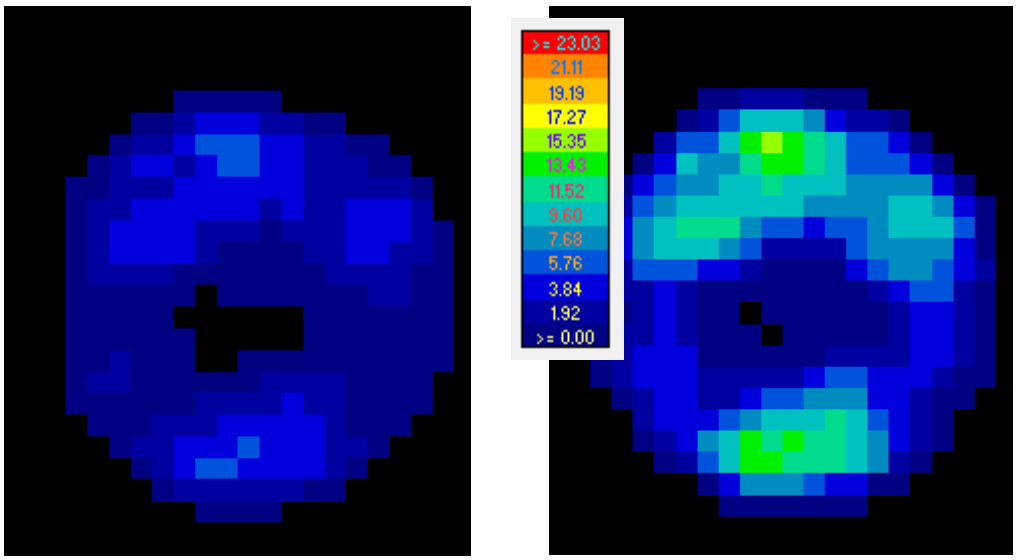

Figure 3-4: Tekscan 4000 calibration with default sensitivity (left) and Mid 2 sensitivity (right) settings.

A two-load calibration procedure, where $F_2 > 2F_1$ was developed where the sensor was first loaded to F_1 = 500N and the calibration function in the software was set to take a calibration reading after 30 seconds, allowing the sensor to settle. The second load point of the calibration was F_2 = 3000N, which was also allowed to settle for 30s before a reading was captured by the software. The I-Scan software then calculated the calibration value using the exponential Power Law equation $Y = AX^b$ where; Y is the load, A the slope scale factor, X the digital output (between 0-255), b the exponent which determines the curvature of the line between the two load points [144]. The resulting calibration file was saved and was then imported into the software converting the raw digital values to the engineering units which in this case were pressure values.

3.2.3.2 Total Knee Replacement Methods

Two Tekscan sensors were used on TKR bearing surfaces using two alignment conditions including mechanical alignment and patient specific alignment. The sensors were attached to the surface of the tibial insert using double sided tape. Each sensor was used on one TKR bearing each, this was due to the sensor sensels becoming slightly damaged when removed from one bearing surface and attached to another. Tekscan sensor 1 with TKR bearing 1 is referred to as Test 1, Tekscan sensor 2 with TKR bearing 2 is referred to as Test 2.

Two Tekscan sensors were used to check the repeatability of the methods developed in this study. The methods were also repeated on two TKR bearings to investigate the repeatability of the results. Since this was a preliminary study to develop a methodology it was not considered necessary to use a larger sample size.

The measurements for MA were repeated twice for both Test 1 and Test 2 and twice for the AA alignment for Test 2. There was only one repeat of the measurement of AA with Test 1 because the sensor became too damaged to obtain reliable data.

To complete a gait cycle measurement the TKR specimens were secured in the simulator without the sensors to set the zero/reference position using the AMTI software. Once the zero position was established the sensors were secured to the tibial components tape so that the distal part of the sensors was secured to the most anterior part of the insert surface (Figure 3-5). The sensors were gently smoothed into the curved condyle surface of the insert removing any air bubbles which could cause errors in the pressure readings. The femoral component alignment was also verified to be at a zero angle position using an inclinometer.

To initialise the setup, the Tekscan sensor was secured into the Tekscan Data Handle to connect to the I-Scan software setup with the appropriate calibration settings. A 100N load was applied to the components using AMTI software (VIVOCONTROL) to check that the contact maps on the I-Scan software were registering the contact.

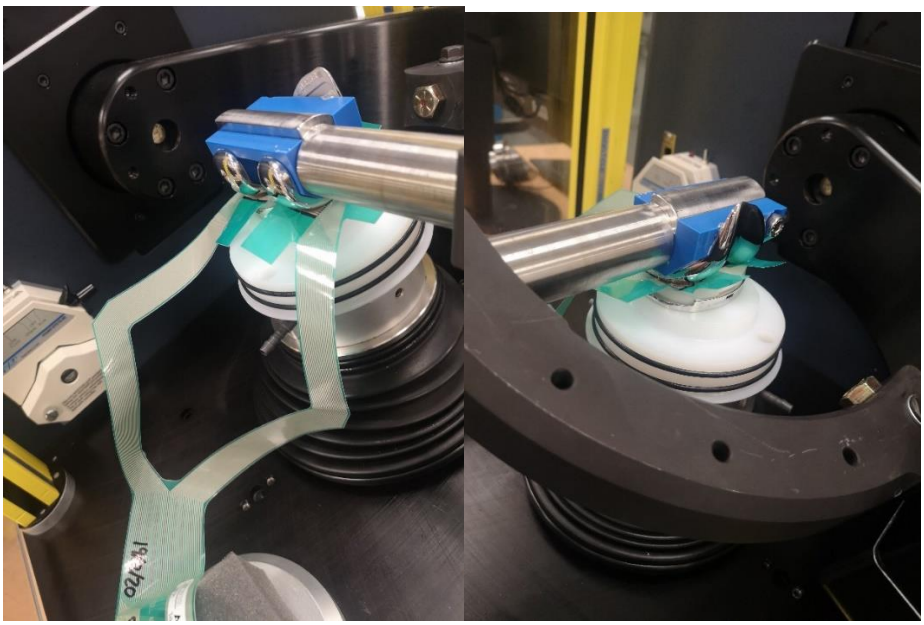

Figure 3-5: TKR components setup on AMTI single station ViVo with Tekscan 4000 sensors, posterior view (left) and anterior view (right)

Each measurement was taken as an individual point of the gait cycle at 10% intervals from 0%-100% of the gait cycle using five degrees of freedom controlled using a displacement or angle and an axial force, being the only axis in load control, applied through the tibial fixture. Once the components were moved to their required position, an initial 100N load was applied which was increased gradually until reaching the demand load for the measurement. The I-Scan software was used to take a snapshot of the pressure map which was saved as an ASCII file for future analysis. To record the exact displacements, rotations and load applied to the bearing, a screenshot of the values reached by the simulator was saved.

3.2.3.3 Kinematic Inputs

Existing load control inputs were adapted from kinematic profiles (Figure 3-6) extracted from a previously validated 6-DOF joint simulator “mechanical alignment cruciate retaining fixed bearing” and “anatomic alignment cruciate retaining fixed bearing” setup conditions [127, 130]. The anatomic alignment condition parameters are consistent with the category of patient specific alignment as defined in this study.

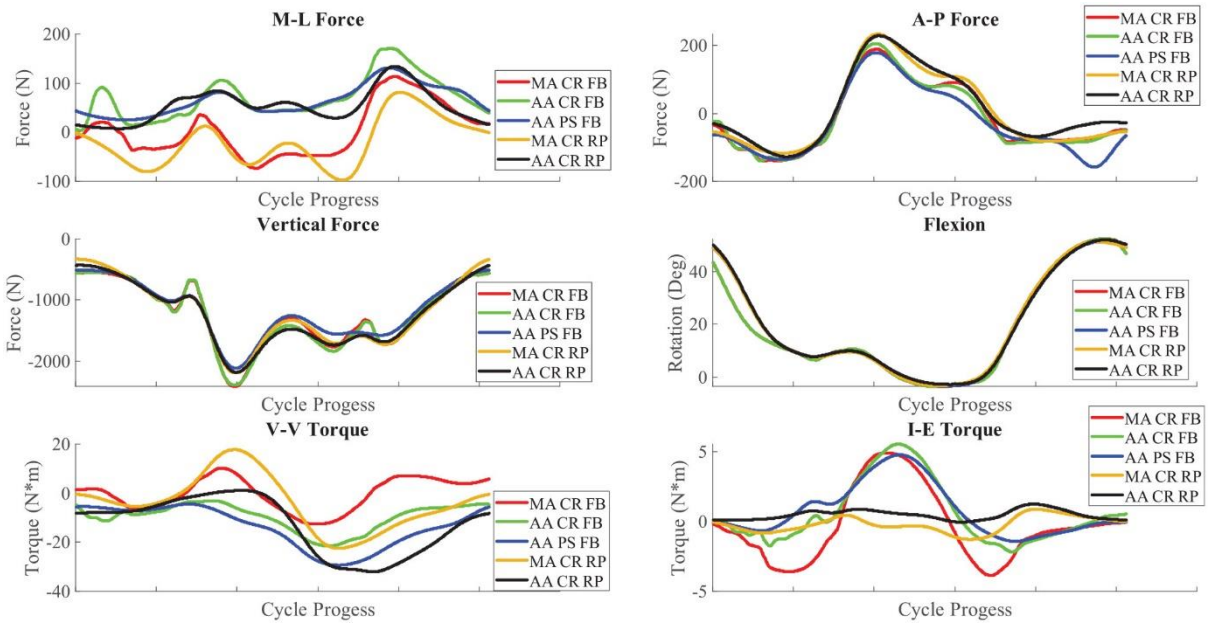

Figure 3-6: Kinematic profiles for mechanical alignment (MA) and anatomic alignment (AA) Tekscan study on AMTI VIVO as extracted from 6-DOF joint simulator model for cruciate retaining (CR) and posterior stabilised (PS) bearing designs. Including medial-lateral (ML) force, anterior-posterior (AP) force, Vertical force, flexion, varus-valgus (VV) torque and internal-external (IE) torque. (reproduced with permission from Maag et al., 2021 [130])

The profiles were loaded into the simulator software and a 1500 cycle simulation at 1Hz was completed using Attune AOX components lubricated with petroleum jelly. The software was setup to record kinematic outputs for each of the 6 degrees of freedom at 100 cycle intervals using a Grood & Suntay joint coordinate system [19]. Kinematic outputs were recorded so that fixed profiles of various points through the gait cycle could be created as inputs for contact mechanics measurements. Using kinematic inputs to control the axes of the simulator was a more preferable method to using kinetic inputs due to the increased level of control and repeatability in positioning the components before taking a pressure reading. The only DoF controlled by kinetic inputs was the AF axis (axial load).

The output profiles exported from the simulator software included: flexion angle and axial load (Figure 3-7), anterior-posterior and medial-lateral displacement (Figure 3-8), and internal-external and abduction-adduction rotation (Figure 3-9) The kinematic profiles were individually plotted over the 1500 cycle simulation to assess whether the displacement applied at component level in response to the loads applied reached a steady value. All kinematic profiles eventually reached a steady gait cycle and therefore the values for the fixed input profiles were taken from the final output results at cycle 1500.

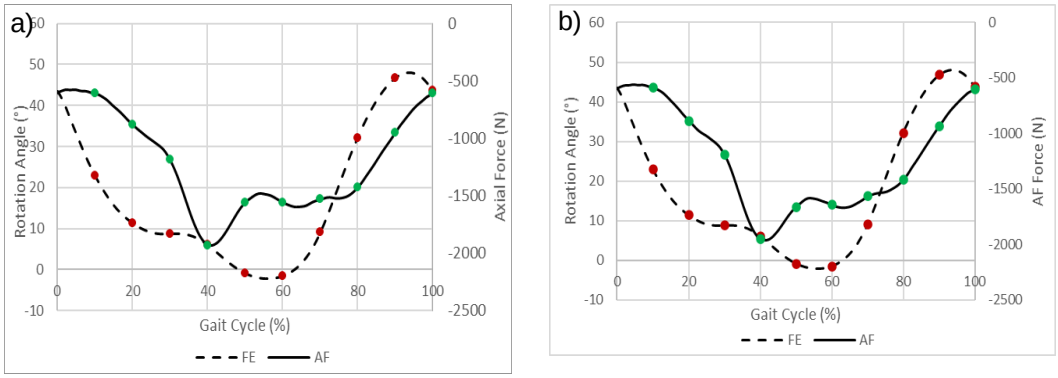

Figure 3-7: VIVO output for flexion/extension angles and axial loads with the study input points located on the profile in a) MA b) PSA

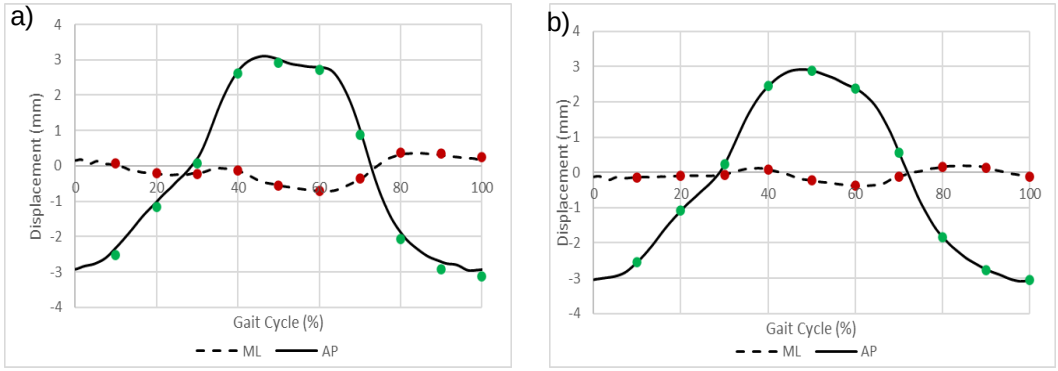

Figure 3-8: VIVO output for medial/lateral and anterior/posterior displacement with the study input points located on the profile in a) MA b) PSA

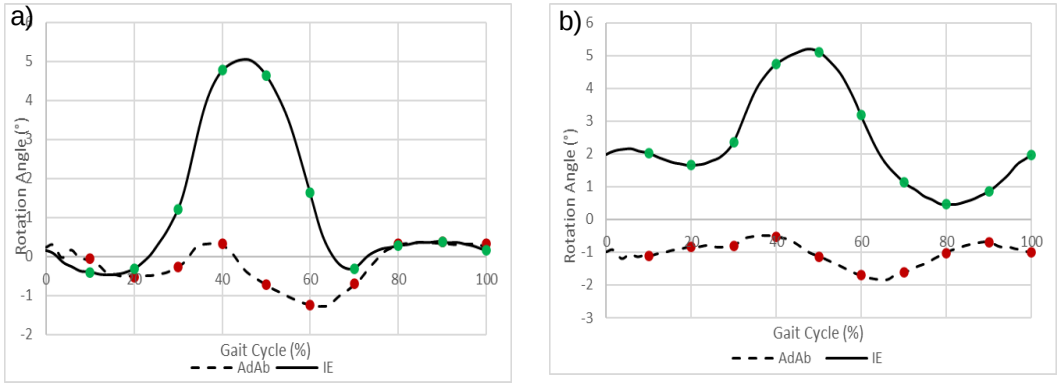

Figure 3-9: VIVO output for adduction/abduction and internal/external angles with the study input points located on the profile in a) MA b) PSA

Static input profiles were created at 10% intervals of the gait cycle from 10% to 100%. An additional position of 0% was created as a baseline position where all kinematic axes were in their zero position and an axial force of 0% of the gait cycle was applied. The profiles for each of the 11 points in the gait cycle are shown in Table 3-1 for mechanical alignment and in Table 3-2 for patient specific alignment.

Table 3-1: Mechanical Alignment Input Profiles

% of Gait Cycle	AF Load [N]	ML [mm]	AP [mm]	FE [deg]	AA [deg]	IE [deg]
0	-576.786	0	0	0	0	0
10	-606.38	0.07	-2.51	23.02	-0.06	-0.67
20	-880.28	-0.21	-1.16	11.35	-0.52	-0.37
30	-1182.24	-0.23	0.06	8.78	-0.28	1.26
40	-1929.5	-0.12	2.61	6.06	0.32	4.94
50	-1560.5	-0.57	2.91	-0.8	-0.72	4.81
60	-1556.72	-0.71	2.71	-1.5	-1.24	1.43
70	-1527.51	-0.35	0.89	9.12	-0.69	-0.53
80	-1429.71	0.38	-2.07	32.15	0.33	0.18
90	-949.42	0.34	-2.93	46.74	0.38	0.19
100	-607.88	0.25	-3.13	43.73	0.32	-0.2

Table 3-2: Patient-specific Alignment Input Profiles

% of Gait Cycle	AF Load [N]	ML [mm]	AP [mm]	FE [deg]	AA [deg]	IE [deg]
0	-572.456	0	0	0	0	0
10	-588.88	-0.14	-2.55	23.03	-1.11	2.02
20	-886	-0.1	-1.08	11.37	-0.85	1.65
30	-1187.74	-0.06	0.22	8.79	-0.81	2.36
40	-1949.33	0.09	2.45	6.05	-0.53	4.74
50	-1661.5	-0.22	2.89	-0.81	-1.13	5.11
60	-1639.9	-0.38	2.38	-1.5	-1.71	3.18
70	-1566.18	-0.11	0.55	9.1	-1.61	1.14
80	-1416.43	0.16	-1.83	32.15	-1.03	0.46
90	-935.55	0.14	-2.76	46.75	-0.69	0.86
100	-601.19	-0.12	-3.06	43.72	-1	1.97

3.2.4 Results

3.2.4.1 Tekscan Load and Contact Pressure results

The applied contact load and the load measured by the tekscan sensor at each point of the gait cycle was recorded for both Test 1 and Test 2 (Table 3-3). The comparison of these values shows that during Test 1, the Tekscan sensor measured loads different from the simulator applied load. This difference between values was smaller during Test 2 but did appear to be affected by the alignment setup of the total knee replacement.

Table 3-3: Percentage difference between simulator applied load and Tekscan sensor measured load. Includes 101 (test 1, repeat 1), 102 (test 1, repeat 2) and 201 (test 2, repeat 1)

	Test 1			Test 2			
Gait Point (%)	**MA 102**	**MA 201**	**PSA 101**	**MA 101**	**MA 201**	**PSA 101**	**PSA 201**
0	16%	9%	14%	-3%	-6%	12%	-1%
10	23%	22%	23%	14%	17%	31%	15%
20	24%	24%	27%	7%	6%	23%	15%
30	43%	27%	36%	2%	1%	19%	10%
40	70%	35%	37%	1%	-2%	7%	4%
50	31%	27%	35%	-2%	-2%	5%	6%
60	40%	34%	28%	5%	1%	13%	13%
70	33%	32%	33%	6%	3%	18%	19%
80	42%	33%	40%	14%	9%	17%	16%
90	44%	29%	32%	8%	7%	20%	11%
100	38%	28%	21%	2%	2%	15%	7%

For both mechanical alignment and patient specific alignment, Test 2 measured higher contact pressures than Test 1 which shows that there may be an inherent variability between sensors. There was also damage incurred on Sensor 1 early in Test 1 due to the experimental nature of securing the sensors to the tibial insert surface. Therefore, the results of Test 1 and Test 2 were analysed independently.

The contact pressure maps in Figure 3-11 show the heat maps of the Tekscan sensor (scale shown in Figure 3-10) at 10% intervals of the gait cycle from 0% to 100% for MA and PSA kinematic conditions for Test 2 measurement repeat 2. The plots were created using the exported .csv files of the I-Scan movie file and were recreated in .html files using R code. The heat map plots show the movement of the contact area over the surface of the tibial insert as the input kinematics changed over the gait cycle intervals (Figure 3-11). The top of the plots is the posterior part of the insert, the left plot is the lateral compartment and the right is the medial compartment. The plots clearly show the distribution of the contact pressure between the two compartments depending on the stage of the gait cycle. Grey results show that there was no contact pressure pick up in the measurement.

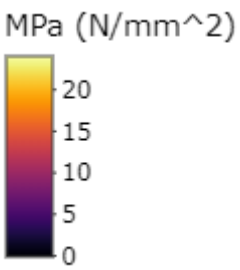

Figure 3-10: Contact pressure heat map scale

Measurement Point (%Gait Cycle)	Test 2 – Repeat 2			
	MA		PSA	
	lateral	medial	lateral	medial
0%	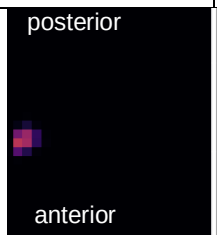	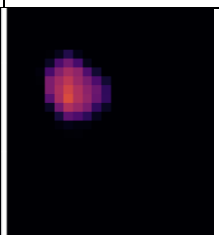		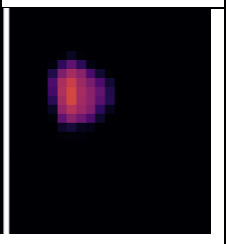
10%	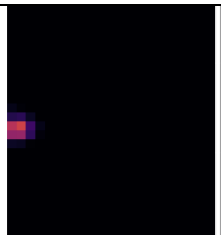	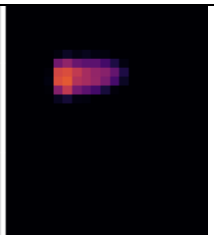	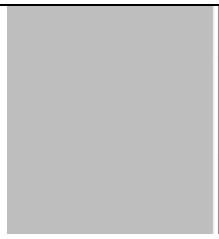	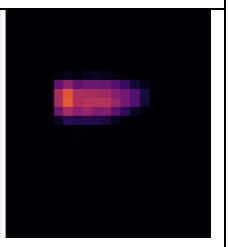
20%	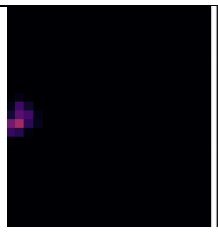	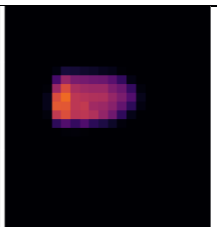		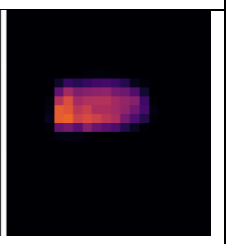
30%	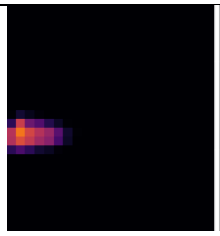	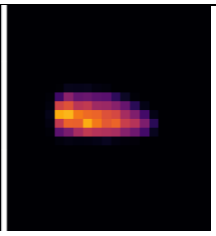	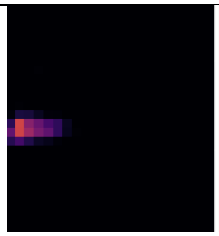	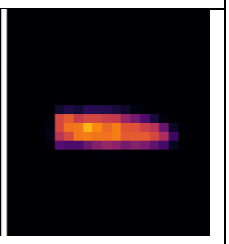
40%	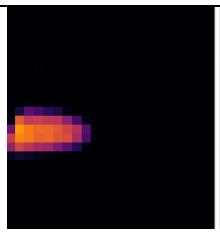	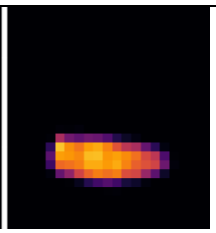	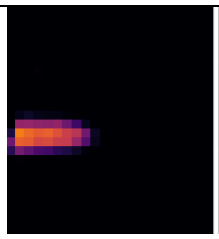	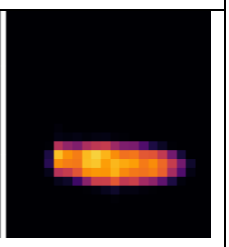
50%	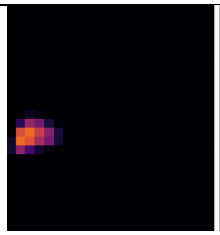	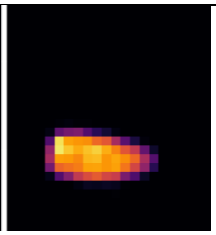	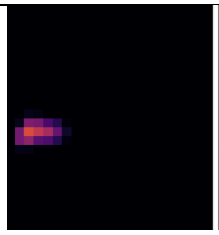	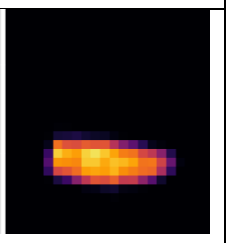
60%	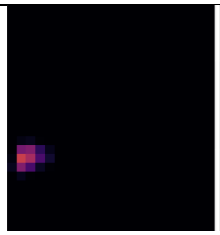	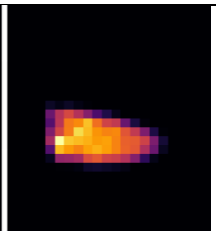	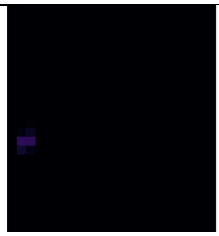	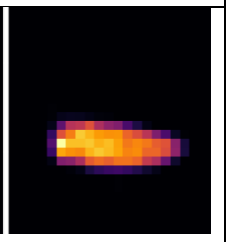

Measurement Point (%Gait Cycle)	Test 2 – Repeat 2			
	MA		PSA	
	lateral	medial	lateral	medial
70%	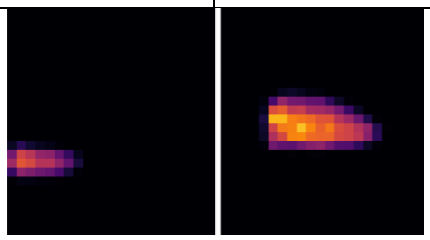		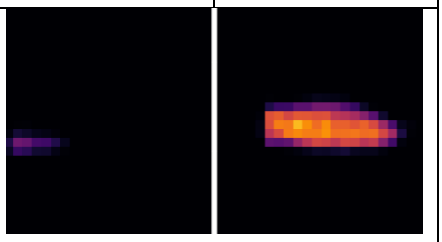	
80%	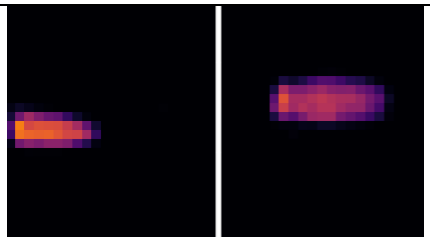		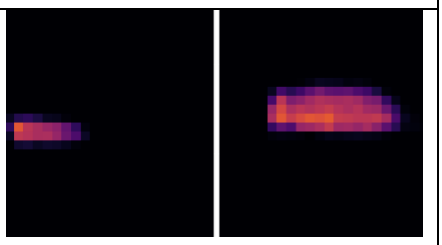	
90%	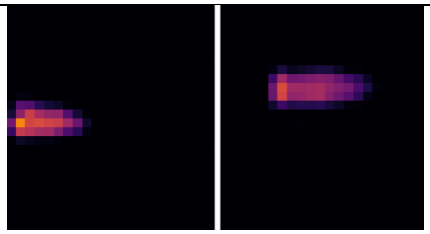		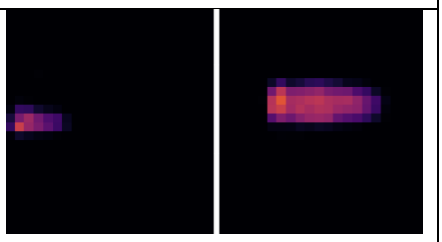	
100%	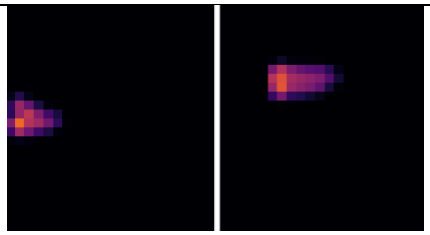		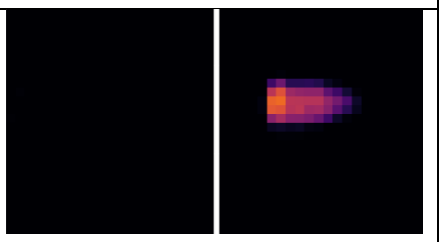	

Figure 3-11: Test 2, repeat 2 contact pressure maps of MA and PSA over all 11 fixed points of the gait cycle. Greyed results represent no contact pressure on that sensor pad.

3.2.4.2 Mechanical Alignment Compartment Contact Pressures

The medial and lateral compartment peak contact pressures (MPa) measured by the Tekscan sensor during Mechanical alignment Test 1 are shown in Figure 3-12. The same comparison for Test 2 results are shown in Figure 3-13. The results from Test 1 show that at 0% of the gait cycle peak pressure started between 5.8MPa and 8.1MPa. The pressure on the medial compartment increased initially until 50% of the gait cycle and then decreased, until a peak pressure around 10MPa for 80%, 90% and 100% of the gait cycle. In comparison, the peak pressure on the lateral condyle decreased at 10% and 20%, followed by a gradual increase in peak pressure to 70% of the gait cycle which reached the highest peak pressure (16.5MPa) of either

compartment during the study. The results from Test 2 showed at 0% of the gait cycle a peak pressure on both compartments between 10MPa and 15MPa. The medial compartment peak pressure increased up to a value of 24.2MPa at 60% followed be a decrease in pressure to around 15MPa at 80%, 90% and 100%. The lateral compartment peak pressure during Test 2 decreased to a value of 10.4MPa at 20% and then increased to 18.7MPa at 40%. Subsequent measurements between 50% and 100% of the gait cycle ranged from 12.9MPa to 17.8MPa.

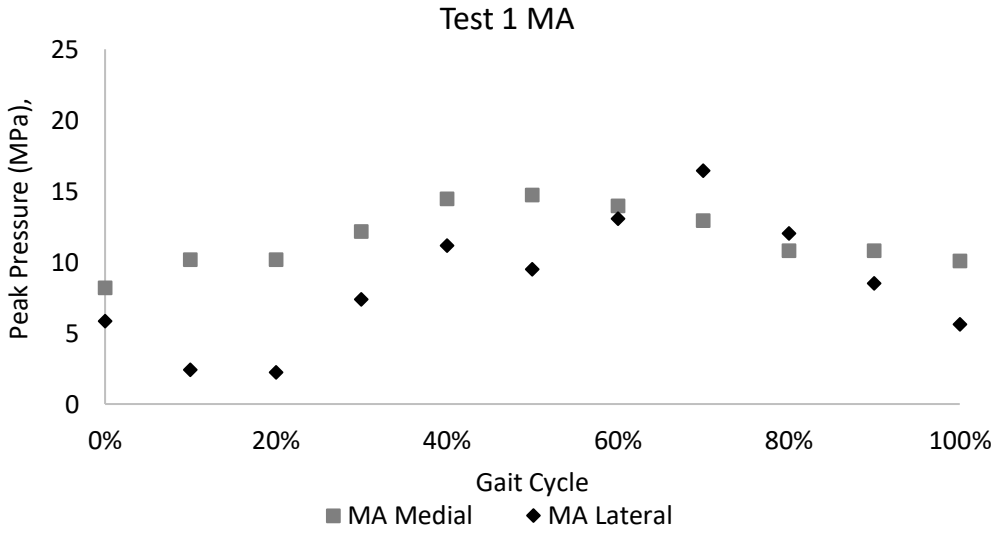

Figure 3-12: Peak Contact Pressure (MPa) for MA Test 1 medial and lateral compartments.

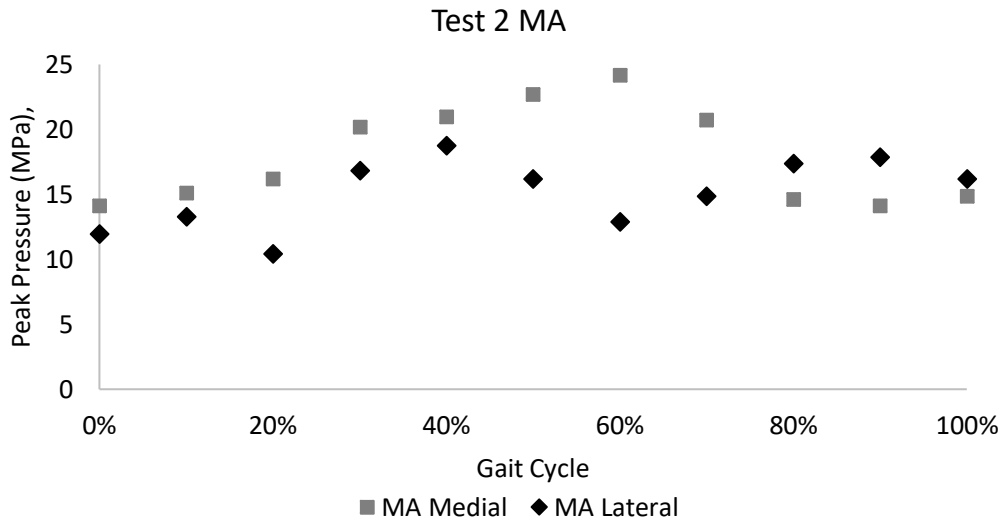

Figure 3-13: Peak Contact Pressure (MPa) for MA Test 2 medial and lateral compartments.

3.2.4.3 Patient Specific Alignment compartment contact pressures

Figure 3-14 and Figure 3-15 show the difference between compartment measured peak contact pressures for Test 1 and Test 2 PSA respectively. During Test 1 PSA the peak contact pressure on the medial compartment reached a maximum of 16.5MPa at 40% and minimum of 9.5MPa at 20%. After 40% the peak contact pressure continuously decreased in value to 10.5MPa 100%. The peak pressure on the lateral compartment reached a maximum of 9.9MPa at 40% and a minimum of 0MPa at 10% and 100% positions. The lateral compartment peak pressure varied throughout the gait cycle positions with an initial decrease to 10% followed by an increase to 40%, a decrease to 60%, a second increase to 80% and a final decrease to 0MPa at 100%.

During Test 2 of the PSA setup condition, both compartment peak pressures had a value of 13.1MPa at 0% and 14MPa at 80%. Between these gait positions the peak pressure of the medial compartment was continuously larger in value than the lateral compartment. The lateral compartment had a minimum value of 0MPa at 10% and 100% gait positions compared to a peak value of 16.2MPa at 40%. The medial compartment, in comparison, had a minimum value of 13.1MPa at 0% and a maximum value of 22.7MPa at 60%.

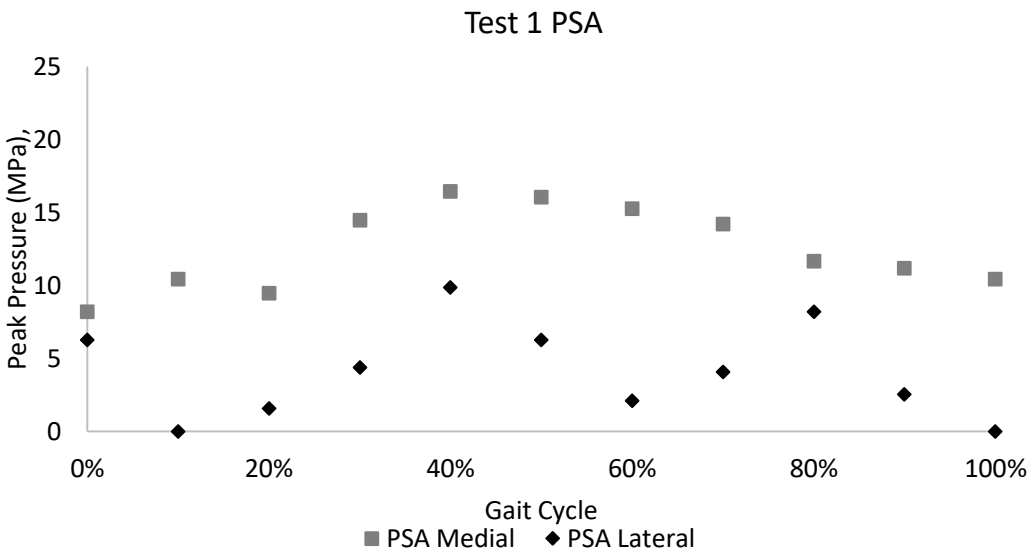

Figure 3-14: Peak Contact Pressure (MPa) for PSA Test 1 medial and lateral compartments.

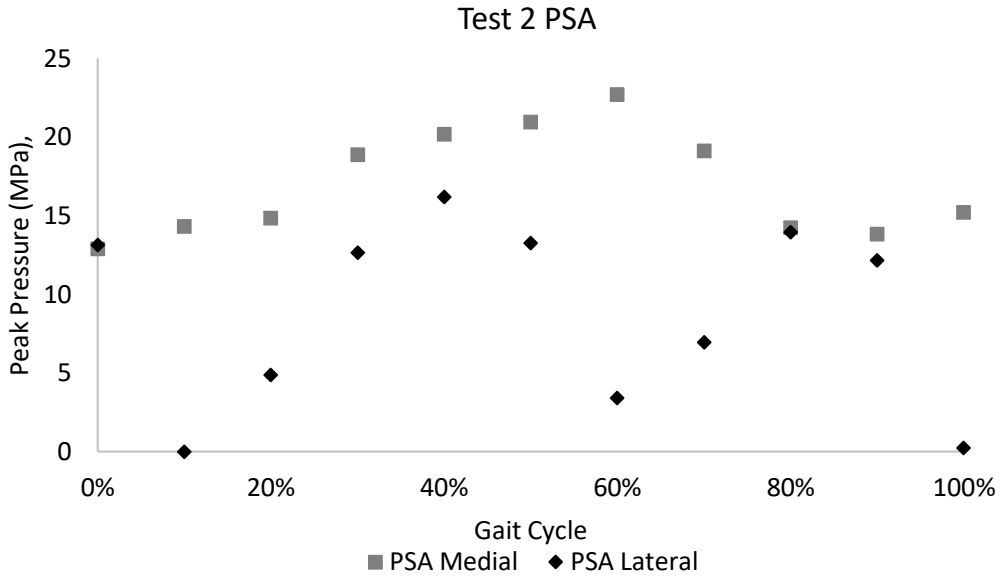

Figure 3-15: Peak Contact Pressure (MPa) for PSA Test 2 medial and lateral compartments.

3.2.5 Discussion

The peak contact pressure values recorded in this study show that overall, the contact pressure in Test 2 reached higher peak values than Test 1. The results also show that in PSA, there are points of the gait cycle where only the medial compartment is loaded. These preliminary results show that the peak contact pressure values differ between the two compartments and that the values are dependent on the position of the gait cycle.

Sensor-to-sensor variability was assessed in this study by comparing the differences between the loads measured by the load cell at the samples and the load recorded by the Tekscan sensor during the measurement. Sensor 1 was secured and removed from the bearing more than sensor 2 as the methodology for securing the sensor on the bearing was developed. This process of using double sided tape to secure the sensors caused damage to the sensels which also affected the accuracy of the sensor measurements. There was only one repeat of Sensor 1 in PSA due to sensel dropout and there was no recorded contact pressure for certain sensels due to damage. Furthermore, this study showed that it was important to calibrate the sensors regularly to ensure that the error of the sensels is accounted for. It may therefore be useful to find an alternative method of securing the sensors to the surface so that they are not damaged when being transferred between surfaces. Further method development should investigate alternate methods for positioning the sensors in the study setup.

3.3 Preliminary Study 2 - Prosim Simulator Total Knee Replacement method development

3.3.1 Rationale

Preliminary Study 1 showed that joint simulators can be used effectively to load total knee replacements in fixed positions to determine contact pressures using Tekscan sensors. The methods developed to measure the contact pressure of the total knee replacement bearing on the AMTI ViVo simulator were adapted to be completed on the ProSim electromechanical knee simulator. Due to the differences between the two simulators this required different fixtures and positioning control methods so a second preliminary study was completed to investigate these variables.

The objectives of Preliminary study 2 include:

- Adapt the calibration procedure into a refined methodology specific for the ProSim simulators with improved repeatability of measurements.
- Determine an appropriate method for positioning the sensor on the tibial insert component to prevent sensor damage caused by removal of the sensor from the tibial insert bearing surface.
- Standardise the appropriate timing for the sensors to settle before a measurement was taken.
- Establish a method of applying the fixed position inputs to the simulator to position the components, taking into account the capabilities of the ProSim simulator with 4 actively controlled degrees of freedom

3.3.2 Materials

3.3.2.1 Calibration Materials

Studies were completed on one station of a ProSim 6-station knee simulator to develop a repeatable calibration method using the plates and disks created in the AMTI study. Additional equipment was added to remove the need for double-sided tape which was damaging the sensors and making the study expensive.

The study was carried out with the same equipment as the AMTI ViVo study with a few exceptions. A standard ProSim tibial base fixture was used to create a flat surface and support for the base of the calibration fixture. A femoral dummy fixture with a typical femoral component radius typically used for flexion-extension and axial

loading movements only in trial setups, was used as a fixture to apply the force to the top of the calibration setup. The fixture was used because it was easily secured into the flexion rocker of the simulator. A flat plate was positioned on the top of a tibial fixture to create a flat surface for the calibration setup.

An alternate method was trialled using Vaseline between a piece of polythene mesh and the metal fixture, adapted from work published measuring contact pressures of cadaveric ankles, to evenly distribute the contact load and remove any points of concentrated pressure [142]. The Tekscan 4000 sensor was placed on top of the polythene mesh and connected to the Tekscan data handle (Figure 3-16). The software used to take measurements was Tekscan I-Scan 6.03.

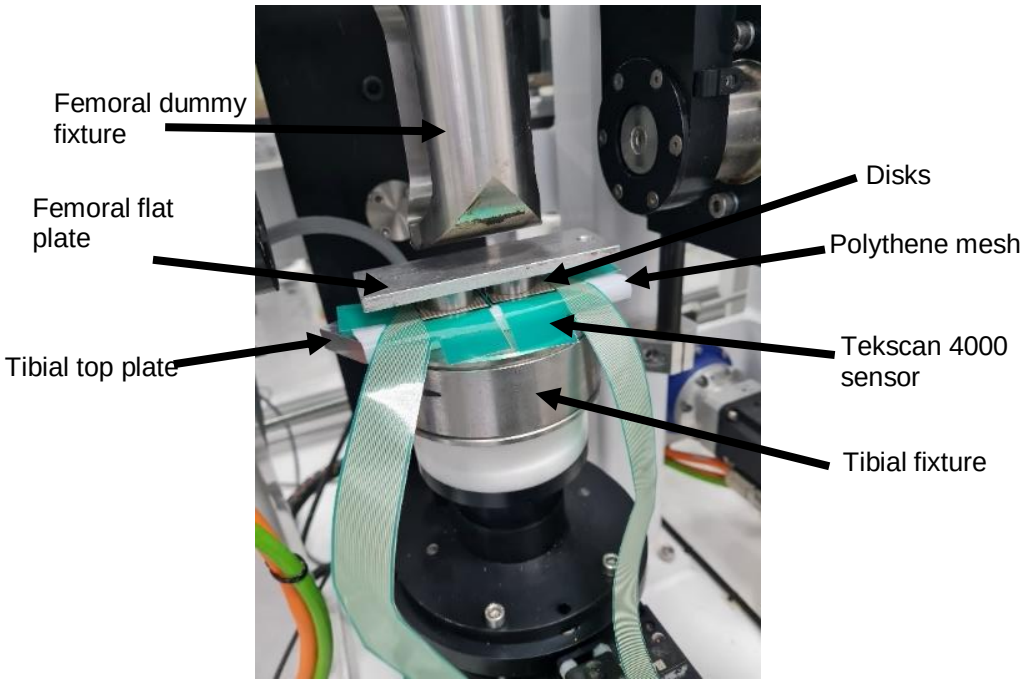

Figure 3-16: Tekscan Prosim Calibration Setup

3.3.2.2 Total Knee Replacement Setup Materials

Setup of the total knee replacement study required one Attune femoral component cemented onto an Attune femoral fixture, one Attune tibial tray cemented into a standard ProSim tibial fixture, and one Attune AOX tibial insert. This setup was adapted from the setup used in the AMTI VIVO study to remove the use of adhesive tape which caused damage to the sensors. In this study, a thin layer of Vaseline was applied to the superior surface of the tibial insert and a piece of polythene mesh was placed onto the same surface and smoothed into the condyles with caution not to fold the material and to remove any air bubbles which would affect the contact pressure.

The Tekscan 4000 sensor was placed between the two components and the femoral component lowered into place using the station load spring (Figure 3-17). The sensor was connected to a Tekscan data handle. Tekscan I-Scan 6.03 software was used to take measurements from the sensors while they were loaded at different kinematic positions.

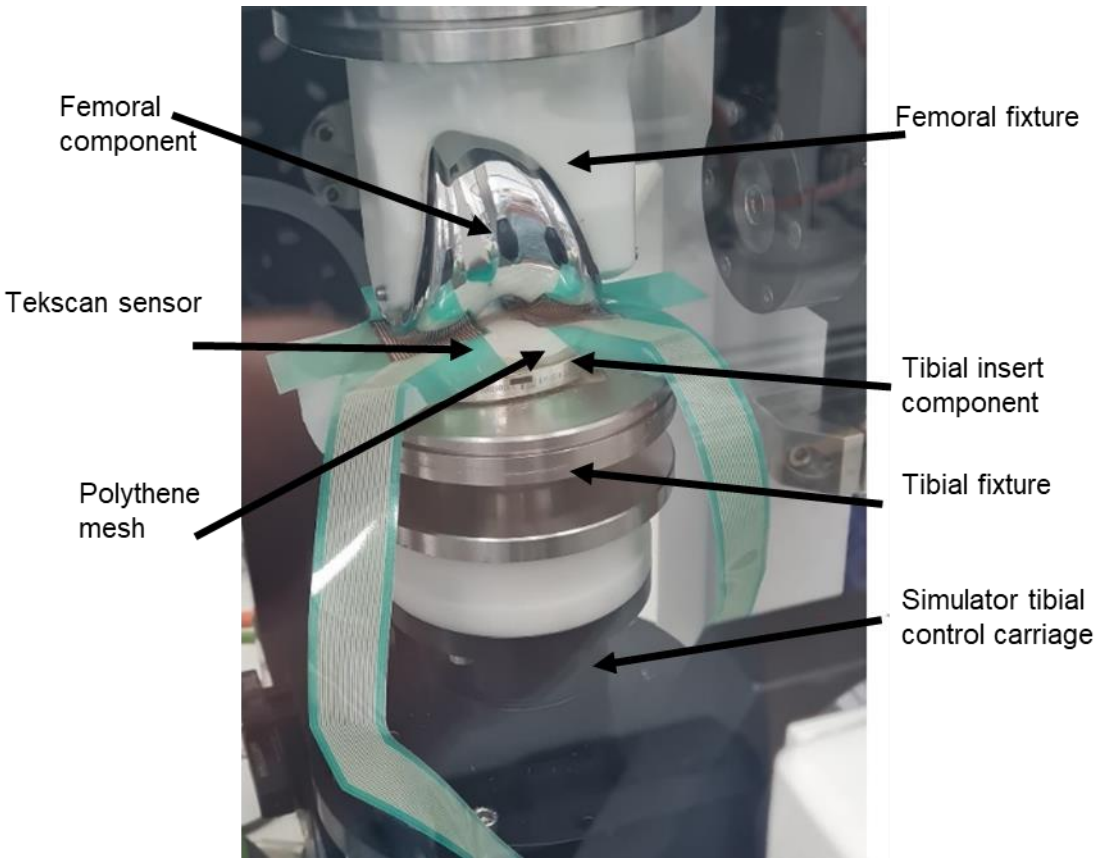

Figure 3-17: ProSim Total Knee Replacement Tekscan setup

3.3.3 Methods

3.3.3.1 Calibration Methods

The calibration procedure was completed using the I-Scan software to take a reading from the Tekscan sensor and the ProSim software to apply a load to the setup. A two-point load calibration curve was created at 500N and 3000N using Mid1 sensitivity. The calibration fixtures were assembled on the station with the Tekscan sensor positioned below the two stainless-steel calibration disks. The ProSim simulator was initialised and “fixed demands” was used to apply a 500N load to the station. The I-Scan software “calibration” feature was used to adjust the sensitivity of the sensors based on the contact legend spectrum which indicated high pressure (red) and low pressure (blue) areas. The appropriate sensor sensitivity was

determined to be “Mid-1” which was applied to all measurements. The first pressure measurement was recorded after 30s of being loaded at 500N by the joint simulator. The ProSim simulator was then used to apply a 3000N load and the I-Scan software took a second pressure measurement after another 30s of being loaded at 3000N. The pressure that the sensor was calibrated to was around 30MPa, slightly higher than the maximum contact pressure expected from the gait cycle study. If the recording wasn’t reaching this reading it indicated that there was too much Vaseline or the disks weren’t positioned on the sensors correctly.

3.3.3.2 TKR Setup

One ramp cycle included six measurements with the components at 0° flexion and the components loaded axially at the following loads; 50N, 100N, 500N, 1000N, 2000N, 3000N. For each measurement, the load was applied and a snapshot was taken on the I-Scan software after a 30s interval to allow the sensors to relax. “Ramp Up” refers to six consecutive measurements increasing the load from 50N to 3000N, “Ramp down” refers to six consecutive measurements decreasing the load from 3000N to 50N. This method was used to remove any potential error caused by gradually adding load to the sensor versus gradually reducing it and any effects this would have on the pressure. It was also used so that both 50N measurements and 3000N measurements were taken after a calibration of the sensors so that there was a fresh layer or Vaseline and minimal drift in the calibration.

3.3.4 Results

The average contact pressure measured by the Tekscan equipment in preliminary study 2 showed little difference between subsequent ramps (Figure 3-18). There was also little difference between output contact pressures caused by reapplying Vaseline between ramps (Figure 3-19). These sets of results also show that the setup of the TKR bearing on the Prosim simulator with the Tekscan sensors showed an increase in measured contact pressure with increase in applied load. Overall, these sets of results show that the difference in contact pressure measured is repeatable in the current setup and that twelve contact pressure measurements can be taken between applying Vaseline to the setup.

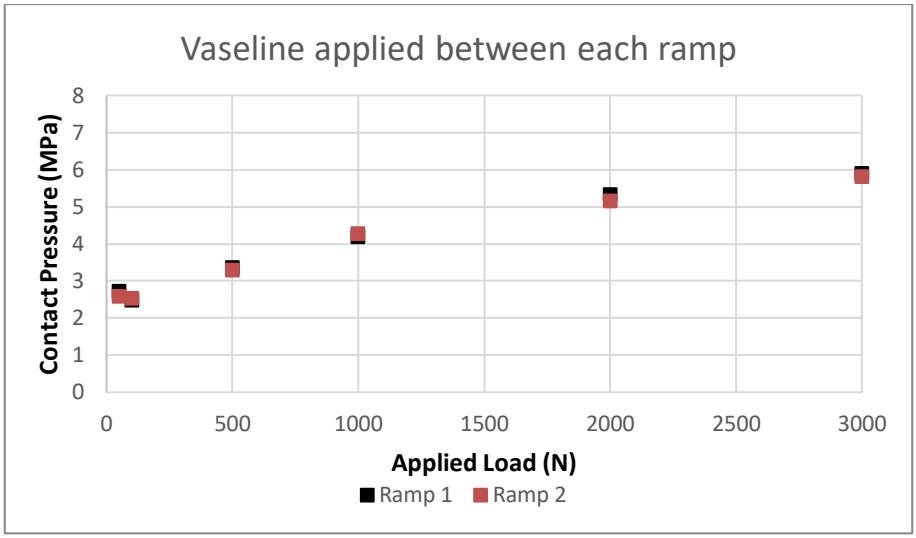

Figure 3-18: Output contact pressure of applied load to TKR bearing with Vaseline applied after 6 measurements

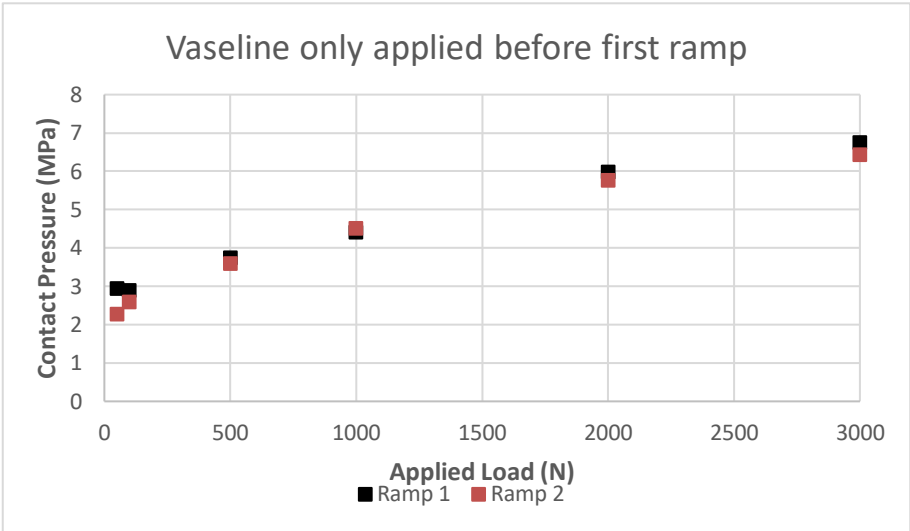

Figure 3-19: Output contact pressure of applied load to TKR bearing with Vaseline applied after 12 measurements

The additional study to investigate the effect of changing the frequency of calibration between average contact pressure values of the TKR bearings, these results are shown in Figure 3-20. The results indicate that reducing the frequency of repeating calibrations between measurements, up to 18 repeats, has little or no effect on the repeatability of the contact pressure measurement.

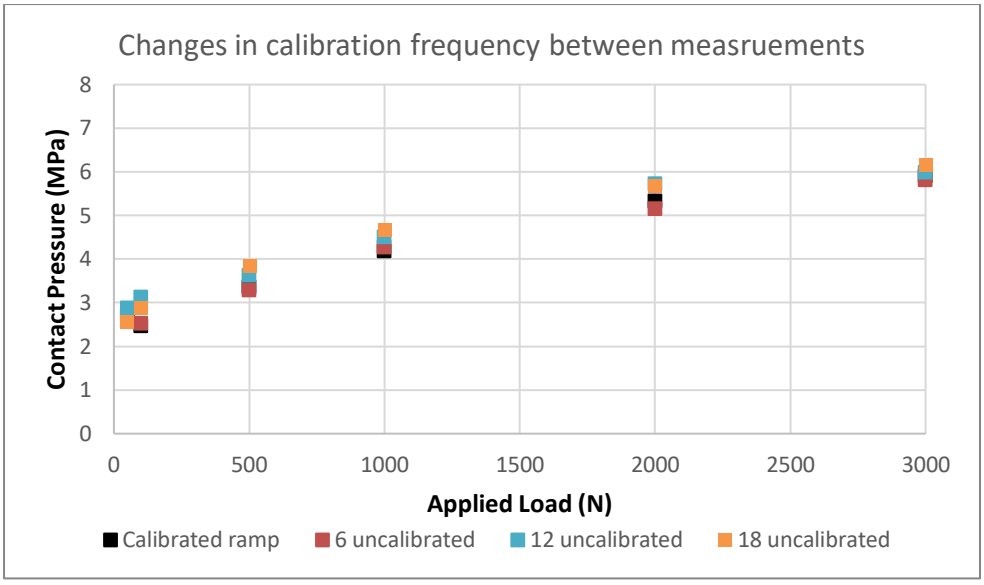

Figure 3-20: Output contact pressures of applied load to TKR bearing with a reduced frequency of calibrations between measurements, including each ramp, 6 ,12 and 18 additional measurements.

3.3.5 Discussion

The same Tekscan 4000 sensor was used throughout this study without any visible damage to the sensor or sensel dropout. This shows that the method of placing the sensor on the tibial insert bearing surface with Vaseline and polythene mesh helped to keep the sensors in good condition while allowing good contact pressure pickup. The main limitation to this method is that the sensor was not secured on the surface which resulted in slight movements of the sensor placement when the load was applied. In this set of preliminary studies, any movement of the sensors as a result of not being secured in position does not appear to have had any noticeable impact on the repeatability of measurements. This Vaseline setup method will be used in further studies using the Tekscan sensors on the ProSim simulators.

The additional investigations in this preliminary study have shown that increasing the number of repeated measurements between calibrations of the sensors did not impact the repeatability of the measurements.

3.4 ProSim Attune Baseline Tekscan Study

3.4.1 Rationale

Preliminary studies have been completed to develop procedures for calibrating Tekscan sensors and measuring the contact pressures of a total knee replacement. The findings of these studies will be used to develop a procedure in this section for measuring the contact pressure of a total knee replacement bearing at fixed positions of the gait cycle, using a ProSim joint simulator. Only contact stresses were measured during this study, contact area was not included. This was as a result of the pressure sensors chosen for the study, Tekscan sensors, which are optimised for measuring contact stresses. The limitations of the methodology discussed previously, which highlighted challenges in securing the Tekscan sensor on the tibial insert bearing, meant that it was not possible to accurately measure the contact area in this study. The results of this section will provide insight into the contact pressure of the Two studies were completed on the total knee replacement setup which include:

- A flexion study to investigate the sensitivity of the sensor setup to changes in flexion and the contact pressure output
- A gait cycle study to determine the contact pressure values at a range of positions throughout the gait cycle.

3.4.2 Methods

3.4.2.1 Study 1 - Flexion

An initial study was completed where the flexion angle of the femoral component was varied from -30° to +30° in steps of 10° at a range of loads (50N, 100N, 500N, 1000N, 2000N, 3000N). The flexion angle was adapted from the flexion angle range of 0° to +60° stated in ISO 14243-2009 [112] due to the capabilities of the simulator. The simulator input profile was limited to -30° to +30° which was accounted for when developing the femoral component fixture with a built in 30° flexion angle. For each measurement the components were secured in the ProSim simulator using fixtures, “fixed demands” was used on the software to send the femoral component to the desired flexion angle, and then the load was also applied using “fixed demands” for the measurement. Once the sensor was loaded, a snapshot was taken of the contact pressure after a 30s delay to allow the sensors to settle. An ASCII file for each measurement was exported. This method was repeated to n=6 on the same bearing samples.

3.4.2.2 Study 2 – Gait Cycle

The gait cycle study was completed with the components positioned on the simulator using fixtures and with two degrees of freedom active on the tibial components (anterior-posterior translation and internal-external rotation), and with two degrees of freedom active on the femoral component (flexion-extension and axial force). The tibial component carriage was uncontrolled in abduction-adduction and left free to move in response to loads. Medial-Lateral displacement of the tibial insert was fixed in a neutral position and not free to move during the study. Before the kinematic positions were applied to the components, the sensor was placed between the femoral component and the polythene mesh, which was placed with Vaseline on top of the tibial insert.

The Tekscan gait cycle study input kinematics were determined from the outputs of the baseline wear simulation on the ProSim Simulator which was simulated in load control. The output displacement values for anterior-posterior translation, internal-external rotation, flexion-extension angle and axial load were calculated from a 100-cycle average (with ±1 standard deviation) of all six loaded stations of the wear study (Table 3-4).

Table 3-4: Tekscan gait study input values at 10% intervals from 0%-100% for 4-degrees of freedom

Gait %	Axial Force (N)	Flexion-Extension (°)	Anterior-Posterior (mm)	Tibial Rotation (°)
0	328.9	0.0	-0.7	1.6
10	1880.5	12.0	-0.9	-0.5
20	1506.9	15.1	-0.7	-0.2
30	1074.2	9.3	0.2	3.5
40	2158.0	5.2	-0.1	4.0
50	1837.7	16.0	0.9	5.2
60	191.9	39.2	3.6	6.8
70	184.4	56.9	-4.0	-1.5
80	160.5	48.6	-1.8	0.0
90	251.3	20.2	1.0	1.4
100	252.2	0.1	-0.6	1.6

Using the ProSim software, the femoral component was sent to the desired flexion position, followed by the anterior-posterior position of the tibial insert and finally the internal-external rotation position of the tibial insert. Once all kinematic positions were applied to the components for the measurement, the desired axial force was applied to the femoral component. A 30s settling period was allowed before the snapshot of the resulting contact pressure was taken and the ASCII file was exported.

The exported ASCII files from I-Scan were combined into a CSV file for each ramp (i.e. 50N-3000N for the flexion study and 0%-100% for the gait cycle study). An R script was used to read the values of contact pressure for each sensel in these files and to generate a map of the contact pressure and a table of outputs for average contact pressure, peak contact pressure and contact area. The average contact pressure (± 1 standard deviation) for n=6 repeats was determined by averaging the values of all the sensels in the scan which recorded a value.

3.4.3 Results

3.4.3.1 Study 1 - Flexion

The flexion study average contact pressure results show that the results varied by around 1.5MPa to 2MPa between the different flexion angles (Figure 3-21). In general, the larger angles of flexion resulted in higher contact pressures and lower angles of flexion resulted in lower contact pressures. The average contact pressures were affected by the applied load value with lower contact pressures at 50MPa between 2-4MPa compared to between 7.5-10MPa at a 3000N. The results showed that the sensors and setup were responsive to changes in applied load and kinematic positioning of the femoral component.

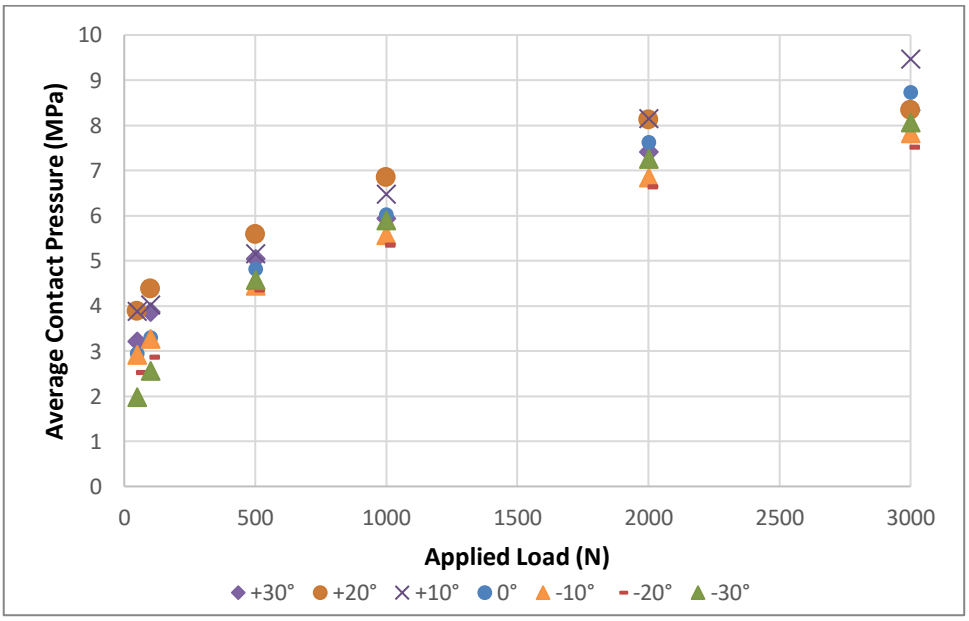

Figure 3-21: Average Contact Pressure at an applied load with varying femoral flexion angles

3.4.3.2 Study 2 - Gait Cycle

The output contact pressure heat maps were plotted where one box is one sensel and the contact pressure (MPa) colour coded values were normalised over the 11 gait cycle loading points (Figure 3-22). The pressure map was split into outputs on the lateral condyle and medial condyle and one heat map was generated for each measurement which visually shows how the contact pressure and size varied over the gait cycle (Figure 3-23: Attune baseline contact pressure heat maps for one gait cycle at 10% intervals.Figure 3-23).

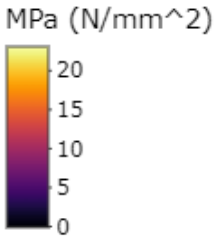

Figure 3-22: Attune baseline Tekscan heat scale

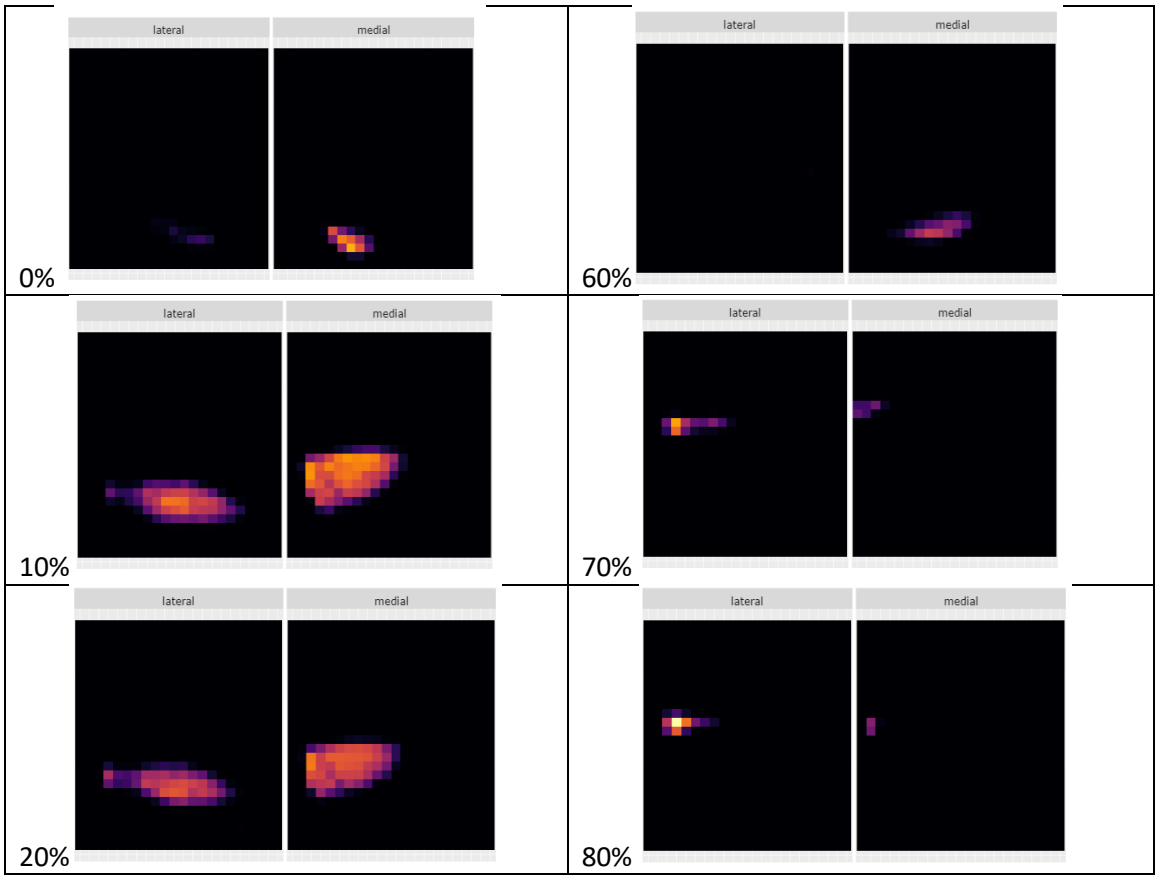

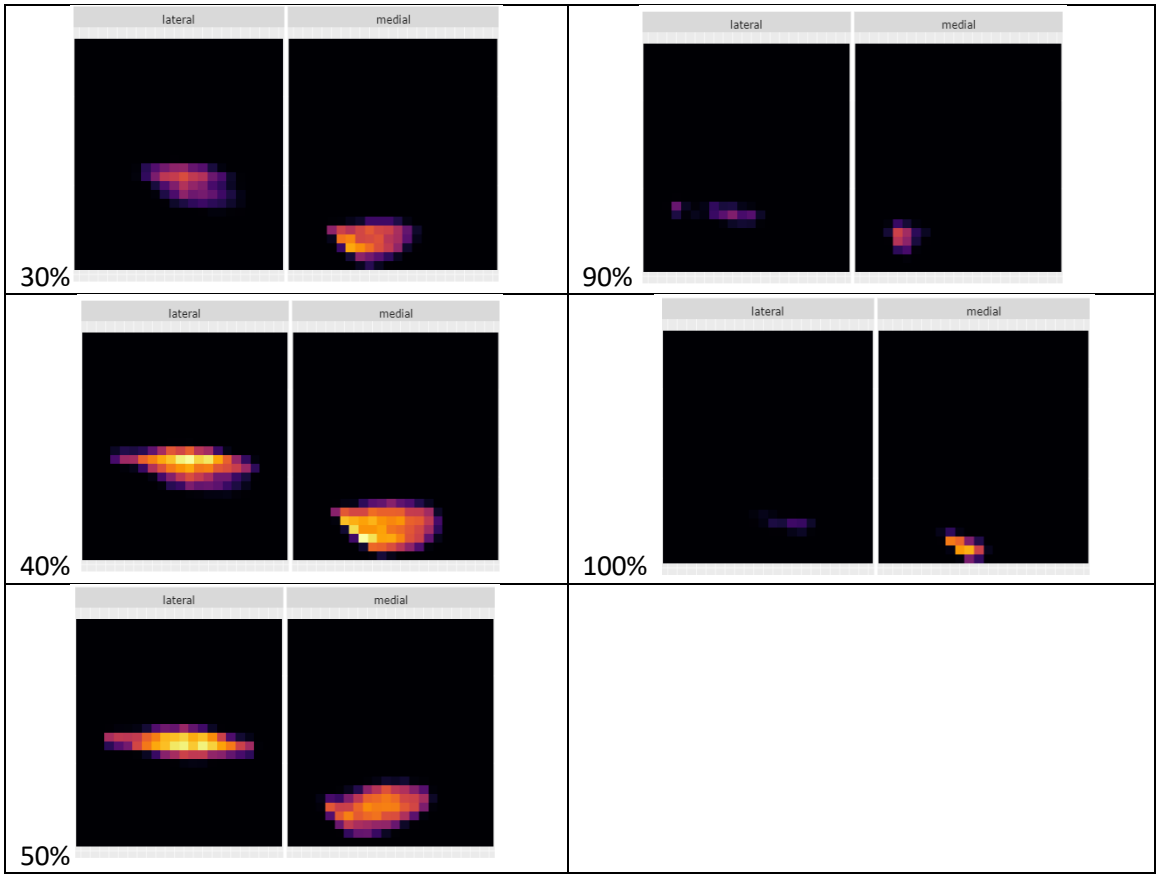

Figure 3-23: Attune baseline contact pressure heat maps for one gait cycle at 10% intervals.

The average contact pressure in response to varying positions in the gait cycle were responsive to changes in load and component positioning. The maximum contact pressure was 7.31MPa at 40% of the gait cycle. The lowest contact pressure was 2.26MPa at 60% of the gait cycle where the load cycle reaches its minimum point (Figure 3-24).

The results were split into average contact pressure for the medial and lateral compartments to understand how the contact pressure shifted between the compartments during the gait cycle positions (Figure 3-25). There was a large difference between the starting average contact pressure at 0% gait cycle position which was 5.7MPa on the medial compartment and 2.3MPa on the lateral compartment. Both compartment contact pressure increased at 10% followed by subsequent decreases at 20% and 30%. The medial compartment had a maximum value of 8MPa at 40% and a minimum of 3.4MPa at 80%. In comparison, the lateral compartment had a maximum value of 6MPA at 50% followed by a minimum of 0.6MPa at 60%.

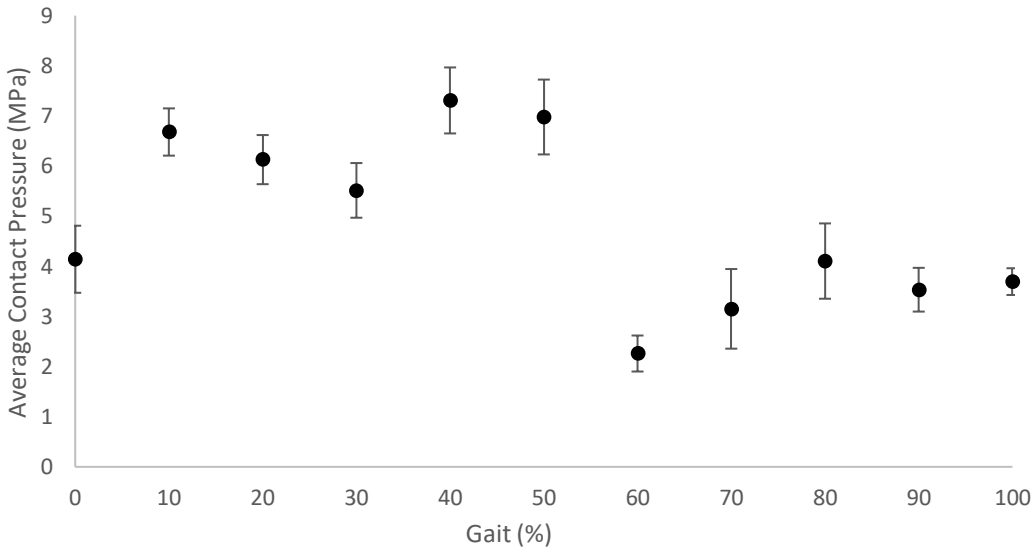

Figure 3-24: Average ±1 standard deviation contact pressure at 10% intervals of the gait cycle with input load of an ISO 14243-1:2009 standard walking gait cycle.

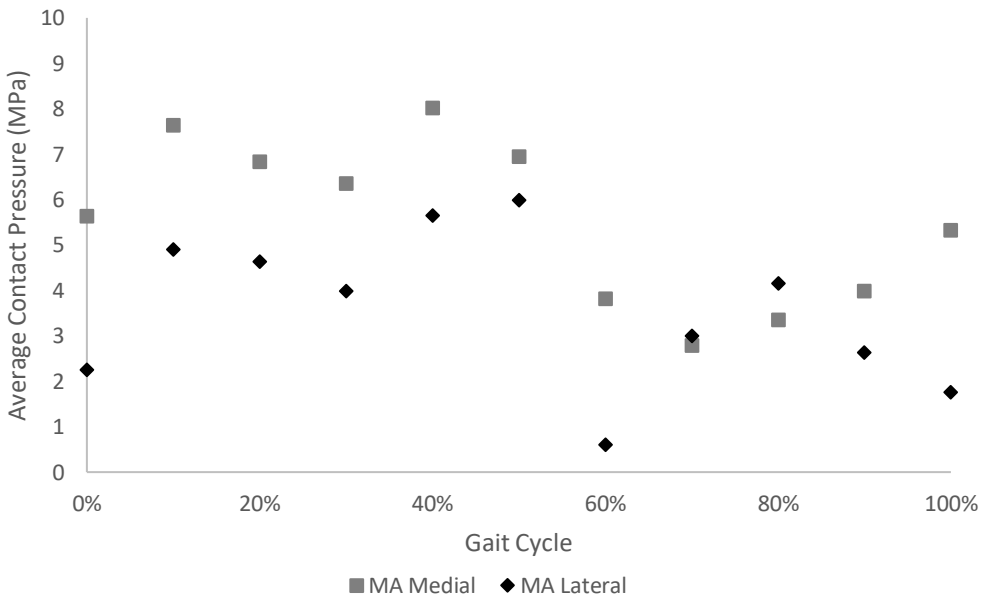

Figure 3-25: Average Contact Pressure (MPa) of medial and lateral compartments measure by the Tekscan sensor on ProSim simulator in Mechanical alignment

3.4.4 Discussion

The ProSim Attune Baseline Tekscan Study was able to combine methods developed in previous preliminary studies to refine a test protocol capable of measuring contact pressures on a tibial insert bearing surface.

The study has shown an insight into how the contact pressure values change with kinematics, the value of applied load, and how they differ between the medial and lateral compartment. The flexion study showed that an increase in load increased the average contact pressure for all angles of femoral flexion. The results also showed a small range of average contact pressures between the flexion angles. The contact pressure maps created from the exported files from Tekscan show how the contact pressure on the tibial insert surface changes throughout the 10% intervals of the gait cycle.

3.5 Measuring Contact Mechanics Using Pressure Sensors Discussion

The methods developed in this study were novel for examining the contact pressures of total knee replacement bearings using a ProSim Simulators at intervals of the gait cycle with 4 controlled degrees of freedom. The average contact pressure values ranged from 2.26MPa to 7.31MPa and were dependent on the kinematic positions of the gait cycle and applied load. There was higher contact pressure measured on the medial compartment in comparison to the lateral compartment at all gait cycle intervals except 70% and 80%. Investigations into the effect of flexion angle and load on the average contact pressure, with all other kinematic positions set to neutral, showed that larger angles of flexion generally resulted in higher contact pressure outputs and that higher loads resulted in larger contact pressure, although this relationship was not linear.

A series of preliminary investigations were completed as part of the objectives of this study to develop repeatable experimental methodologies using pressure sensors to reliably investigate the effect of load and kinematics on the contact mechanics of TKR bearings at intervals of a gait cycle. Tekscan was chosen as the appropriate sensor equipment for this study as a result of a review of literature. The literature found that Tekscan sensors are more accurate at measuring contact stresses and Fuji Film sensors are more accurate at measuring contact areas in comparison the contact stresses [141]. However, Fujifilm has been found to be less effective at measuring contact areas of highly conforming bearing surfaces [145]. As a result, Tekscan

sensors were chosen as the most appropriate for this experimental study due to the focus on measuring contact stress. Further work to develop methodologies of using Fuji Film in addition to the Tekscan sensors may facilitate evaluating the effect of kinematic inputs on the contact area of Attune AOX total knee replacements.

A calibration procedure was developed which could be repeated on different sensors to set up the pressure range to convert the raw measurement values. Regular calibration of the sensors reduced error in the measurements later in the study by neutralising any drift. A non-linear two-load calibration procedure was adopted because the experimental measurements would involve a large load range, it was important that the sensor was accurate at both low and high loads.

As the methodology was developed, it was found that securing the sensors with tape damaged sensels quickly which in turn made results less reliable and became expensive to replace the Tekscan Sensors. As a result, an alternative method of creating a contact surface was developed. In this new method, the sensors were not secured to the bearing surface meaning that contact area could not be determined from this study. However, previous studies investigating the contact pressure of a cadaveric ankle joint used petroleum jelly to lubricate the sensor to reduce shear forces [142]. This method was adapted into this study with the addition of a polythene sheet between the petroleum jelly and Tekscan sensor to preserve the sensor. This setup resulted in repeatable contact pressure measurements with up to 18 measurements between calibration and no damage to the pressure sensor.

Further studies could include repeating the study on additional total knee replacement bearings and using different ProSim simulator stations to complete the study. Furthermore, studies have found that the measured contact pressure is susceptible to surface wear [145]. It may therefore be useful to repeat the Tekscan measurements on samples after a 3 million cycle wear simulation study. Additional steps to improve repeatability of the sensor readings could also be included in further work using a Tekscan equilibrator to apply a pneumatic uniform load [144]. This device preconditions the sensor, normalising the sensitivity of each sensel, which reduces drift and hysteresis. The advantage of equilibrating the sensors would be especially important after increased use of the Tekscan sensors drift of individual sensels becomes more common.

The outlook of this study is for the results to be used to check for agreement between experimental results and computational predictions and to compare the TKR surface contact pressures between mechanical alignment and patient specific alignment. The series of preliminary studies completed in this chapter facilitated a structured

approach to developing methods which were then applied in the final study. The results were analysed at each stage to determine the repeatability of the methods and to adapt the setup where required. As a result, there is confidence in the accuracy of the results presented in the ProSim Attune Baseline Tekscan study and they will be used in future studies to compare model predictions to experimentally measured values.

Chapter 4
Finite Element Methods

4.1 Introduction

Traditional methods of assessing the pre-clinical performance of total knee replacements includes experimental simulations using joint simulators, following guidelines published by international standards. These experimental methods are limited to the capabiities of such simulators which are manufactured to adhere to such standards, and are also expensive in both time and resources. As patient cohorts to total knee replacements become more diverse and the technologies used to implant the components becomes more advanced, the requirements for other methods of pre-clinical assessment to assist these well established experimental methods are essential. Using finite element methods to recreate the experimental simulation setup which can be subjected to the same displacements and forces as in a physical environment, could prove useful in ensuring that a wider patient cohort is accounted for in pre-clinical assessments. The main advantges of finite element simulations are that virtual components can be arranged into complex setups with more extreme inputs without the same limitations as an experimental simulator, and that once the methods are well established, they can process many variables in shorter periods of time and with multiple analyses processed simultaneously.

This chapter outlines the method development of creating a finite element model of a total knee replacement in a setup to replicate experimental methods with ISO-14242-1 inputs to predict output kinematics and contact mechanics. The first part of this model development was to initially create a simplified contact model using simple geometrical surfaces to develop an understanding of how input parameters can be applied to the model, how outputs can be exported from the model and how the results can be analysed to determine the contact mechanics between the two materials under different conditions. Simplified models require less CPU time to complete and therefore studying these variations on less complex geometries reduces the time demands of developing this knowledge.

The aim was to have a reliable total knee replacement model, in good agreement with experimental outputs, which can be used in future work to investigate the effect of surgical alignment variables on the biomechanics of the joint replacement.

4.2 Development of Finite Element Simple Geometry Models

4.2.1 Introduction and Background

4.2.1.1 Hertzian Contact Theory

Hertzian theory, developed by Heinrich Hertz in 1882 [146], demonstrates how the contact of two surfaces is related to their contact area and pressure relationship when a concentrated load is applied to a single point on the top of one surface. For this theory to be valid, the criteria of a rigid metallic solid loaded in contact with a relatively soft elastic component must be met. Since wear can be a function of contact pressure [147], this is an important factor to consider when investigating the tribology of contacting surfaces. In order to apply this theory to understand the interaction between two contacting surfaces, the contact area must be significantly smaller than both the size of each body and the radii of the curvature of the surface(s). Additionally, the surfaces must be assumed to be frictionless, this means that the pressure applied can only be normal to the surface to avoid any frictional effects. Due to this, Hertz theory only models the total contact pressure created and does not account for any changes in forces due to deformation of the surfaces [148].

4.2.2 Cylinder on Plate model

4.2.2.1 Rationale

A Standard Implicit finite element model was developed in Abaqus/CAE 2017 (Dassault Systèmes Simulia Corp., Johnston, RI, USA). To investigate how changes in loads and kinematics impact contact mechanics, a simplified geometry model of a total knee replacement was created using implicit finite element methods. In this simplified model the cylinder replicated the femoral component and the plate tibial component.

4.2.2.2 Setup Methods

The plate dimensions were 70mm length, 70mm width, 10mm height and the cylinder dimensions were 63.5mm diameter, 63.5mm length. Material properties for the plate study were determined from previous finite element models which reported a Young's modulus of 400MPa [149] and Poisson's ratio of 0.46 [150] for Ultra-High-Molcular-Weight Polyethylene (UHMWPE).

A frictionless interaction property with "hard"/"default" normal behaviour was assigned to the contact surface of the two components. The cylinder was assigned

the main (master) surface and the plate the secondary (slave) surface. A constraint was created over the whole cylinder body and was assigned a rigid constraint using a reference point (RP). This RP was used to apply constraints, known as boundary conditions (BCs), and loads to the cylinder. BCs were applied to the bottom of the plate surface to constrain it in all degrees of freedom (translational and rotational) and applied to the cylinder to allow movement only in the y direction (i.e. the direction of the applied load.

An initial displacement step was created to bring the parts into contact by establishing a small (<1MPa) contact pressure. A second 'load' step was created to apply 2.52kN (the maximum axial load under standard walking force control) to the reference point of the cylinder in the y direction as shown in Figure 4-1.

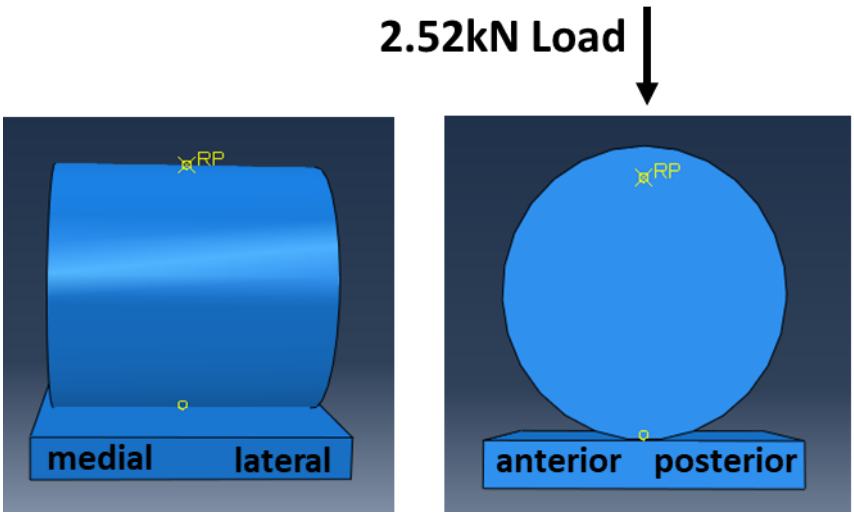

Figure 4-1: Cylinder on Plate model assembly

The output maximum contact pressure (MPa) was determined from the visualisation module. The FEA stress contours on Figure 4-2a show that there was a concentration of pressure where the plate contacts the edge of the cylinder. To resolve the issue of a concentrated pressure at the edges of the cylinder, the cylinder length was increased to longer than the contact length. The cylinder diameter and length was increased to 76mm. Figure 4-2b shows that extending the length of the cylinder past the contact length resulted in the maximum contact pressure at the contact point of the base of the cylinder on plate.

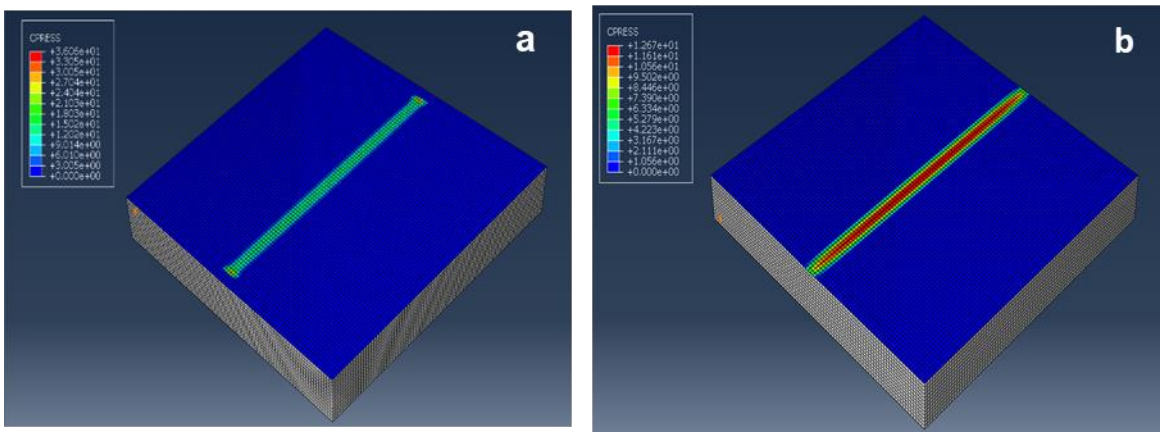

Figure 4-2: Abaqus Cylinder on Plate Model - Plate stress contours a) 63.5mm cylinder length b) 70+mm cylinder length

4.2.2.3 Mesh Convergence Study

A mesh convergence study was completed where both components were meshed at a 1 to 1 ratio. The mesh was gradually refined from a coarse mesh into a fine mesh until the change in the maximum predicted contact pressure was less than ±5% in further mesh refinements. The maximum contact pressure (MPa) was recorded and plotted against the size of the assigned global mesh elements (shown in Figure 4-3).

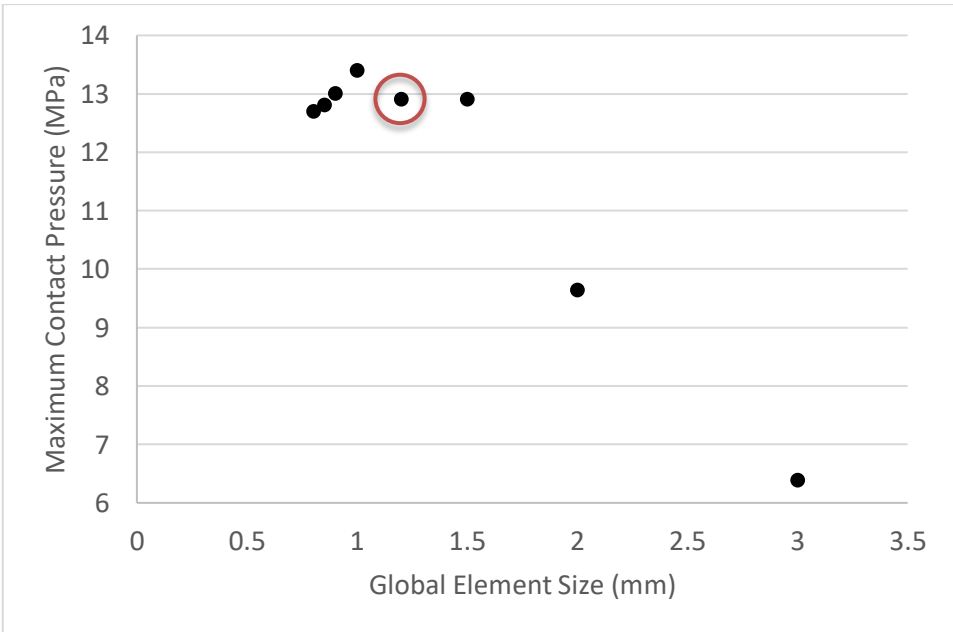

Figure 4-3: Cylinder mesh convergence study with the result for convergence circled in red.

From this convergence study an appropriate global mesh size of 1.2mm was selected with a total number of 272,108 elements for the contact pressure measurement circled in red in Figure 4-3. This value was chosen because all subsequent results for increasing total number of elements did not vary by ±5%. The Hertzian peak contact pressure prediction for the material properties used in this model was 12.4MPa which compares to the value of 12.9MPa predicted by this model setup.

4.2.2.4 Sensitivity Study

A second study investigated the efficacy of the model to predict contact pressure values in agreement with theoretical values calculated using Hertzian contact theory (Equation 4-1, Equation 4-2 and Equation 4-3). The theoretical values of contact pressure for loading a cylindrical object onto a flat plate were determined using the following formulae which is adapted from the formula published by K.L. Johnson (1985) [148]:

$$\frac{1}{E'} = \frac{(1 - {v_1}^2)}{E_1} + \frac{\left((1 - {v_2}^2)\right)}{E_2}$$

Equation 4-1: Young's Modulus – Poisson's Ratio relationship in Hertzian prediction

$$b = \sqrt{\frac{2Fd}{\pi l E'}}$$

Equation 4-2: Semi-contact width (Cylinder on Plate)

$$p_{max} = \frac{2F}{\pi b l}$$

Equation 4-3: Maximum Contact Pressure (Cylinder on Plate)

E1 = Young's Modulus of cylinder E2 = Young's modulus of plate v1 = Poisson's ratio of cylinder v2 = Poisson's ratio of plate F = load on cylinder d = diameter of cylinder l = length of cylinder b = semi-contact width Pmax – Maximum contact pressure

The final step of developing a simplified model to predict the contact pressure of a cylindrical surface in contact with a plate was to investigate the sensitivity of the model to changes in material properties. The values for moderately cross-linked polyethylene XLK found under compression conditions were E = 553MPa and v = 0.32 [119].

Contact pressure values were calculated using the Hertzian equations for a range of values of Young's modulus values and Poisson's ratio values of 0.46 and 0.3, which include the values of different UHMWPE materials reported in literature [119, 150]. The cylinder contact pressure (*CyPmax*) values calculated (shown in Table 4-1), where *b* is the semi-contact width (Equation 4-2), were compared with finite element model predicted values.

Table 4-1: Extended cylinder Hertzian Predicted PMax values for a range of polyethylene material properties

v2	**0.3**	**0.3**	**0.3**	**0.3**	**0.46**	**0.46**	**0.46**	**0.46**
E2 (MPa)	200	300	400	500	200	300	400	500
b	2.82	2.30	1.99	1.78	2.62	2.14	1.86	1.66
CyPmax (MPa)	8.14	9.96	11.50	12.86	8.74	10.70	12.35	13.81

The finite element model predicted values showed that the contact pressure increased with increasing values of Young's Modulus. The model also showed that higher values of Poisson's ratio (0.46) resulted in a higher value of contact pressure compared to the lower value (0.3) (Figure 4-4). These results indicate that the model was sensitive to changes in these material properties.

The model with a Poisson's ratio of 0.46 predicted contact pressures in good agreement with the Hertzian contact theory calculated values (Figure 4-5). As the value of Young's Modulus increased to 500MPa, there became less agreement between the values and the model predicted values drifted outside of a 5% agreement with the Hertzian predicted value.

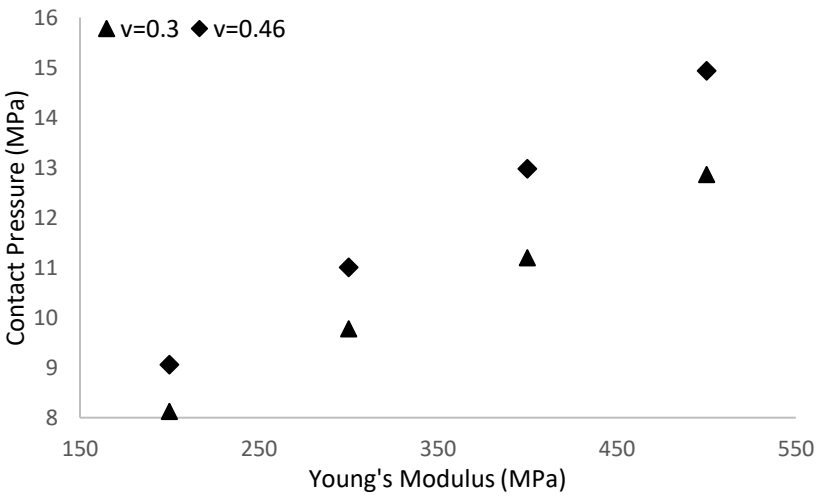

Figure 4-4: Cylinder on Plate model predicted contact pressure for a range of material properties with differing values of Young's Modulus and Poisson's Ratio

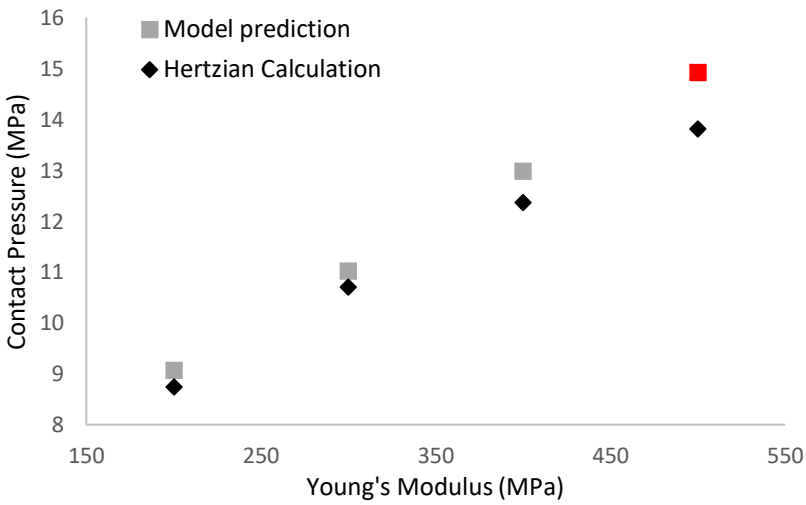

Figure 4-5: Cylinder on Plate model predicted values for v=0.46 plotted with calculated values using Hertzian contact theory. Value highlighted red to show outside of 5% agreement

One reason for the difference between the theoretically calculated values and the model predicted values is the change in geometry of the cylinder at the ends which may have created regions of concentrated stress on the plate. To reduce this error the geometry of the curved surface should be changed to have a radius on these edges or to change the geometry completely from a cylinder to a sphere which has no edges. Overall, the cylinder on plate model shows good sensitivity to changes in material values and also predicts contact pressure values in good agreement with the Hertz contact theory calculated values.

4.2.3 Sphere on Plate model

4.2.3.1 Rationale

An alternative geometry was investigated to understand how a change in contact area from a geometry change affects the contact mechanics. A sphere loaded onto a plate is a much simpler model to investigate the effect of displacements and load on the contact mechanics. The same BCs, loads, interaction properties and constraints were applied as in the cylinder on plate model.

4.2.3.2 Mesh Convergence study

A mesh convergence study was completed with a sphere of diameter 63.5mm, loaded onto an elastic plate with a compressive load of 2.52kN. The global mesh element size was reduced and the maximum contact pressure was predicted by the model. These results are shown in , which indicate that an appropriate element size of 1.2mm, resulting in a maximum contact pressure of 52.3MPa, should be used in future sphere on plate models. This value was chosen because further decreases in element size showed no considerable impact (more than 5% deviation) on the maximum contact pressure value.

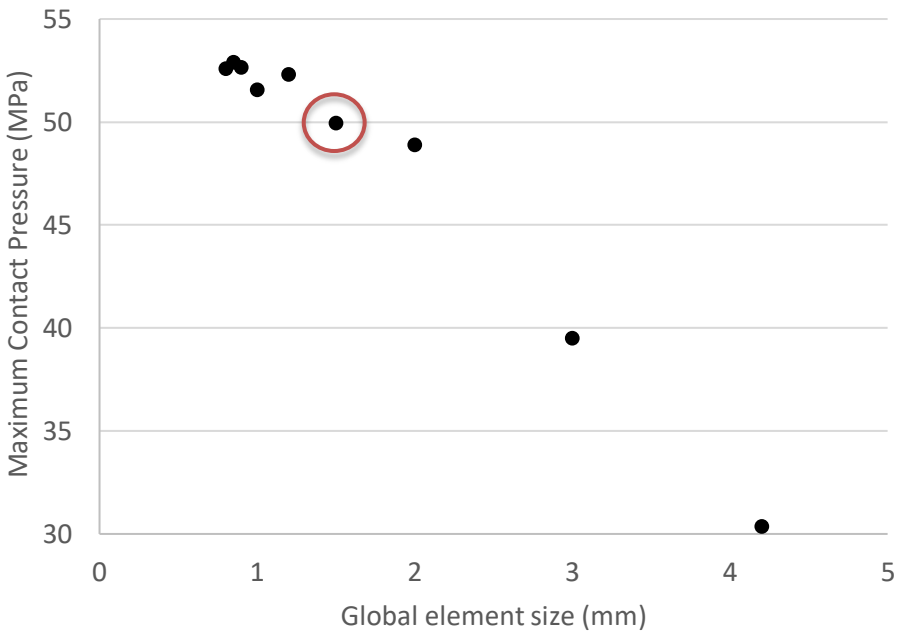

Figure 4-6: Sphere on plate mesh convergence study with maximum contact pressure values at a range of global element sizes with the result for convergence circled in red.

4.2.3.3 Sensitivity Study

Hertzian contact theory was reassessed for a sphere on plate model to determine model sensitivity to changes in material properties. The values were recalculated for a sphere (with a diameter of 63.5mm) model using Hertzian theory of elastic contact for a sphere on plate published by K.L. Johnson (Equation 4-4 and Equation 4-5), where R is the radius of the sphere (Johnson, 1985b) (Figure 4-7).

$$a = \sqrt[3]{\frac{3FR}{4E'}}$$

Equation 4-4: Radius of the contact circle

$$Pmax = \frac{3F}{2\pi a^2}$$

Equation 4-5: Maximum contact pressure for a sphere on plate

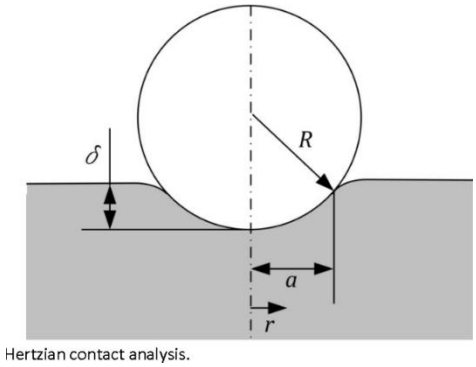

Figure 4-7: Hertzian Contact model of a sphere on plate (Cheneler et al., 2013)

Using this contact theory, a value of 49.4MPa was calculated as the maximum contact pressure for the sphere on plate with 2.52kN applied compression load and material properties of E = 400, v = 0.46. This is in good agreement with the value predicted in the model simulation of 52.3MPa.

A sensitivity study was completed on the sphere on plate size with both components assigned a global mesh size of 1.2mm which was selected as the optimal mesh size for convergence. The Sphere on plate Hertzian predicted values are shown in Table 4-2.

Table 4-2: Hertzian predicted peak contact pressure values for a sphere loaded onto a plate with varying Young's Modulus and Poisson's ratio values

v2 E2 (MPa)	0.3 200	0.3 300	0.3 400	0.3 500	0.46 200	0.46 300	0.46 400	0.46 500
A	6.49	5.67	5.15	4.78	6.19	5.41	4.91	4.56
Sphere Pmax (MPa)	28.57	37.42	45.32	52.57	31.43	41.17	49.86	57.83

The results from the sphere on plate models with differing values of Young's Modulus and Poisson's ratio show that the model is sensitive to changes in material properties. The model with material properties of v=0.46 had consistently higher values of contact pressure in comparison to the equivalent model with v=0.3 properties (Figure 4-8). This indicates that higher values of Poisson's ratio result in higher values of contact pressure. Furthermore, the contact pressure value increased with increasing values of Young's Modulus applied to the model material.

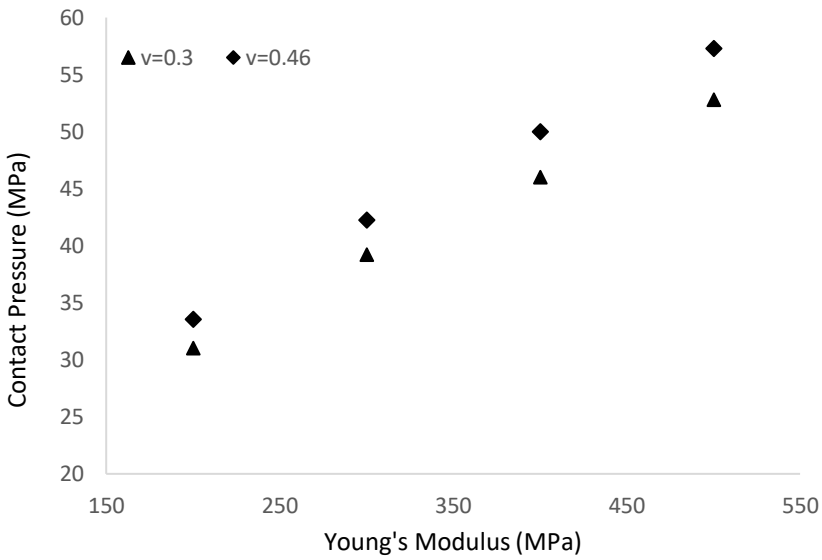

Figure 4-8: Sphere on Plate model predicted contact pressure for a range of material properties with differing values of Young's Modulus and Poisson's Ratio

The comparison of the predicted values calculated for the sphere on plate model (Table 4-2) with the model predicted values for the same material property combinations shows good agreement within 5% for all values of Young's Modulus with a Poisson's ratio of 0.46 (Figure 4-9). The good agreement between the calculated and model predicted values gives confidence in the appropriateness of the finite element model setup and inputs to predict accurate values of contact pressure for a spherical surface contacting a flat plate.

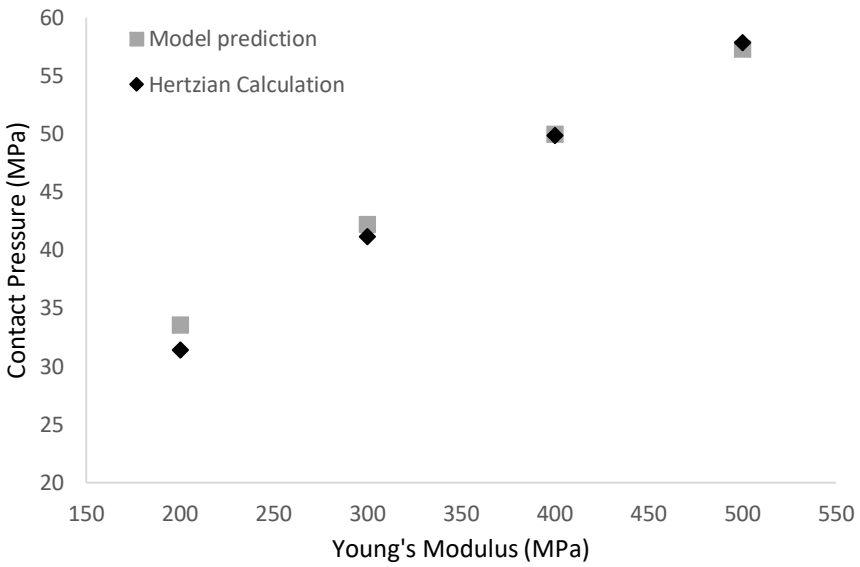

Figure 4-9: Sphere on Plate model predicted values for v=0.46 plotted with calculated values using Hertzian contact theory.

An additional study investigated the sensitivity of the model to changes in coefficient of friction of the contacting surfaces. The coefficient of friction value was chosen based on the typical approximated value for UHMWPE TKR's of μ=0.04 used for the contacting surfaces of an Attune TKR [130]. Values either side of this coefficient of friction were assigned to the model along with a frictionless model resulting in four models studies (μ = 0, 0.02, 0.04, 0.06). The results show that there was a slight decrease in contact pressure (0.14MPa) between a frictionless surface and a surface with a small coefficient of friction value (Figure 4-10).

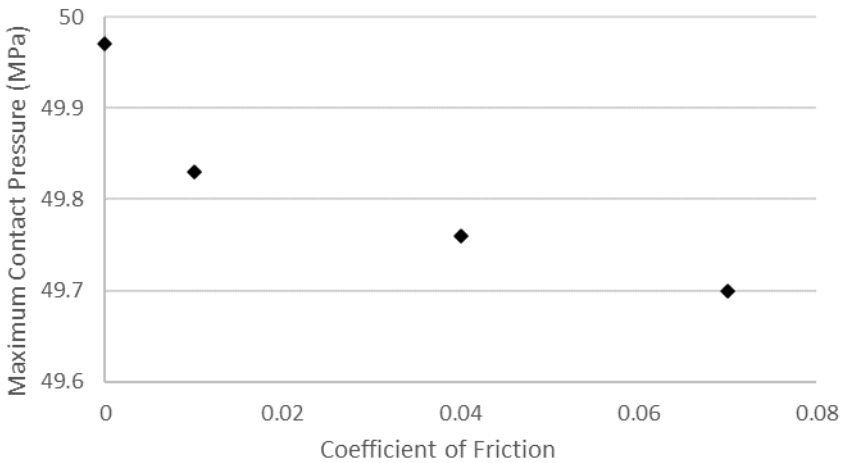

Figure 4-10: Peak contact pressure results at a range of coefficient of friction values

Once a value of friction was assigned to the surface interaction properties, the contact pressure linearly decreased with increasing coefficient of friction values. This response in the outputs of the model predictions shows sensitivity to changes in surface interaction properties which provides confidence in the validity of the model's surface contact setup and inputs.

Overall, the sphere on plate model showed good accuracy in predicting contact pressures and sensitivity to inputs. The sphere geometry contacting a flat surface is a good simplified geometry model of a total knee replacement bearing surface where the rounded condyles of the femoral component contact the elastic tibial insert surface which is relatively flat. The principles developed in this section to develop and mesh a finite element model will be applied to further models developed throughout this section.

4.2.4 Dynamic Models

4.2.4.1 Rationale

The static, general model, where a concentrated load was applied to the sphere to initiate contact with a stationary plate, was adapted into a dynamic, implicit model with both components controlled in two degrees of freedom. The setup developed in the dynamic model permitted displacements and rotations to simulate a simplified displacement control ISO 14243-3:2014 standard walking gait movement, with incremental changes in loads and kinematics at specific time points. The aim of this study was to investigate the ability of the simplified geometry model to move in different ranges of motion and to verify that the output kinematics of the model were in agreement with calculated values.

4.2.4.2 Methods

The conditions applied to this model used ISO 14243-3:2014 displacement control [114] kinematics as motion inputs to the model using forces and boundary conditions. Displacement control applies the kinematics and axial loading to the bearings but does not apply restraining forces through springs to replicate soft tissue restraints. It was therefore suggested by Brockett et al. (2016) that this control method is the most appropriate to use when testing requires careful control of the kinematic positions [117].

Motions included anterior displacement (0-5.2mm) applied to the plate, angular rotations including flexion (0°-58°) applied to the sphere and IE rotation (-5.7°-1.9°) applied to the plate, and an axial force (168-2600N) applied to the sphere (Figure

4-11). All other degrees of freedom were constrained except abduction-adduction rotation of the plate which was unconstrained. The contact of the articulating surfaces in this simulation were frictionless.

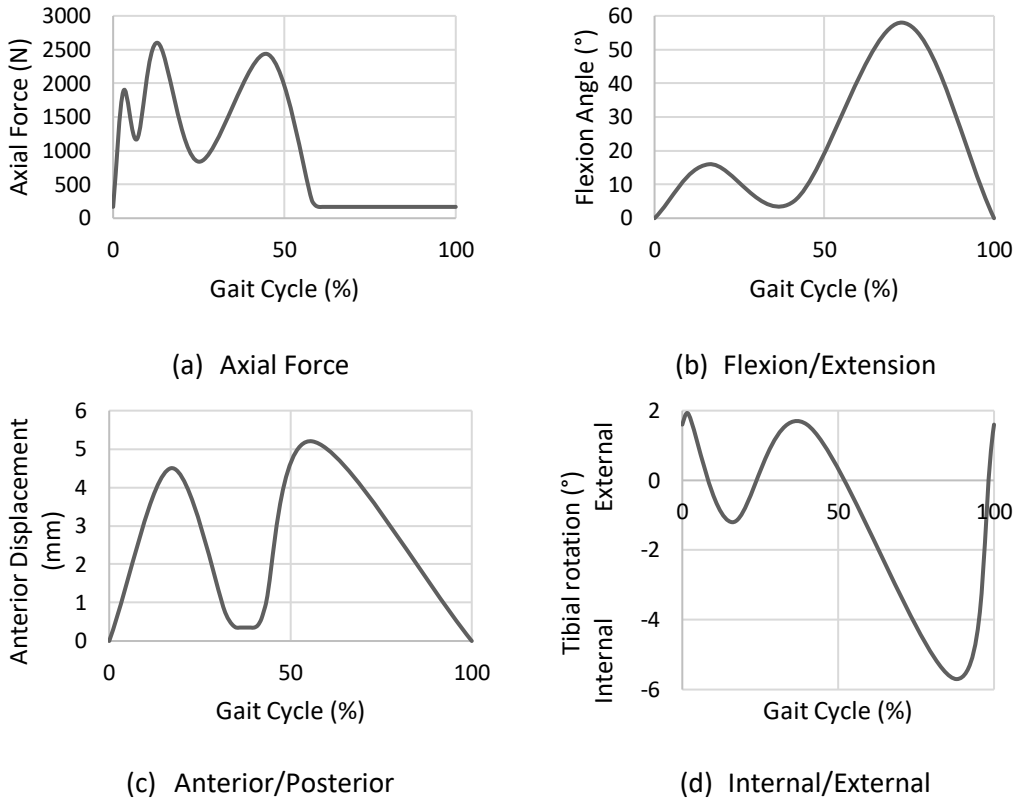

Figure 4-11: Gait profiles for standard walking under displacement control adapted from (ISO 14243-3:2014) [114]

4.2.4.3 Results

The maximum contact pressure (MPa) and total contact area (mm^2) of all nodes on the plate contact surface after one full gait cycle were exported from ABAQUS and are plotted in Figure 4-12. The maximum contact pressure found was 53.8 MPa. The graph shows that the contact mechanics of the sphere on plate model under displacement control ISO 14243-3:2014 input conditions is sensitive to changes in applied load. The output contact area and pressure values showed a double peak at 20% and 40% of the gait cycle.

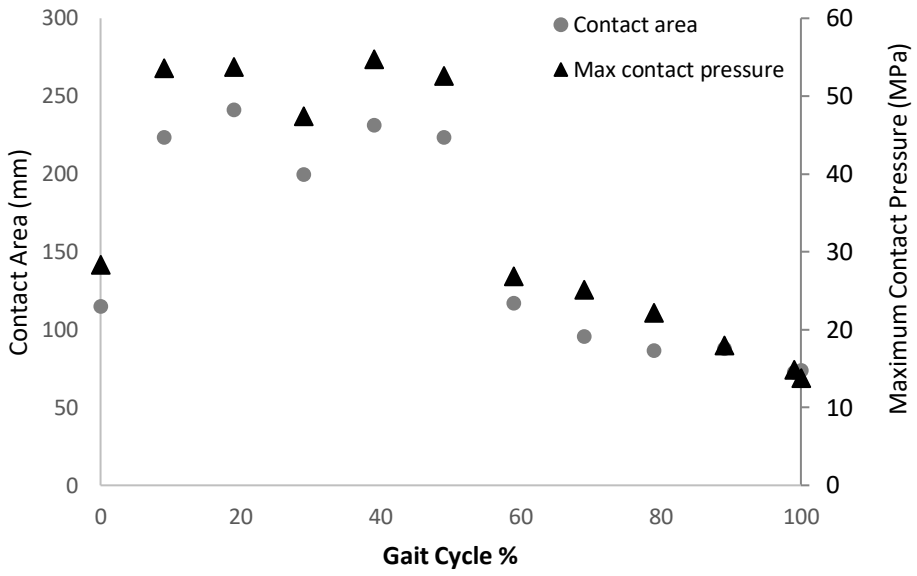

Figure 4-12: Sphere on plate output contact area and contact pressure for one gait cycle

An additional dynamic model of the sphere on plate was created with adapted inputs to control the plate using load control motions as per ISO 14243-1: 2009 [112]. The motion control of the sphere remained the same, the plate was controlled by a central control reference point connected to two wire connectors' assigned properties to act as springs. The loads applied to the reference point included anterior-posterior force and rotation torque (Figure 4-13). All other motions on both parts were constrained except abduction-adduction of the plate which was unconstrained.

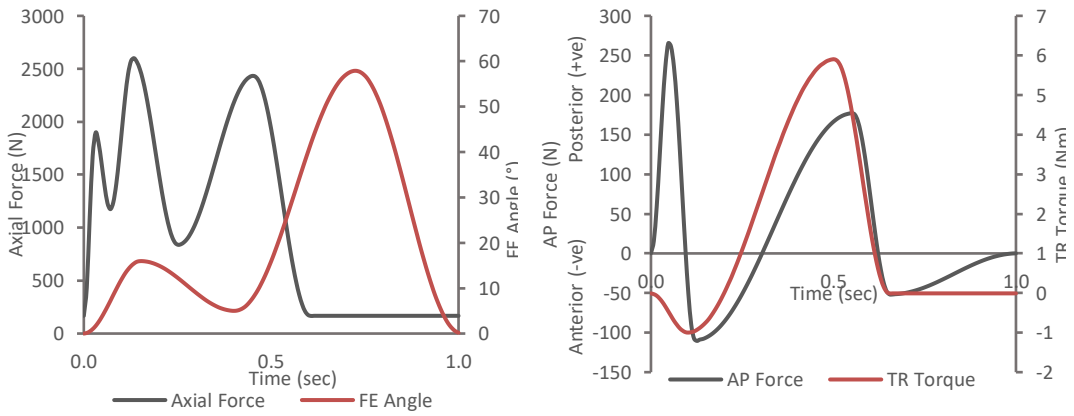

Figure 4-13: ISO 14243-1:2009 force control input profiles for AF, FE, AP and TR at a 1Hz frequency [112]

Linear elasticity values applied to the two wire connectors were 9.3N/mm for the anterior-posterior force spring and 0.36Nm/° for the plate rotation spring. With the applied loads and spring values known, the expected output motions were calculated using Hooke's law and compared to the actual outputs from the model for one full gait cycle for anterior-posterior displacement (Figure 4-14) and for internal-external rotation (Figure 4-15). The results for both kinematic outputs were in good agreement with the calculated value with an r^2 value of 1.

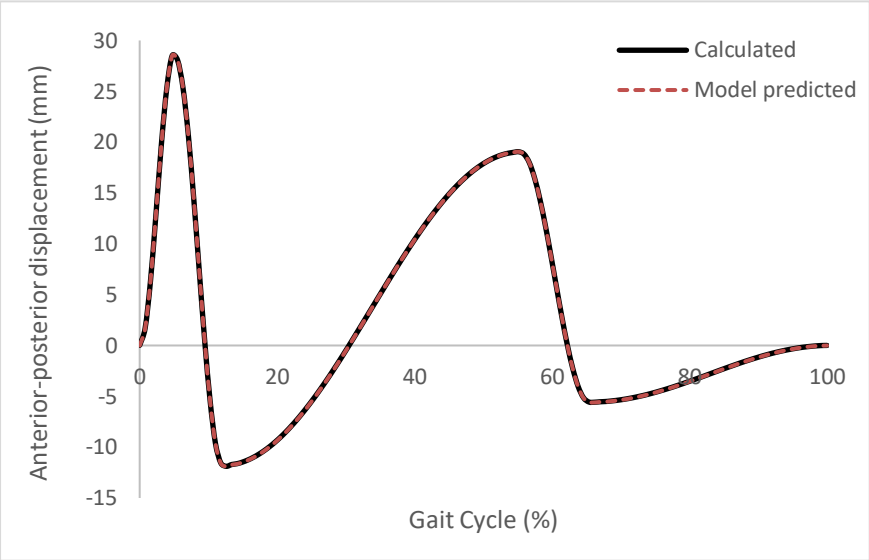

Figure 4-14: Sphere on plate load control model predicted output anterior-posterior displacement and calculated value for one gait cycle

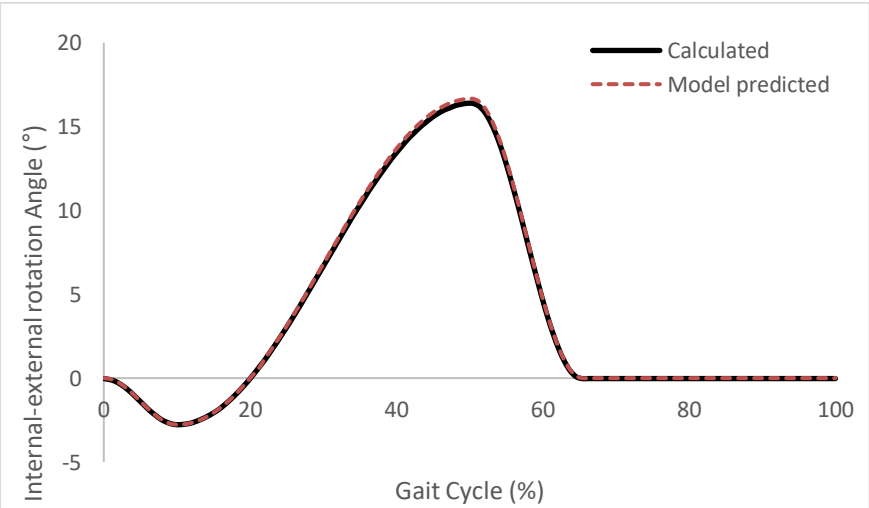

Figure 4-15: Sphere on plate load control model predicted output internal-external rotation and calculated value for one gait cycle

4.2.5 Discussion

A simple geometry, dynamic finite element model was used to simulate ISO 14243-3:2014 displacement control and ISO 14243-1:2009 load control standard walking kinematics of a total knee replacement. The displacement control model showed that the model output contact mechanics were susceptible to changes in load and kinematics. The model controlled through spring constraints was validated against theoretical values. It was important to check the functionality and sensitivity of a simple geometry model to develop confidence in methods of applying input conditions such as loads and boundary conditions, materials, surface interactions and meshes.

Both kinematic outputs of the model were in very good agreement with the calculated values (r^2=1). These results give confidence in the model motions being correct and the connector wires functioning correctly as springs. This methodology of applying load control to the parts will be used in the total knee replacement model to control the motion of the tibial insert.

4.3 Development of a Displacement Control Attune Total Knee Replacement Model

4.3.1 Rationale

The aim of this section was to develop a finite element computational model of an Attune design total knee replacement and to establish confidence in its biomechanical function by comparing outputs with experimentally determined kinematics and contact mechanics. The model started as a static concentrated load model to investigate the initial contact of the components and to determine an appropriate mesh size through mesh convergence studies. Subsequent studies involved dynamic models of multiple loaded steps which simulated a full ISO 14243-1:2009 load control standard walking gait cycle to predict output kinematics and contact pressure. The outputs were compared to experimental values to establish confidence in the efficacy of the model as a preclinical assessment tool of standard walking on a TKR bearing.

4.3.2 Finite Element Model Setup

A finite element model of an Attune TKR was developed in ABAQUS. To develop the model the component designs were supplied by DePuy Synthes (Attune size 5 cruciate retaining femoral condyle and Attune AOX cruciate retaining, fixed bearing

size 5 tibial insert) were imported into the ABAQUS software. The components were aligned with the longitudinal axis passing through the centre of rotation of each component. Each component also has its own centre of rotation used as a control point for the application of the kinematics and kinetics profiles. The centre of rotation (CoR) of the femoral component was determined using guidance from ISO 14243-1:2009 which states that the CoR of a femoral component with multiple radii should be determined by an average of the distal and posterior radii which were at 30° and 60° in this component design [112]. According to the same standard, the CoR was also offset towards the medial condyle by 7% of the width of the femoral component, this was a 4.7mm medial translation for the mid-size attune cruciate retaining design. The CoR of the tibial component was also moved to be aligned with the femoral CoR in the longitudinal axis.

The points identified as the centre of rotation for each component were assigned a reference point which was constrained to control the component in all six degrees of freedom. The femoral reference point was constrained as a rigid body, the tibial component was constrained using kinematic coupling. All loads and boundary conditions for each component were applied to these two reference nodes. A global coordinate system was used to control both components shown in Figure 4-16, the positive directions of each axis of displacement and rotation were medial (x), posterior (y), inferior (z), flexion (Mx), abduction (My), interior (Mz).

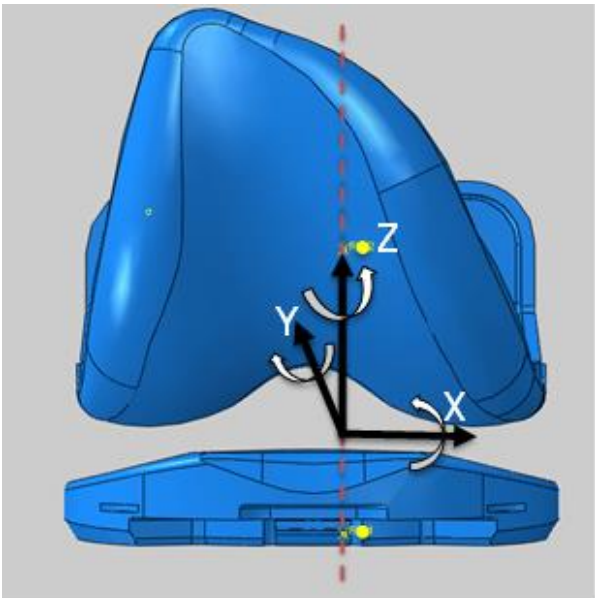

Figure 4-16: Right: TKR Model setup with coordinate system of reference. +X is medial, Y+ is posterior and Z+ is superior. The directions of rotation are Mx+ is flexion, My+ is abduction and Mz+ is internal rotation.

Surface to surface interaction properties were created between the contacting surfaces where the femoral component was assigned the main (master) surface and the tibial insert component assigned the secondary (slave) surface. Surface to surface discretization method where the contact considers surrounding slave nodes, although biasing the nearest slave node. This method helps with accuracy in edge loading situations where stresses may be concentrated to a node by calculating an average slave node position based on surrounding nodes. A friction coefficient of 0.04 was assigned to the contact interaction [64].

4.3.3 Convergence Studies

4.3.3.1 Study 1 – XLK Material

A convergence study was completed which included investigating different types of meshing options in two software applications including ABAQUS and HyperMesh (Altair Engineering, Inc). A two-week trial educational software license was obtained to use the HyperMesh software for this study. HyperMesh software was trialled for creating the mesh on the total knee replacement components due to the improved mesh size control capabilities. For the ABAQUS meshing method developed, a global element size was assigned to the components. In comparison, HyperMesh facilitated both a maximum element size and minimum element size to be specified. The mesh used in HyperMesh was tri tetras (second order) C3D10, the ABAQUS mesh used 10-node modified quadratic tetrahedron (C3D10M) elements. The material properties of the tibial inserts used XLK polyethylene values from the cylinder on plate study which were E=553MPa and v=0.32 [119]. To complete the study using HyperMesh, the meshes were exported from the software and uploaded into ABAQUS with the Job input file to complete a static loading cycle where a contact displacement step followed by a static load step of 220N was used. For the mesh convergence study both types of mesh element sizes were gradually reduced to increase the total number of elements in the model. Figure 4-17 shows the maximum contact pressure output from the two models meshed in ABAQUS and HyperMesh for a range of maximum global element size for each model.

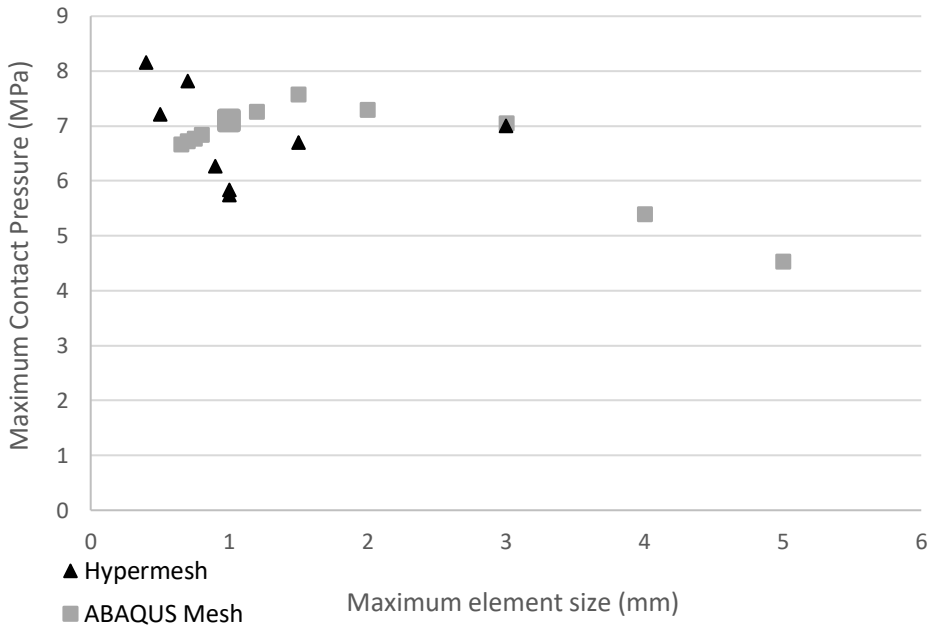

Figure 4-17: Convergence study of the TKR contact pressure under a static load of 220N at a range of element sizes for finite element mesh created in HyperMesh versus ABAQUS software

The resulting contact pressure at full mesh convergence was around 7MPa, which was at a point of around 500,000 elements for HyperMesh and around 220,000 elements for ABAQUS Standard mesh. From the results of this study the mesh created in ABAQUS was determined as the suitable software for meshing the components. Although HyperMesh offered more specific control over the types and size of element used there were challenges with importing the meshed components into ABAQUS which compromised the efficacy of the model. In comparison, the ABAQUS meshing method was simple and resulted in mesh convergence.

4.3.3.2 Study 2 - AOX Material

An additional mesh convergence study was completed in ABAQUS with a single concentrated load of 667N applied to the femoral component. This value was chosen because it resulted in a maximum contact pressure value of around 20MPa which is larger than the maximum contact pressure value measured in the previous Tekscan study (17MPa). This method ensured that mesh convergence was established at the maximum range of loads which would be measured by the model. Material properties were assigned to each component, CoCr with Young's Modulus (E) of 193000MPa and Poisson's ratio (v) of 0.29 and Attune AOX with E = 348MPa and v = 0.35 [151]. From the outputs an appropriate mesh size was determined using the element size

at which no further reduction in size changed the output contact pressure by ±5%. This point is highlighted red in Figure 4-18 and represents a global element size of 1mm, with 204,748 elements assigned to the femoral component and 137,527 assigned to the tibial insert component.

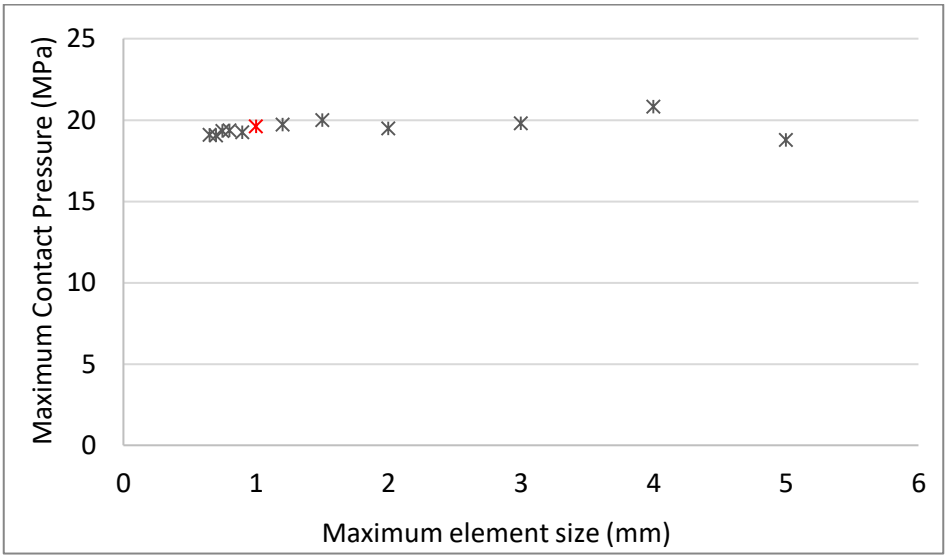

Figure 4-18: Mesh convergence study using ABAQUS mesh with a static load demand of 667N applied to a TKR finite element mesh with decreasing global element sizes (global element size of 1 highlighted red)

4.4 Development of a Load Control Attune Total Knee Replacement Model

4.4.1 Rationale

To facilitate load control motion in the model, wire connectors were created and assigned elastic spring constraint properties as per the ISO 14243-1:2009 standard. The methods to implement this into the model began with a linear spring model to ensure that the output kinematics were in agreement with calculated values. The next step was to adapt the wire connectors into non-linear spring constraints with three phases of elasticity. The aim of this section is to create accurate motions of the model which are in agreement with experimental kinematic outputs determined from the ProSim experimental wear simulation.

4.4.2 Linear Spring Model

The static, general TKR model was adapted into a dynamic, implicit model to simulate a walking gait cycle under ISO 14243-1:2009 standards plotted in Figure 4-13 [112]. An ISO 14243-1:2009 standard walking 128-point gait cycle input from the

electromechanical Prosim simulators with ISO input were input to the model setup with spring constraints added to control the tibial insert component.

Spring constraints were added to the model using wire connectors between the tibial insert control node and two reference points located externally from the part (Figure 4-19). A cartesian wire connector was created for the anterior-posterior spring and a rotational wire connector was created for the tibial rotation spring.

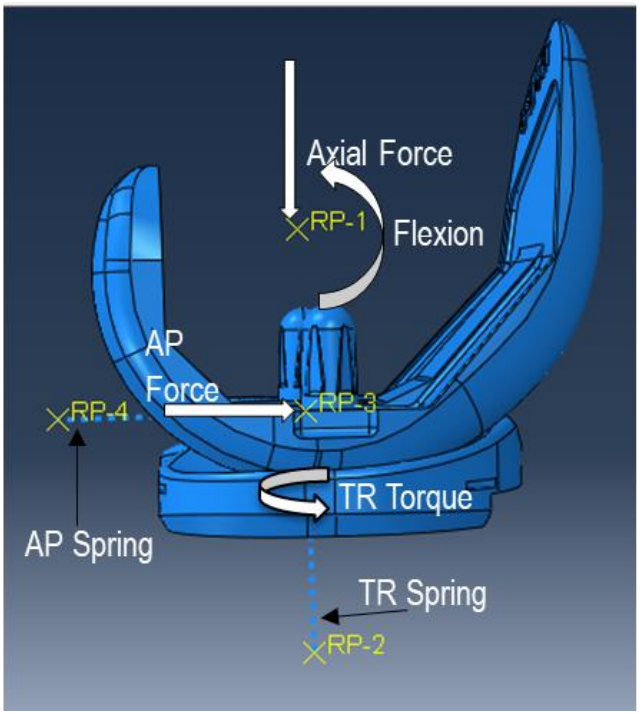

Figure 4-19: Wire elements applied to Attune finite element model to act as anterior-posterior spring and tibial rotation spring.

A initial tibia only model was studied first to verify the control of the spring constraints by comparing the output kinematics for AP displacement and TR angle to calculated values using Hooke's law (Equation 4-6: Hooke's Law). Initially linear spring constraint values were used, the AP connector had a value of 44N/mm and the TR connector had a values of 0.36Nm/° as per ISO 14243-1:2009 [112]. This equation was used to calculate spring profiles between -30 to 30mm AP displacement and -30° to 30° tibial rotation for the linear spring values stated (Figure 4-20).

$$\frac{F}{k} = x$$

Output Displacement

Applied Load/Torque

Spring stiffness

Equation 4-6: Hooke's Law where F is applied force, k is spring stiffness and x is the displacement.

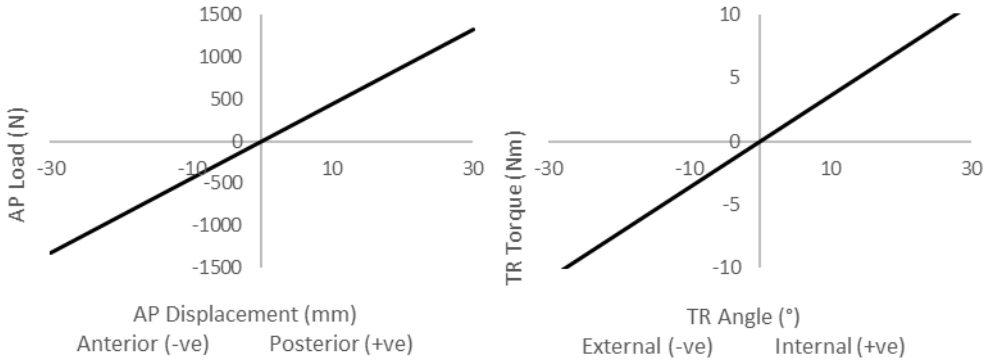

Figure 4-20: Linear spring model stiffness profiles for AP displacement (mm) and tibial rotation angle (°)

The model output AP displacement (mm) and TR angle (°) and the values calculated using Hooke's law are plotted in Figure 4-21 as 'calculated value' with the prediction kinematics from the model using 30mm spring lengths.

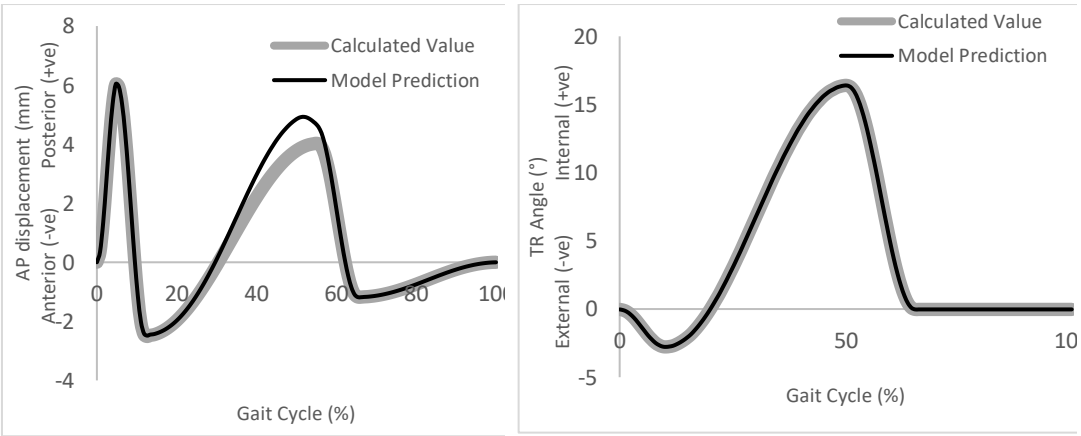

Figure 4-21: Linear spring model predicted kinematic values vs calculated values using Hooke's law -F=kx for AP displacement (left) and TR angle (right)

The spring lengths were adapted to investigate their effect on the output kinematics to determine the most suitable way to set up the springs. Models with point-to-point connectors with spring lengths of 30mm and 20mm and a model with point-to-ground were created for this investigation. All output anterior-posterior kinematic values were compared to the calculated output value based on the spring value and input load.

The 30mm AP spring length compared with the calculated displacements and rotations had an r^2 value of 0.97. Additional repeats of this model were spring lengths which included 20mm, 30mm and a spring connected to ground. The r^2 value for the AP spring lengths of 30mm, 20mm and to ground were 0.97, 0.99 and 1 respectively (Figure 4-22).

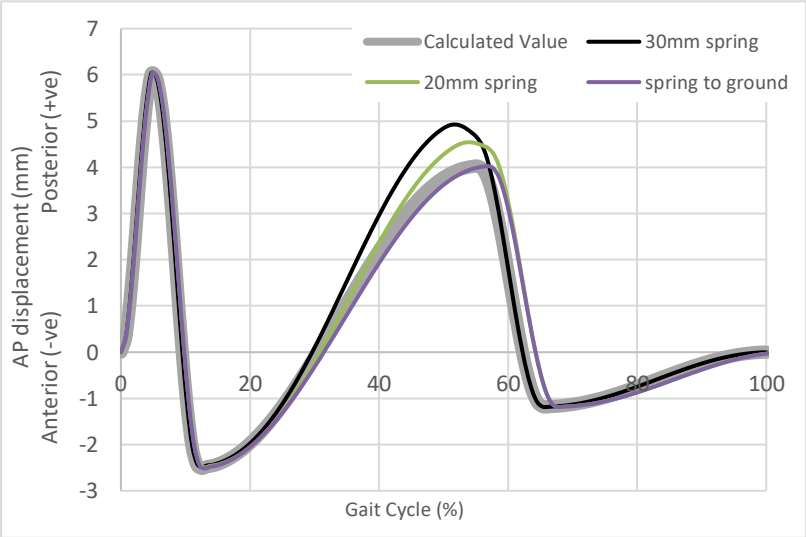

Figure 4-22: Linear spring model predicted kinematic values vs calculated values using Hooke's law -F=kx for AP displacement for spring lengths of 20mm, 30mm and to ground.

The springs connected to ground resulted in the best agreement between model output AP displacement and the calculated value. As a result, it was determined that spring connected to ground was the appropriate method of setup for the springs.

4.4.3 Non-linear Spring Model

Once the tibia only model was confirmed to produce accurate kinematic output values for both anterior posterior translation and tibial rotation angle, a full TKR model with tibial insert and femoral component was assembled to complete a whole ISO 14243-1:2009 standard walking gait cycle (Figure 4-23). Boundary conditions were used to fix the tibial component in medial-lateral translation, flexion-extension and superior-inferior translation, it was unconstrained in abduction-adduction. Boundary conditions were also used to constrain the femoral component in all degrees of freedom except FE and AF. An initial contact step was created using boundary conditions to apply a small vertical displacement to the femoral control node. The displacement was altered until the initial maximum contact pressure between the components was <1MPa.

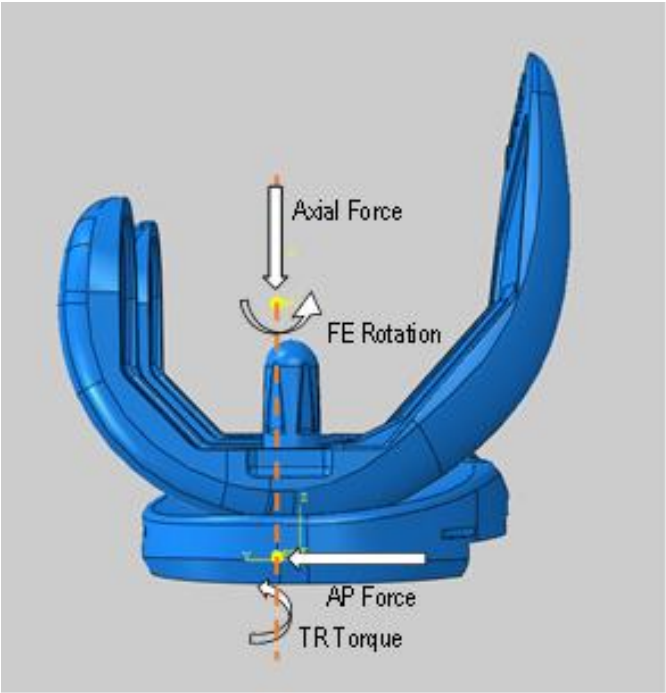

Figure 4-23: TKR model setup with the active kinetic and kinematic controls applied to each reference point constrained to the two components.

The FE rotation of the femoral component was controlled using boundary conditions while the axial force was applied using a load. The movement of the tibial component was controlled in the same way as the previous model, however the AP load and TR torque were applied using non-linear spring constraints to more accurately represent the soft tissue actions within the knee (Figure 2-4). There was an adaption to these input profiles, due to the capabilities of the model, which required a small load to be applied during the “free range” section of the spring profile.

To apply the gait cycle, there was an initialisation step added after the contact step to move the components to their initial starting positions before the first step of the 1Hz gait cycle was started. Individual steps for each of the 128 points of the gait cycle were created with the same boundary and load conditions. Amplitude plots were created with the load, torque and rotation values for each of the four controlled degrees of freedom which were applied per time increment throughout the step.

The model was simulated over one gait cycle where outputs were requested at each of the 128 points of the gait cycle for AP displacement, TR angle, FE angle, contact pressure, contact area, and sliding distance.

4.4.4 Results

To determine the accuracy of the TKR finite element model to produce outputs in agreement with experimental simulations, specific outputs were compared and their agreement was analysed. The two outputs assessed were the kinematic outputs of the tibial insert in AP and TR and the contact pressure between the surface of the bearing at intervals of the gait cycle.

The kinematic outputs for AP displacement and TR angle were recorded at the reference node of the tibial insert at each step of the gait cycle. These outputs were compared with a 100-cycle average of all six wear stations of the baseline Attune experimental wear study output kinematics between 0-1MC. A 95% confidence interval of the six stations was calculated over the gait cycle to indicate an upper and lower boundary of the results range.

The maximum anterior displacement predicted by the model was 4.38mm and the maximum posterior displacement was 3.22mm. The AP displacement output showed good agreement between the model prediction and experimentally determined values where the model prediction was within the 95% confidence interval range of the experimental data for the majority of the gait cycle (Figure 4-24). Between 0-50% and 80-100% of the gait cycle there was very good agreement, however the agreement was less good between 50-80% of the gait cycle.

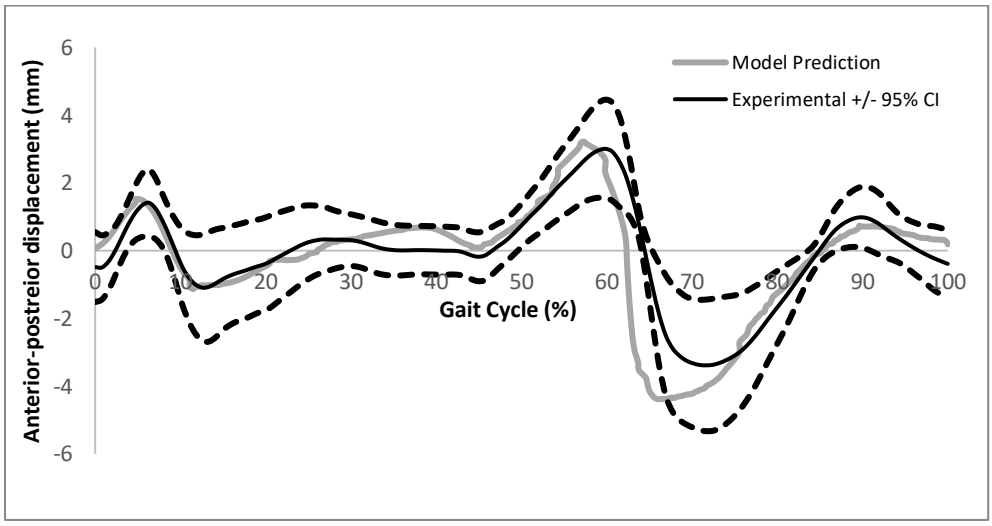

Figure 4-24: Model predicted AP displacement of the tibial component and experimental simulation measured 100 cycle average AP displacement with ±95% CI (represented with dashed lines) (r^2 = 0.766)

The model predicted tibial rotation values were within the 95% confidence interval of the experimental simulation output values over the whole gait cycle indicating a good agreement between the two simulation methods (Figure 4-25). The maximum internal angle of the model prediction was 7.94° and the maximum external rotation was -1.18°. The results show slight fluctuations in the model predicted tibial rotation angle between 80-100% which may be due to the low load on the spring constraints.

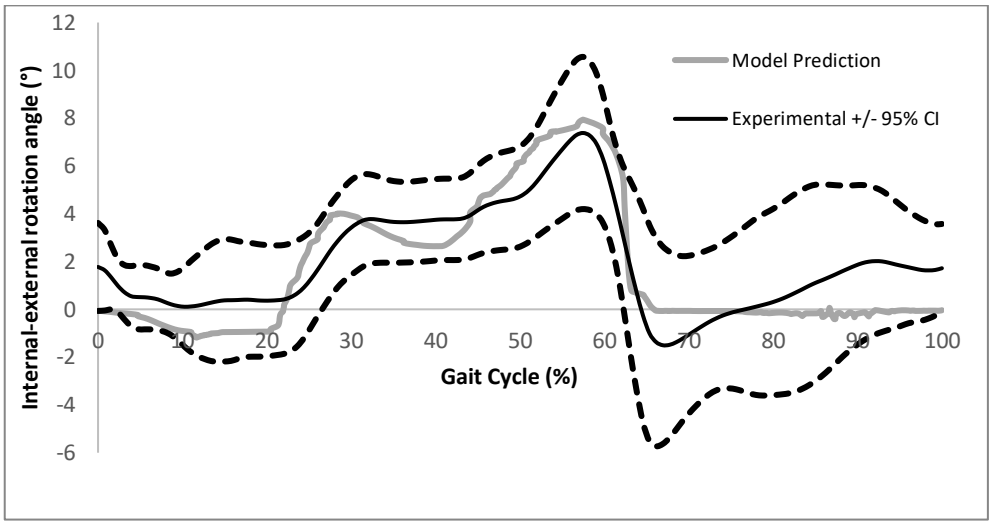

Figure 4-25: Model predicted TR angle of the tibial component and experimental simulation measured 100 cycle average TR angle with ±95% CI (represented with dashed lines) (r^2 = 0.828)

Root-mean-square-error (RMSE) was calculated to determine the difference between the predicted (finite element model output) and observed (experimental simulation) values. The AP displacement had an RMSE of 1.60% and the TR angle had an RMSE of 0.95% indicating that the internal-external rotation of the model was in closer agreement with the experimental data than the anterior-posterior displacement values.

4.4.5 Discussion

An Attune total knee replacement finite element model, actively controlled in 4 degrees of freedom, has been developed. The model is capable of being controlled using displacement control and load control inputs, with output kinematics for anterior-posterior displacement and tibial rotation angle. The initial static implicit model, which was developed to measure contact pressure under a compressive load, has been successfully adapted into a dynamic implicit model with 128 gait cycle

steps, where the tibial insert is controlled through wire connectors in anterior-posterior motion and tibial rotation motion.

Development of the load control inputs began with an initial study using linear spring control profiles where the predicted output kinematic values were calculated and compared with the model predicted values. The results from this study allowed the capabilities of the model to move through the control of wire connectors to be validated.

The non-linear control spring model proved to be more challenging to develop, with the “free range” section of the spring profile causing errors in the completion of the model. A small, negligible load was applied to overcome the error caused by stiffness range values of 0.

The results of the model development and completion of a whole gait cycle showed that the Attune AOX non-linear load control model was capable of predicting both anterior-posterior displacement and tibial rotation angles in agreement with experimental data from the experimental wear simulation study.

4.5 Using the Attune Total Knee Replacement Model to Investigate Contact Mechanics

4.5.1 Rationale

Contact pressure outputs are an essential element of understanding the wear of total knee replacement. As such, the accuracy of the model to predict contact pressure outputs in agreement with experimentally measured values was determined to be an important additional study. The computational contact mechanics study was created based on the methodology developed in the experimental section “3.4 ProSim Attune Baseline Tekscan Study” and integrated into the Attune finite element model.

4.5.2 Model Development Methods

The contact pressure values were determined at 10% intervals of the gait cycle where the components were set to specific kinematic positions before having a load applied. As such, the finite element model had to be adapted to replicate this setup and changed to singular loading measurements rather than the 127-step gait cycle model outlined previously in this chapter, which will be referred to as the full gait cycle baseline model in this section.

All geometries, materials and surface interactions were maintained from the full gait cycle baseline model. However, since the inputs were now simple displacement

applied to position the components for the individual loading measurement, the spring constraints were not included and boundary conditions were used to set the position in the anterior-posterior axis and about the tibial rotation axis. Flexion-extension angle of the femoral component was also positioned using boundary conditions and the only load applied to the model was an inferior load at the femoral components control node. Abduction-adduction of the tibial insert was left unconstrained in this model and all other motions of both components were fixed.

At each 10% interval a new model was simulated which consisted of an initialisation step to send the components to their desired translation or rotation, followed by a displacement step to initiate contact. Contact pressure outputs from the displacement step were used to determine that an initial contact pressure of <1MPa was established before the loading step. The load step applied a force to the femoral component and contact pressure (CPRESS) and contact area (CNAREA) field outputs were calculated by the model. These steps were repeated for all eleven intervals of the gait cycle and the requested outputs were exported for all nodes for each model.

The contact pressure for all tibial insert nodes, defined in the surface set, were exported to excel for analysis. An average contact pressure was calculated for all nodes with a positive value (i.e. the nodes which were in the contact area). The contact pressure calculated for the whole contact surface was further split into average contact pressure values on the medial compartment and lateral compartment at each gait interval. The values were determined by the node coordinates where all medial compartment nodes had a positive x value coordinate and lateral compartment nodes had a negative x value coordinate.

4.5.3 Results

The images in Table 4-3 show a colour indicated contour (Figure 4-26) of the contact pressure over the medial and lateral compartments at each 10% interval of one gait cycle (Figure 4-27). The images show how the distribution of in contact pressure between the medial and lateral condyles changed throughout the gait cycle. The predicted outputs had a maximum average contact pressure of 6.68MPa (peak of 16.91MPa) at the 40% gait cycle interval and a minimum average contact pressure of 2.08MPa (peak of 5.47MPa) at 80% gait cycle interval Table 4-4.

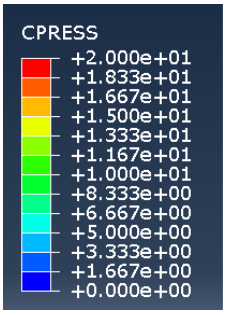

Figure 4-26: Contour scale for tibial contact images

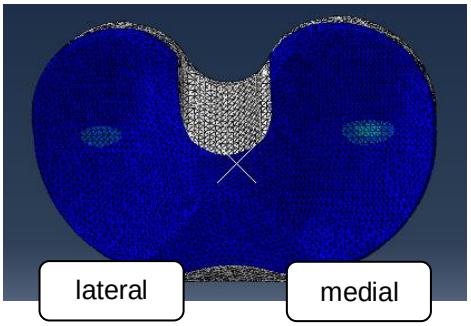

Figure 4-27: Tibial insert model contact heat map medial and lateral condyles

Table 4-3: Contour images of the tibial component contact area at 10% intervals of the gait cycle

0% 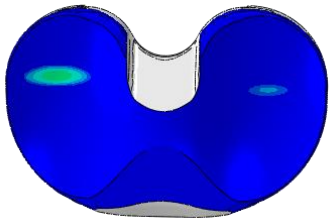	10% 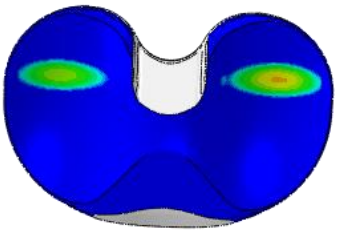	20% 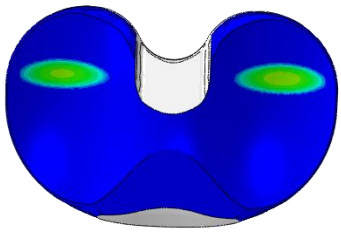
30% 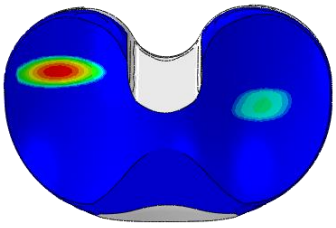	40% 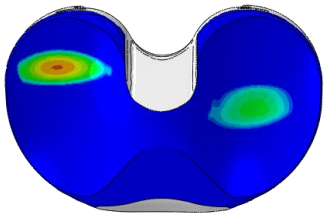	50% 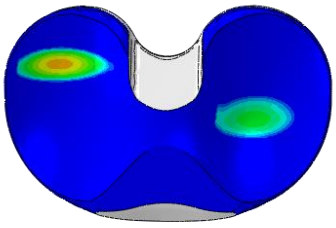
60% 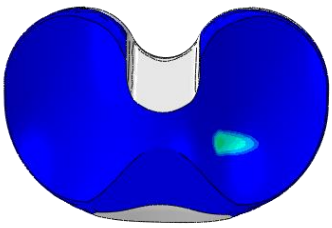	70% 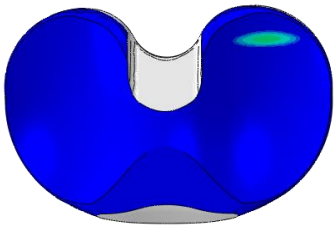	80% 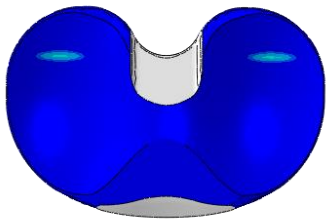
90% 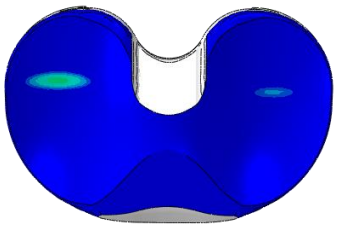	100% 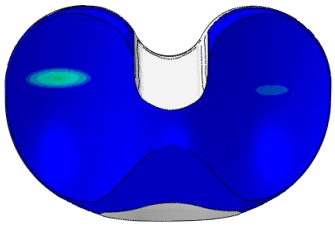	

Table 4-4: Average and peak contact pressure predictions of TKR baseline model

Gait %	Model Average Contact Pressure (MPa)	Model Peak Pressure (MPa)
0	3.03	7.74
10	6.98	15.35
20	6.24	13.32
30	5.02	13.29
40	6.68	16.91
50	6.43	16.07
60	3.24	7.81
70	3.28	7.54
80	2.08	5.47
90	2.63	7.16
100	2.59	6.90

The predicted average contact pressures showed maximum values at high load and minimum values at low load indicating that the model was sensitive to changes in forces applied to the bearing (Figure 4-28). The average contact pressure for the two compartments were overlayed on the total contact surface values to show how the contact pressure was distributed over the two compartments at each of the gait cycle intervals.

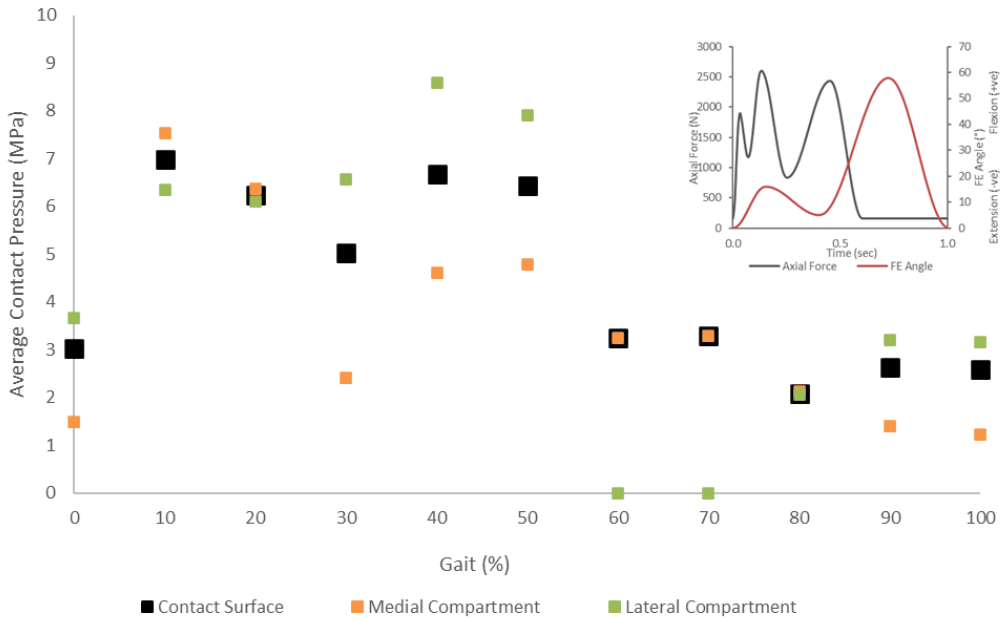

Figure 4-28: Average contact pressure of baseline TKR model contact surface (black) medial compartment (orange) and lateral compartment (green). With axial force and flexion-extension graphs inputs of one gait cycle

The results show that at the 20% and 80% gait cycle points, the two compartments had similar average contact pressure values indicating that the load was evenly distributed between the two compartments at these points. The gait interval points with the largest difference between the two compartments were at 30% and 40% of the gait cycle which recorded a difference in average contact pressure between the two compartments of 4.16MPa and 3.97MPa respectively. Furthermore, these results show that at 60% and 70% gait interval points the lateral compartment measured no contact pressure in comparison to over 3MPa measured on the medial compartment.

Overall, the model predicted average contact pressure values were in good agreement with the average contact pressure values determined from the baseline Tekscan study completed in Chapter 3. At high loads the predicted values fall within the standard deviation range of the experimental values, indicating that the model is accurate at higher loads. There is slightly less agreement between the model outputs and experimental values at lower loads with five out of six predicted values falling outside of the standard deviation range during the swing phase (Figure 4-29).

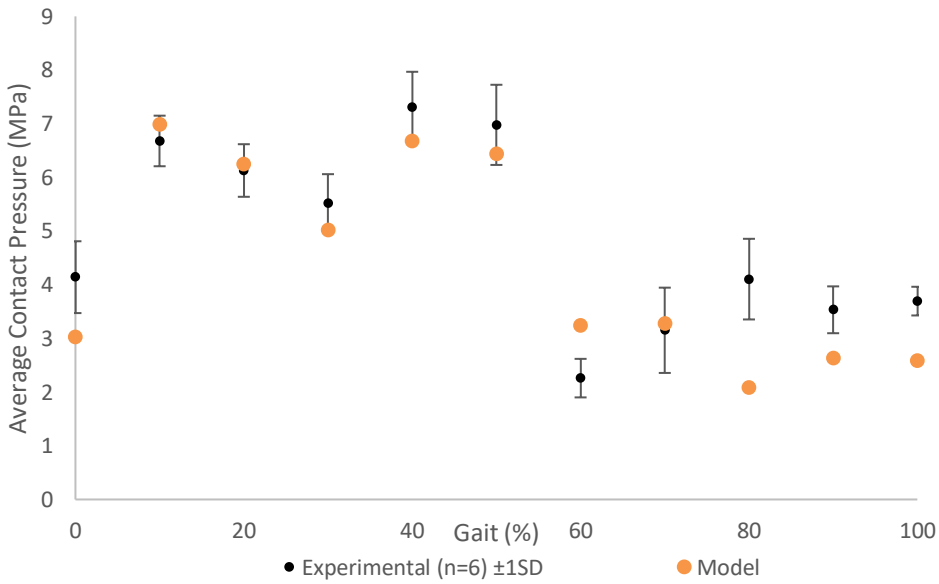

Figure 4-29: Average contact pressure of baseline TKR model plotted with average baseline Tekscan study outputs with ±1 standard deviation.

4.5.4 Discussion

The Attune total knee replacement model was used to investigate the contact pressure of the bearing at 10% intervals of the gait cycle. Results from the contact pressure study using the finite element model provide a detailed insight into the location, size and intensity of pressure using contact pressure heat maps. The model predicted average contact pressure results have been found to be in agreement during higher loads with the experimentally measured values using Tekscan pressure

sensors. However, at lower loads there was less agreement which may be due to limitations in the accuracy of measuring contact pressure at lower loads.

The advantages of the model are highlighted in this study. Where the Tekscan method was unable to secure the pressure sensors on the tibial insert without resulting in shear stresses acting on the sensors, the model has the advantage of not requiring additional equipment to measure the contact pressures. As such, the model advantages in predicting contact mechanics are highlighted in this study.

4.6 Finite Element Model Discussion

A finite element model of an Attune AOX total knee replacement bearing was developed in ABAQUS. Overall, the model predicted kinematics and contact mechanics were in good agreement with experimentally determined values for the same setup and input conditions. Kinematic outputs of the non-linear TKR model were in good agreement with experimental simulation results with an RMSE value of 1.60 and 0.95 for anterior-posterior displacement and internal-external rotation respectively. The maximum average contact pressure was 6.68MPa at 40% gait and minimum was 2.08MPa at 80% of gait. The peak contact pressure was 16.91MPa. The contact pressure between the compartments varied depending on the gait cycle alignment and there were two intervals where there was no contact pressure measured on the lateral compartment (60% and 70%). In comparison, the experimental Tekscan study also showed low contact pressure on the lateral compartment at 60% (0.6MPa), but did not show a relatively low contact pressure at 70% (3.01MPa). The limitations of the experimental Tekscan setup methodology previously discussed, including the challenges of securing the sensor in place and movements of the sensor once the components were brought into contact, may offer some insight into the differences between these values. The results from this finite element model investigation of the contact pressures of the two compartments highlights specific measurement points where additional method development of the experimental study may require focus in future studies to understand why the results at 70% are different between the two studies.

Methods of applying pre-clinical simulation inputs to a TKR model were initially developed on simple geometries, including cylinder on plate and sphere on plate model configurations. The simplified geometry outputs were verified against theoretical values determined from Hertzian contact theory equations. The verified models were then adapted into the appropriate setup of the model in terms of mesh type, the alignment of the components and application of loads and boundary conditions, the setup of spring constraints and determining the steps required to

initialise the model and run a full gait cycle. This setup considered the creation of control nodes at the centre of rotation of each component and the axis of alignment. The setup methodology for the simplified geometry was then applied to the TKR model.

Mesh convergence studies were completed to assess the suitability of different element sizes for the Attune TKR geometry. To complete this step, an initial study was completed where the component materials were assigned values of XLK material properties. A mesh applied in ABAQUS showed convergence under a 220N load of 7.3MPa. An additional convergence study was completed on the XLK mesh, where a mesh was applied in HyperMesh. The HyperMesh software, in comparison to ABAQUS, allows more control over the element size on the surface which reduces the chance for concentrated areas of small element sizes at regions of sharp geometry changes, such as the edge of the tibial insert surface. This mesh resulted in similar maximum contact pressure values in comparison to the ABAQUS mesh, however there was more variation in values even at the refined mesh sizes. There were challenges with the method of importing the HyperMesh components into ABAQUS resulting in elements that were too small to be effective. However, these elements were not on the contact surface of the tibial component so were deleted from the mesh to resolve the issue. As a result, ABAQUS was selected as the most appropriate software to use to complete the meshing step of the model development. An independent mesh convergence study in ABAQUS with AOX material properties and an applied compressive load of 667N as performed. The study resulted in a maximum contact pressure around 20MPa to encompass the maximum values expected during future studies using this model. Considering contact pressure results and CPU time, a global element size of 1mm with 204,748 elements assigned to the femoral component and 137,527 assigned to the tibial insert component was selected as optimal for this total knee replacement design.

Although there was confidence in the method of setup and application of variables to the TKR model, validation of the outputs was still necessary but required experimental investigation to support the computational predictions of kinematic outputs and contact mechanics. The differences in anterior-posterior translation between 60-80% is possibly due to the inherent variability of using spring constraints to control motion and physical mechanical factors which cannot be accounted for computationally, such as friction. Overall, the output kinematics of the model were in good agreement with the experimental values and were within the 95% confidence intervals.

The AP displacement did deviate from being within the experimental 95% CI between 60-65% of the gait cycle. One explanation for this deviation is that the computational model does not fully account for the mechanical variables of the simulator and any friction as a result of motion or the control springs. This could be accounted for by adapting the model to include the electromechanical components of the simulator, however this would require significantly more development and CPU time. Additionally, the confidence interval of the experimental simulation had a relatively small confidence interval during this phase of the gait cycle, resulting in a smaller range of values for the model prediction to fall within. Alternatively, a consistent range to test for agreement between the two outputs may be more appropriate.

It may be noted that there was a larger posterior translation between 0-10% of the gait cycle than has been reported by List et al. 2020 for the Attune design in vivo using a moving fluoroscope [85]; this may have been driven by the ISO standard which is generic for all fixed bearing implant designs but may be efficiently investigated in future by this model.

The contact mechanics studies in this baseline model of Attune were used to investigate the responsiveness of the model to changes in loads and kinematics, to allow a direct comparison to experimental values determined from the same setup, and to create inputs for the wear framework which will ultimately determine a computationally predicted wear rate for Attune AOX TKRs. The changes in the average contact pressure over the gait cycle shows that the model has good response to changes in applied load.

The position of the contact area at 10% intervals showed the response to tibial rotation and AP translation and larger shifts of the lateral condyle compared to the medial condyle. In addition, the medial condyle showed larger contact pressure measurements on the contour map (indicated by red areas) compared to the lateral condyle. This was expected due to the medial shift applied to the model setup and reflects what would be found in-vivo.

Overall, this study of baseline model predicted kinematics and contact mechanics gives confidence in the efficacy of the model to predict these outputs in agreement with experimental simulation outputs.

Chapter 5
Patient Specific Alignment Experimental Simulation

5.1 Introduction

Patient specific alignment (PSA) of total knee replacements is a change to conventional alignment approaches to the procedure, where each patient's native, constitutional limb alignment is accounted for during the surgical planning and implantation of the total knee replacement [88]. Patient specific alignment encompasses true kinematic alignment, restricted kinematic alignment and other procedures in-between [92].

Patient specific alignment procedures are typically completed in one of three ways, with procedure specific instrumentation [94], with pre-made cutting blocks [13, 152], or with computer navigated surgical systems [89, 153].

These procedures offer good early surgical outcomes and have increased patient satisfaction [90, 154]. However, there is little understanding of the effect of patient specific alignment on offsets in compartment loading and the long-term impact this may have on the wear of total knee replacement polyethylene components.

The aim of this chapter is to review the surgical procedure techniques of PSA, and determine how to simulate the input parameters in an experimental environment so that the tribology and biomechanics can be assessed. The first steps will be to determine the surgical alignment parameters of interest and then to assess the capabilities of the electromechanical simulators to simulate these alignment parameters. A wear simulation and contact mechanics study will then be completed using methods outlined in Chapter 2 and Chapter 3, to determine experimental kinematics of the tibial insert, contact pressure, and wear over 3 million cycles of gait in the PSA setup.

The outcomes of this chapter will be compared to the baseline mechanical alignment results to evaluate the impact of alignment on experimental simulation outputs. The results will also be used as part of future studies to implement PSA in the computational finite element environment.

5.2 Patient Specific Alignment Background

Traditional mechanical alignment surgical approaches involve systematically creating a neutral long leg axis during total knee replacement surgery. However, the inherent anatomical variation between patients means that a patient specific approach to joint alignment, where the patient's native anatomy is accounted for, may be more suitable. In mechanical alignment procedures where the natural alignment is altered, there can be detrimental effects on the soft tissue structures surrounding the knee causing instabilities, loss of full kinematic range of motions and reduced patient satisfaction [13, 106, 155] As a result, alignment procedures that are considerate of the patients native anatomy have become increasingly popular over recent years. The evolution of patient specific procedures has occurred over the last 15 years, with early studies published between 2008 and 2010 investigating the variability between patient anatomy and how surgical procedures could restore native anatomy [156-159].

There is still uncertainty around the appropriate boundaries of patient specific alignment procedures. Where restoring the native anatomy might improve surgical outcomes in one patient, this may not be true for all patients and could be affected by a range of variables. It is therefore important to understand the individual variables in a patient specific alignment approach, how these variables vary within patient cohorts, determine whether outlier populations exist and finally establish research based safe boundaries for all patients. This section will systematically review current literature on patient specific alignment post-operative outcomes and evaluate the ranges of alignment parameters, including joint axes and angles, identified in these studies.

5.2.1 Patient Specific Alignment Axes and Angles

There are three kinematic axes of the knee which include; the transverse axis about which the tibia flexes and extends, the longitudinal axis about which the tibia internally and externally rotates, the transverse axis about which the tibial flexion-extension occurs and the transverse axis about which patellar flexion-extension occurs (Figure 5-1) [155].

The femur mechanical axis is the line joining the centre of the femoral condyle with the head of the femur and the tibial mechanical axis joins the centre of the tibial plateau with the centre of the tibial plafond. The long bone axis joins the centre of the head of the femur with the centre of the tibial plafond (Figure 5-2).

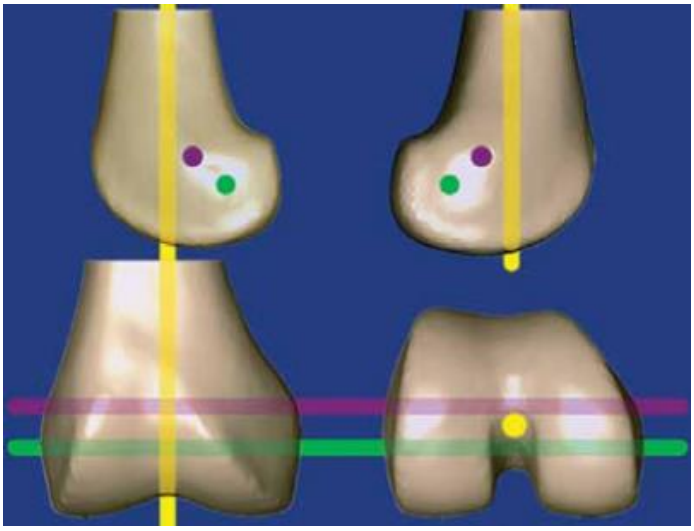

Figure 5-1: The three axes that define tibiofemoral and patellofemoral kinematics including the longitudinal axis (yellow), transverse axis of tibial flexion (green) and transverse axis of patellar flexion (magenta) [155]

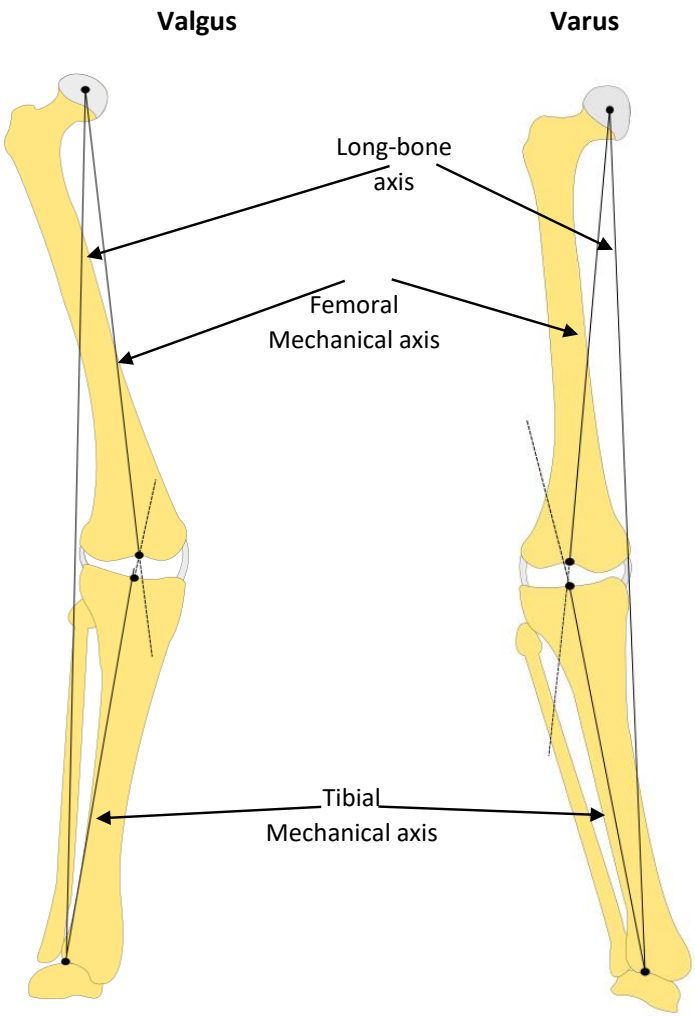

Figure 5-2: Frontal view leg axes in valgus and varus alignments, including the long bone axis, the femur mechanical axis and the tibia mechanical axis.

Once the mechanical and anatomic axes of the limb are defined, the angles between the joint line and the axes can also be defined, which facilitates the assessment of the overall alignment of the joint. The obliquity of this joint line determines the alignment of the joint. When determining the pre-operative alignment it is important to first measure on a radiography the parameters detailed in Table 5-1 which include the mechanical and anatomic axes, the joint lines of the knee surfaces and the overall HKA angle of the lower limb (Figure 5-3).

Table 5-1: Lower limb alignment axes and angles terminology [94, 160]

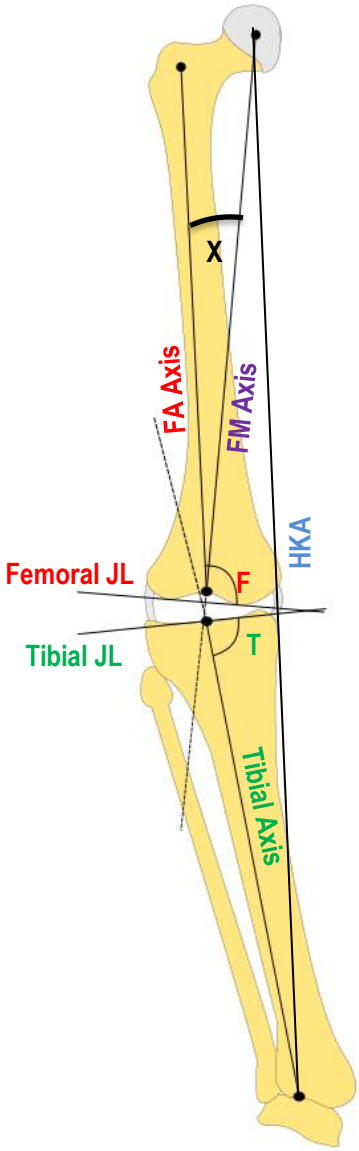

Figure 5-3: Frontal view lower leg alignment axes, angles and joint lines (JL) [94]

Axis/Angle	Definition
Femoral mechanical axis (FM)	A line that runs distally from the centre of the femoral head to the centre of the femoral condyle
Femoral anatomic axis (FA)	A line that runs distally from the anterior superior iliac spine to the centre of the femoral condyle
Tibial axis	A line from the centre of the tibial plateau running distally to the centre of the tibial plafond.
Femoral valgus angle (F)	Angle between the femoral joint line and the femoral anatomic axis.
Tibial joint line angle (T)	Angle between the tibial joint line and the tibial mechanical axis.
Femoral anatomic axis angle (X)	Angle between he femoral anatomic axis and femoral mechanical axis
Hip-Knee-Ankle angle (HKA)	Angle between the femoral mechanical axis and the tibial mechanical axis. In neutral alignment this angle is 180°.
Joint line orientation angle (JLOA)	joint line perpendicular to the weight bearing axis.

5.2.2 Patient Specific Alignment Outcomes in Literature

5.2.2.1 Overview of Systematic Review

A systematic review of published literature was completed to investigate the range of knee joint alignment variables in patient's post-operative outcomes after TKR surgery. The review covered studies investigating the difference between patients undergoing a mechanical alignment procedure versus patients undergoing patient specific alignment procedures. Terminology outlined in Table 1-2 can be referred to for the alignment procedure nomenclature used in this thesis, where anatomic alignment is a systematic approach to applying a 3° varus angle to patients, kinematic alignment is true resurfacing of the joint, and restricted kinematic is resurfacing the joint within specific boundaries. The procedures used on patient cohorts for these studies are summarised in Table 5-2 which were either randomised control trials (RCT) where subjects are randomly assigned a treatment group or retrospective case control (RCC) where two or more groups are identified, controlled by the researcher and compared in the study. Studies were included if they included post-operative evaluation of both a MA and PSA procedure, included the surgical approach for each procedure, stated alignment parameters for the femoral and tibial joint line angles and reported post-operative functional outcomes.

Table 5-2: Summary of reviewed literature on mechanical alignment versus patient specific alignment outcomes

Journal Article	Patients	Procedure		Trial type	PSA Alignment approach
		MA	PSA		
Dossett (2014) [13]	MA = 60 PSA = 60	Standard MRI using intermedullary (IM) rods and standard cutting jigs.	Patient specific cutting blocks using MRI	RCT	KA
Young (2017) [152]	MA = 50 PSA = 49	Computer-assisted navigation	Patient specific cutting blocks using MRI	RCT	KA
McNair (2018) [161]	MA = 15 PSA = 14	Cohort of patients post-op	Cohort of patients post-op	RCC	KA
Blakeney (2019) [153]	MA = 18 PSA = 18	Computer-assisted navigation	Restricted KA protocol. Computer assisted navigation	RCC	rKA

Different surgical approaches were adopted by the studies included in this review. Two studies used cutting blocks for the patient specific alignment approach [13, 152] and one used computer assisted navigation [153]. For mechanical alignment, two studies used computer assisted navigation [152, 153], one used traditional surgical instrumentation including intermedullary rods and cutting jigs [13]. The remaining study was a post-operative review of a selected patient cohort and did not report the individual surgical techniques used for the cohort [161].

Additionally, there were variations in the patient specific alignment approach adopted by the surgeons in each study. Three of the studies assessed true kinematic alignment procedures [13, 152, 161] and one set “safe boundaries” to operate under a restricted kinematic alignment approach [153]. The “safe boundary” was defined as an overall HKA alignment within ±3° and femoral joint line and tibial joint line angles within ±5°. Two studies applied an exclusion criteria from their studies of above a 15° varus/valgus deformity [152, 161].

5.2.2.2 Alignment Angle Outcomes

The post-operative measurements of the patients’ alignment angles for the reviewed literature, summarised in Table 5-3, includes the overall HKA angle and joint line angles in the coronal plane, sagittal plane and transverse plane. All four studies reported no significant difference in HKA angle between the PSA and MA patient cohorts. The range of values reported for the tibial coronal angle was -0.88° to 0° for MA compared to -3.0° to -2.2° for PSA. All studies, except McNair at al., (2018) which found no significant difference in any alignment angle outcomes, reported that the tibial component was significantly more varus in PSA compared to MA. There was also a significant difference reported for the femoral coronal alignment by Dossett et al., (2014), Young et al., (2016) and Blakeney et al., (2019) where the femoral component was more valgus in PSA compared to MA. The range of tibial slope values reported by the studies was +1.1° to +5° in MA compared to +3.7° to +4° in PSA. Femoral sagittal angle was only reported by Blakeney et al., (2019) and was not significantly different between the MA and PSA procedure. Finally, Young et al., (2016) reported that the femoral component was significantly more internally rotated in PSA compared to MA.

Table 5-3: Post-operative joint alignment angles of the literature review of MA and PSA procedures

Joint Alignment Average (SD)	**McNair (2018)**		**Blakeney (2019)**		**Dossett (2014)**		**Young (2016)**	
	MA	PSA	MA	PSA	MA	PSA	MA	PSA
HKA angle (°)	-0.88 (1.7)	-0.14 (2.8)	-0.5 (2.3)	0 (3.3)	0.1 (2.5)	-0.1 (2.8)	-0.7 (2)	-0.4 (3)
Tibial coronal angle (°)	-0.88 (2.1)	-2.7 (2.5)	0 (1.9)	-2.5 (2.0)	0 (2.1)	-2.2 (2.6)	-0.7 (1.8)	-3 (3)
Femoral coronal angle (°)	0.38 (1.3)	1.9 (2.2)	0 (2.5)	2.5 (2.1)	-0.8 (2.7)	1.3 (2.0)	0.5 (1.6)	2 (2.5)
Femoral internal rotation angle (°)	1.6 (3.1)	0.07 (2.4)					1.5 (2.5)	-0.5 (2.5)
Tibial slope angle (°)	1.1 (2.3)	3.7 (3.2)	5 (3.0)	4 (3.0)			1.3 (2)	4 (2.5)
Femoral flexion angle (°)			3.5 (3.8)	3 (4.2)				

* -ve values Varus, +ve values Valgus for coronal angles

5.2.2.3 Functional Outcomes

Post-operative kinematic motions were reported by the studies to assess the functional outcomes of each surgical procedure. A randomised control trial of 120 patients, evenly split between MA and KA procedures found that the KA approach resulted in a larger range of flexion motion by 8.5° [13]. Other studies have also found a difference in functional outcomes, reporting an increase of 10° in the maximum flexion angle achieved in patients who had undergone a KA approach in comparison to MA [152]. In comparison, some studies have reported no significant difference between maximum flexion motion of PSA and MA [153, 161], although in one study the maximum flexion motion of MA was significantly lower than that of a healthy control group [153]. Hutt et al., (2015) did not report post-operative functional outcomes. Overall, studies have reported that PSA procedures are more restorative of healthy knee flexion range of motion.

5.2.2.4 Summary of Systematic Review

Four studies were included as part of this systematic review in accordance with the selection criteria which was a post-operative evaluation of both a MA and PSA procedure, details of the surgical technique and reported outcomes to include component alignment angles and kinematic range of motion. Overall, studies found that PSA did not significantly impact the overall HKA angle of the lower limb but that specific component alignment angles were significantly different between PSA and MA. Regarding the studies which did find a difference, the femoral coronal angle, tibial coronal angle and femoral internal rotation angle were all significantly increased in PSA [13, 152, 153].

When comparing studies of patient surgical outcomes, it is important to consider the variability of individual surgeon in addition to the different alignment approaches and surgical techniques used. Each surgeon has preferred methods of operating and inherent error in the procedure. Furthermore, some studies stated an exclusion criterion from the patient cohort which may have skewed averages due to a more condensed study sample.

5.2.3 PSA Surgical Guidelines

The surgical alignment procedures provided by manufacturers for variants of patient specific alignment state safe boundaries for the implantation of their medical devices. One such set of guidelines from DePuy Synthes states how to calculate the angles of the pre-operative joint and how to determine the cutting angles for placement of the total knee replacement [94]. These cutting guidelines have boundaries for the safe alignment of the components, using angles and axes defined in Table 5-1, which are as follows, where X is the angle between the mechanical axis of the femur and the anatomical axis of the femur (Figure 5-4).

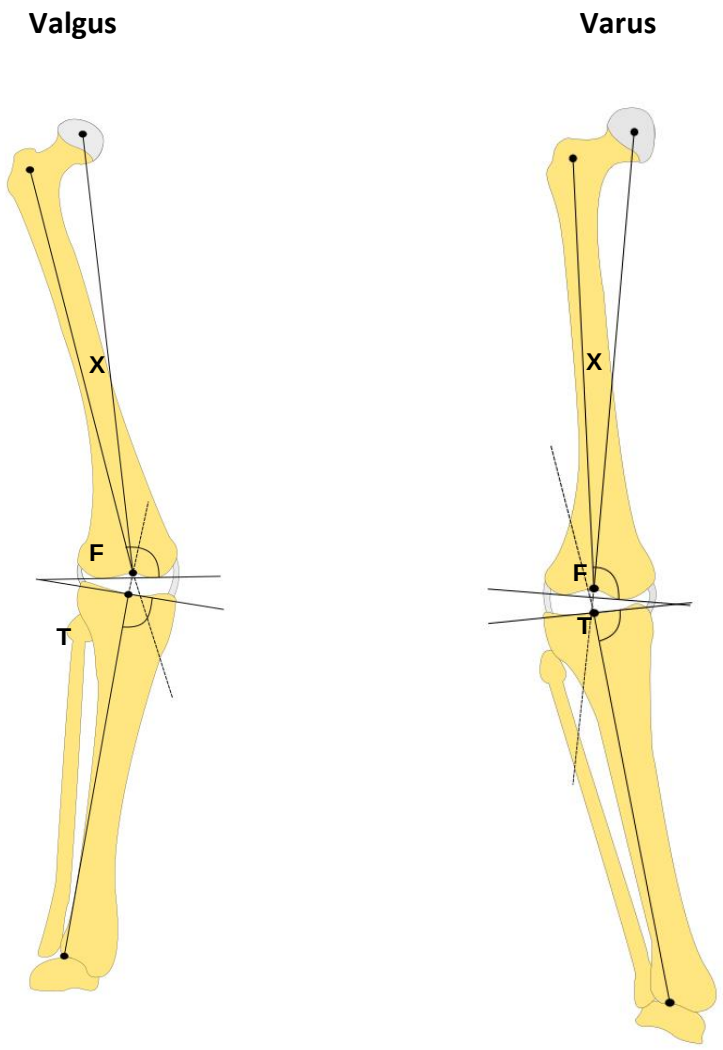

Figure 5-4: Total knee replacement patient specific alignment angles and axes for pre-operative cutting calculations [94].

The HKA angle can be determined by the equation F + T – X = HKA angle [94]. The "safe boundaries" stated in the DePuy Synthes femur first PSA instrumented technique specific to the ATTUNE Knee System are as follows:

- T safe boundary 87° – 90°
- HKA safe boundary 177° – 183
- F safe boundary <99°
- T should be adjusted for HKA to fall within the boundary, T should not be >3 degrees varus.

An example of adjusting the alignment angles to ensure that the patients' TKR procedure is within the "safe boundaries" is outlined in Table 5-4. An example of how this would be adjusted in the patients long-leg anatomy is shown in Figure 5-5. The guidelines given are considerate of the error found to be the typical range of surgeons which is +/-2° [162], the "safe boundaries" take this value into account.

Table 5-4: Example of patient with out of "safe boundary" tibial coronal angle as per DePuy Synthes ATTUNE Knee System femur first PSA instrumented surgical technique

Angle	Safe boundary	Example X-Ray value	Adjusted surgical alignment angle
T	87° – 90°	85°	87°
F	<99°	98°	98°
HKA	177° – 183°	177°	177°
x	/	6°	8°

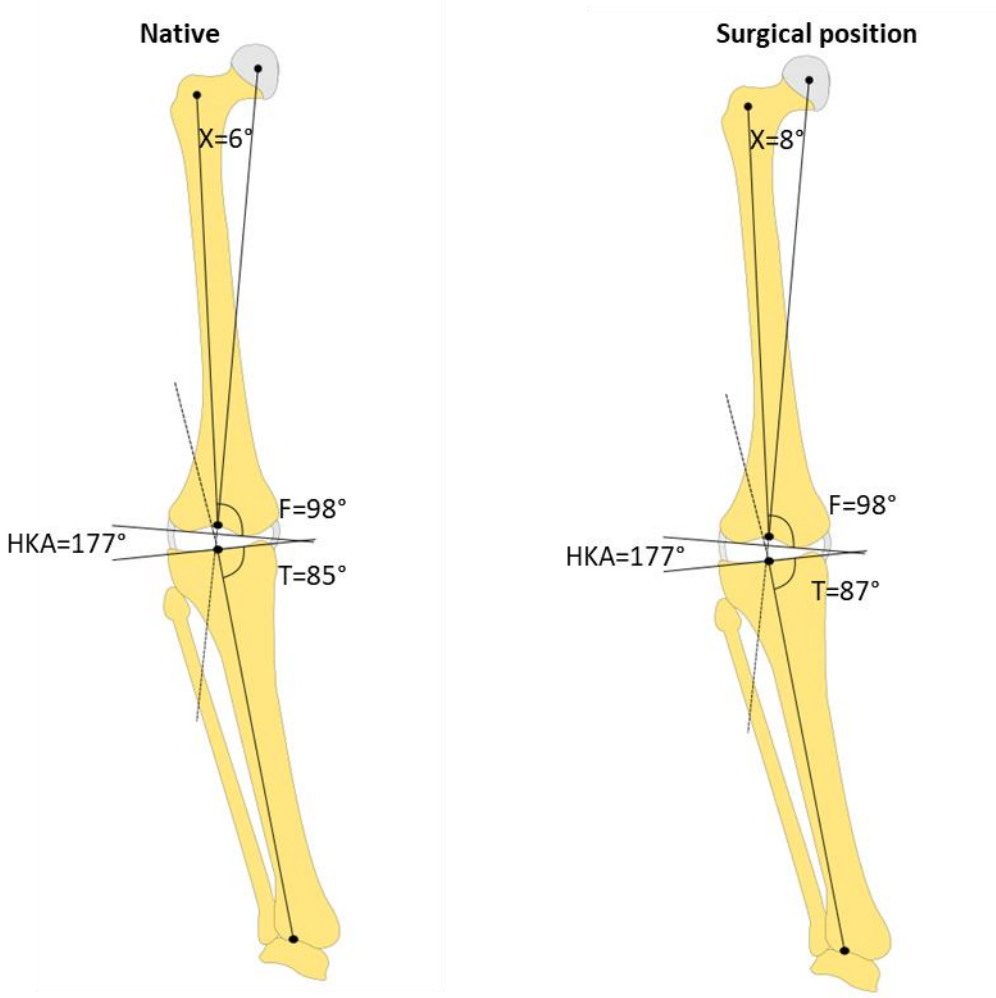

Figure 5-5: Illustrated example of cutting angles to restore patients' post-operative alignment to within DePuy Synthes "safe boundaries"

5.2.4 Conclusions

Firstly, the coronal alignment of the total knee replacement was established. The summary of literature established that constitutional varus and valgus are defined as a HKA angle larger than ±3° [88]. Therefore, the alignment selected to be studied was 4° varus to investigate an alignment within the envelope of what would be determined constitutional varus, but within the range of surgical error of ±2° of

restricted kinematic alignment surgical guidelines which stated a maximum of 3° varus from neutral HKA alignment [94]. An additional consideration for selecting a 4° varus alignment as the study subject was to align the study with previously published literature. Studies which have investigated the kinematics and wear of total knee replacements under patient specific alignments have created 4° varus alignment setups. Using this alignment as the primary study alignment allows results to be compared to literature [121, 129].

There are three planes of alignment in a total knee replacement on each side of the joint. These planes of alignment require femoral cuts and tibial cuts during operation determined pre-operatively as per the surgical procedure being followed. The compensation for cartilage thickness is also accounted for in the calculation, which is typically 2mm thick [163].

5.3 Development of Experimental Methods of Patient Specific Alignment

5.3.1 Rationale

The purpose of this study was to use previously developed pre-clinical assessment methods to investigate the effect of patient specific alignment on the tribological and biomechanical performance of the total knee replacement. Previous sections have detailed a methodology of pre-clinical assessment of kinematics, contact mechanics and wear of a total knee replacement bearing in mechanical alignment. This section will adapt the methods to simulate patient specific alignment variables in a pre-clinical in-vitro study. The adaptions to the baseline mechanical alignment setup will include the following objectives:

- Evaluate the capabilities of the ProSim electromechanical total knee replacement joint simulator to create 4° varus coronal alignment angles.
- Investigate methods of adapting component fixtures to create 4° varus coronal alignment angles.
- Determine how to implement the pre-defined centre of rotation for the Attune TKR bearing samples with 4° varus coronal alignment during simulator setup.

5.3.2 Simulator Capabilities

The capabilities of the ProSim 6-station electromechanical simulator were investigated to establish whether using the abduction-adduction carriage of the simulator to create a varus alignment was feasible. Two methods of using the carriage to control the varus alignment were investigated on the University of Leeds ProSim 6-station electromechanical knee simulator, which were as follows:

- Trial 1 – using the carriage to apply a displacement demand to rotate the tibial component. The axis would then be locked in position before applying a load (Figure 5-6a)
- Trial 2 – Creating an abduction-adduction displacement profile to control the motion of the tibial component through the gait cycle.

During Trial 1, the components were setup as per the baseline Attune simulator setup on mechanical alignment fixtures, with Vaseline between the bearing for lubrication and the abduction-adduction bar secured to the axis. The simulator controls were used to move the abduction-adduction axis of the simulator to values of 1° to 5° in increments of 1°. At each position, the component was loaded to a 50N load and 2000N load. An inclinometer was used in combination with outputs from the simulator software to show when the axis, when unloaded, reached the desired angle. When aligned at the required angle, the lateral compartment visually separated from being in contact with the tibial insert Figure 5-6b.

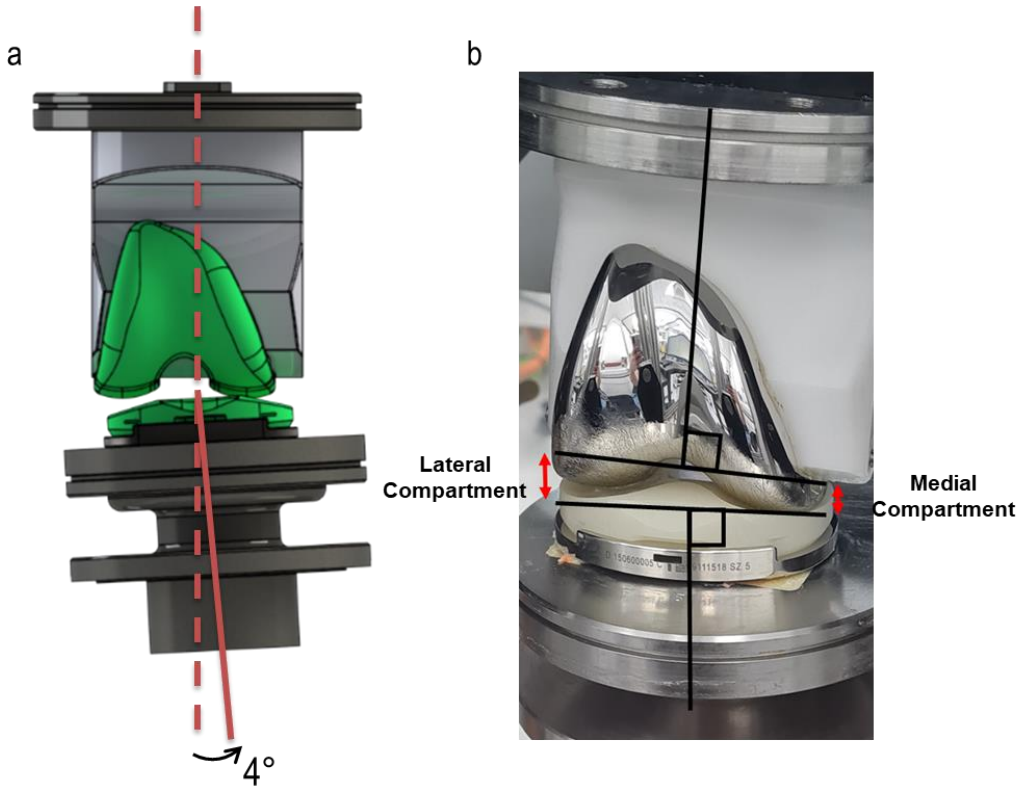

Figure 5-6: Trial 1 - 4° tibial angle setup using abduction-adduction carriage a) CAD depiction of adaption to component alignment b) component alignment during simulator alignment trial

Once the angle of orientation of the abduction-adduction axis was confirmed using an inclinometer, the station was loaded. When walking peak gait cycle loads of up to 2000N were applied, the tibial carriage was not able to maintain the adduction angle and rotated in reaction to the applied load to create a 0° tibial angle. It was therefore determined that the axes could not be used to control the varus angle of the components.

In Trial 2 the 127-point input profile for the simulator was adapted to include a value for the abduction-adduction axis. The setup of the simulator was the same as the baseline Attune AOX study but with the abduction-adduction control bar in place to allow control of the axis rocker. The output files requested from the simulator showed that the tibial carriage was not capable of maintaining the requested value when completing a gait cycle (Figure 5-7). It was deduced that this method of control was not suitable for this study. As a result, the simulator controls were not capable of applying the varus angle to the components. Fixtures were determined to be the more suitable solution.

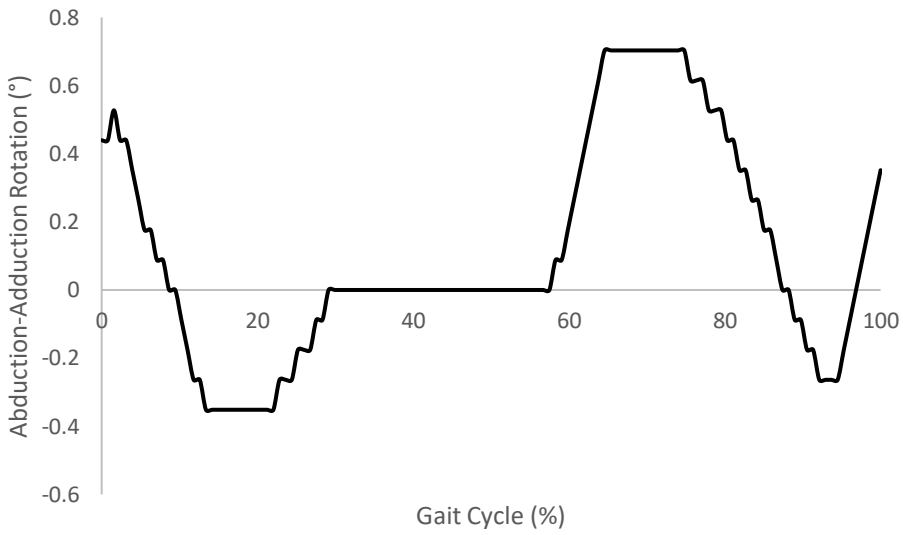

Figure 5-7: Trial 2 – Abduction-adduction rotation angle output kinematic profile with 4° adduction angle profile applied to simulator tibial carriage

5.3.3 Designing Fixtures

To design the fixtures for the 4° varus setup, further consideration to the capabilities of the simulator was required. From the previous studies, it was shown that the simulator did not have the capability to maintain an angle on the abduction-adduction carriage, and therefore on the tibial component while the femoral component was at a different angle of alignment. Once a load was applied through the femoral component, the abduction-adduction carriage moved to create an aligned dwell point between the components.

As a result, the study had to be limited to investigating the effects on kinematics, contact mechanics and wear of the total knee replacement bearing while both components were in the same coronal plane of alignment. Consequently, patient specific alignment as explain above was not created for the experimental study of alignment, both components were assigned a 4° varus alignment which was created using fixtures.

Existing tibial fixtures at 4° varus of alignment at the University of Leeds were used. New bespoke fixtures for the Attune design of the femoral component at 4° were created and manufactured using Delrin. One important consideration when adapting the fixture setup for the experimental simulator to the 4° varus alignment was the axis of alignment of the components in the simulator and the resulting location of the axis of applied load through the femoral component. The control axes and coordinate system were built in characteristics of the joint simulator meaning that adaptions to

alignment and loading position had to be built into the new component fixtures. The 4° varus angle created on the femoral fixture would have resulted in a shift in the centre of load if no further adaptions were made to the fixture. To account for this, the femoral base screw holes were repositioned using SolidWorks Premium 2018 x64 Edition (Dassault Systèmes SolidWorks Corp, US) to align the new 4° varus fixture with the femoral fixture base (Figure 5-8). Once the fixture was assembled with the Attune femoral component fixed in position on the Delrin fixture, new screw holes were created on the base of the Delrin fixture which aligned with the screw holes in the femoral base plate (Figure 5-9).

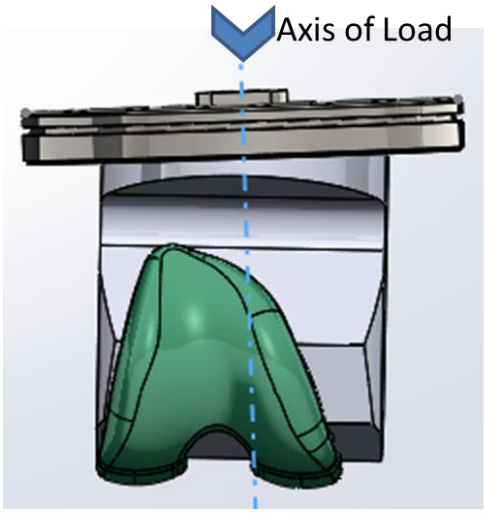

Figure 5-8: 4° varus femoral Delrin fixture aligned with femoral fixture base to align screw holes for positioning in the joint simulator

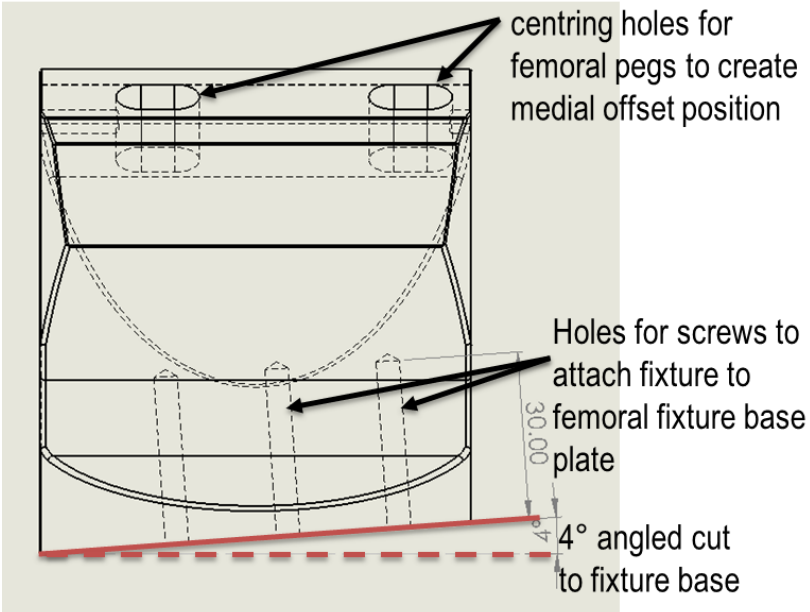

Figure 5-9: 4° varus alignment femoral fixture drawing with adapted base, base plate screw holes and femoral peg centring holes

5.4 Study 1 - 4° Varus Experimental Kinematics and Wear

5.4.1 Methods

A three million cycle wear study was completed using a ProSim 6-station electromechanical knee simulator. The components were setup for the wear simulation study using new 4° varus alignment fixtures and standard kinematic motions were applied as inputs to the simulator. All other methodology for setup of components and evaluating outputs remained the same as outlined in Section 2.3. The outputs from this study were volumetric wear rates and kinematics (anterior-posterior displacement, internal-external tibial rotation and abduction-adduction rotation).

5.4.1.1 Attune AOX Components

The components used in this study are shown in Table 5-5 which include six wear bearing components and two additional tibial inserts for unloaded soak controls. Corresponding sample information including lot numbers are recorded in Appendix A. The components were rotated onto a new wear station at each one million cycle wear interval to reduce any inter-station variability. The pairings of the samples and wear station at each test interval is shown in Table 5-5. There were also two tibial insert unloaded soak control samples assigned to this test, C1 and C2. During the 0-1MC wear interval the tibial insert from sample 5 was damaged by unknown third-body wear. On restarting the simulator after the one million cycle wear interval, a simulator software fault caused the sample to dislocate resulting in damage to the tibial insert from sample 6. The tibial insert unloaded soak control samples (C1 and C2) were then used as wear samples, C1 as sample pairing 5 and C2 as sample pairing 6. The two unloaded soak control samples were replaced with inserts X1 and X2.

Table 5-5: 4° varus experimental wear simulation sample pairings with corresponding wear station at each wear interval

Sample Pairing	Insert	Tibial Tray	Femoral Component	Station Number		
				0-1MC	1-2MC	2-3MC
1	X7	T1	F7	1	2	3
2	X8	T2	F8	2	3	4
3	X9	T3	F9	3	4	5
4	C10	T4	F10	4	5	6
5	X11/C1	T5	F11	5	6	1
6	X12/C2	T5	F12	6	1	2

5.4.1.2 Simulator Setup Methods

Six new 4° femoral fixtures were manufactured and then the Attune femoral components were cemented in position using the same PMMA methods as detailed in Chapter 2. Tibial fixtures were reused from previous studies. These were solid stainless steel machined fixtures with a 4° angled cut on the top of the fixture in the coronal plane. To position the tibial tray in the correct position to be aligned correctly with the axis of load, the tibial tray stems were adapted to fit in the centring hole of the fixture. To do this, material was taken off the side of the tray stem to allow it to be positioned far enough laterally on the fixture to not impinge on the edge of the fixture, allowing enough cement to fill around the stem to secure the tibial tray in place for the duration of the study.

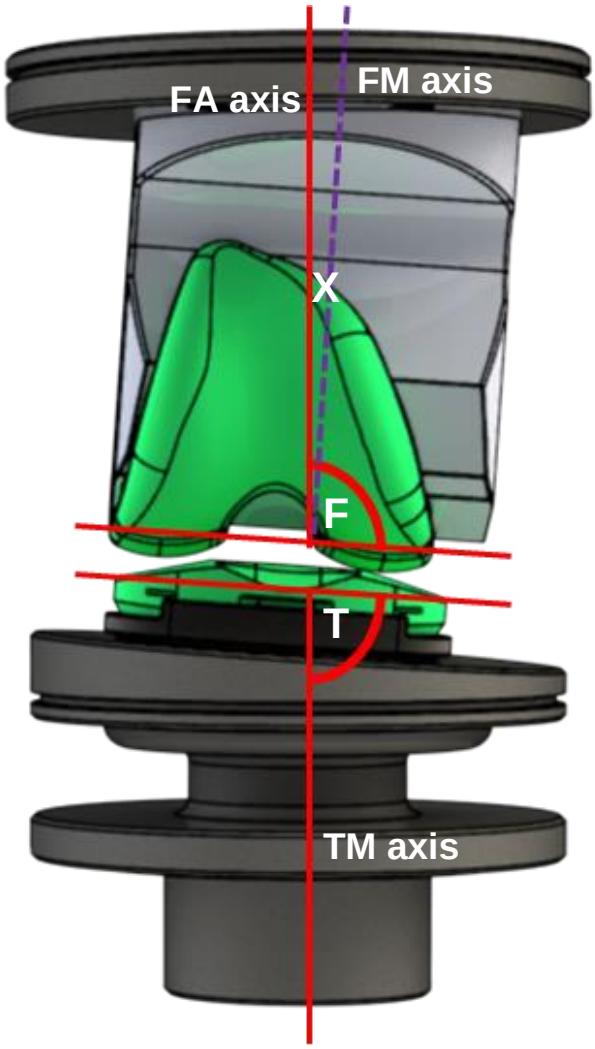

Figure 5-10: 4° varus experimental simulator setup with fixture adaptions. Axes of alignment labelled in accordance with DePuy alignment guidelines as femoral anatomical (red line) axis, femoral mechanical (purple dashed line) axis and tibial mechanical (red line) axis. F and T are the femoral joint line angle and tibial joint line angle respectively.

The procedure from Section “2.3.3 Sample Setup Methods” was followed to secure the tray in position using PMMA cement and ensuring the tibial insert was positioned correctly for the contact with the femoral component by using the simulator to align the components as per the schematic in Figure 5-10.

5.4.1.3 Kinematic Input Profiles

ISO 14243-1:2009 load control input kinematics were applied to this study [112]. Although variations to the alignments of the knee joint in-vivo would result in differences in the gait of patient’s and the ratio of loading over the two compartments of the knee leading to larger joint reaction forces [153], this simplified study did not account for this. The primary reason for this was that the gait and knee adduction moment is completely specific to the individual patient with a patient specific aligned implant. It would therefore require further studies to investigate the effect of patient gait and compartment loading for a specific patient case with this specific alignment, which is out of scope of this study. A secondary reason was to ensure that only specific variables were being investigated individually, to limit the effects of interactions of numerous input variables. As a result, the only variable in the inputs of this study was the angle of alignment of the components.

5.4.1.4 Output Kinematics Analysis and Wear Determination

Outputs from each wear interval were calculated as 100-cycle averages of all six stations. Comparing the output kinematic averages at each wear interval allows a comparison between the output kinematics over the three million cycles wear study.

The 100-cycle average was taken from kinematic outputs from the 0-1MC wear interval to allow direct comparison between the experimental outputs and the finite element model outputs. This interval was used because the samples were unworn making the bearing surface equivalent to the unworn sample geometry used to develop the finite element model outputs.

5.4.2 Results

5.4.2.1 4° Varus Kinematics Results

The average values for the kinematic outputs at each wear interval is shown in Figure 5-11 for AP displacement, Figure 5-12 for internal-external tibial rotation angle and Figure 5-13 for abduction-adduction rotation. For all simulation intervals, the outputs had the same amplitude with only slight changes in phase which may be the result of wear of the insert or due to the small variability in cementing alignment between each

sample resulting in slightly shifted output kinematics when rotated onto different wear simulation stations of the simulator. The output abduction-adduction angle was also plotted for this study. Since the fixtures positioned the components at 4°varus, it was important to understand how the alternate alignment angle affected the abduction-adduction angle over the gait cycle (see Figure 5-13).

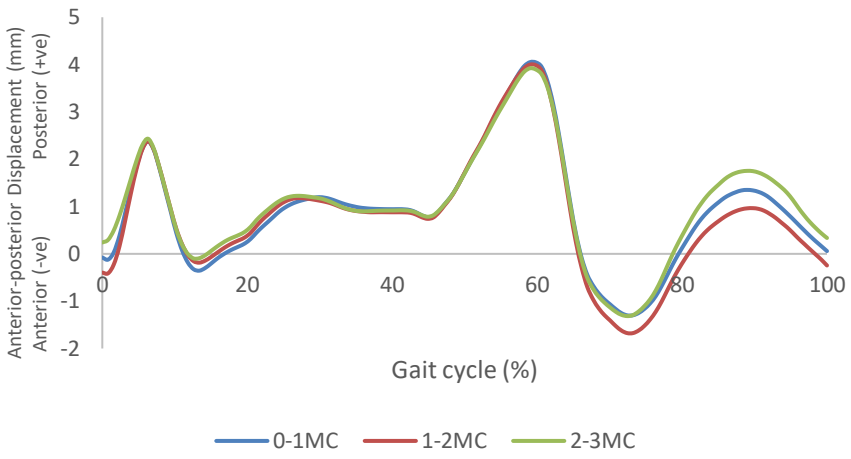

Figure 5-11: 4° varus alignment anterior-posterior displacement at each wear interval (100-cycle average of 6 stations)

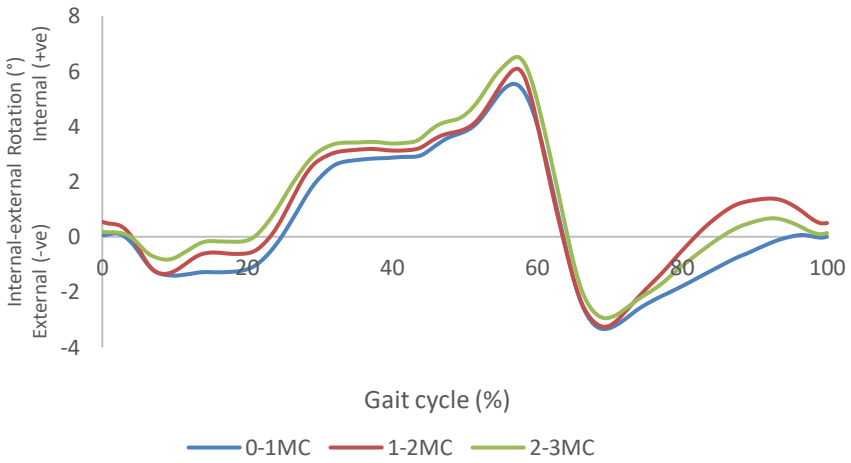

Figure 5-12: 4° varus alignment internal-external rotation angle at each wear interval (100-cycle average of 6 stations)

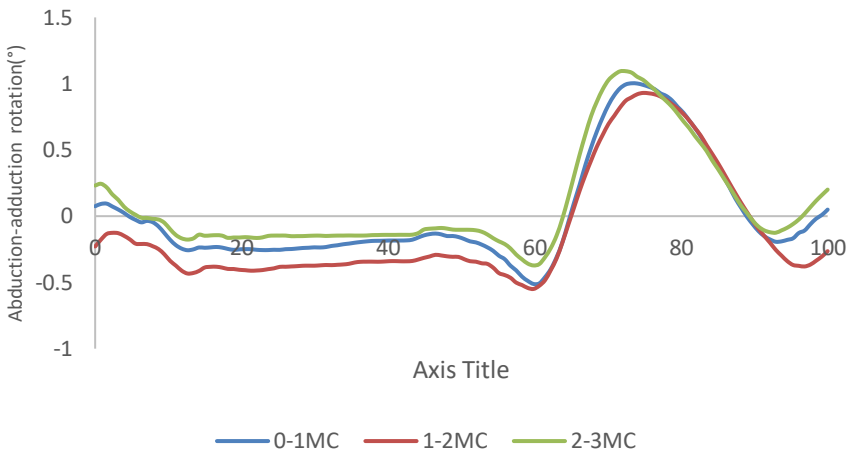

Figure 5-13: 4° varus alignment abduction-adduction rotation angle at each wear interval (100-cycle 6 station average)

The anterior-posterior displacement 0-1MC average with 95% confidence intervals was plotted to show the spread of the data for the six stations (Figure 5-14). The 4° varus alignment setup resulted in an initial posterior displacement reaching a peak of 2mm, followed by an anterior shift at 15% and a plateau at 1mm posterior position between 25-40%. An increase in posterior displacement to reach a peak posterior position of 4.3mm occurred at 60% while peak anterior displacement occurred at 73%. A net neutral displacement position was found at 100% of the gait cycle.

The internal-external rotation 100-cycle average with 95% confidence intervals (n=6) is shown in Figure 5-15. The output kinematics show a peak internal rotation of 5.5° at 59% and peak external rotation of 3.3° at 70%. There was net internal rotation between 25% and 63% of the gait cycle and net external rotation between 5.5% and 23% and between 63% and 92%. Abduction-adduction outputs were also analysed for the 100-cycle average shown in Figure 5-16 with 95% confidence intervals. There was a plateau in adduction rotation between 12% and 55% of the gait cycle followed by peak adduction of 0.5° at 60%. There was then an abduction rotation motion between 60% and 75% of the gait cycle reaching a peak of 1° followed by a final abduction motion during the end of the swing phase.

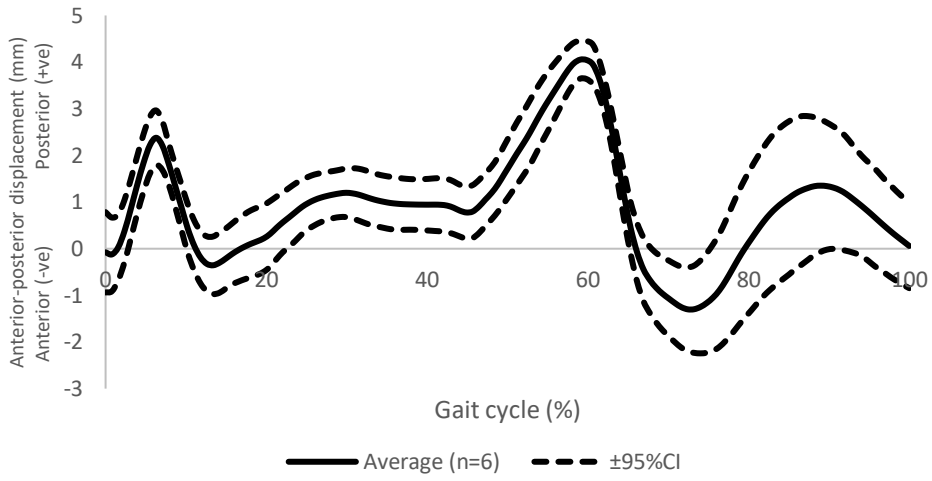

Figure 5-14: PSA 4deg anterior-posterior displacement 0-1MC 100-cycle average with 95% confidence intervals

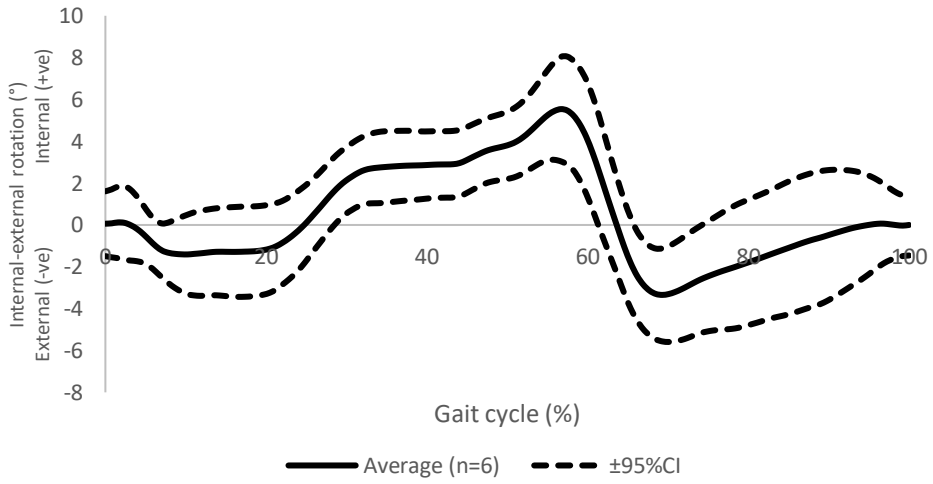

Figure 5-15: PSA 4deg internal-external rotation angle 0-1MC 100-cycle average with 95% confidence intervals

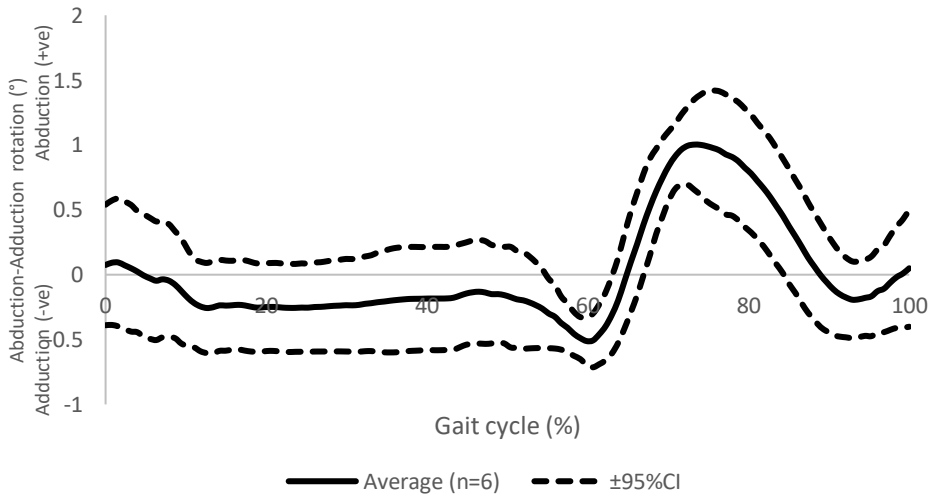

Figure 5-16: PSA 4deg abduction-adduction rotation angle 0-1MC 100-cycle average with 95% confidence intervals

The kinematic outputs of the 4º varus model were compared with the kinematic results of the baseline study to understand the impact of a 4º varus joint line on the output kinematics of an experimental simulated wear study (Figure 5-17). The anterior-posterior displacement 100-cycle average with 95% confidence intervals show that the baseline average start position was 1mm more anterior to the 4º varus start position. This difference was maintained over the whole gait cycle, but there was overlap of the confidence intervals throughout the gait cycle and the amplitude of the outputs between the two setups were similar.

The comparison of the internal-external rotation kinematic outputs of the two alignment studies showed a phase shift between the studies with the 4º varus alignment rotating less internally. The maximum internal rotation of the 4º varus alignment study was 5.5º in comparison to peak internal rotation in mechanical alignment which was 7.5º. However, there was continued overlap of the 95% confidence intervals over the whole gait cycle (Figure 5-18).

The abduction-adduction carriage of the simulator was left free to move in response to the motion of the bearings during the simulation. The outputs of the baseline and 4º varus simulations were also compared to understand the effect of changing the joint alignment to 4º varus would have on the motion of the abduction-adduction rotation in response to the experimental simulation inputs (Figure 5-19).

The 100-cycle average angle was similar between the two setups over the first 60% of the gait cycle and overlap of confidence intervals. However, there was less agreement in the final 40% of the gait cycle which is the swing phase of gait. The 4º varus simulation showed an increased average abduction to a peak of 1º compared to the baseline swing phase abduction which reached an average of 0.5º. The peak average abduction angle of the baseline setup was lower in value than the lower 95% confidence interval range of the 4º varus setup at this point of the swing phase.

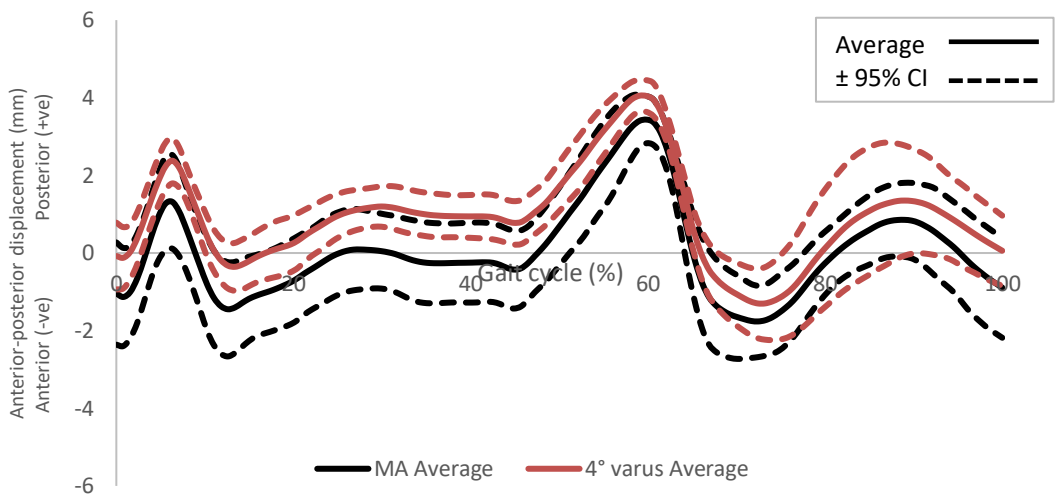

Figure 5-17: Baseline and 4º varus anterior-posterior displacement 100-cycle average with 95% confidence intervals

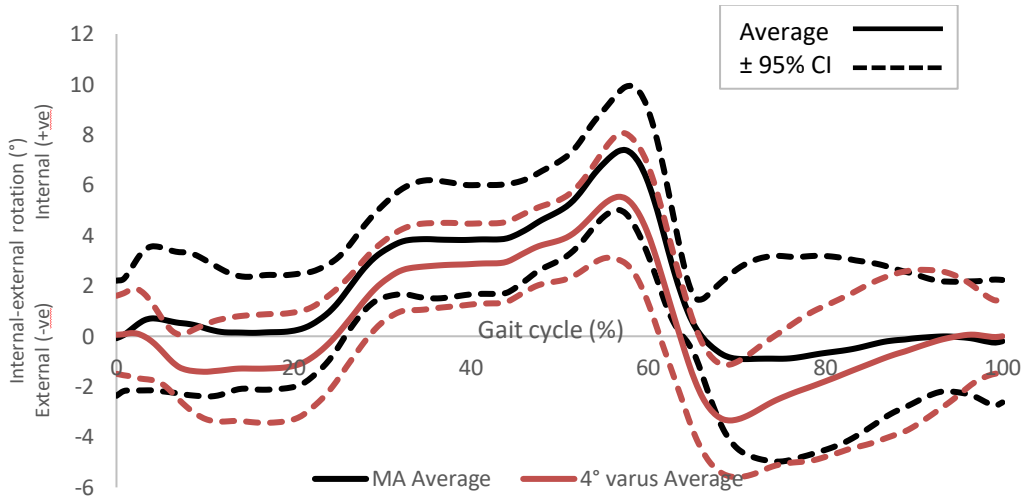

Figure 5-18: Baseline and 4º varus tibial rotation angle 100-cycle average with 95% confidence intervals

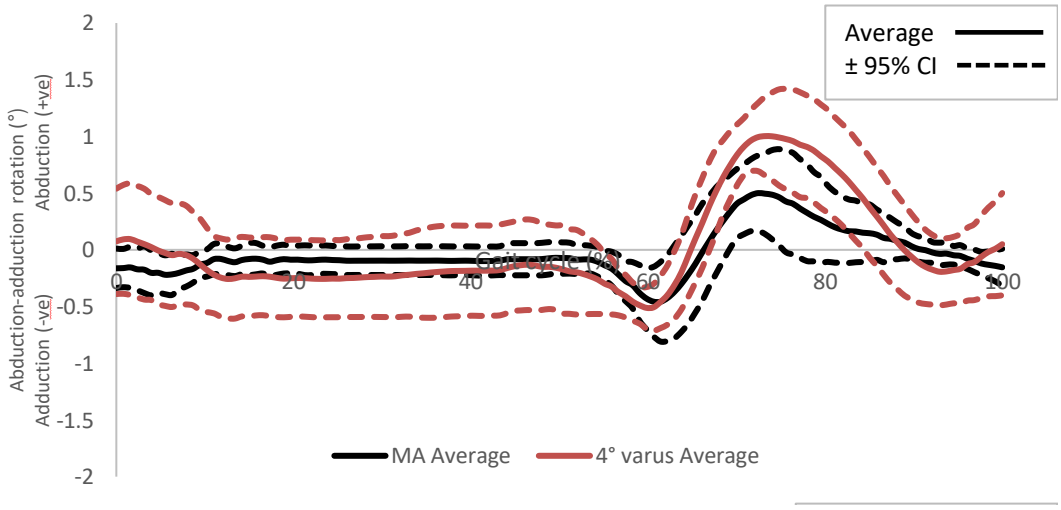

Figure 5-19: Baseline and 4º varus abduction-adduction rotation angle 100-cycle average with 95% confidence intervals

5.4.2.2 4° Varus Wear Results

The cumulative volumetric wear (mm^3) was calculated for each sample and a linear regression fit determined the volumetric wear rate (mm^3/mc). An average volumetric wear rate of the wear samples was determined after three million cycles of wear (Table 5-6).

During the wear simulation one sample was removed from the study after 1mc of wear due to third-body abrasive damage. A replacement tibial insert was used to simulate 2mc of wear which is presented in the data in this section. An additional sample was lost when the simulator was restarted for the 1-2MC wear interval due to a simulator fault causing the bearing to dislocate, this tibial insert was replaced for wear intervals 1-2mc and 2-3mc. The 1mc wear value for sample 6 was calculated from one tibial insert (X12) and the 2mc and 3mc wear intervals for sample 6 were calculated from a new tibial insert (C2). As a result, the 3mc volumetric wear rate was only calculated using n=5. The overall average volumetric wear rate for 4° varus of 5 samples was 3.3±0.5mm^3/mc .

Table 5-6: Cumulative wear (mm^3) of each wear sample at wear intervals, with 3mc volumetric wear rate (mm^3/mc) for each sample

Wear Cycles	Cumulative wear/sample number					
	1	2	3	4	5	6
0	0	0	0	0	0	0
1000000	6.5	6.0	4.8	1.2	2.8	1.5
2000000	8.9	9.8	6.9	3.6	8.3	5.4
3000000	11.6	11.0	8.7	10.7		7.3
Volumetric wear rate mm^3/mc	3.7	3.7	2.8	3.5		2.6

The mean cumulative volumetric wear values for the six wear samples (five-samples only for 4° varus 3 million cycle interval) for the baseline and 4° varus experimental simulations show that the mechanical alignment setup had lower average cumulative wear values than 4° varus at each wear interval (Figure 5-20). A 1-way ANOVA of the average volumetric wear rate of the 4° varus (3.3±0.6mm^3/MC) and mechanical alignment (2.7± 1.1mm^3/MC) experimental wear studies at 3 million cycles of wear found that they were not significantly different *(p=0.12)*.

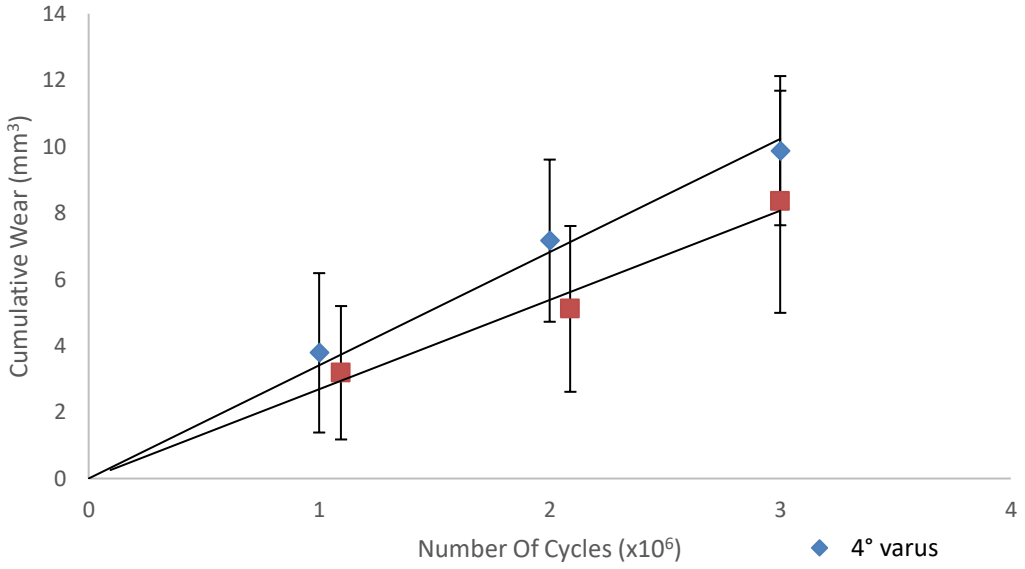

Figure 5-20: 4° varus and MA average cumulative wear with 95% confidence intervals at wear intervals over 3mc, and regression line with intercept at zero

5.4.3 Discussion

In summary, the 4º varus setup did not have a notable impact on the output kinematics of the experimental wear simulations. There was overlap of the 95% confidence interval range during the whole gait cycle for anterior-posterior displacement and tibial rotation, and for the stance phase of abduction-adduction rotation. The kinematic outputs of the 4º varus alignment simulation showed an increase in the abduction of the knee during swing phase in comparison to a mechanically aligned bearing. This suggests that altering the joint line angle, with no further adaptions to any other input variables, had an effect on the abduction-adduction rotation of the bearing.

Regarding the impact of 4º varus alignment on the wear of a total knee replacements, the results found no significant difference from wear rates in mechanical alignment after 3 million cycles of ISO 14243-1:2009 standard walking gait. In both studies, volumetric wear increased linearly between each wear interval.

5.5 Study 2 - 4° Varus Experimental Contact Pressure

5.5.1 Methods

The fixtures from the 4° varus wear study were also used to complete tekscan pressure sensor measurements of the bearing during points in the gait cycle. The

output kinematics from the wear study were used to calculate the average value in FE position, AP position and TR position at 10% intervals of the gait cycle. These values were input into the simulator to position the components before the required load was applied. The tekscan equipment was used to measure the pressure between the bearing at each of the eleven gait points.

5.5.1.1 Setup of Contact Sensor Equipment

The experimental investigation of the contact mechanics of a 4° varus alignment followed the methodology outlined in Section 3.3.3 and Section 3.4.2. The fixtures from the 4° varus wear study were used to align the components in the specified position and the abduction-adduction bar was removed to allow the tibial carriage to adjust the dwell point of the bearing based on the input conditions.

Following calibration of the Tekscan equipment, the TKR bearings and Tekscan sensor were assembled in the simulator. Vaseline and the poly mesh were placed between the tibial insert and the Tekscan sensors to improve the pick-up of contact pressure and to prevent the sensors becoming damaged (Figure 5-21). Once the eleven measurements were recorded at the 10% intervals, the sensors were re-calibrated using the calibration procedure and the same measurements on the total knee replacement bearing were repeated 6 times.

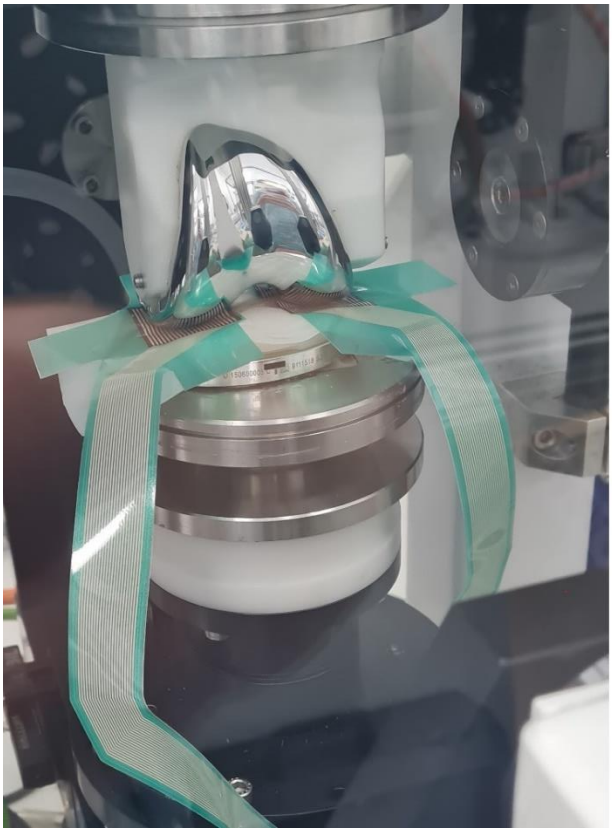

Figure 5-21: 4° varus alignment experimental Tekscan setup in simulator

Care was taken at gait points with high flexion to ensure that there was correct contact between the bearing and the sensor on both condyles during the measurement. This was a result of movement of the Tekscan sensor during motion at the femoral condyle when it was sent to the flexion position. An additional step was used when required to manually bring the components into contact and to assess the contact of both condyles with the sensor before applying full load and taking a measurement. If there was not contact, the sensors were repositioned on the bearing surface.

5.5.1.2 Creating Kinematic Positions

The position of the femoral component and tibial component at the 10% intervals of the gait cycle were determined from the average of 100-cycle kinematic outputs of the 4° varus wear simulation study for; flexion-extension, anterior-posterior position, tibial rotation, and applied axial force. The values for the 11 points are in Table 5-7.

Table 5-7: 4° varus 10% gait interval tekscan input positions.

Gait %	Axial force (N)	Flexion/Extension (°)	Anterior/Posterior (mm)	Tibial Rotation (°)
0	328.9	-30.0	-0.7	1.6
10	1880.5	-18.0	-0.9	-0.5
20	1506.9	-14.9	-0.7	-0.2
30	1074.2	-20.7	0.2	3.5
40	2158.0	-24.8	-0.1	4.0
50	1837.7	-14.0	0.9	5.2
60	191.9	9.2	3.6	6.8
70	184.4	26.9	-4.0	-1.5
80	160.5	18.6	-1.8	0.0
90	251.3	-9.8	1.0	1.4
100	252.2	-29.9	-0.6	1.6

5.5.1.3 Analysis of I-Scan measurements

The contact pressure outputs from the sensor at each of the 10% intervals were recorded in I-Scan software which was then exported and analysed using an R script. For each of the six repeated measurements are each of the 10% intervals, an average and standard deviation was calculated for the medial compartment, lateral compartment and total contact surface.

5.5.2 Results

The average contact pressure at the points of the gait cycle show that the value changed with changes in applied load (Figure 5-22). The highest points of flexion are after 60% of the gait cycle, which is where there are larger values of standard deviation in the data set. The contact pressure was higher on the medial compartment in comparison to the lateral compartment at all gait cycle intervals except 70% (Figure 5-23). The maximum difference in the contact pressure measured on the two compartments was at 80% gait cycle where the medial compartment contact pressure was 1.57MPa higher than the lateral compartment.

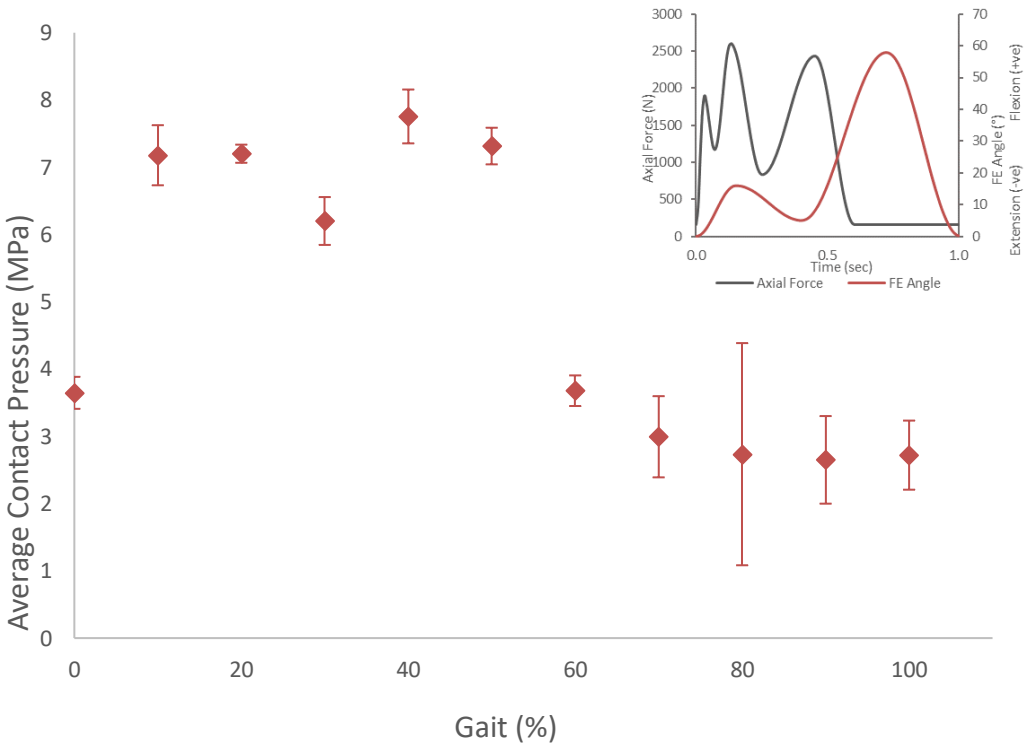

Figure 5-22: PSA Tekscan average contact pressure and standard deviation (n=6) and input load and flexion of one gait cycle

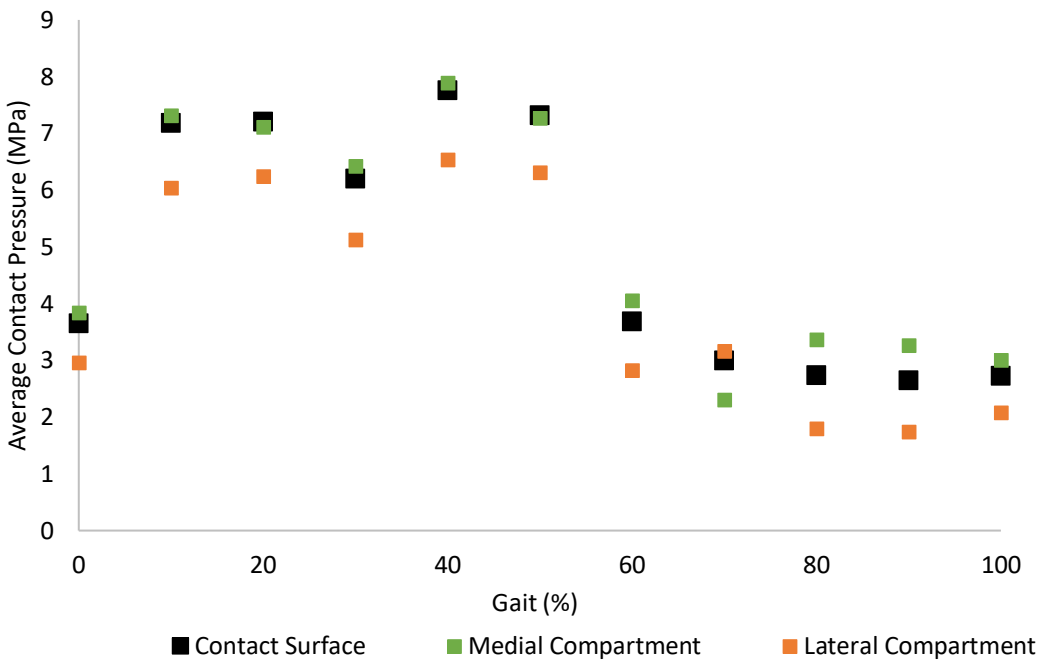

Figure 5-23: Tekscan average contact pressures (n=6) for the total contact surface, the medial compartment, and the lateral compartment for each of the 10% gait cycle intervals

The average contact pressure from the patient specific alignment bearing setup was compared to the average contact pressure from the mechanical alignment setup to determine differences between the values and the standard deviation ranges (Figure 5-24). At early positions of the gait cycle (10% to 60%) the 4° varus alignment setup consistently measured a higher contact pressure than the mechanical alignment setup. Comparing the contact pressures measured on the medial and lateral compartments of the bearing in the two studies highlights the differences in compartment loading during the gait cycle (Figure 5-25). At 0° and 100° there was a relatively large difference in contact pressure (1.8MPa and 2.32MPa respectively) on the medial compartment between the MA and 4° varus studies. However, during the rest of the gait cycle measurements there was a only small differences between the two studies. The lateral compartment contact pressure showed more difference in values between the two studies with a maximum difference of 2.23 MPa at the 60% gait cycle position. At all gait cycle positions, except 70% and 80%, a lower contact pressure was measured on the lateral compartment for both the MA and 4° varus alignments. At 70% both studies measured a higher contact pressure on the lateral compartment than the medial. However, at the 80% measurement point, the MA setup resulted in a higher lateral compartment pressure than the medial compartment

while the 4° varus resulted in a lower lateral compartment pressure than the medial compartment.

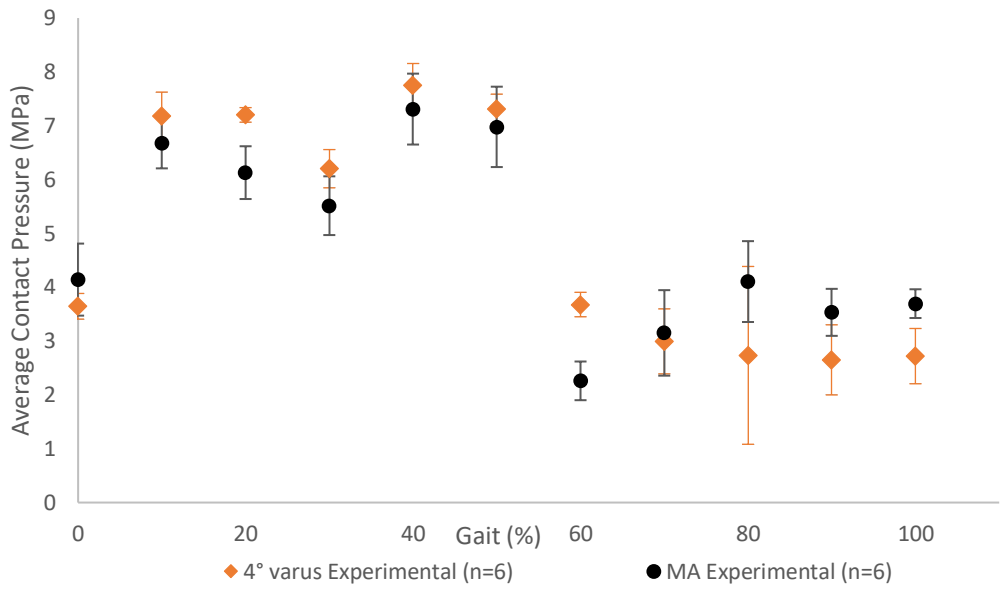

Figure 5-24: 4° varus and MA experimental total contact surface contact pressure average and standard deviation at 10% intervals of the gait cycle

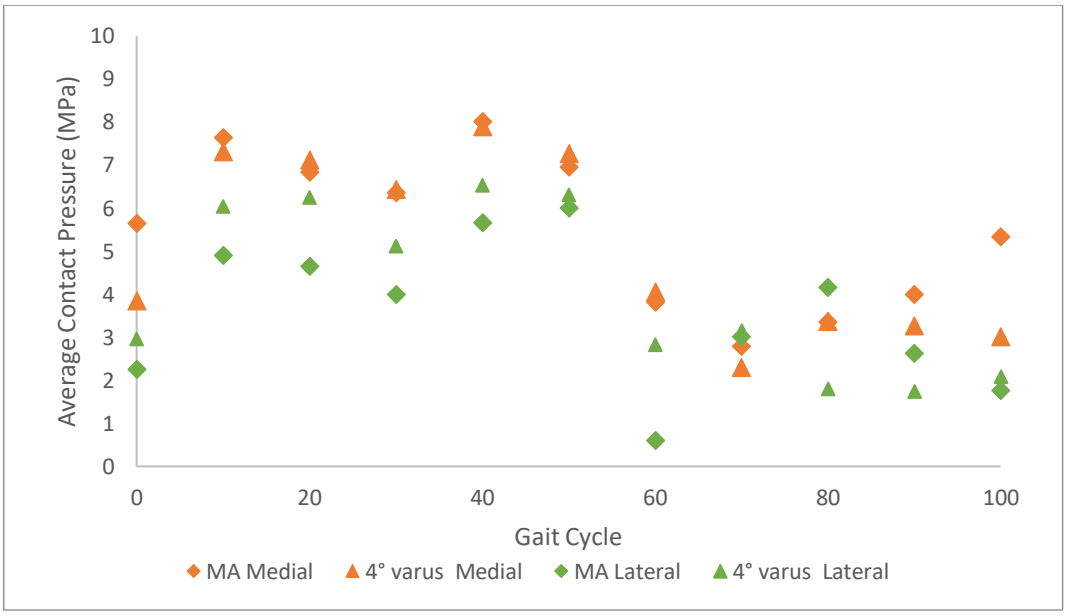

Figure 5-25: 4° varus (triangles) and MA (diamonds) experimental contact pressure average at 10% intervals of the gait cycle for the medial compartment (orange) and lateral compartment (green)

5.5.3 Discussion

Experimental methods of measuring total knee replacement contact pressures using pressure sensors was successfully adapted to evaluate a 4° varus alignment setup. The study measured higher contact pressures during stance phase and also less variability between repeats during stance phase in comparison to swing phase. Higher axial load values during stance phase may have resulted in improved stability of the study setup during measurement and therefore resulted in improved repeatability between measurements. In addition, the comparison of the medial and lateral compartment contact pressure showed that the measurement point with the largest variation (80%) was the same point with the largest difference between medial and lateral compartment contact pressure.

5.6 Discussion

This chapter investigated the kinematics, contact mechanics and wear of a TKR bearing at an alternate joint line orientation angle to the mechanically aligned TKR previously studied. Studies in this chapter involved adapting setup methodologies to adapted alignment conditions and evaluating the capabilities of the ProSim electromechanical knee simulator to control these variables.

Creating the 4° varus alignment setup required an in-depth review of the current procedures of patient specific alignment, how they vary between patient cohorts, outliers in the patient population and finally the limits which are set on these procedures, often termed “safe boundaries”. A 4° varus alignment value was picked as being a value greater than the limit of constitutional varus, but also within the surgical error of 2° allowed for in surgical procedures which state “safe boundaries” as an overall HKA angle of 3°.

The study found that a 4° varus alignment setup resulted in a phase shift of 1mm more posterior in comparison to the MA setup during the majority of the gait cycle. The overall anterior and posterior motions were not impacted by the change in alignment. There was also a phase shift in internal-external rotation resulting in the 4° varus alignment simulation reaching a peak internal rotation value 2º less than in the MA simulation. The average abduction was increased by 0.5º during swing phase in the 4° varus alignment simulation in comparison the MA. There was no significant difference between the wear rate in the two simulations (*p=0.12)*.

Previous studies on the effect of total knee replacement PSA variables on kinematics and wear rates have shown no significant impact of varus alignments between 3°-5°. The two studies which physically altered the bearing angle using a combination of

fixtures and simulator adaptions, reported kinematic outputs of anterior-posterior displacement and internal-external tibial rotation for 4° varus alignment of Sigma and Attune designs [121, 129]. Both studies reported similar anterior-posterior displacement and internal-external rotation kinematic outcomes, while the study by Johnston et al., (2019) also reported similar outcomes for abduction-adduction rotation on Sigma XLK components. The present study determined that the altered joint line orientation had an effect on the abduction-adduction rotation of Attune AOX components during swing phase, with a peak abduction angle in PSA double the peak value in MA. The results of the present study also reported no significant difference in wear rate between the two alignment setups which was also reported by Johnston et al., (2019) [164].

The contact pressure distribution between the two compartments was an additional research focus of this study in addition to the kinematics and wear. The study found that there was higher contact pressure on the lateral compartment in PSA in comparison to the MA setup. There was little difference between the contact pressure on the medial compartment between the two alignment setups, except at 0% and 100% gait cycle points where there was a higher medial compartment contact pressure on the MA setup in comparison to the PSA setup.

The results of this chapter, investigating the impact of coronal effects of rotating the joint alignment to a varus angle on the biomechanics and tribology of the joint, will be of use in future work. As established in the literature review of this chapter, the effect of patient specific surgical approached to the alignment of total knee replacements affects a range of variables and only one of which is the coronal angle alignment of the components. Additional variables include the sagittal alignment, compartment loading offset and input kinematics. Methodologies developed in this study will be applied to the previously developed finite element model of a total knee replacement to predict the impact of both coronal alignment and other variables on kinematics, contact mechanics and wear of the implant. The work completed here will be useful in determining the validity of the model results and will contribute to understanding key, long term impacts of patient specific alignment.

Chapter 6
Computational Modelling of Patient Specific Alignment and Wear

6.1 Introduction

Investigating the effect of patient specific alignment of total knee replacements on the kinematics, contact mechanics and wear using experimental simulation methods had limitations as a result of the physical constraints of the joint simulator. As demonstrated in “Section 4.5 Using the Attune Total Knee Replacement Model to Investigate Contact Mechanics”, finite element models offer an environment which can simulate the same conditions as an experimental simulator and predict outcomes in agreement with such experimental investigations. They also have the capacity to push past the confines of a physical environment to simulate control of total knee replacements in all six degrees of freedom in both displacement and load control and with feedback of the exact location of the components relative to each other. These advantages of the model may prove useful when investigating the variables of patient specific alignment in three-dimensions including all three planes of alignment.

This chapter will use the previously developed finite element model of a total knee replacement in mechanical alignment and will adapt it to patient specific alignment as defined in the 4º varus alignment package. As with previous methods applied to the finite element model, boundary conditions will be used to simulate the constraining effects of fixtures, wire constraints will be used to simulate spring control, and input loads will be used to simulate the loading profiles.

The predictions of the finite element model rotated to 4º varus alignment will be compared to the experimental results in Chapter 5 in an attempt to develop confidence in the capabilities of the model to predict accurate outputs of kinematics, and contact mechanics in a coronal alignment.

The results of both the baseline and 4º varus finite element models will be used to calculate a wear prediction using a previously developed computational framework [119]. The framework calculates a wear prediction using outputs from the finite element model including sliding distance, contact stresses and material properties. The results of the wear calculation will be compared to the experimental wear results of the baseline model and 4º varus model to facilitate an extra level of understanding

of the efficacy of the model to be used as a preclinical tool for total knee replacements.

Furthermore, the model predictions will be used to determine any future developments still required to improve the reliability of the model so that it can be used to investigate patient specific alignment in all 3 planes of alignment. The future use of such a model is vast including; individual patient combinations of alignment, studies into the effects of loading position on the outputs, studies into the effect of alignment on knee adduction moment, the combined effect of patient specific alignment and total knee replacement bearing design and materials, and many more applications.

6.2 Developing 4 º Varus Alignment Finite Element Model

6.2.1 Rationale

The purpose of this model was to use it to predict kinematics and contact mechanics outputs in 4° varus alignment. The predictions from this model will be compared to the results from the experimental study to determine the robustness of the model in alignment setups different from mechanical alignment. This is an important step in evaluating the usability of the model to investigate more complex setups. It is intended that the model should be capable of being adapted into patient specific alignments outside of the bounds of capability of the experimental simulator, although trust in the efficacy of the model needs to be established first.

6.2.2 4º Varus Model Setup Methods

The methods included in this section outline the steps taken to create the 4° varus alignment between the components, boundary conditions and kinematic inputs to the model, the suitability of the model spring constraints to control the new alignment setup, how the model was used to predict kinematic outputs of one gait cycle and how the model was used to predict contact mechanics at 10% intervals of the gait cycle.

Creating the 4° varus alignment experimental setup in a computational environment involved accounting for the rotation of the components relative to the axes of applied load and relative to each other. In the ABAQUS environment a coordinate system was assigned to the assembly which was used to position the datum points, used as individual control nodes, at the centre of rotation of each component to which reference points were assigned. RP-1 was assigned to the tibial insert and RP-2 was assigned to the femoral component (Figure 6-1).

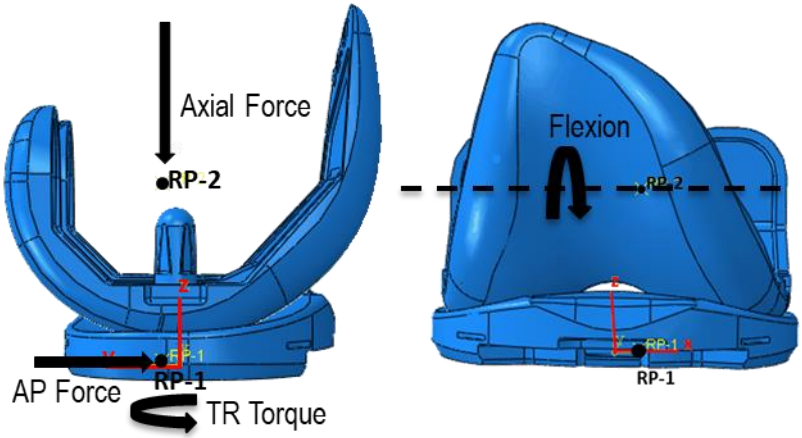

Figure 6-1: 4° varus model alignment side and front views of setup of control nodes and coordinate system with control reference points of each component including the tibial insert (RP-1) and the femoral component (RP-2).

“Instance” and “translate” functions in the assembly of the model were used to rotate the components at the centre of rotation, about the y-axis of the coordinate system, by 4°. This setup ensured that the original applied axis of load was not altered from the baseline finite element model setup. As with the experimental setup, the physical axis of applied load was not altered from its central position above the fixtures, the parameters which were changed in the setup were the positioning angles of the components relative to the axes of the simulator. Translating this into the finite element model setup, the applied axes of load and constraints remained the same as the baseline mode, however the physical angle of the component was altered to 4° varus, replicating the effect of 4° varus angled components (Figure 6-2). An alternate method of applying this would be to use boundary conditions to rotate the angle of the component during the displacement step of the model. However, this would equate to using the abduction-adduction carriage of the simulator to rotate the angle of alignment of the components. Since this was not possible to achieve in the simulator, it was not the preferred method of orienting the samples in the computational environment.

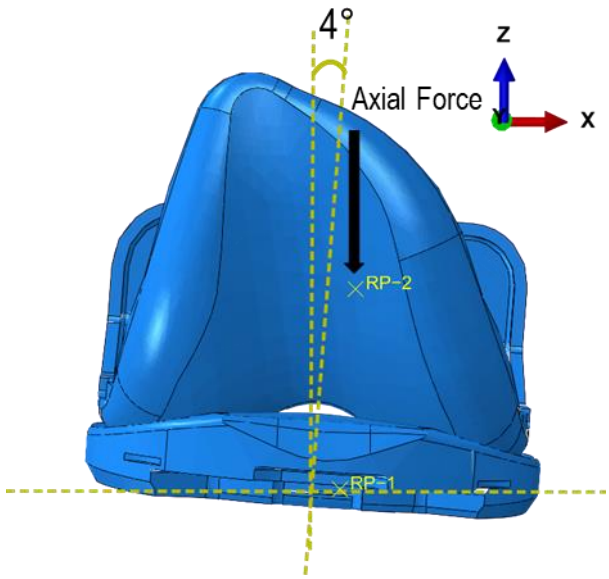

Figure 6-2: 4° varus alignment in finite element environment with axes and coordinate system

Other model setup parameters were maintained from the Mechanical Alignment model setup including:

- Surface-to-surface interaction properties (femoral main surface and tibia secondary surface) with a friction coefficient value of 0.04
- Meshing of each component with quadratic tetrahedral elements of type C3D10M. Both components were assigned global element size of 1mm which resulted in a total of 204748 elements on the femoral component and 137527 elements on the tibial component.
- AOX material properties assigned to the tibial insert including an elastic modulus of 348MPa and Poisson's ratio of 0.35. Cobalt Chrome material properties assigned to the femoral component including an elastic modulus of 193000 and Poisson's ratio of 0.29.
- Boundary conditions applied to the control nodes of each component to constrain the movement of the bearing. All motions of both components were constrained except abduction-adduction of the tibial insert which was left unconstrained to move in response to the femoral component motions.

6.2.3 Investigating Initial Contact

An initial displacement only simulation was completed with two purposes. The first was to determine the displacement step required to create an initial contact between

the two components resulting in a small but negligible contact pressure of less than 1MPa. The second purpose was to determine the location of the contact area at initial contact to ensure that the initial contact was at the dwell point of the bearing contact (Figure 6-3). This was important to ensure that the centre of the contact area for the starting positioning of this model setup was comparable with both the baseline setup and future alignment setups.

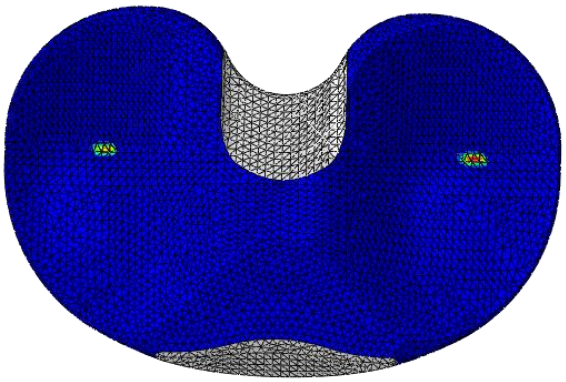

Figure 6-3: 4° varus alignment with small vertical displacement applied through femoral component, with initial contact pressure of 0.62MPa located at the bearing dwell point

6.3 4º Varus Model Gait Cycle Simulation in Load Control

6.3.1 Methods of Simulation

6.3.1.1 Steps

Steps were used to apply the motion and load conditions at each iteration of the gait cycle. After the initial contact step, there was a step to send the components to their respective positions at the start of the gait cycle (0%). An additional 127 individual steps were created for each individual point of the gait cycle input profiles. The total time of all 127 steps was 1 second.

6.3.1.2 Boundary Conditions

Boundary conditions were applied to the control nodes of each component to replicate the constraints of the fixtures assigned to the control coordinate axes. Flexion-extension of the femoral component was also applied through a displacement/rotation boundary condition. Loads were used to apply the action of the

axial force to the femoral component as a compressive force in the z-axis. Loads were also applied to the tibial component including a compressive force in the y-axis to apply anterior-posterior load and a moment in the z-axis to apply internal-external tibial rotation torque. The axial force and anterior-posterior loads were applied as concentrated forces, the tibial rotation torque was applied as a moment. Boundary conditions were used to constrain the components in all other degrees of freedom except rotation in the y-axis of the tibial component to allow abduction-adduction rotation response to the motions of the bearing.

6.3.1.3 Load Profiles

The input kinematics to the finite element model followed the ISO 14243-1:2009 load control inputs explained in “Section 2.3.2 ISO 14243-1:2009 Force Control Inputs” which applies flexion-extension motion kinematically to the femoral component and all other actively controlled degrees of freedom using load inputs. The load driven axes include an axial load applied to the femoral component, anterior-posterior load and tibial rotation torque through spring controls to the tibial component and leaves the tibia abduction adduction axis unconstrained. In the finite element model, these input profiles were applied using a combination of boundary conditions, load inputs and spring constraints.

The spring constraints were added to the model using wire connectors where one end of the wire was connected to the tibial insert CoR control node (RP-1) and the other end connected to ground. The anterior-posterior wire was created as a Cartesian connector and connected to ground in the y-direction, the internal-external rotation wire was created as a rotational connector and connected to ground in the z direction. The elastic values of the wires were assigned as 3-phase profiles (Figure 2-4).

6.3.1.4 Model Outputs

The outputs were requested from the finite element model simulation at the final frame of each step for anterior-posterior translation position, tibial rotation angle position, contact displacement values and the contact pressure of the contact surface. The model simulations were completed on a local computer system using Abaqus/CAE 2017 (Dassault Systèmes Simulia Corp., Johnston RI, USA.) using 4 Centeral Processing Units (CPUs) and a General-Purpose Graphics Processing Unit (GPGPU) acceleration of 2. The simulation took 10 days to complete.

The results were exported from ABAQUS using a python (Python Version 2.7.3) script (Appendix B) which exported the displacement (U), rotation (UR), tangential

motion of contact surfaces (CSLIP) and the contact pressure (CPRESS) for each step of the gait cycle. The node labels were also extracted for the tibial insert component. The steps were converted into the percent of the gait cycle and the output values were plotted in Excel and compared to the 4° varus experimental results and the baseline alignment model predictions.

6.3.2 Spring constraints study

6.3.2.1 Methods

A study was conducted to gain an understanding of the influence of the spring constraints on the kinematic outputs. The 4° varus alignment model was adapted to have spring control profiles with (Figure 6-4) and without (Figure 6-5) the ISO 14243-1 free-range phase, where the constant of proportionality was zero. The finite element model completed one gait cycle for each of the spring constraint profile combinations which included; (1) both AP and TR with “free-range”, (2) both AP and TR with no “free-range”, (3) TR with no “free-range” and AP with “free-range”.

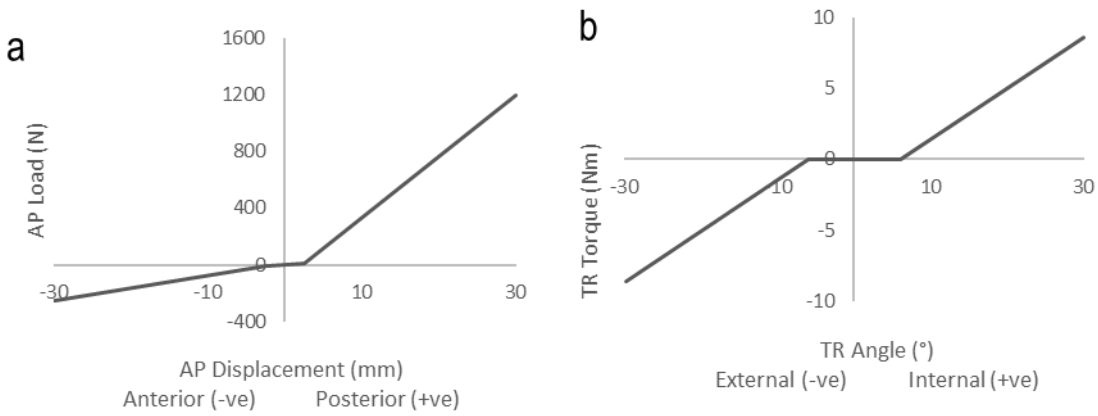

Figure 6-4: Input profiles with “free-range” for a) anterior-posterior load and b) internal-external tibial torque

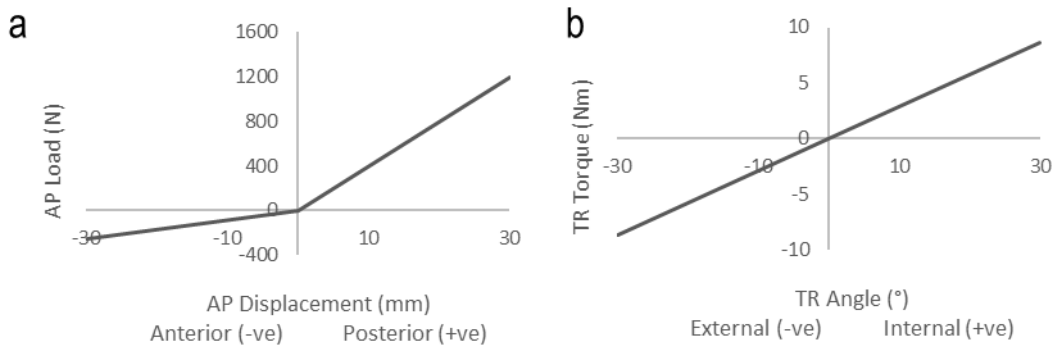

Figure 6-5: Input profiles with no "free-range" for a) anterior-posterior load and b) internal-external tibial torque

6.3.2.2 Results

The anterior-posterior (AP) translation results showed that the "free range" of the anterior-posterior spring constraint impacted the kinematic output (Figure 6-6). In the model adaption where anterior-posterior had free range but tibial rotation (TR) had no free range (3), the output anterior-posterior kinematic value was not affected except a slightly larger peak posterior value in the model with no tibial rotation free range.

Additionally, the steep change in tibial rotation direction at 65%, seen in the model with a free-range included in both springs (1), was not seen in the model adaptions where the tibial rotation spring had no free-range (2) and (3) (Figure 6-7).

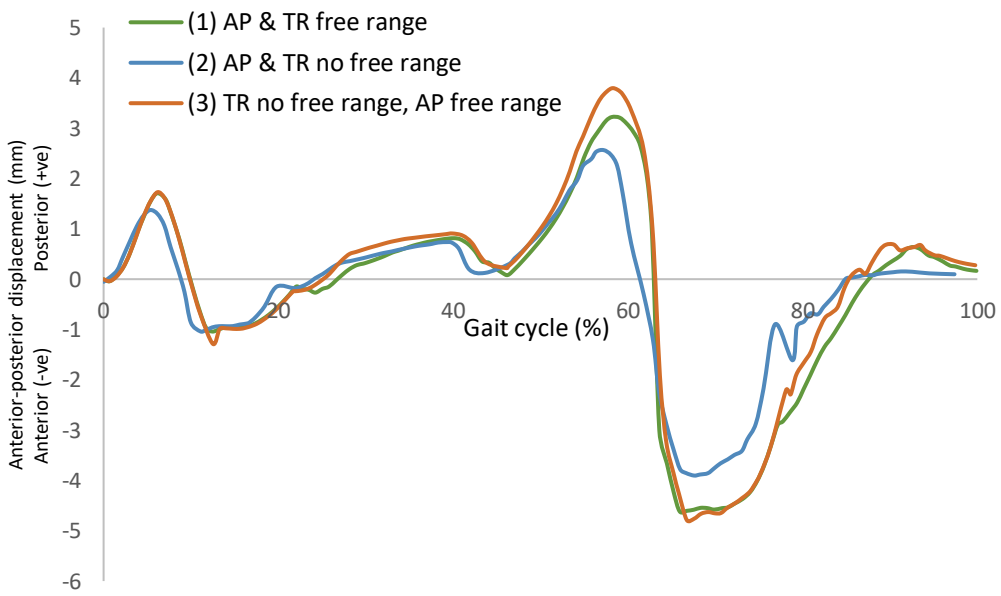

Figure 6-6: 4° varus alignment anterior-posterior displacement output with varying spring profile combinations (1), (2) and (3).

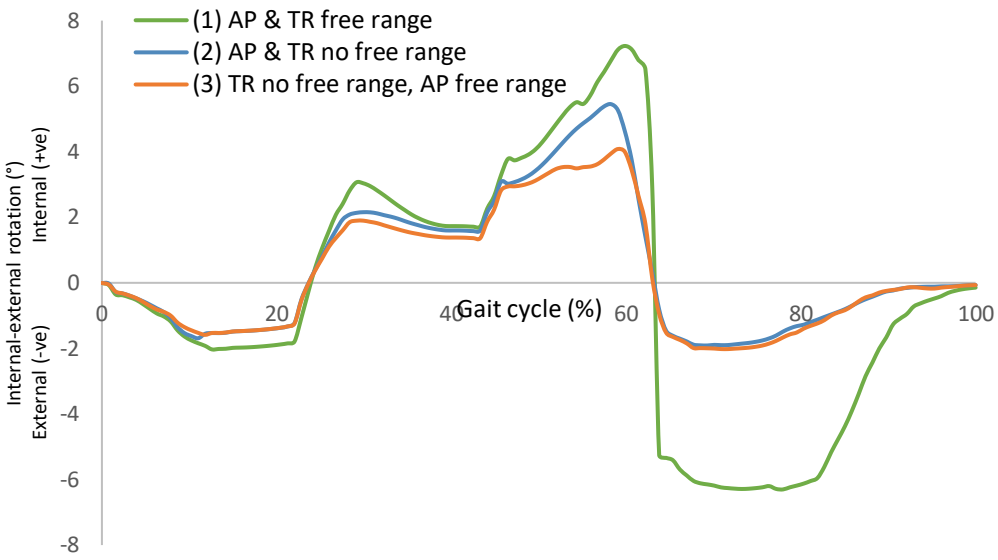

Figure 6-7: 4° varus alignment internal-external rotation angle output with varying spring profile combinations (1), (2) and (3).

Contact pressure maps show the location and size of the contact between the bearings at individual frames of the model simulation. The pressure map shown in Figure 6-8, taken at 65% of the gait cycle during the simulation with “free range” anterior-posterior translation and tibial rotation, shows concentrated contact pressure at the medial edge of the medial compartment.

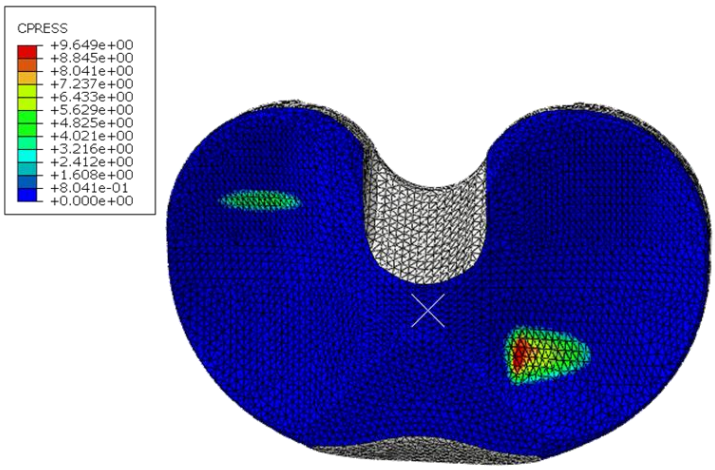

Figure 6-8: Contact pressure map of tibial insert during 4° varus alignment gait cycle with both tibial rotation spring and anterior-posterior spring containing a “free range”.

6.3.2.3 Discussion

Adapting the model to have no “free range” in the TR spring profiles resulted in removing this sudden tibial rotation and the output was a profile in closer agreement with the experimental kinematic results. This appears to be caused by the new alignment of the component causing compartment edge contact which is not seen in mechanical alignment setups. This contact at the edge of the tibial insert medial compartment may have restricted the external rotation of the bearing and therefore resulted in the results shown for “Free range TR and AP” with a dramatic shift in rotation angle between 60%-70% of the gait cycle. This study shows that the “free range” input had an effect on the output AP displacement and tibial rotation during the early swing phase of the gait cycle.

6.3.3 4º Varus Model Simulation Kinematics Results

6.3.3.1 Parameters of the Final Simulation Model

The 4° varus finite element model simulated to predict kinematics during one full gait cycle was developed to include 3-phase spring inputs (Figure 6-4). This spring profile was chosen because it was identical to the inputs for the mechanical alignment model and therefore permitted direct comparison of the MA outputs to the 4° varus alignment outputs.

6.3.3.2 4º Varus Model Kinematic Motions

Kinematic outputs from the 4° varus alignment finite element model were plotted over one full gait cycle for anterior-posterior displacement (Figure 6-9a) and internal-external rotation (Figure 6-9b). The results show a peak posterior displacement of 3.2mm at 58% gait and peak anterior displacement of 4.6mm at 66% gait. There was peak internal rotation of 7.2° at 60% gait and peak external rotation of 6.3° at 78% gait.

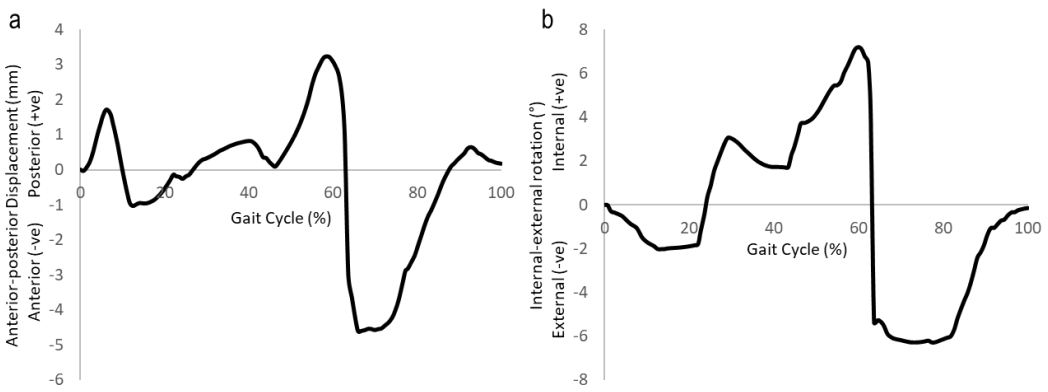

Figure 6-9: 4° varus finite element model output kinematics of one gait cycle for a) anterior-posterior displacement and b) internal-external rotation

6.3.3.3 4º Varus Model Comparison to Experimental Kinematics

The 4° varus finite element model kinematic motions of the tibial insert in anterior-posterior displacement (Figure 6-10) and tibial rotation angle (Figure 6-11) were compared to the same kinematic results from the 4° varus experimental simulation. The model anterior posterior translation motions showed agreement between the outputs for the first 50% of the gait cycle, with the model results following the lower range of the 95% confidence interval of the experimental results. However, when the gait cycle entered the high-flexion swing phase of the gait cycle there was less agreement between the results with a maximum anterior translation of the model tibial insert reaching 4.6mm. Similarly, the tibial rotation model predictions were in good agreement with the experimental average ±95% confidence interval during the stance phase and less close agreement in the final 40% of the gait cycle.

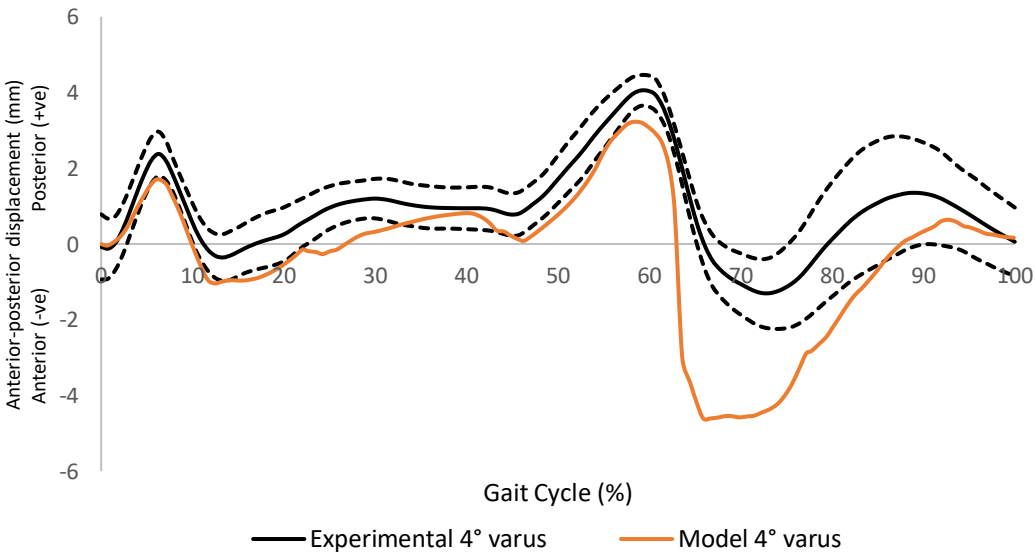

Figure 6-10: Anterior-posterior displacement 4° varus output kinematics for experimental (±95%CI) and finite element model predicted outcome.

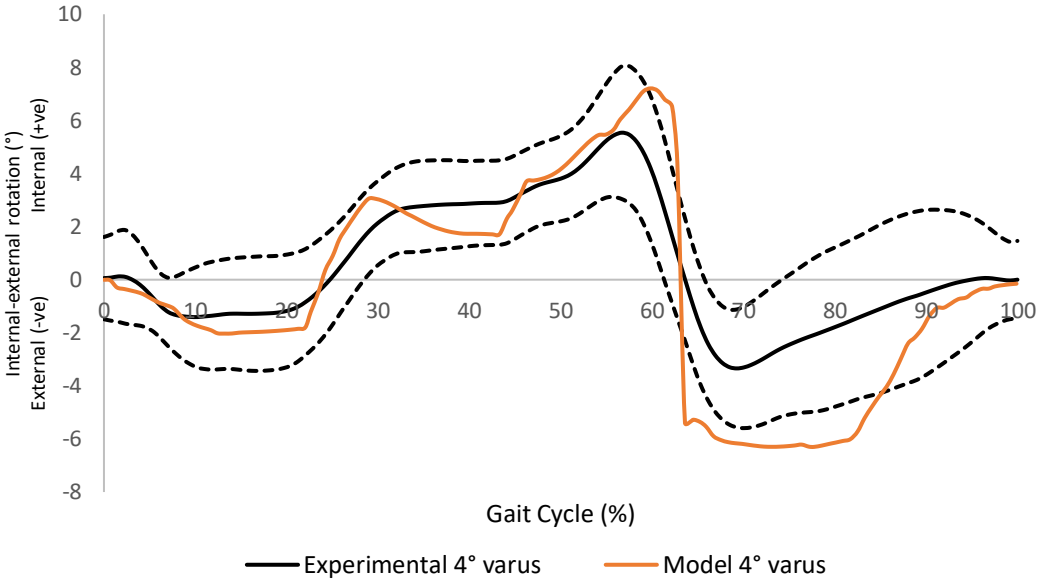

Figure 6-11: Internal-external rotation angle 4° varus output kinematics for experimental (±95%CI) and finite element model predicted outcome.

6.3.3.4 4º Varus Model Comparison to MA Model Kinematics

The kinematic results from the 4° varus alignment model were also compared to the baseline model kinematic results to compare how the change in alignment affected the output kinematics for anterior-posterior displacement and internal-external rotation angle. The close agreement between the anterior-posterior displacement results indicates that the change in alignment did not affect the anterior-posterior translation of the tibial insert by any notable amount during the whole gait cycle (Figure 6-12). The 4° varus alignment model had a peak internal rotation value of 7.2° compared to 7.9° in the baseline model setup (Figure 6-13). This difference was exacerbated during the swing-phase of the gait cycle where the baseline model maintained a neutral rotational angle of the tibial insert, but the 4° varus alignment model externally rotated to a maximum of -6.3°.

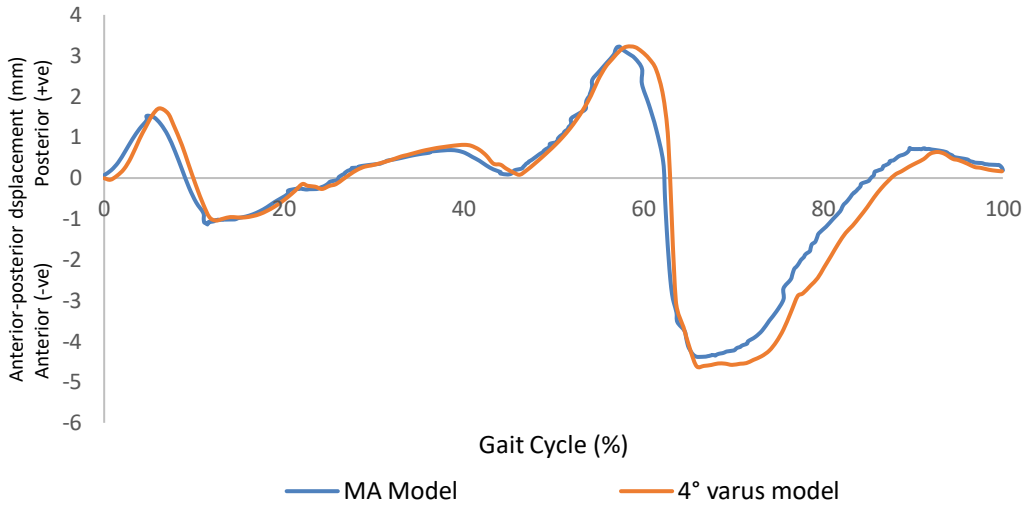

Figure 6-12: Anterior-posterior displacement kinematic output for MA and 4° varus finite element model outputs

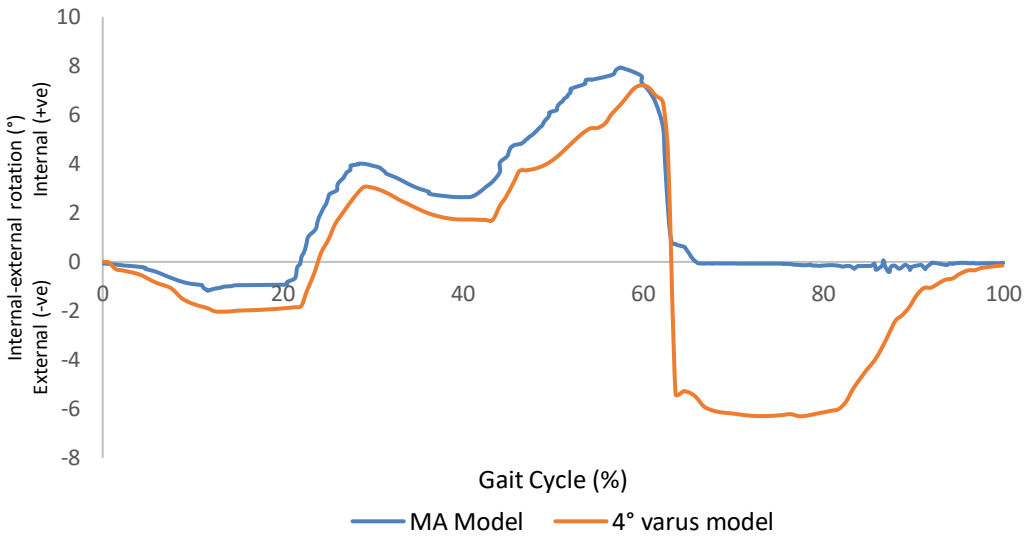

Figure 6-13: Internal-external rotation angle kinematic output for MA and 4° varus finite element model outputs

6.3.4 Discussion

ISO 14243-1:2009 standard walking gait input parameters were applied to the 4° varus finite element model to investigate the impact of the coronal alignment of the implants on the output kinematics. Overall, the model simulation shows that the angle of alignment of the components to 4° varus, while applying a 3-phase spring setup,

resulted in a large external rotation of the tibial insert, which was not seen in the mechanical alignment setup.

The comparison of the model predicted anterior-posterior displacement and internal-external rotation kinematics to the experimental simulation results showed poor agreement during swing phase. The finite element model setup included boundary conditions to implement the constraining effect of the fixtures in the experimental environment, but did not account for other mechanical factors. This simplification of the setup in comparison to the experimental environmental conditions cannot account for frictional effects caused by rotation the angle of alignment or by the edge contact of the bearing in the 4° varus alignment model.

A comparison of the 4° varus model output kinematics to the MA model output kinematics showed little difference in the anterior-posterior displacement and stance phase internal-external rotation. There was a difference between the output internal-external rotation of the two alignment models during swing phase, where the MA model outputs plateaued at 0° but the 4° varus setup externally rotated to -6.3°. The noted edge loading in the 4° varus model setup as a result of the 3-phase spring profile may have resulted in these differences as no similar edge loading was found in the model or the experimental simulation. Other factors which may have contributed to differences between the model and experimental output include uncontrolled variables in the experimental simulator, such as friction, which were not accounted for in the finite element model inputs.

6.4 4º varus Model Contact Mechanics Study

6.4.1 Rationale

In this section, the contact mechanics were determined computationally and compared to experimental results. The experimental study investigating the contact mechanics of the 4° varus alignment setup using sensor mapping equipment (Tekscan) outlined in Section “5.5 Study 2 - 4° Varus Experimental Contact Pressure ” were combined with the finite element contact pressure study adaptation methods outlined in Section “4.5.2 Model Development Methods”. The 4° varus alignment finite element model was used to complete this study.

6.4.2 Steps

The finite element model of 4° varus alignment was adapted into eleven setups, according to the kinematic positions in Table 5-7, for the respective 10% intervals of the gait cycle. The model was set up with a two-step configuration:

- Displacement - to create initial contact between the components
- Initialisation - to send components to the positions of the measurement point

The initialisation step was created as static, general step since this was a single concentrated load static stress analysis.

6.4.3 Boundary Conditions

Boundary conditions were applied to constrain the components and to apply displacements to position the components at each gait cycle interval. For each of the eleven models, the displacement increment for initial contact was determined through running a preliminary model with only the displacement step activated. The correct displacement increment was determined as the smallest value to result in a contact pressure between the bearing surface of less than 1MPa. In the initialisation step, the femoral component was set to a flexion angle using a displacement angle, the tibial insert set to an anterior-posterior position using a linear displacement and the tibial insert set to an internal-external rotation position using a displacement angle. The abduction-adduction of the tibial insert was left unconstrained, to allow the tibial insert to freely move to the correct position for alignment on the dwell point. The required load for the 10% interval setup was also applied during the initialisation step.

6.4.4 Model Outputs

Field outputs were requested at the final frame of the initialisation step, these included displacement values (U and UR) and contact stress (CPRESS) values. The Tekscan study finite element model input files (.inp) were created from Abaqus 2017 software on the local computer. All eleven model configuration input files were imported to the University of Leeds ARC3 High Performance Computing facilities (HPC) to allow the queuing of Jobs and to reduce the Job completion time. The HPC was accessed remotely through a Secure Shell (SSH) gateway using MobaXterm. The models were run for a maximum of 48 hours using 8CPUs. Results file (.odb) were exported from the HPC onto the local computer and contact pressure data was extracted using a python script.

6.4.5 4º Varus Model Contact Pressures

An average contact pressure was determined for all tibial surface nodes with a non-zero value, for each of the eleven models. Additional contact pressure values were determined for each of the compartments by averaging only the medial compartment nodes with a non-zero contact pressure value and the lateral compartment nodes

with a non-zero contact pressure value. The results show that there was a difference between the contact pressure measured on the medial and lateral compartments and that it was dependent on the gait cycle interval measurement point (Figure 6-14). At 0% and 100% of the gait cycle, the contact pressure was similar on the two compartments. However, at the majority of the gait cycle points there was a large difference in contact pressure on the two compartments with a maximum difference of 5.8MPa at 20% and 40% of gait cycle intervals. At most intervals, the medial compartment measured a higher contact pressure than the lateral compartment, except at 30%, 40% and 50% where there was a higher contact pressure measured on the lateral compartment.

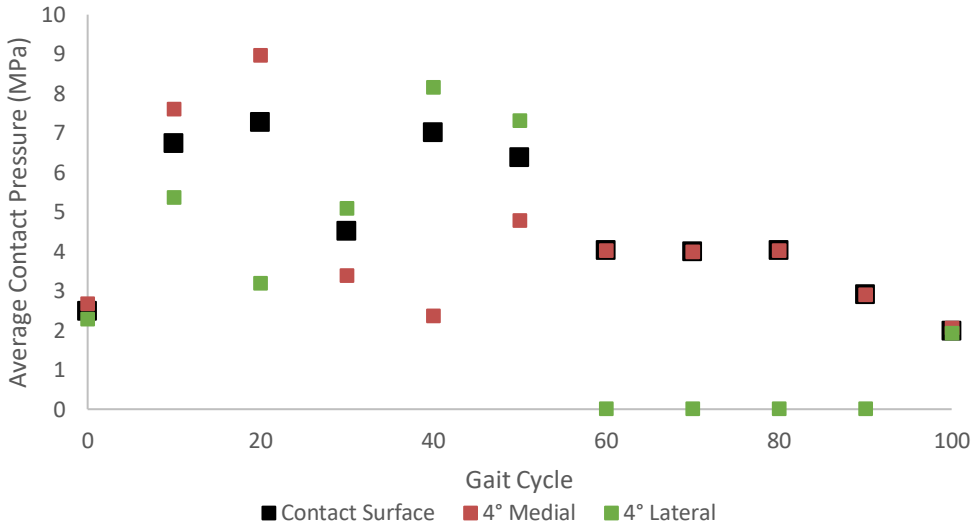

Figure 6-14: Finite element model predicted medial and lateral compartment contact pressures at 10% gait intervals in 4° varus alignment

6.4.6 4º Varus Model Comparison to Experimental Contact Pressures

The results were compared to the experimental average contact pressure ±95% confidence intervals (n=6) to determine whether the model predicted values were in agreement with the experimentally measured values (Figure 6-15). The model predicted values were outside of the standard deviation range of the experimental results except for the 60%, 80% and 90% models, during the swing phase of gait. The results also show that generally the model predicted contact pressure values lower than the experimental values in stance phase, but higher than the experimental values in swing phase.

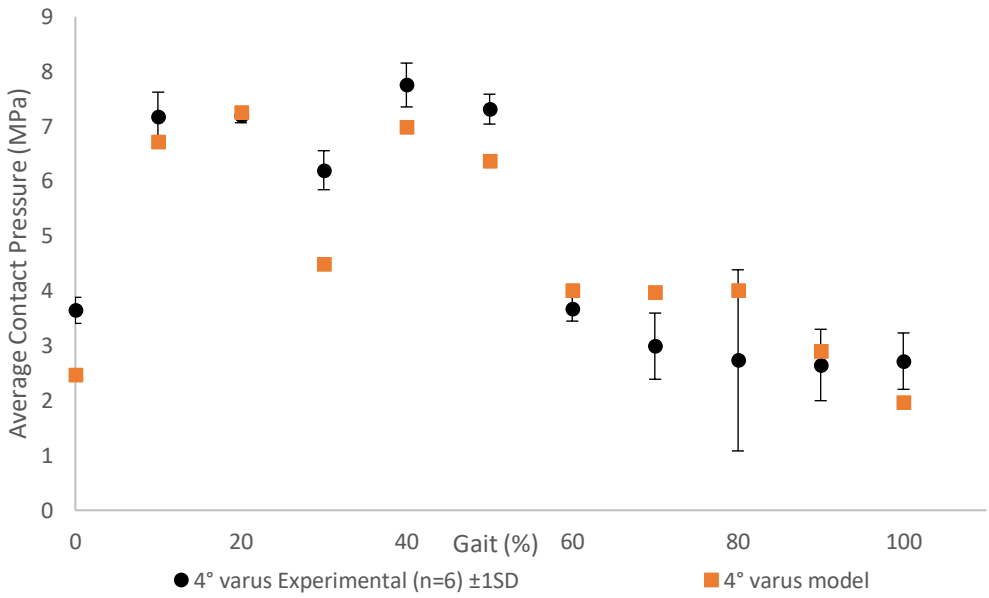

Figure 6-15: Finite element model PSA average contact pressure and experimental contact pressure with ±1 standard deviation at 10% intervals of the gait cycle

There was a large difference between the model predicted value (4.4MPa) and the experimental average (6.2MPa) contact pressure in the 30% configuration. The contact pressure heat maps from the experimental study (Figure 6-16) and the finite element model study (Figure 6-17) may offer some insight into the differences between these two results, including the position and size of the bearing contact. The model contact pressure shows a peak value on the medial condyle of 10.6MPa whereas the peak contact pressure in the experimental Tekscan study was 13.5MPa and also on the medial condyle.

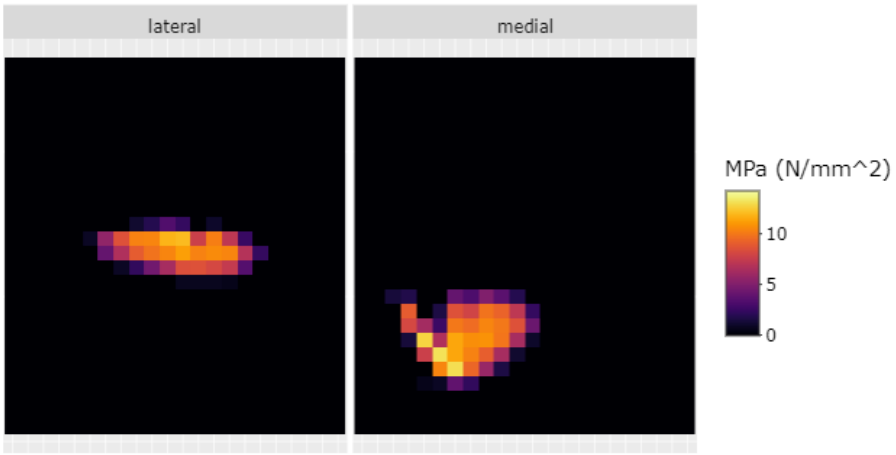

Figure 6-16: 4° varus experimental Tekscan contact pressure heat map at 30% configuration repeat-1

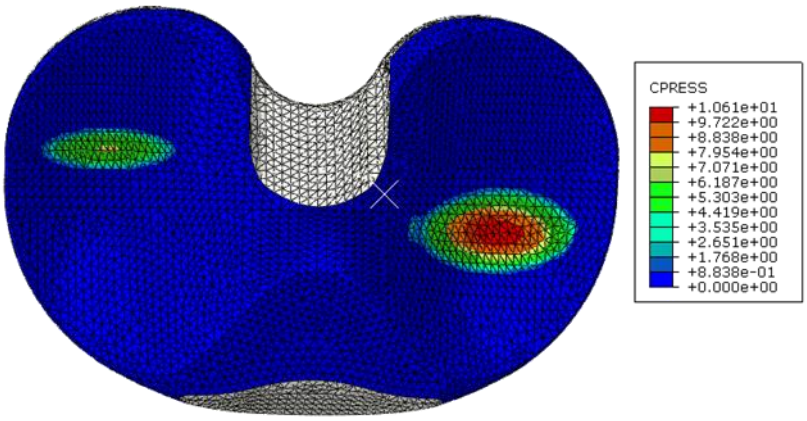

Figure 6-17: 4° varus 30% model contact pressure heat map

6.4.7 4º Varus Model Comparison to MA Contact Pressures

The average contact pressure value for the contact nodes at each of the eleven configurations of the MA model and 4° varus model were compared to determine the effect of the alignment of the bearings on contact pressure (Figure 6-18). The difference between the average contact pressure values of the two models (MA model - 4° varus model) had a median of -0.02MPa. The 80% gait configuration models resulted in the largest difference of -1.6MPa.

Figure 6-18: Finite element model predicted average contact pressure at eleven 10% intervals of the gait cycle for baseline mechanical alignment and 4° varus alignment.

6.4.8 Discussion

Investigating the cause of the difference in average contact pressure outputs between the 4° varus experimental and model results highlights the limitations of the experimental study methods. The first limitation is that the contact area and relative position was not quantified due to the inherent challenge of securing the sensors in the experimental study. As previously explored, this was not part of the methodology due to the damage adhesives had on the sensors. However, being unable to determine the differences between the experimental and model results contact area size and location does not allow a comparison of these variables.

Furthermore, there were differences in the individual point measurements on the contact surface measured by the experimental method and computational model method. Tekscan sensors are composed of sensels and a contact pressure value is determined per each sensel. The model determined contact pressure per contact node rather than a uniform square area. This limitation could be overcome by adapting the model mesh to represent the sensel area of the Tekscan sensor. However, this would compromise accuracy of the model as the mesh would not be optimised for the surface geometry of the tibial insert.

6.5 The Effect of Coronal and Sagittal Alignment on Kinematics

6.5.1 Rationale

The work completed in the previous sections of this chapter, as a result of the alignment parameters determined in Chapter 5 Patient Specific Alignment , have involved one alternate alignment of the knee replacement components in the coronal plane. However, as explained in the literature review of patient specific alignment of total knee replacements, three planes of alignment are altered using surgical cuts to position to components. The three planes of alignment interact with each other to set the overall alignment of the joint which also impacts the gait outcomes post-surgery [11].

The total knee replacement finite element model developed throughout this research has been shown to be capable of predicting kinematic outputs and contact pressures in good agreement with experimental results even in alternate coronal alignments. The model can be adapted further into other alignment positions in the coronal plane, but also in the sagittal and transverse plane. These adaptions offer a method to quickly investigate the biomechanical impact of joint alignment with little cost or time.

Although a full gait cycle with a 1mm mesh model takes 10 days, multiple models can be submitted to the HPC simultaneously and they can be queued to run consecutively depending on CPU capabilities. In this study, a further 15 models with a combination of coronal and sagittal alignments were developed in Abaqus2017 and submitted to the HPC for simulation.

6.5.2 Alignment Input Parameters

The coronal alignment and sagittal alignment of a total knee replacement include setting the varus/valgus angle of the tibial insert, the varus/valgus angle of the femoral condyle, the slope of the tibial insert, and the flexion angle of the femoral component (Figure 6-19). The degree to which these alignment parameters were positioned may have a direct effect on the kinematics of the joint replacement, and their combined effect may have an additional effect on the kinematics. The finite element model was adapted to a range of values for these planes of alignment and the kinematics and contact mechanics was determined to understand the influence of each variable.

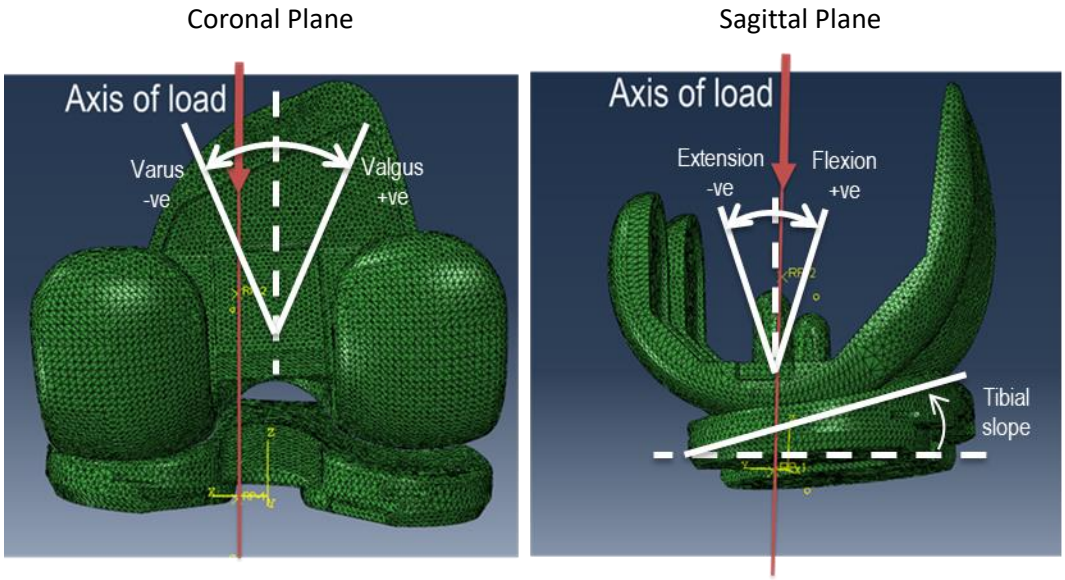

Figure 6-19: Finite element model setup of coronal and sagittal planes of alignment

The three angles of alignment in the coronal plane included 3°, 5° and 7° varus on both components and three angles of alignment in the sagittal plane 5°, 6° and 7° on the tibial component only. The combinations of alignment of the two components for the configurations are identified where C is coronal, S is sagittal and the number following each letter is the angle of alignment for the model. These combinations for the first level of the study, with individual plane of alignment variables, are listed in Table 6-1.

Table 6-1: Femoral and tibial component angle configurations in coronal and sagittal planes for first level of experiments

Alignment condition	Coronal Plane		Sagittal Plane	
	Femoral angle (°)	Tibial angle (°)	Femoral angle (°)	Tibial angle (°)
Baseline MA	0	0	0	0
C3S0	3	3	0	0
C5S0	5	5	0	0
C7S0	7	7	0	0
C0S5	0	0	0	5
C0S6	0	0	0	6
C0S7	0	0	0	7

For the second level of the interaction study, the planes of alignment were combined to include combinations of all three coronal angles with all three sagittal angles resulting in a further nine simulations. These second level combinations are detailed in Table 6-2.

Table 6-2: Femoral and tibial component angle configurations in coronal and sagittal planes for second level of experiments

Alignment condition	Coronal Plane		Sagittal Plane	
	Femoral angle (°)	Tibial angle (°)	Femoral angle (°)	Tibial angle (°)
C3S5	3	3	0	5
C3S6	3	3	0	6
C3S7	3	3	0	7
C5S5	5	5	0	5
C5S6	5	5	0	6
C5S7	5	5	0	7
C7S5	7	7	0	5
C7S6	7	7	0	6
C7S7	7	7	0	7

In total 16 simulations were completed in this study and the output kinematics were obtained from the finite element results file. The maximum and minimum points were determined for each kinematic output including anterior-posterior displacement, internal-external rotation and abduction-adduction rotation.

6.5.3 Adapting Coronal and Sagittal Alignment Assembly

To adapt the model, the methodology used to orientate the components in the ABAQUS environment in Section “6.2 Developing 4 º Varus Alignment Finite Element Model” was implemented in this setup. A central coordinate system was created and the components were rotated at their respective centre of rotation point using this coordinate system. For the coronal alignment the components were rotated about the

y-axis of the coordinate system while the sagittal alignment setup rotated the components about the x-axis.

6.5.4 Level 1 Alignment Kinematic Results

The model kinematic outputs for anterior-posterior displacement for the coronal only alignment and sagittal only alignment are presented in Figure 6-20. The coronal alignment anterior-posterior displacement values did not appear to be affected by the change in angle. However, the sagittal plane alignment did show an overall anterior phase shift which increased with increasing sagittal angle, but the amplitude did not appear to be affected.

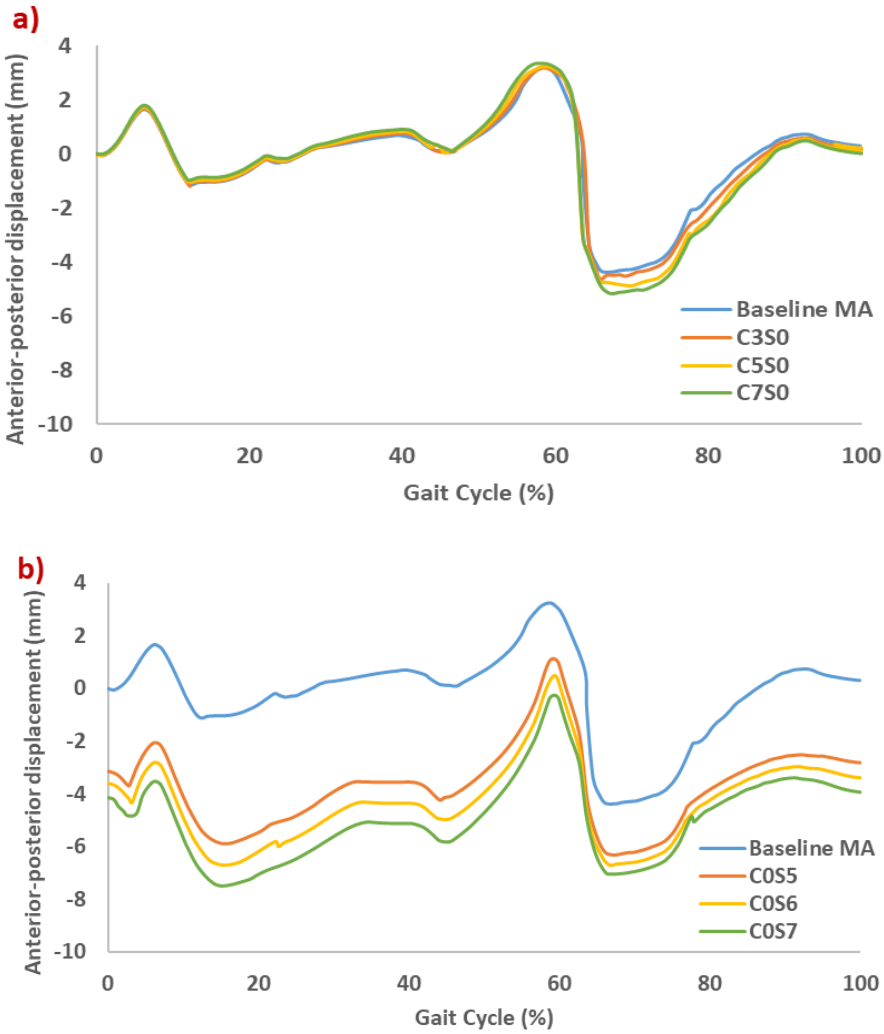

Figure 6-20: AP displacement kinematic outputs from the first level of interaction studies for a) coronal alignment and b) sagittal alignment and including baseline MA output kinematics

The tibial rotation angle for coronal alignment had a large external rotation at around 60% of the gait cycle, similar to the results seen in the 4° varus alignment study (Figure 6-21). The sagittal angle showed an increase in internal rotation at 40% of the gait cycle in comparison to the baseline model, towards the end of the stance phase. The early stance phase and swing phase did not show a difference in phase or amplitude between the sagittal alignment and the baseline alignment models.

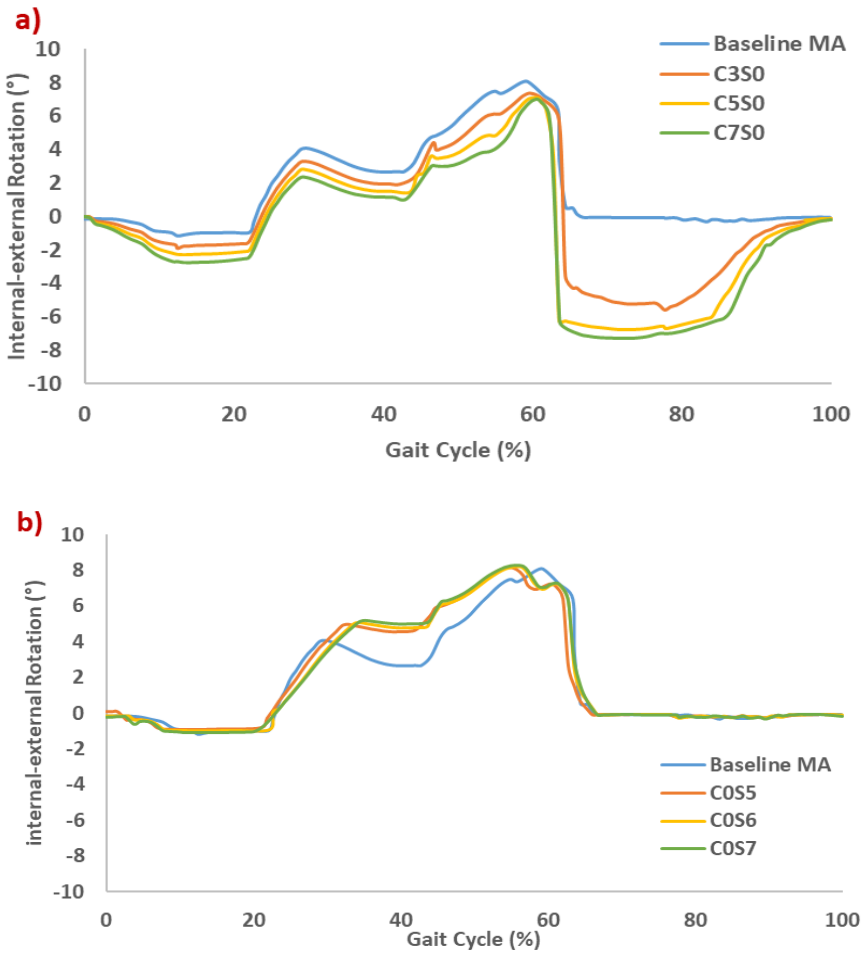

Figure 6-21: Internal-external angle kinematic outputs from the first level of interaction studies for a) coronal alignment and b) sagittal alignment and including baseline MA output kinematics

The output kinematics for abduction-adduction angle of the sagittal model showed similar overall kinematics to the baseline model, with a 1° increase at 60% of the gait cycle (Figure 6-22). Increasing angles of sagittal alignment did not appear to have any further affect in this increased peak. The coronal alignment model showed a 1° increase in adduction between the 3° coronal alignment and the baseline alignment model between 60% and 90% of the gait cycle. This increase of 1° adduction increased by a further 1° in the 5° coronal model and again by 1° in the 7° coronal model.

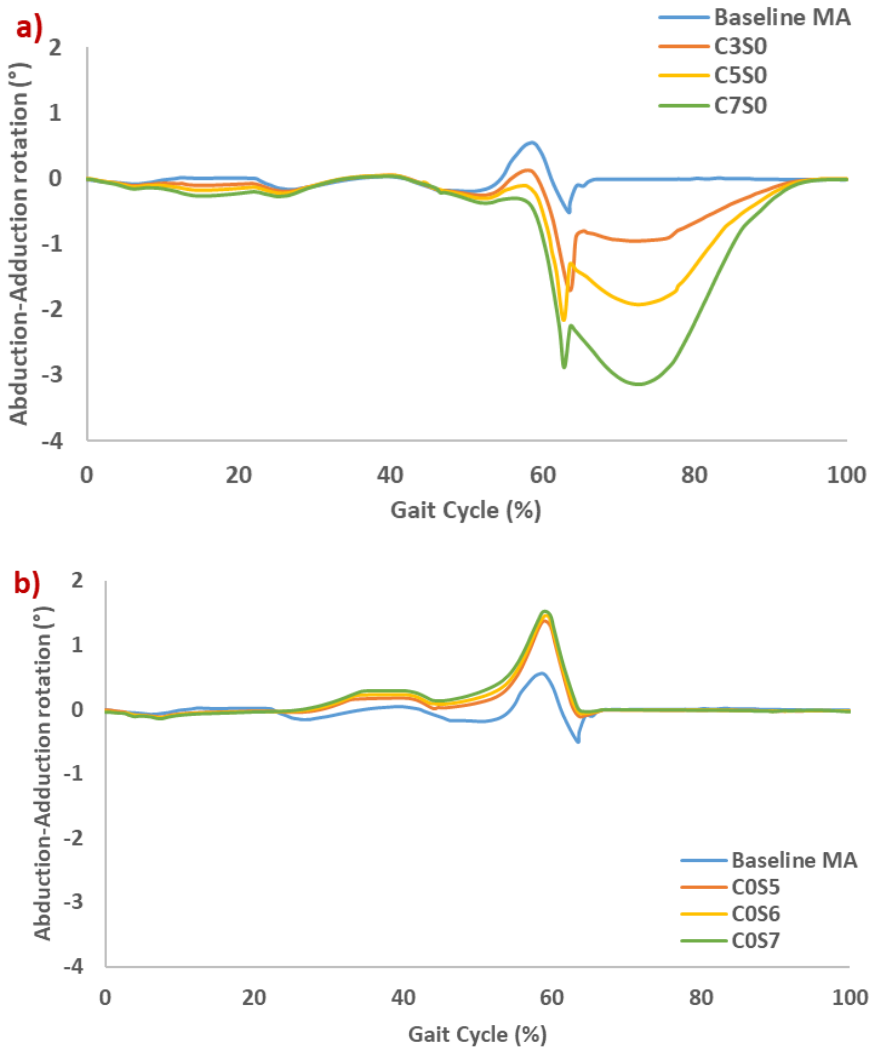

Figure 6-22: Abduction-adduction angle kinematic outputs from the first level of interaction studies for a) coronal alignment and b) sagittal alignment and including baseline MA output kinematics

6.5.5 Level 2 Alignment Kinematic Results

The Level 2 alignment kinematic outputs of the tibial insert were exported from the Abaqus software for anterior-posterior displacement (Figure 6-23), internal-external rotation (Figure 6-24) and abduction-adduction rotation (Figure 6-25). The maximum and minimum points for each of the kinematic output profiles are summarised in Table 6-3 in addition to the corresponding maximum and minimum values reported from the mechanical alignment model.

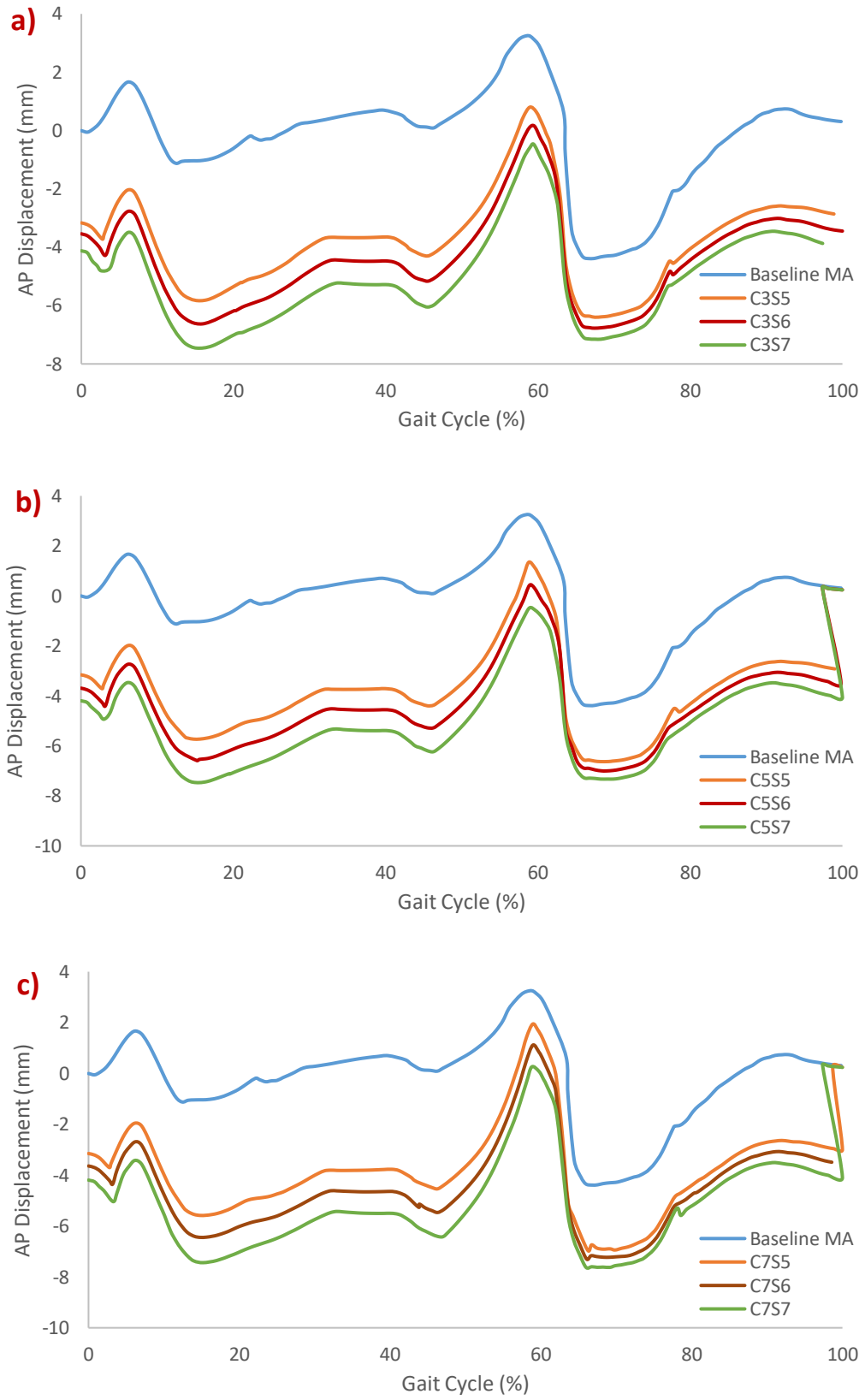

Figure 6-23: Anterior-posterior displacement kinematic outputs from Level 2 model alignment study including a) coronal 3° sagittal 5°-7°, b) coronal 5° sagittal 5°-7°, c) coronal 7° sagittal 5°-7°

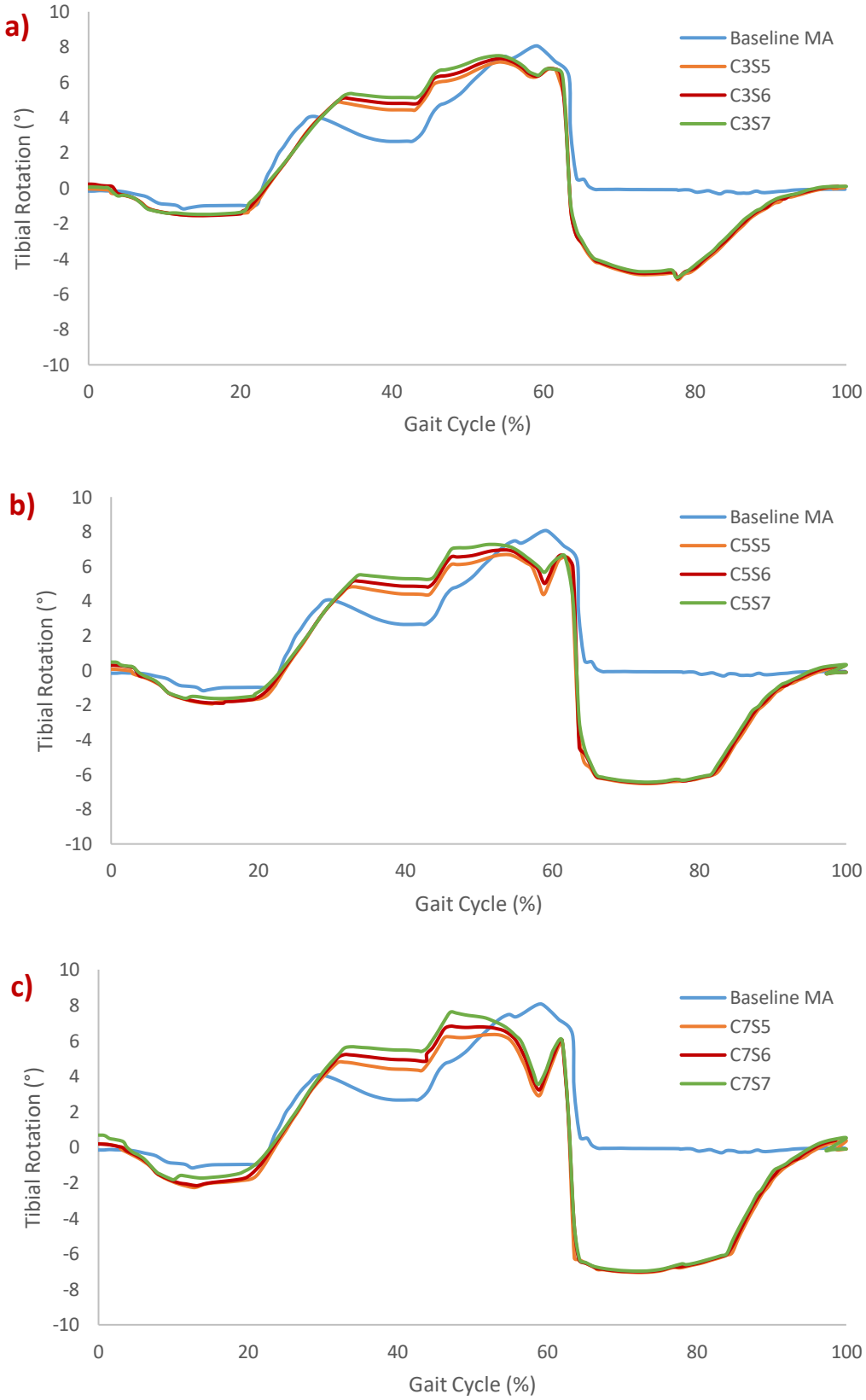

Figure 6-24: Internal-external rotation kinematic outputs from Level 2 model alignment study including a) coronal 3° sagittal 5°-7°, b) coronal 5° sagittal 5°-7°, c) coronal 7° sagittal 5°-7°

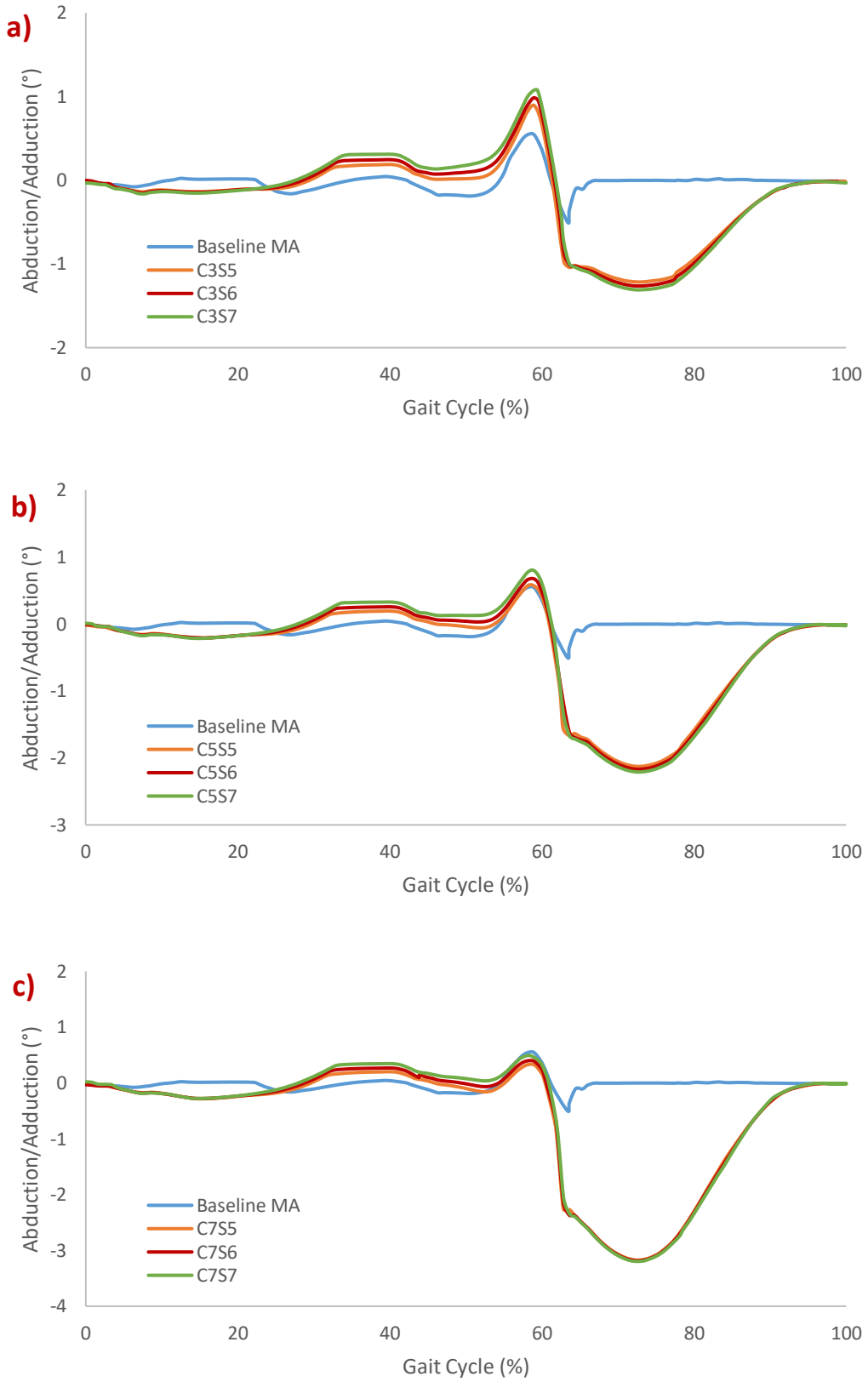

Figure 6-25: Abduction-adduction rotation kinematic outputs from Level 2 model alignment study including a) coronal 3° sagittal 5°-7°, b) coronal 5° sagittal 5°-7°, c) coronal 7° sagittal 5°-7°

Table 6-3: Summary of maximum and minimum kinematic outputs for anterior-posterior displacement, internal-external rotation and abduction-adduction rotation for Level 2 alignment model simulations

Alignment condition	Anterior-posterior displacement (-ve anterior +ve posterior)		Internal-external rotation (-ve external +ve internal)		Abduction-adduction rotation (-ve adduction +ve abduction)	
	Min	Max	Min	Max	Min	Max
MA (C0S0)	-4.39	3.25	-0.22	8.04	-0.50	0.56
C3S5	-6.40	0.80	-5.18	7.13	-1.21	0.89
C3S6	-6.77	0.15	-5.10	7.32	-1.26	0.98
C3S7	-7.15	-0.47	-5.06	7.46	-1.31	1.08
C5S5	-6.63	1.35	-6.52	6.58	-2.13	0.58
C5S6	-7.00	0.43	-6.47	6.81	-2.17	0.68
C5S7	-7.33	-0.47	-6.44	7.02	-2.21	0.80
C7S5	-6.98	1.94	-7.06	6.08	-3.17	0.33
C7S6	-7.30	1.12	-7.01	6.38	-3.18	0.40
C7S7	-7.63	0.26	-6.98	6.62	-3.20	0.49

The anterior-posterior displacement minimum values show that the peak anterior displacement increased with both increasing coronal and sagittal angle. All minimum values were in a more anterior position than in mechanical alignment. The maximum anterior-posterior displacement values show that a coronal alignment values of 3° and 5° combined with increasing sagittal angle results in a less posterior peak position and in 7° sagittal alignment a peak position in net anterior translation of the tibial insert. The 7° coronal alignment resulted in a decreasing peak posterior position and the 7° sagittal alignment resulted in a peak position of net posterior translation of 0.26mm. All maximum points were less posteriorly translated than the maximum posterior translation in mechanical alignment.

The internal-external rotation minimum values showed increased external rotation with increased coronal angle but a decreased peak external rotation position with increasing sagittal alignment angle. The maximum external rotation was found to be -7.06° in the 7° coronal and 5° sagittal alignment. All minimum values were more externally rotated than in mechanical alignment. The change in alignment had the opposite effect on the peak position which decreased in value (less internal rotation) with increasing coronal angle and increased in value (more internal rotation) with increasing sagittal angle. The peak internal rotation was 7.46° in the 3° coronal and 7° sagittal alignment. All alignment resulted in a lower peak internal rotation than mechanical alignment.

The alignment model configurations all resulted in more adduction rotation during swing phase in comparison to the mechanical alignment model. The adduction rotation increased with increasing coronal alignment by large increments of over 1°.

There was also an increase of adduction rotation with increasing sagittal alignment but only by small increments. All alignments resulted in more adduction rotation during swing phase of gait than in mechanical alignment. An increase in coronal alignment to resulted in a decrease in peak abduction rotation and an increase in sagittal angle resulted in an increase in adduction rotation. The maximum abduction rotation was 1.08° in 3° coronal and 7° sagittal alignment. The 3° coronal alignment configurations all had an increased peak abduction rotation and the 7° a decreased peak abduction rotation in comparison to mechanical alignment.

6.5.6 Discussion

Overall, the changes in plane of alignment in the coronal plane and the sagittal plane resulted in a change in the kinematics outputs for anterior-posterior displacement, internal-external angle and abduction-adduction angle in comparison to mechanical alignment.

Increased coronal angle resulted in a small anterior shift in displacement, there was no overall change to the phase and amplitude of the output kinematics. Increased sagittal angle resulted in a larger anterior shift than the effect of coronal alignment. There was also a large increase in the external rotation of the tibial insert during swing phase with increase coronal alignment, there was little effect caused by an increase in sagittal alignment on internal-external rotation.

The Level 1 coronal alignment resulted in an increased adduction during swing phase, sagittal angles increased the peak abduction at 60% of gait. However, in the Level 2 models the effect of increased tibial slope on the peak abduction value was only seen in the 3° coronal alignment and not at larger coronal angles. This may imply that a combined non-zero coronal and sagittal angle may have a different effect on the abduction motion of the tibial insert in comparison to Level 1 alignments.

6.6 The Effect of Coronal Alignment on Wear

6.6.1 Introduction

In comparison to kinematic analysis and the study of contact mechanics which offer insights into the instantaneous impact of altering the joint alignment, wear rates are able to predict the long-term function of the total knee replacement by determining the material loss caused by different inputs. Pre-clinical assessment of wear through gravimetric experimental methods has been the foundation of the biotribology of total joint replacements for decades. However, the new finite element methods demonstrated in previous chapters have been shown to be capable of investigating

the core principles of the biotribology and biomechanical function of total knee replacements. Therefore, computational methods of calculating wear rates from these finite element outputs have been developed to utilise these new technologies and to produce predictions of bearing wear during walking gait and other daily activities [119]. To use such a wear framework to predict the wear of Attune AOX bearings, the calculation must be tailored to the unique material properties of AOX including Young's Modulus and Poisson's ratio and wear factors determined from pin on plate studies. This has involved internal work at The University of Leeds and work is yet to be published on its findings [151, 165]. However, the computational framework created by Abdelgaied et al., 2018 [119] has been applied in this study using the preliminary material data from this internal work.

This section will outline the background of the wear model, how it has been adapted for the purpose of this study and the inputs taken from the finite element model to calculate a wear prediction. A computational wear prediction is calculated for both the baseline model and the 4° varus alignment model and the results of each will be compared to the experimental results. The aim of this section is to determine whether the wear prediction from the computational simulations is in agreement with the experimental simulations and to compare the predicted wear rate between two alignment setups.

6.6.2 Background on Total Knee Replacement Wear Models

The wear framework is an algorithm developed to incorporate the components calculating the wear coefficient of a polyethylene tibial insert bearing. The theory and development of this wear calculation is detailed in the published work [119]. The first component of the wear calculation is the cross-shear ratio which is calculated using the combined theory of [59] and [126]. The principle first calculates the principal molecular orientation as the primary direction of the largest sliding distance. The cross-shear ratio (CS) can then be calculated as the frictional work perpendicular to the PMO ($E_{cross\text{-}shear}$) divided by the total frictional work (E_{total}).

The contact pressure, calculated from the finite element model and the elastic modulus of the material are the final two components of the calculation for the wear coefficient shown in Equation 6-1.

$$\mathrm{C} = \mathrm{fun}(\mathrm{CS}, \tfrac{\mathrm{P}}{\mathrm{E}})$$

Equation 6-1: Non-dimensional wear coefficient for UHMWPE as a function of cross shear and non-dimensional contact stress [119]

6.6.3 Inputs to Attune AOX Wear Model

The finite element model was developed to output the variables required to be used as components in the computational wear framework which include translation (U), rotation (UR), tangential motion of contact surfaces in the x-axis and y-axis (CSLIP) and the contact pressure (CPRESS) for each step of the gait cycle. The node labels were also extracted for the tibial insert component. The values form the components of the non-dimensional wear coefficient calculation which is formulated specifically for AOX polyethylene material.

This calculation was completed using a Matlab code previously developed by the University of Leeds in collaboration with Nottingham Trent University [166], which incorporated the AOX material wear factor determined from pin-on-plate studies. The Matlab code calculated the principal molecular orientation direction in x and y direction from the CSLIP1 and CSLIP2 outputs which was then used to calculate the average cross shear ratio. Finally, the non-dimensional wear coefficient was calculated using contact pressure values (CPRESS) and accounting for the elastic modulus of AOX polyethylene.

6.6.4 MA and 4º Varus Alignment Computational Wear Predictions

The wear calculation was used to predict a volumetric wear rate for the baseline mechanical alignment and the 4° varus alignment setups. The outputs of the MATLAB code for each of these alignment configurations includes Maximum contact stress (MPa), Average contact stress (MPa), Average cross-shear ratio, and Wear rate (mm^3/mc) (Table 6-4). The computational predictions showed a 0.1MPa increase in average contact pressure in the 4° varus alignment and an overall decrease in volumetric wear rate of 0.1 mm^3/mc for the first 100,000 gait cycles.

Table 6-4: Computational predictions of contact stress, cross shear ratio and wear rate calculated in MATLAB using the computational wear framework developed by Abdelgaied et al., 2018 [119]

Test condition	Max contact stress (Mpa)	Average Contact stress (Mpa)	Average cross-shear ratio	Wear rate (mm3/mc)
MA condition	19.4	4.1	0.03	3.0
4° varus condition	19.4	4.2	0.03	2.9

6.6.5 Comparison of Computational and Experimental Wear Rates

The wear rate predictions from the wear framework calculation were compared to the experimental wear rates for both the baseline alignment and the 4° varus alignment. The mechanical alignment computational wear rate prediction of 3.0mm^3/mc was within the 95% confidence interval of the experimental mechanical alignment 3 million cycle wear rate (n=6) of 2.7±1.1mm^3/MC (Figure 6-26). The computational wear rate predicted value for the 4° varus alignment model was 2.9mm^3/MC which was within the 95% confidence interval of the 3 million cycle experimental 4° varus alignment wear study average wear rate (n=5) of 3.3 ± 0.5mm^3/MC (Figure 6-27).

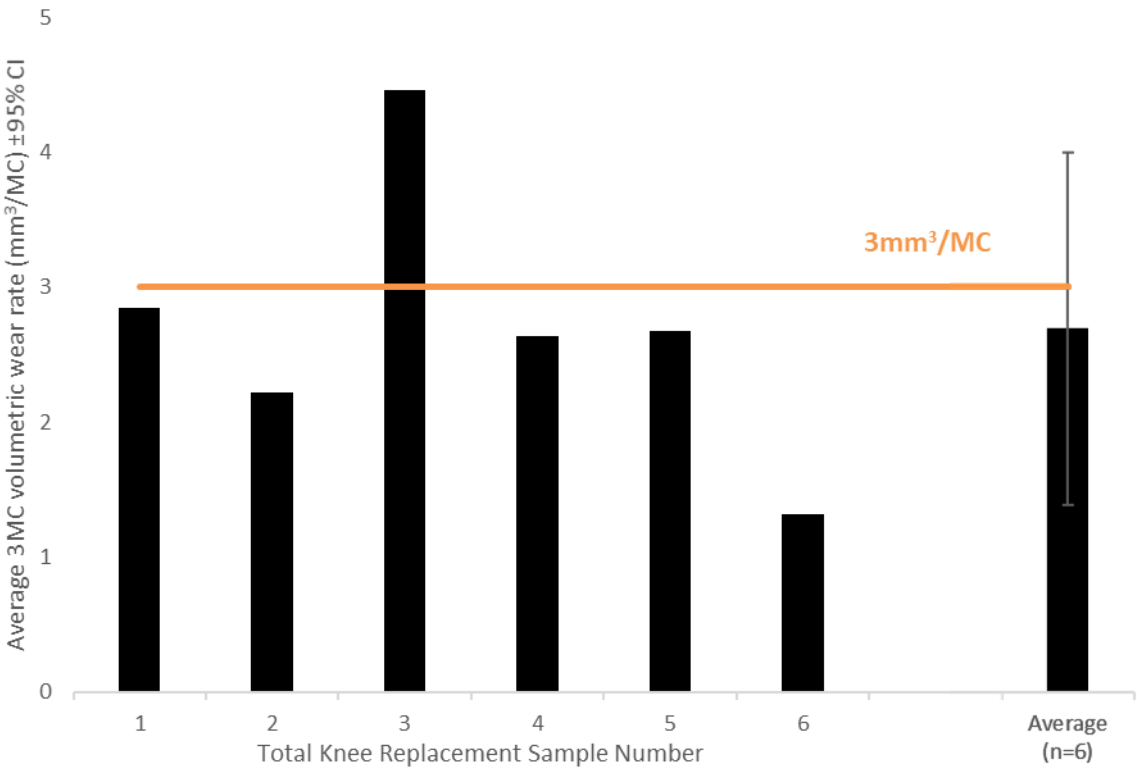

Figure 6-26: Average 3 million cycle wear rates of baseline experimental study for each of the six wear stations, the experimental average wear rate with ±95% confidence interval, and the computational wear prediction in orange

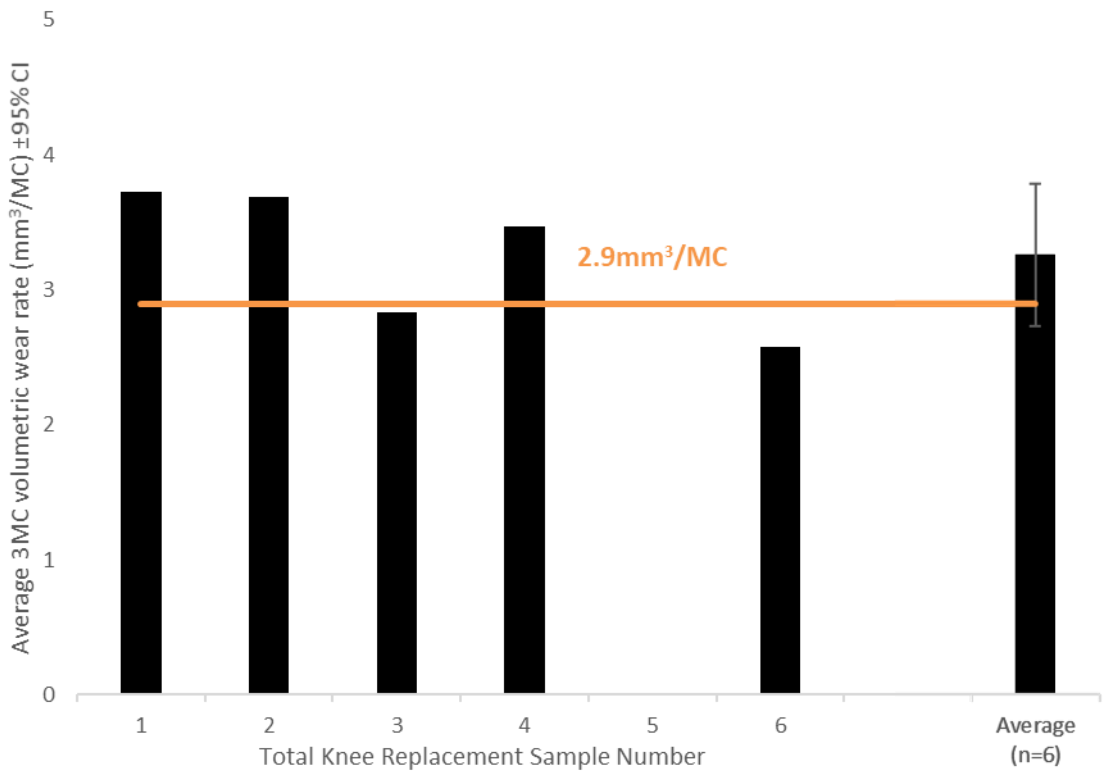

Figure 6-27: Average 3 million cycle wear rates of 4° varus experimental study for each of the five wear stations, the experimental average wear rate with ±95% confidence interval, and the computational wear prediction in orange

6.6.6 Summary of Wear Model

Overall, the model predicted volumetric wear rate for both baseline alignment and 4° varus alignment were in good agreement with the experimentally determined average wear rates and 95% confidence limits after 3mc of wear simulation. This shows that the Attune AOX finite element model is a reliable tool for predicting kinematics and contact mechanics for the conditions investigated. The study also shows that the wear framework for the AOX polyethylene material is suitable for calculating wear rates when combined with the finite element model output parameters. It further shows that the model methodology is sensitive to adaptations in component alignment in the coronal plane and continues to be reliable in predicting volumetric wear rates.

6.7 Discussion

This chapter adapted the Attune AOX finite element model to varus alignment conditions to predict kinematics and contact mechanics. The output kinematics and contact mechanics were compared to experimental data and compared to

mechanical alignment model predictions. The model outputs were used in combination with AOX material parameters to calculate a wear prediction using a computational wear framework.

The objectives of this chapter were:

1. Adapt mechanical alignment finite element setups to patient specific alignment to investigate the efficacy of the model to predict pre-clinical outputs at an alternate alignment and compare to experimental results
2. Computationally determine the wear under patient specific alignment setup of Attune AOX and compare with standard alignment conditions and experimental wear data

To address the first objective, the components were rotating in the ABAQUS environment to the required alignment position. Additional setup steps were included to investigate the effects of spring constrain inputs on output kinematics and contact between the components. These studies found that the spring profile used in the mechanical alignment setup, containing a “free-range” spring phase resulted in edge loading on the tibial insert, restricting the tibial rotation motion. It was found that removing the “free range” section from the tibial rotation spring overcame the issue of tibial edge loading. These findings were not reported in the experimental study which suggests there may be additional reasons for the edge loading in the alignment model caused by variables such as fixtures or internal simulator friction.

The fixed bearing, cruciate retaining TKR design model simulated under ISO 14243-1:2009 standard walking conditions in this study found more external rotation in the 4° varus alignment model in comparison to MA. However, the anterior-posterior translation results were not notably different to the outputs form the MA model motions.

Additional models were simulated in this study to understand the individual impact of coronal and sagittal alignment variables on the kinematic motions of the TKR bearing. The results showed that, both coronal alignment and sagittal alignment had an effect on the output kinematics in comparison to mechanical alignment. During stance phase, there was little difference between internal-external rotation and abduction adduction rotation between all alignments. All alignments resulted in more anterior positioning of the tibial insert in comparison to mechanical alignment. Overall, the study of changing coronal alignment and sagittal alignment showed that the angle of these two planes of the knee had an impact on kinematic motions.

Further work outside the scope of this study should be completed to validate the kinematics and contact mechanics outputs of this study using experimental data. This would require further component assembly adaptions. Once validated, these output kinematics and the contact mechanics from the model simulation could be used to determine the interaction of alignment planes with output kinematics and contact pressure. The model outputs may also be used with the Attune AOX wear framework to predict a wear rate for each simulation combination.

Investigation of the contact mechanics predicted by the model showed good agreement with experimental data which was measured using pressure sensor (Tekscan) equipment. The maximum average contact pressure for the whole contact surface was 7.2MPa. Further evaluation of the differences in contact pressure between the two compartments showed that the medial compartment had a higher contact pressure at more points of the gait cycle and between 60%-90% of gait there was no contact pressure measured on the lateral compartment. Overall, there was not a large difference between the contact pressure of the MA model in comparison to the PSA model at the majority of the gait measurement points. The largest difference was at 80% of gait were there as a 1.6MPa difference between the average contact pressure of the two alignments.

In comparison a study has found that contact pressure increases under PSA conditions and with increasing values of flexion with a peak contact stress of 39MPa on the lateral compartment at 90° flexion and a 5° varus alignment [133]. However, this study was conducted under a load of 4kN and without any other input kinematics other than flexion angle of the femoral component.

The kinematics and contact mechanics outputs of the 4° varus alignment model were used as functions of the volumetric wear calculation. The second objective was addressed using an Attune AOX specific wear formulation, incorporating a wear factor determined for the AOX material in a pin on plate study. A MATLAB script previously developed by the University of Leeds in collaboration with Nottingham Trent University [166], using the computational wear framework in combination with the finite element model outputs, was created specifically to predict the volumetric wear rate of Attune AOX. The volumetric wear rate calculated was applicable for the first 100,000 cycles of wear. Further adaptions to the surface geometry of the tibial insert bearing would need to be included in further work to investigate the volumetric wear rate over more wear cycles. The wear rate was calculated for both mechanical alignment (3.0 mm^3/MC) and 4° varus alignment (2.9 mm^3/MC). The wear rate

predictions for the two alignment models were similar and were both within the 95% confidence intervals of the corresponding experimental volumetric wear rates.

Overall, the model has been tested in alternate alignment angles and used to predict kinematics, contact mechanics and volumetric wear rate in a 4° varus alignment. The model results showed good agreement with experimental data in the same alignment and shows a promising outlook for future use in studying the effect of patient specific alignment variables in more depth. The models easy adaptability to different planes of alignment and competency for predicting kinematic and contact mechanics outputs may also prove to be useful in driving future improvements to the experimental pre-clinical methodology to investigate patient specific alignment configurations. Adaptions of this model in the future may offer a critical insight into the effect of planes of alignment on the biomechanics and tribology of total knee replacements.

Chapter 7
Discussion and Limitations

7.1 Introduction

The aim of this research was to develop combined experimental and computational approaches to investigate the influence of patient specific alignment surgical procedures on the kinematics, contact mechanics and wear of an Attune AOX Total Knee Replacement. A 4° varus coronal alignment did appear to impact output kinematics and contact mechanics in swing phase. Overall, there was no significant difference found between the wear rate in traditional alignment and patient specific coronal alignment.

Experimental pre-clinical methods were developed to simulate ISO-14243-1:2009 load control standard walking conditions on an Attune AOX TKR to investigate kinematics and wear. The output motions of the tibial component would be important in comparing the effect of the alignment of the TKR bearings on output kinematics. Pressure mapping sensors were used to measure the effect of ISO-14243-1:2009 load control standard walking kinematics on the contact pressure of the TKR bearing surface.

Experimental simulation ISO-14243-1:2009 load control inputs were applied to a finite element model of an Attune AOX TKR developed in ABAQUS 2017. Mesh convergence studies determined the appropriate mesh size for the Attune TKR design and sensitivity studies were completed investigate the efficacy of the Attune AOX TKR model to measure contact mechanics. Outputs from the model simulation, including kinematics and contact mechanics, were compared to experimental data to develop trust in the model capabilities.

The combined method of developing methodologies of TKR simulation in an experimental joint simulator and measuring outputs, followed by applying the same inputs to a finite element model simulation and comparing outputs to experimental data was used to investigate the effect of patient specific alignment variables on the performance of a TKR bearing.

The principle behind patient specific alignment approaches is to restore the native anatomy of the lower limb post-surgery. It was proposed that systematic approaches to the alignment of total knee replacements, such as mechanical alignment and anatomic 3° alignment were not necessarily producing optimal patient outcomes for patient cohorts with constitutional varus alignments [88, 155]. Literature has reported

good early-stage clinical outcomes with faster restoration of functional capabilities as a result of patient specific alignment procedures in comparison to mechanical alignment [13, 91]. Although overall, the functional outcomes at 2-year follow up are similar between the two procedures [152].

Total knee replacement bearings containing polyethylene tibial components that are susceptible to wear which has been well established in literature as being dependent on patient activity levels and frequency of use [62, 66]. Literature has also reported that medial wear damage is increased under conditions of total knee replacement compartment lift-off, where the coronal positioning of the tibial component caused loss of surface contact on the lateral compartment [135].

Determining the efficacy of patient specific alignment procedures on the longevity of TKR implants requires a comprehensive investigation into the combined impact on kinematics, contact mechanics and wear. Although studies have independently investigated the impact of alignment parameters on kinematics and wear in an experimental environment, there are yet to be validated methods of developing computational models to investigate the impact of TKR alignment on wear rates. Furthermore, physical limitations of joint simulators prevent the study of daily activities on more adverse alignment parameters outside of the range of constitutional varus/valgus alignments. This study utilised the combination of experimental and computational methods to develop a finite element of a TKR which can be adapted into a range of coronal and sagittal alignment positions to predict kinematics and contact mechanics.

Furthermore, the study utilised previously developed computational wear frameworks to predict the wear rate of a TKR in varus alignment to determine whether there is likely to be any effect on the wear of the tibial insert because of these alignment parameters.

7.2 Experimental Simulation of Attune AOX Total Knee Replacements Under ISO 14243-1:2009 Load Control in Mechanical Alignment.

A 3 million cycle wear study was completed on Attune AOX TKR bearings using a 6-station ProSim electromechanical knee simulator to determine kinematics and wear during ISO-14243-1:2009 load control inputs. The method of simulation, outlined in Chapter 2, was initially validated on the Sigma XLK TKR design and the wear rate (5.6±2.1 mm^3/MC) was found to be not significantly different ($p = 0.36$) from wear rates published in literature by Johnston et al., 2018 (4.7±1.3 mm^3/MC). There were differences reported in the kinematic outputs of these studies with the present study

translating to an anterior position in swing phase, which was not found in the literature. Both studies were completed under load control using virtual springs tuned using a PID controller, variability in these tuning parameters may have contributed to the differences reported in output kinematics.

The methods were then developed to investigate the wear of Attune AOX TKRs, which included creating new bespoke fixtures for the Attune Gradius design. The study was simulated under ISO-14243-1:2009 load control inputs for 3 million cycles. The Attune AOX wear rate was 2.7±1.1mm^3/MC. The lower wear rate, although not statistically different, reported on the Attune TKR bearing may be a result of the optimised design with a gradually reducing femoral sagittal radius to attenuate loads through increasing angles of flexion. The antioxidant-stabilised UHMWPE material used in the AOX tibial inserts may also contribute to the reduced wear rate in comparison to the moderately cross-linked XLK material. The accuracy of the methodology to measure differences in wear at these low wear rates should be considered and may have been impacted by uncontrolled system errors such as friction. Specifically, at wear rates lower than 5mm^3/MC, it has been found that simulator error may make identifying differences in wear rates between samples challenging [124]. Other studies, which have simulated walking kinematic conditions derived from lower limb musculoskeletal models, have found Attune AOX wear rates of 3.8 mm^3/MC [130]. This study was simulated using an AMTI VIVO joint simulator and Grood & Suntay coordinate system in comparison to the global coordinate system used in this present study.

The anterior-posterior translation of Attune design found under the ISO-14243-1:2009 load control conditions was similar in motion to the Sigma bearing design, although the peak posterior position at 60% and peak anterior position at 70% were lower in value for Attune. There was an anterior shift in motion found at around 30° flexion in both bearing designs. Studies have found that this anterior motion is eliminated in-vivo due to the Gradius design resulting in lateral femoral rollback which is more representative of native knee kinematic motion [85]. The simulator motion control input parameters under ISO-14243-1:2009 conditions may have had an impact on the overall kinematic output motions of the Attune bearing.

Input kinematics of Attune in-vivo knee motion may be used in future to more accurately represent the true kinematic outputs with this design. Furthermore, a wider range of kinematic inputs representing other activities of daily living such as stair ascent and deep squat may provide further insight into the performance of the Attune design.

7.3 Experimental Investigation of Attune AOX Total Knee Replacement Contact Mechanics Using Pressure Sensors at a Range of Kinematic Positions and Loads

Contact mechanics of the Attune AOX TKR were measured using pressure mapping sensors at 10% intervals of the gait cycle. Contact stress was the parameter of interest in this study. Tekscan equipment was determined as the most appropriate choice of pressure sensor for this study due to high accuracy measuring contact stress [141, 167]. Methodologies of calibration of the sensors, setup of the test materials and analysing results were developed in Chapter 3 using methods reported in literature and from a series of preliminary studies outlined in this research. The studies found maximum average contact pressure of 7.31MPa at 40% of the gait cycle, with higher contact pressures measured on the medial compartment. This finding is in agreement with published literature which found the average contact pressure of Attune AOX under gait conditions to be between 7MPa and 12MPa [127].

The results showed that appropriate calibration procedures returning contact pressures with no drift between values with up to 18 measurements completed between sensor re-calibration. The methods developed to measure the contact pressure of the Attune TKR bearing were initially studies for repeatability at different input loads without input kinematics, followed by investigating the impact of a range of flexion positions on contact pressure at applied loads between 50N and 3kN. The results showed average contact pressures at 50N between 2MPa and 4MPa while contact pressures increased with increasing load with values between 7.5MPa and 9.5MPa at 3kN of load. These initial studies provided confidence in the suitability of the calibration and setup procedures, which facilitated the measuring of contact pressures of the Attune AOX total knee replacement at 10% intervals of the gait cycle under a compressive load.

7.4 Developing an Attune AOX Finite Element Model to Predict Kinematics and Contact Mechanics Under ISO-14243-1:2009 Load Control Simulation Input Conditions

A finite element model of an Attune total knee replacement system was developed in Chapter 4, by importing part geometries of the femoral component and tibial insert into Abaqus. Boundary conditions were applied to constrain the components in space according the fixture constraints of the experimental wear simulation. Both components were assigned a 10-node modified quadratic tetrahedron (C3D10M) element mesh with a global element size of 1mm. ISO-14243-1:2009 load control inputs were applied through boundary conditions and loads in addition to wire

elements used to apply soft tissue restraint profiles for tibial insert control. The AOX tibial insert material properties were determined under experimental compressive test conditions combined with computational simulations according the methods presented by Abdelgaied et al., (2018) [119].

The material mechanical properties (E =348MPa and v=0.35) were assigned to the tibial insert material in the finite element model. The computational simulation of the TKR model for a load control walking gait cycle predicted output profiles of tibial kinematics (including anterior-posterior displacement and internal-external rotation), sliding distance of tibial insert coordinates throughout the gait cycle in both x and y directions, and contact pressure values measured by the bearing surface nodes.

The model simulation over one gait cycle resulted in kinematic predictions in good agreement with the experimental kinematic outputs for anterior-posterior displacement (RMSE = 1.60%) and internal-external rotation (RMSE = 0.95%). Contact pressure values predicted a maximum average contact pressure of 6.68MPa at 40% of the gait cycle. This was in good agreement with the experimentally measured maximum average contact pressure at 40% gait of 7.5MPa. The close agreement between the experimental and computational results created trust in the efficacy of the model specifically for predicting kinematics and contact mechanics of an Attune AOX TKR bearing under ISO-14243-1:2009 walking conditions.

7.5 Creating Experimental Preclinical Methods of Simulating Patient Specific Alignment Joint Angles to Predict Kinematics, Contact Mechanics and Wear Rates.

The work presented in Chapter 5 outlines how a combination of literature and surgical guidelines was used to develop patient specific alignment parameters to simulate and evaluate the impact on kinematics, contact mechanics and wear of an Attune AOX TKR. The experimental studies were developed to create a varus joint line of 4°, which was implemented through fixture adaptions of both the tibial component and femoral component. An offset was incorporated into the fixture to align the components with the loading axis at the centre of rotation. The wear simulation methodology was maintained from the mechanical alignment simulation, which included using ISO 14243-1:2009 standard walking inputs, with anterior-posterior translation and tibial rotation motions constrained through virtual springs.

The results of the experimental studies showed that the tibial insert translated approximately 1mm more posterior in 4° varus alignment, compared to MA,

throughout the whole gait cycle with a peak of 4.1mm posterior in 4° varus compared to 2.7mm in MA. Internal-external output kinematics showed a lower peak internal rotation of 5.5º in 4° varus compared to 7.5º in MA. The 4° varus alignment resulted in a 0.5º increase in abduction during the swing phase compared to MA.

During the wear simulation, one sample was found to be damaged at the 1 million-cycle wear interval so was removed from the study. The fixed bearing, Attune AOX, 4° varus alignment experimental wear rate was 3.3±0.5mm^3/MC (n=5) after 3 million cycles. The wear rate of mechanical alignment after 3 million cycles was 2.7± 1.1mm^3/MC (n=6). A 1-way ANOVA on the wear rates of the two studies at 2 million cycles of wear, both with n=6, found no significant difference (*p=0.12*).

Recent studies presented in literature have investigated the effect of coronal alignments on kinematics, contact mechanics and wear of the total knee replacement bearing. One study, performed during the duration of this research, adapted the simulator control axes positions to place the tibial component in 4° varus alignment and the femoral component in 4° valgus alignment [121]. This method of altering the alignment of the flexion-extension axis and internal-external rotation axis resulted in a configuration such that the control of the implant kinematics were at the new desired angle but that the axis of superior-inferior load of the joint was unchanged. Their study, also using a fixed bearing, cruciate retaining Attune AOX TKR, simulated under ISO 14243-1:2009 load control inputs, found that there was no difference ($p > 0.99$) in wear between the kinematic alignment setup (4.1mg/mc) and the mechanical alignment setup (3.8mg/mc) [121]. Other studies created a 4° varus alignment setup using angled femoral and tibial fixtures have found lower wear rates in varus alignment (1.79±1.64mm^3/mc) in comparison to mechanical alignment (3.06±1.57 mm^3/MC) under ISO 14243-1 kinematic inputs [129]. This study was completed on a 6-station ProSim electromechanical TKR simulator on the Sigma dual radius TKR design with XLK tibial insert material. Maag et al., (2021) investigated wear using an AMTI VIVO simulator with input kinematics determined from a computational simulation of Attune AOX in a lower limb musculoskeletal model. The alignment parameters were applied using these kinematic profile inputs, the Attune samples were mounted in the simulator using the same fixtures as the mechanical alignment study. The study reported no significant difference (*p=0.144*) between wear rates at 4.5 million cycles in a 5° varus alignment (2.59 ± 2.11mg/mc) and mechanical alignment (3.76 ± 0.51 mg/mc) [130].

Different joint simulators were used for these three studies, including a 6-station ProSim electromechanical simulator by Johnston et al., (2019) and an AMTI VIVO

simulator by Schroeder et al., (2022) and Maag et al., (2021). Although these studies used similar methodologies for determining the output kinematics and wear scar area; differences in the application of kinematic inputs, use of fixtures for component alignment and the use of the control systems of the simulators, make direct comparison of the results challenging. However, all three studies found no significant difference between the mechanical alignment simulation results and the patient specific alignment results which is in agreement with the results found in this study.

The average contact pressure for the contact surface in patient specific alignment was similar to mechanical alignment. However, a more detailed look at the average contact pressure on the medial compartment compared to the lateral compartment showed that the patient specific alignment setup had a larger difference between the contact pressure measured on each compartment with the offset of pressure greater on the medial compartment in comparison to the lateral compartment.

7.6 Applying Alignment Simulation Parameters to an Attune AOX Finite Element Model to Predict Kinematics and Contact Mechanics

A computational simulation method for a 4° varus TKR alignment was developed in Chapter 6. The new alignment parameters for 4° varus, developed for experimental simulation in Chapter 5, were adapted into the computational model. The samples were rotated in Abaqus, about the central coordinate system aligned with the centre of rotation of the component, to the 4° varus alignment orientation. The 4° varus alignment finite element model simulation resulted in anterior-posterior displacements at the same phase and amplitude as in mechanical alignment, but more external rotation in the swing phase.

Computational models reported in literature of fixed bearing cruciate retaining TKR designs, have found that patient specific alignment results in more anterior translation on the medial compartment and more posterior translation on the lateral compartment in comparison to corresponding models in MA [133, 168]. These two computational model studies of the effect of PSA on TKR kinematics only reported the impact of increasing angles of flexion on the output kinematics and did not investigate the impact of daily activities such as walking. The study by Ishikawa et al., (2015) studied alignment conditions of 3° varus and 5° varus and found an increase in femoral rollback in the PSA models [133]. The study by Theodore et al., (2017) used CT scans of 20 patients to assign component alignments relative to their native anatomy. The average coronal alignment was 3.0° ± 2.4° tibial varus, 3.0° ± 2.3° femoral valgus and average tibial slope was 7.2° ± 6.6°, the study found little difference in femoral

rollback [168]. These values closely align with what was found in the literature review of patient specific alignment surgical procedure studies and is similar to what was studied here in the coronal alignment which reported averages of between 2.2° to 3° tibial varus and 1.3° to 2.5° femoral valgus [13, 152, 153, 161].

To investigate patient specific alignment in the finite element model, the components were rotated in the coronal plane to represent the 4° varus alignment. The initial results of this study highlighted that the setup of the spring constraints used in the mechanically aligned finite element model resulted in loading on the edge of the tibial insert when the components were rotated to a coronal alignment. A short study investigated the impact of a three-phase spring profile and a two-phase spring profile on the outputs of the model which showed no loading on the edge of the insert. A two-phase spring prevented the incidence of edge loading and allowed kinematic motions closer in agreement with experimental outputs. However, the three-phase spring inputs were used in the wear prediction study to ensure that the input parameters were consistent with the experimental and mechanical alignment model inputs. Further studies may be required to investigate the cause of the edge loading in the three-phase spring PSA model and to investigate the impact of two-phase spring inputs on output kinematics both experimentally and computationally.

Further adaptations to the model were made, to evaluate the impact of a larger range of alignment values including a range of coronal alignments, sagittal alignment and a combination of both. This study implied that the coronal and sagittal positioning of the tibial insert had an effect on kinematic motions including more anterior translation, more external rotation in swing phase and more abduction in swing phase.

The 4° varus alignment simulation study used the 3-phase spring constraints to maintain input parameters with the mechanical alignment model inputs. However, published studies have investigated the impact of spring input conditions on output kinematics, contact mechanics and wear using experimental and finite element model simulations [129, 164]. The studies found that a 4° varus alignment resulted in similar kinematic outputs and significantly lower wear rates than in mechanical alignment. It was also reported that a sagittal tibial slope alignment resulted in increased anterior translation throughout the whole gait cycle, in agreement with the results presented here.

7.7 Using Computational Methods to Determine the Wear Rate of Attune AOX Simulated Under Mechanical Alignment and 4° Varus Alignment Conditions

The computational formulation used in this study to calculate wear volume of the TKR bearing was previously developed in the work by Abdelgaied et al., (2018) and revised with Attune AOX material properties. The linear wear depth of the TKR bearing was calculated using sliding distance values, an output from the finite element model, and the wear coefficient. The wear coefficient calculation [125] accounting for cross-shear of polyethylene materials [59], was adapted to be applicable for calculating the wear volume of total knee replacements by methods presented in [61] and [169]. These methods were applied to AOX polyethylene material to derive a non-dimensional wear coefficient, independent of contact pressure, using multi-directional pin on plate studies. The computational wear volume formulation was optimised using these values for the wear prediction of Attune AOX material properties using the methodologies outlined in [119]. The volumetric wear rates calculated in Chapter 6 for the two finite element models were 3.0 mm^3/mc for mechanical alignment and 2.9 mm^3/mc for 4° varus alignment.

The computational values were within the 95% confidence interval range of the confidence intervals of the experimental values. The agreement between the model and experimental kinematic outputs, contact pressures and wear developed further trust in the efficacy of the model when adapted to alternate component alignments.

7.8 Limitations

The Attune AOX total knee replacement system is an optimised design with a gradually reducing radius (Gradius) in comparison to a dual radius found on many other total knee replacements such as Sigma XLK [56]. In comparison to dual radius designs, the Gradius TKR design has been shown to create more natural walking kinematics in-vivo which include lateral compartment femoral rollback (posterior translation) during gait above 30° flexion [85]. The ISO 14243-1:2009 standard setup, where spring constraints are used to control the movement of the tibial insert, may limit the full gait range of motion of the Attune TKR Gradius at high flexion angles. The output kinematics are also only presented for the motion of the whole bearing and were not studied for the individual compartments. Further work is required to determine whether the output kinematics of this study are indicative of kinematics in-vivo, however literature would suggest that they are not. It may also be useful to increase the sample size for these studies. As highlighted in the PSA experimental studies, damage can occur during simulation causing loss of data and a reduced sample size of less than six. Expanding the sample size may improve the reliability of the average wear volume in addition to increased study lengths with increased wear cycle intervals up to the ISO standard cycle number of 5 million cycles.

During the method development of the experimental studies completed, limitations were found which restricted the scope of the studies which could be completed in this body of work. The most restrictive capability of the simulator was the inability to control the abduction-adduction angle using input kinematic profiles. This resulted in a more resource and time-expensive approach where fixtures were developed to achieve the alignment goals. In contrast, the adaption of the mechanical alignment finite element model to the 4° varus alignment configuration was less complex and did not require any further resource. The advantage of computational approaches is that the combination of variables which can be simulated are, in theory, endless. However, it is important to consider the validation of these simulations with experimental data to establish the credibility of the results.

Limitations of using experimental joint simulators to measure wear rates are highlighted when large ranges of input variables are required to simulate a large portfolio of TKR setup parameters. The demand on resources and time makes investigating multiple configurations of patient specific alignment impractical and unjustifiable in a physical experimental simulation environment. However, it is important to highlight the value that these experimental simulations bring to validating the outputs of alternative pre-clinical simulation methods such as computational models.

Limitations of the Tekscan sensor accuracy were found when the pressure distribution was more concentrated to one compartment leaving small pressures on the contralateral compartment. The Tekscan sensors used in this study had a maximum resolution of 62MPa to ensure that they were capable of accurately measuring the maximum contact pressures of the study. However, this may have compromised the sensor accuracy at lower contact pressures. Further work to develop the methods of equilibration of the sensors may help to resolve any resolution issues at lower contact pressures.

Adapting these alignment variables into an alignment package to investigate experimentally on an electromechanical joint simulator with load control inputs was confined by the capabilities and limits of the simulator. Furthermore, when considering modelling the pre-clinical performance of a total knee replacement it may also be useful to develop models incorporating the patient anatomy rather than modelling the simulator setup. This may provide an additional insight into the performance of a total knee replacement in the human body in both mechanical alignment and other alignments. To create a preclinical representation of all variables

effected by patient specific alignment, further work is required to properly align the components at the required axes of the limb.

Literature has shown that varus joint line orientation, after kinematic alignment procedures, results in a significant reduction in peak knee adduction moment (KAM) during walking [170]. The 4º varus alignment fixtures were designed to incorporate adaptions to align the loading axis at the centre of rotation in the simulator. The centre of rotation was determined based on the value stated in ISO 14243-1:2009 which is a medial offset of 7% of the width of the tibial insert. However, this offset value is specific for mechanically aligned total knee replacements and might not be representative of medial offset as a result of patient specific alignment variables. Research into the impact of patient specific alignment on the load distribution between the compartments of total knee replacements using finite element methods, reported a medial shift in load concentration on the tibial insert surface [171]. Further research, using methods of determining the effect of alignment on the loading offset between the medial and lateral compartment, may be able to adapt the setup for patient specific alignment depending on the angle of alignment.

Preliminary alignment trials using the simulator hardware to align the components in the specified 4° varus orientation highlighted the limitations of the simulator to be that the abduction-adduction axis could not be maintained at the angle once an axial load was applied. The applied load overpowered the fixation of the axis, moving the components to settle on a dwell point and therefore forcing the components into the same joint line orientation.

7.9 Future Work

The studies presented on evaluating contact mechanics focussed on measuring contact pressures on the bearing surface and how it is affected by changes in gait parameters. Additional contact mechanics studies could help to contextualise the effect of joint alignment and kinematic inputs on contact area and location. These further studies would require additional equipment and methodologies to evaluate the tibial insert surface. A digital microscope or camera can be used to evaluate the wear scar size and location on the bearing surface. This is a useful method which can be used to quantify the difference between the wear scars of the two compartments and visually assess differences in wear scars between insert components due to different testing parameters.

Further adaptions to the Tekscan methods are required to improve accuracy of measurements at low loads. Alternative methods of securing the sensors and

positioning the simulator axes could be investigated to improve the repeatability of the measurements using the Tekscan. One option would be to use the simulator software to pre-position the flexion angle of the femoral component followed by disabling the axis prior to positioning the Tekscan sensors. This would ensure that the Tekscan sensor is placed in the correct position for the measurement and stops the movement of the flexion of the femoral component moving the Tekscan sensor, therefore improving the repeatability of the measurement and ensuring that the contact of the bearing is picked up correctly by the equipment.

In a clinical environment, where a surgeon determines that a patient specific alignment approach is the most suitable medical intervention for the patient, many parameters are measured to determine the appropriate surgical approach. Pre-operative planning involves using x-rays of the patients' knee to determine the anatomical axes and measure the corresponding angles. Surgical tools, cutting blocks or computer aided surgical systems are used to measure the bone cuts during surgery, to create the new bone surfaces for the implant. New planes of alignment are created when the bones are resurfaced with total knee replacement components. These planes of alignment may be the same as the patients' native anatomy or adapted to be within surgical "safe boundaries".

Investigating these post-operative alignment conditions in a pre-clinical setting requires data inputs from in-vivo conditions so that research can accurately determine the long-term impacts of these alignment procedures. Gathering this data presents challenges, which in time can be overcome by technology and by long-term clinical data. However, since patient specific alignment procedures are a relatively novel approach to total knee replacement surgery, published data on these parameters is limited and concentrated to specific surgeons and patient cohorts. Furthermore, studies appeared to summarise differences between the alignment angles of MA patient cohorts and PSA patient cohorts or the post-operative gait parameters.

Developing in-vitro inputs to simulate patient specific alignment variables which are clinically relevant requires cohesive data sets of patient case studies where the alignment angle parameters match the measured gait outputs. In terms of mechanical alignment, the alignment angles are the same and gait parameters can be determined from the population average or can be developed to simulate worst-case scenarios.

To create a patient specific alignment setup on the ProSim simulators, further adaptions to the hardware or software of the equipment would be required. This could

include adapting the control coordinate system to a Grood & Suntay system, creating a floating axis for anterior posterior translation and varus valgus rotation [19, 127]. This method of assigning a Cartesian coordinate system to both the femur and tibia with a floating axis between the two facilitates a control system where the two components rotate relative to each other rather than relative to a global coordinate system of the simulator. This would be beneficial when simulating a patient specific alignment setup because the rotational alignment of the components could be achieved with a rotation of the internal-external rotation axis for the components. Studies have achieved these alignment conditions using a Grood and Suntay coordinate system by rotating the physical fixture angle of the component in addition to rotating the simulator alignment axis. The result of this method was the alignment of the compressive load axis with the internal-external control axis at the new alignment orientation, in an AMTI joint simulator [121]. A separate study, also using an AMTI simulator with Grood & Suntay coordinate system, did not alter the physical alignment of the components but applied altered kinematic inputs determined from a PID controlled lower limb model with TKR components adapted to PSA conditions [130, 131].

Future work could utilise a collaboration with clinical partners to collect clinical standard walking and other daily activity gait data for patients post-operatively. This would facilitate the development of in-vitro simulation inputs combining post-operative alignment values with post-operative walking loads and kinematics. This would also allow investigations into the long-term impacts of patient specific alignment approaches on patients with anatomies determined as severe cases. It is imperative that research includes “outlier populations” when determining the safety and efficacy of joint replacement designs and surgical procedures. The motivation behind patient specific surgical approaches is to create clinical interventions which are tailored towards being inclusive of wider patient demographics. The risk is that these new and innovative clinical interventions are not backed up by research or more importantly, research which also encompasses these outlier patients. Evaluating the longevity of implants which are positioned on the boundaries of what could be determined as safe cannot be successfully determined using patient averages or even the worst-case scenario of patient averages. These patient outlier populations require a comprehensive understanding of the effects of the combined adaptions to alignment angles, loading offsets and resulting gait parameters to evaluate whether the benefits of restoring a native joint alignment outweigh any implication on the longevity of the implant.

In future, models should be developed taking into account different input kinematics, spring constraints and changes in load caused by the alignment. Models to investigate the effect of PSA on other bearing designs such as posterior stabilised or rotating platform implants may also provide further insight into the impact of alignment on TKR bearing wear. Additionally, further work could be completed to continue to investigate the effect of combinations of coronal and sagittal angles on kinematic outputs and specifically to understand the interaction of the alignment angles on abduction rotation of the tibial insert.

7.10 Conclusion

The aim of this research was to investigate the impact of patient specific alignment on the kinematics, contact mechanics and wear of a total knee replacement through a combined experimental and computational approach. The research objectives were addressed through a combination of experimental and computational studies, where new methods have been developed to simulate ISO 14243-1 load control standard walking in different alignment conditions. There was no significant difference ($p=0.12$) found between the wear rate of the commercially available DePuy Synthes Attune fixed bearing total knee replacement under mechanical alignment and 4° varus alignment conditions after 3 million cycles of standard walking. The wear rate predictions of the computational model simulations were within the 95% confidence intervals of the experimental wear rates. In summary, the finite element model of an Attune total knee replacement was developed and validated under mechanical alignment and 4° varus alignment conditions.

The validated model was used to investigate the independent and combined interaction effects of coronal and sagittal planes of alignment on the output kinematics under ISO 14243-1 load control standard walking input conditions. Changes in both the coronal angle and sagittal angle of alignment resulted in different kinematic outputs in comparison to mechanical alignment. It can be concluded that there are independent impacts of the individual alignment variables on kinematic outputs.

The validated computational model has the potential to be used in the future as an efficient verification tool for the design phase of total knee replacements and to provide surgeons with a tool for pre-operative visualisation of the bearing surface and functional performance outcomes on a patient-by-patient basis. However, further work is required to improve the computational efficiency of the model, the model accuracy at low loads, and to develop methods for quantifying the surface contact areas both experimentally and computationally. The structured experimental and

computational approach presented in this study should be used in the future to create the next iterations total knee replacement pre-clinical simulation models.

Chapter 8

Bibliography

[1] J. Charnley, "Anchorage of the femoral head prosthesis to the shaft of the femur," *The Journal of bone joint surgery. British volume,* vol. 42, no. 1, pp. 28-30, 1960.

[2] National Joint Registry, "NJR's 19th Annual Report," https://www.njrcentre.org.uk/njrcentre/Reports-Publications-and-Minutes/Annual-reports2022.

[3] Versus Arthritis, "Osteoarthritis information booklet," VersusArthritis.org2018, Available: https://www.versusarthritis.org/about-arthritis/conditions/osteoarthritis/.

[4] K. Maiese, "Picking a bone with WISP1 (CCN4): new strategies against degenerative joint disease," *Journal of translational science,* vol. 1, no. 3, p. 83, 2016.

[5] D. Pereira, B. Peleteiro, J. Araujo, J. Branco, R. Santos, and E. Ramos, "The effect of osteoarthritis definition on prevalence and incidence estimates: a systematic review," *Osteoarthritis and Cartilage,* vol. 19, no. 11, pp. 1270-1285, 2011.

[6] J. Fisher, M. Al-Hajjar, S. Williams, L. M. Jennings, and E. Ingham, "In Vitro Measurement of Wear in Joint Replacements: A Stratified Approach for Enhanced Reliability “SAFER” Pre-Clinical Simulation Testing," *Seminars in Arthroplasty,* vol. 23, no. 4, pp. 286-288, 2012/12/01/ 2012.

[7] D. Dowson, "Bio-tribology," *Faraday discussions,* vol. 156, pp. 9-3, 2012.

[8] H. G. Dossett, G. J. Swartz, N. A. Estrada, G. W. LeFevre, and B. G. Kwasman, "Kinematically versus mechanically aligned total knee arthroplasty," *Orthopedics,* vol. 35, no. 2, pp. e160-e169, 2012.

[9] S. Howell and A. Nedopil, *Five Quality Assurance Steps for Balancing a Kinematically Aligned Total Knee Arthroplasty*. 2017, pp. 79-96.

[10] Y. S. Lee *et al.*, "Kinematic alignment is a possible alternative to mechanical alignment in total knee arthroplasty," *Knee Surgery, Sports Traumatology, Arthroscopy,* vol. 25, no. 11, pp. 3467-3479, 2017.

[11] J. D. Roth, S. M. Howell, and M. L. Hull, "Kinematically aligned total knee arthroplasty limits high tibial forces, differences in tibial forces between compartments, and abnormal tibial contact kinematics during passive flexion," *Knee Surgery, Sports Traumatology, Arthroscopy,* vol. 26, no. 6, pp. 1589-1601, 2018/06/01 2018.

[12] S. M. Howell, E. E. Hodapp, J. V. Vernace, M. L. Hull, and T. D. Meade, "Are undesirable contact kinematics minimized after kinematically aligned total knee arthroplasty? An intersurgeon analysis of consecutive patients," *Knee Surgery, Sports Traumatology, Arthroscopy,* vol. 21, no. 10, pp. 2281-2287, 2013/10/01 2013.

[13] H. G. Dossett, N. A. Estrada, G. J. Swartz, G. W. LeFevre, and B. G. Kwasman, "A randomised controlled trial of kinematically and mechanically aligned total knee replacements: two-year clinical results," (in eng), *Bone Joint J,* vol. 96-b, no. 7, pp. 907-13, Jul 2014.

[14] T. Fukubayashi and H. Kurosawa, "The contact area and pressure distribution pattern of the knee: a study of normal and osteoarthrotic knee joints," *Acta Orthopaedica Scandinavica,* vol. 51, no. 1-6, pp. 871-879, 1980.

[15] H. Forster and J. Fisher, "The influence of continuous sliding and subsequent surface wear on the friction of articular cartilage," *Proceedings*

of the Institution of Mechanical Engineers, Part H: Journal of Engineering in Medicine, vol. 213, no. 4, pp. 329-345, 1999.

[16] M. Gupton and R. R. Terreberry, "Anatomy, Lower Limb, Knee," in *StatPearls [Internet]*: StatPearls Publishing, 2018.

[17] R. S. Behnke, *Kinetic Anatomy 3rd Edition*. Human Kinetics, 2012, pp. 243-261.

[18] E. N. Marieb and K. Hoehn, *Human anatomy & physiology*, Tenth, Global / Elaine N. Marieb and Katja Hoehn. ed. (no. Book, Whole). Pearson Education M.U.A: Pearson, 2015, pp. 271-286.

[19] E. S. Grood and W. J. Suntay, "A joint coordinate system for the clinical description of three-dimensional motions: application to the knee," *Journal of biomechanical engineering,* vol. 105, no. 2, pp. 136-144, 1983.

[20] F. R. Noyes, *Noyes' Knee Disorders: Surgery, Rehabilitation, Clinical Outcomes E-Book*. Elsevier Health Sciences, 2009.

[21] M. D. F. Noyes and E. Grood, *Classification of ligament injuries: why an anterolateral laxity or anteromedial laxity is not a diagnostic entity*. 1987, pp. 185-200.

[22] M. A. Lafortune, P. R. Cavanagh, H. J. Sommer, and A. Kalenak, "Three-dimensional kinematics of the human knee during walking," *Journal of Biomechanics,* vol. 25, no. 4, pp. 347-357, 1992/04/01/ 1992.

[23] K. E. Roach and T. P. J. P. t. Miles, "Normal hip and knee active range of motion: the relationship to age," vol. 71, no. 9, pp. 656-665, 1991.

[24] M. Marieswaran, A. Sikidar, A. Goel, D. Joshi, and D. Kalyanasundaram, "An extended OpenSim knee model for analysis of strains of connective tissues," *Biomedical engineering online,* vol. 17, no. 1, p. 42, 2018.

[25] H. Iwaki, V. Pinskerova, and M. Freeman, "Tibiofemoral movement 1: the shapes and relative movements of the femur and tibia in the unloaded cadaver knee," *The Journal of bone and joint surgery. British volume,* vol. 82, no. 8, pp. 1189-1195, 2000.

[26] P. F. Hill, V. Vedi, A. Williams, H. Iwaki, V. Pinskerova, and M. Freeman, "Tibiofemoral movement 2: the loaded and unloaded living knee studied by MRI," *The Journal of bone and joint surgery. British volume,* vol. 82, no. 8, pp. 1196-1198, 2000.

[27] S. Nakagawa *et al.*, "Tibiofemoral movement 3: full flexion in the living knee studied by MRI," *The Journal of bone and joint surgery. British volume,* vol. 82, no. 8, pp. 1199-1200, 2000.

[28] P. Johal, A. Williams, P. Wragg, D. Hunt, and W. Gedroyc, "Tibio-femoral movement in the living knee. A study of weight bearing and non-weight bearing knee kinematics using ‘interventional’MRI," *Journal of biomechanics,* vol. 38, no. 2, pp. 269-276, 2005.

[29] S. Hamai, T.-A. Moro-Oka, N. J. Dunbar, H. Miura, Y. Iwamoto, and S. A. Banks, "In vivo healthy knee kinematics during dynamic full flexion," *BioMed research international,* vol. 2013, 2012.

[30] S. Yamaguchi, K. Gamada, T. Sasho, H. Kato, M. Sonoda, and S. A. Banks, "In vivo kinematics of anterior cruciate ligament deficient knees during pivot and squat activities," *Clinical Biomechanics,* vol. 24, no. 1, pp. 71-76, 2009.

[31] J. D. Blaha, C. A. Mancinelli, W. H. Simons, V. L. Kish, and G. Thyagarajan, "Kinematics of the human knee using an open chain cadaver model," *Clinical Orthopaedics and Related Research®,* vol. 410, pp. 25-34, 2003.

[32] S. Koo and T. P. Andriacchi, "The knee joint center of rotation is predominantly on the lateral side during normal walking," *Journal of biomechanics,* vol. 41, no. 6, pp. 1269-1273, 2008.

[33] M. A. Freeman and V. Pinskerova, "The movement of the normal tibio-femoral joint," *Journal of biomechanics,* vol. 38, no. 2, pp. 197-208, 2005.

[34] J. D. Roth, S. M. Howell, and M. L. Hull, "Native knee laxities at 0, 45, and 90 of flexion and their relationship to the goal of the gap-balancing

alignment method of total knee arthroplasty," *JBJS,* vol. 97, no. 20, pp. 1678-1684, 2015.

[35] D. A. Dennis. (2018, 16/12/2018). *TKA Axial Alignment*. Available: https://www.orthobullets.com/recon/5014/tka-axial-alignment

[36] K. Deep, F. Picard, and J. V. Clarke, "Dynamic knee alignment and collateral knee laxity and its variations in normal humans," *Frontiers in surgery,* vol. 2, p. 62, 2015.

[37] M. Hall *et al.*, "The knee adduction moment and knee osteoarthritis symptoms: relationships according to radiographic disease severity," *Osteoarthritis and Cartilage,* vol. 25, no. 1, pp. 34-41, 2017/01/01/ 2017.

[38] R. H. Miller, R. L. Krupenevich, A. L. Pruziner, E. J. Wolf, and B. L. Schnall, "Medial knee joint contact force in the intact limb during walking in recently ambulatory service members with unilateral limb loss: a cross-sectional study," *PeerJ,* vol. 5, p. e2960, 2017.

[39] S. Meireles, F. De Groote, S. Van Rossom, S. Verschueren, and I. Jonkers, "Differences in knee adduction moment between healthy subjects and patients with osteoarthritis depend on the knee axis definition," *Gait & Posture,* vol. 53, pp. 104-109, 2017/03/01/ 2017.

[40] C. K. Fitzpatrick, C. W. Clary, and P. J. Rullkoetter, "The role of patient, surgical, and implant design variation in total knee replacement performance," *Journal of Biomechanics,* vol. 45, no. 12, pp. 2092-2102, Aug 2012.

[41] S. Meireles, M. Wesseling, C. R. Smith, D. G. Thelen, S. Verschueren, and I. Jonkers, "Medial knee loading is altered in subjects with early osteoarthritis during gait but not during step-up-and-over task," *PloS one,* vol. 12, no. 11, p. e0187583, 2017.

[42] D. T. Felson, "Chapter 100 - Treatment of Osteoarthritis A2 - Firestein, Gary S," in *Kelley and Firestein's Textbook of Rheumatology (Tenth Edition)*, R. C. Budd, S. E. Gabriel, I. B. McInnes, and J. R. O'Dell, Eds.: Elsevier, 2017, pp. 1719-1729.

[43] D. T. Felson, "The epidemiology of knee osteoarthritis: Results from the framingham osteoarthritis study," *Seminars in Arthritis and Rheumatism,* vol. 20, no. 3, Supplement 1, pp. 42-50, 1990/12/01/ 1990.

[44] G. Pezzotti, *Advanced Materials for Joint Implants*. Pan Stanford Publishing, 2016, p. 492.

[45] E. Teeple *et al.*, "Coefficients of friction, lubricin, and cartilage damage in the anterior cruciate ligament-deficient guinea pig knee," *Journal of orthopaedic research : official publication of the Orthopaedic Research Society,* vol. 26, no. 2, pp. 231-237, 2008.

[46] S.-S. Lee, C.-T. Duong, S.-H. Park, Y. Cho, S. Park, and S. Park, *Frictional response of normal and osteoarthritic articular cartilage in human femoral head*. 2013, pp. 129-37.

[47] A. M. Bhosale and J. B. Richardson, "Articular cartilage: structure, injuries and review of management," *British medical bulletin,* vol. 87, no. 1, pp. 77-95, 2008.

[48] D. Kumar, K. T. Manal, and K. S. Rudolph, "Knee joint loading during gait in healthy controls and individuals with knee osteoarthritis," *Osteoarthritis and cartilage,* vol. 21, no. 2, pp. 298-305, 2013.

[49] R. F. Moyer, T. B. Birmingham, D. M. Bryant, J. R. Giffin, K. A. Marriott, and K. M. Leitch, "Biomechanical effects of valgus knee bracing: a systematic review and meta-analysis," *Osteoarthritis and Cartilage,* vol. 23, no. 2, pp. 178-188, 2015/02/01/ 2015.

[50] U. K. Munzinger, J. G. Boldt, and P. A. Keblish, *Primary knee arthroplasty* (no. Book, Whole). London;Berlin;: Springer, 2004.

[51] National Joint Registry, "NJR's 18th Annual Report," https://www.njrcentre.org.uk/njrcentre/Reports-Publications-and-Minutes/Annual-reports2021.

[52] World Health Organization (WHO). (2000-2016, 05/12/2018). *Global Health Observatory (GHO) data: Overweight and Obesity*. Available: http://www.who.int/gho/ncd/risk_factors/overweight_obesity/obesity_adults/en/

[53] P. C. Noble, M. A. Conditt, K. F. Cook, and K. B. Mathis, "The John Insall Award: Patient expectations affect satisfaction with total knee arthroplasty," *Clinical Orthopaedics and Related Research (1976-2007),* vol. 452, pp. 35-43, 2006.

[54] C. E. H. Scott, K. E. Bugler, N. D. Clement, D. MacDonald, C. R. Howie, and L. C. Biant, "Patient expectations of arthroplasty of the hip and knee," *The Journal of bone and joint surgery. British volume,* vol. 94, no. 7, pp. 974-981, 2012.

[55] L. E. Bayliss *et al.*, "The effect of patient age at intervention on risk of implant revision after total replacement of the hip or knee: a population-based cohort study," *The Lancet,* vol. 389, no. 10077, pp. 1424-1430, 2017.

[56] DePuy Synthes. (2017, 30/11/2018). *ATTUNE® Knee System*. Available: https://www.depuysynthes.com/hcp/knee/products/qs/ATTUNE-Knee-System

[57] Z. M. Jin, M. Stone, E. Ingham, and J. Fisher, "(v) Biotribology," *Current Orthopaedics,* vol. 20, no. 1, pp. 32-40, 2006/02/01/ 2006.

[58] J. F. Archard and W. Hirst, "The wear of metals under unlubricated conditions," *Proc. R. Soc. Lond. A,* vol. 236, no. 1206, pp. 397-410, 1956.

[59] A. Wang, "A unified theory of wear for ultra-high molecular weight polyethylene in multi-directional sliding," *Wear,* vol. 248, no. 1, pp. 38-47, 2001/03/01/ 2001.

[60] A. Galvin *et al.*, "Wear of crosslinked polyethylene under different tribological conditions," *Journal of Materials Science: Materials in Medicine,* vol. 17, no. 3, pp. 235-243, 2006/03/01 2006.

[61] A. Abdelgaied, F. Liu, C. Brockett, L. Jennings, J. Fisher, and Z. Jin, "Computational wear prediction of artificial knee joints based on a new wear law and formulation," *Journal of Biomechanics,* vol. 44, no. 6, pp. 1108-1116, 2011/04/07/ 2011.

[62] C. L. Brockett, L. M. Jennings, and J. Fisher, "Wear of knee prostheses," *Orthopedic Research and Reviews,* vol. 4, pp. 19-26, 2012.

[63] R. A. Serway, J. S. Faughn, C. Vuille, and C. A. Bennett, *College Physics: Enhanced*. Cengage Learning, 2006.

[64] A. C. Godest, M. Beaugonin, E. Haug, M. Taylor, and P. J. Gregson, "Simulation of a knee joint replacement during a gait cycle using explicit finite element analysis," *Journal of biomechanics,* vol. 35, no. 2, pp. 267-275, 2002.

[65] J. Fisher *et al.*, "Wear, debris, and biologic activity of cross-linked polyethylene in the knee: benefits and potential concerns," vol. 428, pp. 114-119, 2004.

[66] H. M. J. McEwen *et al.*, "The influence of design, materials and kinematics on the in vitro wear of total knee replacements," *Journal of biomechanics,* vol. 38, no. 2, pp. 357-365, 2005.

[67] I. R. Williams, M. B. Mayor, J. P. J. C. O. Collier, and R. Research®, "The impact of sterilization method on wear in knee arthroplasty," vol. 356, pp. 170-180, 1998.

[68] S. M. Kurtz, O. K. Muratoglu, M. Evans, and A. A. Edidin, "Advances in the processing, sterilization, and crosslinking of ultra-high molecular weight polyethylene for total joint arthroplasty," *Biomaterials,* vol. 20, no. 18, pp. 1659-1688, 1999/09/01/ 1999.

[69] E. M. Arruda and M. C. Boyce, "Evolution of plastic anisotropy in amorphous polymers during finite straining," *International Journal of Plasticity,* vol. 9, no. 6, pp. 697-720, 1993/01/01/ 1993.

[70] M. D' Acunto, F. Dinelli, and P. Pingue, "Nanowear of Polymers," vol. 31, 2015, pp. 545-587.

[71] C. L. Brockett, L. M. Jennings, C. Hardaker, and J. Fisher, "Wear of moderately cross-linked polyethylene in fixed-bearing total knee replacements," *Proceedings of the Institution of Mechanical Engineers, Part H: Journal of Engineering in Medicine,* vol. 226, no. 7, pp. 529-535, 2012.

[72] A. Abdelgaied, J. Fisher, and L. M. Jennings, "Kinematics, Mechanics and Wear Performance of a Total Knee Replacement Under Different International Standards Organization (ISO) Control Regimes and Simulation Inputs," in *IMechE Engineering the Knee: Innovation at the Interfaces for Improved Surgery and Rehabilitation*, London, United Kingdom, 2018.

[73] H. Johnston, A. Abdelgaied, H. Pandit, J. Fisher, and L. M. Jennings, "Representing the effect of variation in soft tissue constraints in experimental simulation of total knee replacements," *Journal of the Mechanical Behavior of Biomedical Materials,* vol. 87, pp. 87-94, 2018/11/01/ 2018.

[74] V. Narayan, R. King, D. Warner, and M. Sharp, "Evaluation of antioxidant-stabilized UHMWPE materials," in *55th Annual Meeting of the Orthopaedic Research Society. DePuy Orthopaedics Warsaw, IN, USA, Las Vegas, NV*, 2009.

[75] V. N. Narayan, R. King, and A. S. Senyurt, "Oxidative Stability Studies in UHMWPE - ASTM Protocol Aging," presented at the 56th Annual Meeting of the ORS, 2010.

[76] R. King, V. Narayan, C. Ernsberger, and M. Hanes, "Characterization of gamma-irradiated UHMWPE stabilized with a hindered-phenol antioxidant," in *The 55th Annual Meeting of the Orthopaedic Research Society*, 2009, pp. 22-24.

[77] M. S. Krista Parran, "Peak Stress Dictates Fatigue Crack Growth in a Hindered Phenol Antioxidant UHMWPE," presented at the ORS 2015 Annual Meeting, 2015.

[78] F. Khan, C. Yeakle, and S. Gomaa, "Characterization of the mechanical properties of a new grade of ultra high molecular weight polyethylene and modeling with the viscoplasticity based on overstress," *Journal of the mechanical behavior of biomedical materials,* vol. 6, pp. 174-180, 2012.

[79] DePuy Synthes. (2019, 19/05/19). *AOX™ Antioxidant Polyethylene*. Available: https://www.depuysynthes.com/hcp/knee/products/qs/AOX-Antioxidant-Polyethylene

[80] D. A. Dennis, "ATTUNE™ Knee System: SOFCAM™ Contact," in "Scientific Evidence," Attuneevidence.com2013, Available: https://www.attuneevidence.com/scientific-evidence.

[81] JnJ Medical Devices. (2019, 21/05/19). *AOX™ Antioxidant Polyethylene*. Available: https://www.jnjmedicaldevices.com/en-US/product/aoxtm-antioxidant-polyethylene

[82] A. Abdelgaied, C. L. Brockett, F. Liu, L. M. Jennings, Z. Jin, and J. Fisher, "The effect of insert conformity and material on total knee replacement wear," *Proceedings of the Institution of Mechanical Engineers, Part H: Journal of Engineering in Medicine,* vol. 228, no. 1, pp. 98-106, 2014.

[83] A. L. Galvin *et al.*, "Effect of conformity and contact stress on wear in fixed-bearing total knee prostheses," *Journal of Biomechanics,* vol. 42, no. 12, pp. 1898-1902, 2009/08/25/ 2009.

[84] C. W. Clary, "ATTUNE TM Knee System : Stability in Total Knee Replacement," 2013.

[85] R. List *et al.*, "Videofluoroscopic Evaluation of the Influence of a Gradually Reducing Femoral Radius on Joint Kinematics During Daily Activities in Total Knee Arthroplasty," *The Journal of arthroplasty,* vol. 35, no. 10, pp. 3010-3030, 2020.

[86] R. E. Willburger and S. Oberberg, "Early and mid-term results with the ATTUNE total knee replacement system compared to PFC Sigma: a prospective comparative study," (in eng), *J Orthop Surg Res,* vol. 17, no. 1, p. 509, Nov 24 2022.

[87] K. Okazaki, "Adopting the Joint Line Theory for Bone Resection in Cruciate-Retaining Total Knee Arthroplasty to Prevent Flexion Gap Tightness," vol. 14, no. 5, pp. 984-989, 2022.

[88] J. Bellemans, W. Colyn, H. Vandenneucker, and J. Victor, "The Chitranjan Ranawat award: is neutral mechanical alignment normal for all patients? The concept of constitutional varus," (in eng), *Clin Orthop Relat Res,* vol. 470, no. 1, pp. 45-53, Jan 2012.

[89] S. J. MacDessi, W. Griffiths-Jones, I. A. Harris, J. Bellemans, D. B. J. B. Chen, and J. Open, "The arithmetic HKA (aHKA) predicts the constitutional alignment of the arthritic knee compared to the normal contralateral knee: a matched-pairs radiographic study," vol. 1, no. 7, pp. 339-345, 2020.

[90] P.-A. Vendittoli, S. Martinov, and W. G. J. F. i. S. Blakeney, "Restricted kinematic alignment, the fundamentals, and clinical applications," vol. 8, 2021.

[91] C. Rivière *et al.*, "Alignment options for total knee arthroplasty: A systematic review," *Orthopaedics & Traumatology: Surgery & Research,* vol. 103, no. 7, pp. 1047-1056, 2017/11/01/ 2017.

[92] C. Rivière, S. Lazic, O. Boughton, Y. Wiart, L. Vïllet, and J. Cobb, "Current concepts for aligning knee implants: patient-specific or systematic?," (in eng), *EFORT open reviews,* vol. 3, no. 1, pp. 1-6, 2018.

[93] S. Nisar, J. Palan, C. Rivière, M. Emerton, and H. J. E. o. r. Pandit, "Kinematic alignment in total knee arthroplasty," vol. 5, no. 7, pp. 380-390, 2020.

[94] DePuy Synthes, "ATTUNE™ Knee System Femur First Anatomic Alignment Surgical Technique," in *Patient Specific Alignment*, ed, 2022, p. 40.

[95] R. S. Jeffery, R. W. Morris, and R. A. Denham, "Coronal alignment after total knee replacement," *The Journal of bone and joint surgery. British volume,* vol. 73, no. 5, pp. 709-714, 1991.

[96] P. Maquet, "Biomechanics of gonarthrosis," *Acta Orthopaedica Belgica,* vol. 38, p. 33, 1972.

[97] C. Rivière *et al.*, "The kinematic alignment technique for TKA reliably aligns the femoral component with the cylindrical axis," *Orthopaedics & Traumatology: Surgery & Research,* vol. 103, no. 7, pp. 1069-1073, 2017/11/01/ 2017.

[98] M. Schiraldi, G. Bonzanini, D. Chirillo, and V. de Tullio, "Mechanical and kinematic alignment in total knee arthroplasty," *Annals of Translational Medicine,* vol. 4, no. 7, p. 130, 03/03/received

03/15/accepted 2016.

[99] C. C. Castelli, D. A. Falvo, M. L. Iapicca, and V. Gotti, "Rotational alignment of the femoral component in total knee arthroplasty," (in eng), *Annals of translational medicine,* vol. 4, no. 1, pp. 4-4, 2016.

[100] M. Pitta, C. I. Esposito, Z. Li, Y.-y. Lee, T. M. Wright, and D. E. Padgett, "Failure After Modern Total Knee Arthroplasty: A Prospective Study of 18,065 Knees," *The Journal of Arthroplasty,* vol. 33, no. 2, pp. 407-414, 2018/02/01/ 2018.

[101] T. P. Andriacchi, T. S. Stanwyck, and J. O. Galante, "Knee biomechanics and total knee replacement," *The Journal of arthroplasty,* vol. 1, no. 3, pp. 211-219, 1986.

[102] A. Srivastava, G. Y. Lee, N. Steklov, C. W. Colwell, Jr., K. A. Ezzet, and D. D. D'Lima, "Effect of tibial component varus on wear in total knee arthroplasty," *Knee,* vol. 19, no. 5, pp. 560-3, Oct 2012.

[103] T. P. Andriacchi, "Functional analysis of pre and post-knee surgery: total knee arthroplasty and ACL reconstruction," *Journal of biomechanical engineering,* vol. 115, no. 4B, pp. 575-581, 1993.

[104] S. Parratte, M. W. Pagnano, R. T. Trousdale, and D. J. J. J. Berry, "Effect of postoperative mechanical axis alignment on the fifteen-year survival of modern, cemented total knee replacements," vol. 92, no. 12, pp. 2143-2149, 2010.

[105] L. A. Whiteside, *Ligament balancing in total knee arthroplasty: an instructional manual*. Springer Science & Business Media, 2012.

[106] J. Hutt, V. Massé, M. Lavigne, and P.-A. Vendittoli, "Functional joint line obliquity after kinematic total knee arthroplasty," *International orthopaedics,* vol. 40, no. 1, pp. 29-34, 2016.

[107] S. Parratte and M. W. Pagnano, "Instability after total knee arthroplasty," (in eng), *Instr Course Lect,* vol. 57, pp. 295-304, 2008.

[108] K. Gromov, M. Korchi, M. G. Thomsen, H. Husted, and A. Troelsen, "What is the optimal alignment of the tibial and femoral components in knee arthroplasty?," (in eng), *Acta orthopaedica,* vol. 85, no. 5, pp. 480-487, 2014.

[109] E. J. Miller, M. W. Pagnano, and K. R. Kaufman, "Tibiofemoral alignment in posterior stabilized total knee arthroplasty: static alignment does not predict dynamic tibial plateau loading," *Journal of Orthopaedic Research,* vol. 32, no. 8, pp. 1068-1074, 2014.

[110] A. M. Almaawi, J. R. B. Hutt, V. Masse, M. Lavigne, and P.-A. Vendittoli, "The impact of mechanical and restricted kinematic alignment on knee anatomy in total knee arthroplasty," *The Journal of arthroplasty,* vol. 32, no. 7, pp. 2133-2140, 2017.

[111] W. Barrett, D. Hoeffel, D. Dalury, J. B. Mason, J. Murphy, and S. Himden, "In-vivo alignment comparing patient specific instrumentation with both conventional and computer assisted surgery (CAS) instrumentation in total knee arthroplasty," (in eng), *J Arthroplasty,* vol. 29, no. 2, pp. 343-7, Feb 2014.

[112] International Organization for Standardization (ISO). (2009, 21/01/19). *BS ISO 14243-1:2009: Implants for surgery. Wear of total knee-joint prostheses. Loading and displacement parameters for wear-testing machines with load control and corresponding environmental conditions for test*. Available: https://www.iso.org/standard/44262.html

[113] International Organization for Standardization (ISO), "BS ISO 14243-2:2016: Implants for surgery. Wear of total knee-joint prostheses. Methods of measurement," ed: British Standards Institute, 2016.

[114] International Organization for Standardization (ISO). (2014, 21/01/19). *BS ISO 14243-3:2014: Implants for surgery. Wear of total knee-joint prostheses. Loading and displacement parameters for wear-testing machines with displacement control and corresponding environmental conditions for test*. Available: https://www.iso.org/standard/56649.html

[115] P. I. Barnett, J. Fisher, D. D. Auger, M. H. Stone, and E. J. J. o. m. s. M. i. m. Ingham, "Comparison of wear in a total knee replacement under different kinematic conditions," vol. 12, no. 10-12, pp. 1039-1042, 2001.

[116] T. Johnson, M. Laurent, J. Yao, and L. J. W. Gilbertson, "The effect of displacement control input parameters on tibiofemoral prosthetic knee wear," vol. 250, no. 1-12, pp. 222-226, 2001.

[117] C. L. Brockett, A. Abdelgaied, T. Haythornthwaite, C. Hardaker, J. Fisher, and L. M. Jennings, "The influence of simulator input conditions on the wear of total knee replacements: An experimental and computational study," *Proceedings of the Institution of Mechanical Engineers, Part H: Journal of Engineering in Medicine,* vol. 230, no. 5, pp. 429-439, 2016.

[118] H. Asano, A. Hoshino, and T. J. Wilton, "Soft-tissue tension total knee arthroplasty1 1No benefits or funds were received in support of this study," *The Journal of Arthroplasty,* vol. 19, no. 5, pp. 558-561, 2004/08/01/ 2004.

[119] A. Abdelgaied, J. Fisher, and L. M. Jennings, "A comprehensive combined experimental and computational framework for pre-clinical wear simulation of total knee replacements," *Journal of the Mechanical Behavior of Biomedical Materials,* vol. 78, pp. 282-291, 2018/02/01/ 2018.

[120] M. R. Dressler, S. Swope, J. Tikka, C. Hardaker, M. Heldreth, and T. Render, "Wear of a total knee replacement with antioxidant UHMWPE and gradually varying sagittal curvature," in *ORS 2012*, 2012.

[121] S. Schroeder *et al.*, "Does Kinematic Alignment Increase Polyethylene Wear Compared With Mechanically Aligned Components? A Wear Simulation Study," p. 10.1097, 2022.

[122] J. Fish and T. Belytschko, *A first course in finite elements* (no. Book, Whole). Chichester: Wiley, 2007.

[123] R. Willing and I. Y. Kim, "A holistic numerical model to predict strain hardening and damage of UHMWPE under multiple total knee replacement kinematics and experimental validation," *Journal of Biomechanics,* vol. 42, no. 15, pp. 2520-2527, 2009/11/13/ 2009.

[124] J. Fisher, L. M. Jennings, A. L. Galvin, Z. M. Jin, M. H. Stone, and E. Ingham, "2009 Knee Society Presidential Guest Lecture: Polyethylene wear in total knees," (in eng), *Clinical orthopaedics and related research,* vol. 468, no. 1, pp. 12-18, 2010.

[125] F. Liu, A. Galvin, Z. Jin, and J. J. P. o. t. I. o. M. E. Fisher, Part H: Journal of Engineering in Medicine, "A new formulation for the prediction of polyethylene wear in artificial hip joints," vol. 225, no. 1, pp. 16-24, 2011.

[126] L. Kang, A. L. Galvin, T. D. Brown, Z. Jin, and J. Fisher, "Quantification of the effect of cross-shear on the wear of conventional and highly cross-linked UHMWPE," *Journal of biomechanics,* vol. 41, no. 2, pp. 340-346, 2008.

[127] C. K. Fitzpatrick, C. Maag, C. W. Clary, A. Metcalfe, J. Langhorn, and P. J. Rullkoetter, "Validation of a new computational 6-DOF knee simulator during dynamic activities," *Journal of biomechanics,* vol. 49, no. 14, pp. 3177-3184, 2016.

[128] I. Kutzner *et al.*, "Loading of the knee joint during activities of daily living measured in vivo in five subjects," vol. 43, no. 11, pp. 2164-2173, 2010.

[129] H. Johnston, A. Abdelgaied, H. Pandit, J. Fisher, and L. M. Jennings, "The effect of surgical alignment and soft tissue conditions on the kinematics and wear of a fixed bearing total knee replacement," *Journal of the mechanical behavior of biomedical materials,* vol. 100, p. 103386, 2019.

[130] C. Maag, I. Cracaoanu, J. Langhorn, and M. Heldreth, "Total knee replacement wear during simulated gait with mechanical and anatomic alignments," *Proceedings of the Institution of Mechanical Engineers, Part H: Journal of Engineering in Medicine,* p. 0954411921991269, 2021.

[131] C. K. Fitzpatrick, M. A. Baldwin, C. W. Clary, L. P. Maletsky, P. J. J. C. m. i. b. Rullkoetter, and b. engineering, "Evaluating knee replacement mechanics during ADL with PID-controlled dynamic finite element analysis," vol. 17, no. 4, pp. 360-369, 2014.

[132] E. A. Morra, C. S. Heim, and A. S. Greenwald, "Preclinical Computational Models: Predictors of Tibial Insert Damage Patterns in Total Knee ArthroplastyAAOS Exhibit Selection," *JBJS,* vol. 94, no. 18, p. e137, 2012.

[133] M. Ishikawa, S. Kuriyama, H. Ito, M. Furu, S. Nakamura, and S. Matsuda, "Kinematic alignment produces near-normal knee motion but increases contact stress after total knee arthroplasty: A case study on a single implant design," *The Knee,* vol. 22, no. 3, pp. 206-212, 2015/06/01/ 2015.

[134] E. A. Morra, M. P. D. Postak, C. S. Heim, and A. S. Greenwald, "The influence of Mechanical versus Kinematic alignment on the knee design performance during walking gait.," presented at the AAOS 2017 Annual Meeting, San Diego, 2017.

[135] L. Jennings, C. Bell, E. Ingham, R. Komistek, M. Stone, and J. Fisher, "The influence of femoral condylar lift-off on the wear of artificial knee joints," *Proceedings of the Institution of Mechanical Engineers, Part H: Journal of Engineering in Medicine,* vol. 221, no. 3, pp. 305-314, 2007.

[136] A. Abdelgaied, J. Fisher, and L. M. Jennings, "A comparison between electromechanical and pneumatic-controlled knee simulators for the investigation of wear of total knee replacements," *Proceedings of the Institution of Mechanical Engineers, Part H: Journal of Engineering in Medicine,* vol. 231, no. 7, pp. 643-651, 2017.

[137] University of Leeds, "SOP.01.02.J - Knee Joint Simulator Studies," in *Knee Simulators 7, 8 & 9* vol. Revision 3, ed, 2020.

[138] University of Leeds, "SOP.06.04 - PMMA cement Handling," vol. Revision 5, ed, 2019.

[139] University of Leeds, "SOP.03.01.B - Mettler Balance XP205," vol. Revision 4, ed, 2021.

[140] E. A. Morra and A. S. J. J. Greenwald, "Polymer insert stress in total knee designs during high-flexion activities: a finite element study," vol. 87, no. suppl_2, pp. 120-124, 2005.

[141] X. C. Liu and G. Schmidig, "TKA Contact Area Contact Stress FEA Validation following ASME V&V 40," in *2019 Frontiers in Medical Devices*, University of Maryland, 2019.

[142] A. M. Fansa, C. D. Murawski, C. W. Imhauser, J. T. Nguyen, and J. G. Kennedy, "Autologous Osteochondral Transplantation of the Talus Partially Restores Contact Mechanics of the Ankle Joint," vol. 39, no. 11, pp. 2457-2465, 2011.

[143] DePuy Synthes, "WI-0550, Mounting Femoral & Tibial Trays and Verification of Contact Area Between the Femoral and Tibial Insert," vol. B, ed, 2020.

[144] Tekscan Inc., "I-Scan® Equilibration and Calibration Practical Suggestions," vol. Rev A, ed, 2003.

[145] P. Postak, C. Heim, and A. J. O. R. L. Greenwald, "Tibial plateau surface stress in TKA: A factor influencing polymer damage series IV-PCL substituting design,'" 1996.

[146] K. Johnson, "One hundred years of Hertz contact," *Proceedings of the Institution of Mechanical Engineers,* vol. 196, no. 1, pp. 363-378, 1982.

[147] B. J. Fregly, W. G. Sawyer, M. K. Harman, and S. A. Banks, "Computational wear prediction of a total knee replacement from in vivo kinematics," *Journal of Biomechanics,* vol. 38, no. 2, pp. 305-314, 2005/02/01/ 2005.

[148] K. L. Johnson, *Contact mechanics* (no. Book, Whole). New York;Cambridge [Cambridgeshire];: Cambridge University Press, 1985, pp. 84-106.

[149] S. M. Kurtz, C. W. Jewett, J. S. Bergström, J. R. Foulds, and A. A. Edidin, "Miniature specimen shear punch test for UHMWPE used in total joint replacements," *Biomaterials,* vol. 23, no. 9, pp. 1907-1919, 2002/05/01/ 2002.

[150] D. L. Bartel, J. Rawlinson, A. Burstein, C. Ranawat, J. W. J. C. O. Flynn, and R. Research, "Stresses in polyethylene components of contemporary total knee replacements," no. 317, pp. 76-82, 1995.

[151] A. Abdelgaied and L. M. Jennings, "GONFS00813 - Development of a predictive computational wear model for Attune," 2019.

[152] S. W. Young, M. L. Walker, A. Bayan, T. Briant-Evans, P. Pavlou, and B. Farrington, "The Chitranjan S. Ranawat Award: No Difference in 2-year Functional Outcomes Using Kinematic versus Mechanical Alignment in TKA: A Randomized Controlled Clinical Trial," *Clinical Orthopaedics and Related Research,* vol. 475, no. 1, p. 9, 2017.

[153] W. Blakeney, J. Clément, F. Desmeules, N. Hagemeister, C. Rivière, and P.-A. J. K. S. Vendittoli, Sports Traumatology, Arthroscopy, "Kinematic alignment in total knee arthroplasty better reproduces normal gait than mechanical alignment," vol. 27, no. 5, pp. 1410-1417, 2019.

[154] S. M. Howell, S. J. Howell, K. T. Kuznik, J. Cohen, and M. L. Hull, "Does a kinematically aligned total knee arthroplasty restore function without failure regardless of alignment category?," *Clinical Orthopaedics and Related Research®,* vol. 471, no. 3, pp. 1000-1007, 2013.

[155] S. M. Howell, M. L. Hull, M. J. I. Mahfouz, and P. E. Scott surgery of the knee. Philadelphia, "Kinematic alignment in total knee arthroplasty," pp. 1255-1268, 2012.

[156] S. M. Howell, K. Kuznik, M. L. Hull, and R. A. J. O. Siston, "Results of an initial experience with custom-fit positioning total knee arthroplasty in a series of 48 patients," vol. 31, no. 9, pp. 857-863, 2008.

[157] S. M. Howell, K. Kuznik, M. L. Hull, R. A. J. C. O. Siston, and R. Research®, "Longitudinal shapes of the tibia and femur are unrelated and variable," vol. 468, no. 4, pp. 1142-1148, 2010.

[158] S. M. Howell, S. J. Howell, and M. L. J. J. Hull, "Assessment of the radii of the medial and lateral femoral condyles in varus and valgus knees with osteoarthritis," vol. 92, no. 1, pp. 98-104, 2010.

[159] B. A. Spencer, M. A. Mont, M. S. McGrath, B. Boyd, and M. F. J. I. o. Mitrick, "Initial experience with custom-fit total knee replacement: intra-operative events and long-leg coronal alignment," vol. 33, no. 6, pp. 1571-1575, 2009.

[160] T. D. Cooke, E. A. Sled, and R. A. Scudamore, "Frontal plane knee alignment: a call for standardized measurement," (in eng), *J Rheumatol,* vol. 34, no. 9, pp. 1796-801, Sep 2007.

[161] P. J. McNair, M. G. Boocock, N. D. Dominick, R. J. Kelly, B. J. Farrington, and S. W. J. T. J. o. A. Young, "A comparison of walking gait following mechanical and kinematic alignment in total knee joint replacement," vol. 33, no. 2, pp. 560-564, 2018.

[162] P. D. Evans, P. D. Marshall, B. McDonnell, J. Richards, and E. J. Evans, "Radiologic study of the accuracy of a tibial intramedullary cutting guide for knee arthroplasty," (in eng), *J Arthroplasty,* vol. 10, no. 1, pp. 43-6, Feb 1995.

[163] G. A. Ateshian, L. J. Soslowsky, and V. C. Mow, "Quantitation of articular surface topography and cartilage thickness in knee joints using stereophotogrammetry," *Journal of Biomechanics,* vol. 24, no. 8, pp. 761-776, 1991/01/01/ 1991.

[164] H. E. Johnston, "The Effect of Surgical Alignment and Soft Tissue Constraints on the Kinematics, Contact Pressure and Wear of a Total Knee Replacement," University of Leeds, 2019.

[165] A. Abdelgaied and L. M. Jennings, "GONFS01018 - Development of a predictive computational wear model for Attune," 2020.

[166] A. Abdelgaied and L. M. Jennings, "GONFS01316 - Development of a predictive computational wear model for Attune," 2022.

[167] J.-J. Liau, C.-K. Cheng, C.-H. Huang, and W.-H. Lo, "Effect of Fuji pressure sensitive film on actual contact characteristics of artificial tibiofemoral joint," *Clinical biomechanics,* vol. 17, no. 9-10, pp. 698-704, 2002.

[168] W. Theodore *et al.*, "Variability in static alignment and kinematics for kinematically aligned TKA," vol. 24, no. 4, pp. 733-744, 2017.

[169] A. Abdelgaied, C. L. Brockett, F. Liu, L. M. Jennings, J. Fisher, and Z. Jin, "Quantification of the effect of cross-shear and applied nominal contact pressure on the wear of moderately cross-linked polyethylene," *Proceedings of the Institution of Mechanical Engineers, Part H: Journal of Engineering in Medicine,* vol. 227, no. 1, pp. 18-26, 2013.

[170] Y. Niki, T. Nagura, K. Nagai, S. Kobayashi, and K. J. K. S. Harato, Sports Traumatology, Arthroscopy, "Kinematically aligned total knee arthroplasty reduces knee adduction moment more than mechanically aligned total knee arthroplasty," vol. 26, no. 6, pp. 1629-1635, 2018.

[171] C. K. Fitzpatrick, C. Clary, T. Nakamura, and P. Rullkoetter, "THE EFFECT OF COMPONENT AND LOWER LIMB ALIGNMENT ON TKA JOINT MECHANICS," in *Orthopaedic Proceedings*, 2016, vol. 98, no. SUPP_1, pp. 131-131: The British Editorial Society of Bone & Joint Surgery.

Appendix

Appendix A – Attune Baseline Component Details

Table A-1: Attune Baseline Component Details

Part Description	Sample ID	Size	Thickness (mm)	REF	LOT	Drawing Number	Rev
Attune AOX Right Tibial Insert FB CR	X1	5	6	1516-20-506	J2677H	DWG-1151620505	C
Attune AOX Right Tibial Insert FB CR	X2	5	6	1516-20-506	J2677H	DWG-1151620505	C
Attune AOX Right Tibial Insert FB CR	X3	5	6	1516-20-506	J2677H	DWG-1151620505	C
Attune AOX Right Tibial Insert FB CR	X4	5	6	1516-20-506	J2677H	DWG-1151620505	C
Attune AOX Right Tibial Insert FB CR	X5	5	6	1516-20-506	J2677H	DWG-1151620505	C
Attune AOX Right Tibial Insert FB CR	X6	5	6	1516-20-506	J2571J	DWG-1151620505	C
Attune AOX Right Tibial Insert FB CR	C1	5	6	1516-20-506	J2571J	DWG-1151620505	C
Attune AOX Right Tibial Insert FB CR	C2	5	6	1516-20-506	J2481X	DWG-1151620505	C
Attune CoCr Right Tibial Tray FB	T1-T5	5		1506-00-005	9111518	DWG-1150600005	D
Attune CoCr Right Tibial Tray FB	T6	5		1506-00-005	9080596	DWG-1150600005	D
Attune CoCr Right Femoral CR	F1-F6	5		1504-00-205	9111012	DWG-1150400205	E

Appendix B – Python script for extracting Abaqus data

Table B-1: Python script for extracting data from Abaqus .odb files to include CPRESS, CSLIP1, CSLIP2, U, UR and node labels.

```
from odbAccess import *
from abaqusConstants import *
import odbAccess
#*********************************************************************
PreferredExtension = '.xls' #Insert the extension for the output file
#*********************************************************************
odb = openOdb(path='XXXXX.odb')
myAssembly = odb.rootAssembly

NameOfFile1 = 'XXXXX_CPRESS'+PreferredExtension
NameOfFile2 = 'XXXXX_CSLIP1'+PreferredExtension
NameOfFile3 = 'XXXXX_CSLIP2'+PreferredExtension
NameOfFile4 = 'XXXXX_U'+PreferredExtension
NameOfFile5 = 'XXXXX_UR'+PreferredExtension
NameOfFile6 = 'XXXXX_nodelabels'+PreferredExtension

SDResultsX = open(NameOfFile1,'w') #CPRESS
SDResultsY = open(NameOfFile2,'w') #CSLIP1
SDResultsZ = open(NameOfFile3,'w') #CSLIP2
SDResultsU = open(NameOfFile4,'w') #U
SDResultsV = open(NameOfFile5,'w') #UR
SDResultsN = open(NameOfFile6,'w') #NodeLabels

#**********************************************************************
lastFrame = odb.steps['Displacement'].frames[-1]
displacement=lastFrame.fieldOutputs['CPRESS']
fieldValues=displacement.values
center = odb.rootAssembly.instances['Tibial Insert-1']
centerDisplacement = displacement.getSubset(region=center)
centerValues = centerDisplacement.values
#nodenumbers
for v in centerValues:
    SDResultsN.write('%10.9E\t' % (v.nodeLabel))
SDResultsN.write('\n')

#**********************************************************************
for stepName in odb.steps.keys():
   lastFrame = odb.steps[stepName].frames[-1]

   contactX=lastFrame.fieldOutputs['CPRESS']
   slipX=lastFrame.fieldOutputs['CSLIP1']
   slipY=lastFrame.fieldOutputs['CSLIP2']
   slidingY=lastFrame.fieldOutputs['U']
   rotationZ=lastFrame.fieldOutputs['UR']

   fieldValues2=contactX.values
   fieldValues3=slipX.values
   fieldValues4=slipY.values
   fieldValues5=slidingY.values
   fieldValues6=rotationZ.values
```

```
  center = odb.rootAssembly.instances['Tibial Insert-1'].nodeSets['INSERT']

  CSContactX = contactX.getSubset(region=center)
  tibialCSValuesX = CSContactX.values

  CSslipX = slipX.getSubset(region=center)
  tibialCSValuesY = CSslipX.values

  CSslipY = slipY.getSubset(region=center)
  tibialCSValuesZ = CSslipY.values

  CSslidingY = slidingY.getSubset(region=center)
  tibialCSValuesU = CSslidingY.values

  CSrotationZ = rotationZ.getSubset(region=center)
  tibialCSValuesV = CSrotationZ.values

 #CPRESS
  for v in tibialCSValuesX:
    SDResultsX.write('%10.9E\t' % (v.data))
  SDResultsX.write('\n')

#CSLIP1
  for v in tibialCSValuesY:
    SDResultsY.write('%10.9E\t' % (v.data))
  SDResultsY.write('\n')

#CSLIP2
  for v in tibialCSValuesZ:
    SDResultsZ.write('%10.9E\t' % (v.data))
  SDResultsZ.write('\n')

#Displacement
  for v in tibialCSValuesU:
    SDResultsU.write('%10.9E\t' % (v.data[1]))
  SDResultsU.write('\n')

#Rotation
  for v in tibialCSValuesV:
    SDResultsV.write('%10.9E\t' % (v.data[2]))
  SDResultsV.write('\n')

#xxxxxxxxxxxxxxxxxxxxxxxxxxxxxxxxxxxxxxxxxxxxxxxxxxxxxxxxxxxxxxxxxxxxxxxxxxxx
#xxxxxxxxxxxxxxxxxxxxxxxxxxxxxxxxxxxxxxxxxxxxxxxxxxxxxxxxxxxxxxxxxxxxxxxxxxxx
SDResultsX.close()
SDResultsY.close()
SDResultsZ.close()
SDResultsU.close()
SDResultsV.close()

#*******************************************************************
#******************************************************************
#*******************************************************************
odb.close()
#******************************************************************
```